UNIVERSITY OF CALIFORNIA,
IRVINE

η^6-Arene Tethered Ruthenium (II) Complexes and Half-metallocene Dithiocarbamate Ruthenium (IV) Complex for Olefin Polymerization: Experimental, Mechanistic, and DFT Studies

DISSERTATION

submitted in partial satisfaction of the requirements
for the degree of

DOCTOR OF PHILOSOPHY

in Chemistry

by

Miguel Angel Camacho Fernandez

Dissertation Committee:
Professor Zhibin Guan, Chair
Professor Kenneth J. Shea
Professor Gregory A. Weiss

2014

DEDICATION

To

my wife Manuela

TABLE OF CONTENTS

LIST OF CHARTS

LIST OF SCHEMES

LIST OF FIGURES

LIST OF TABLES

ACKNOWLEDGMENTS

First, I would like to thank my advisor, Prof. Zhibin Guan for his mentorship, support, teaching, and wise advice not only on my research projects but also in professional and personal matters. A warm thank you to all the UCI Chemistry Department and especially to my committee members Prof. Kenneth Shea and Prof. Gregory Weiss, I really appreciate their comments and questions during my orals exam and thesis defense. Also, I would like to thank Prof. Filipp Furche for his advice on DFT modeling. I thank Prof. Chris Vanderwal, Renee Frigo, and Jaime Albano for their support and advice. Financial support was provided by the University of California Irvine, NSF Grant CHE-1012422 for experimental work, and NSF Grant CHE-0840513 for Green Planet molecular modeling facility.

I would like to thank the catalysis subgroup members and visitors: Tobias Friedberger, Justin Crumrine. Guobin Sun, Yingwei Yang, Hannah K. Nguyen, Lee Anne Wang, and Maike Lukowiak. Special thanks to Tobi and Justin; it has been a lot fun to work with you in the last few years. I thank Davoud Mozdehi for his insanity; it is always good to know that there is someone odder than myself. I also thank the rest of Guan's lab for their support: Olivia Cromwell, Mark Johnson, Jane Bai, Nathan Oldenhuis, Jae Chung, James Neal, Gregory Williams, Yulin Chen, Jason Lusk, Sophia Liao, Ting-Bin Yu, Hiro Urakami, Max Yen, Sergio Ayala, Jonathan Ruiz, Jens Hentschel and especially to my colleagues Hanxiang Zeng and Yi-Xyan Lu. Thanks to my friend Thomas Patko for the support and fantastic lunches with a cold beer, we need to do it more often now.

I must thank Dr. Phil Dennison for his advice with NMR spectroscopy that allowed me to complete the most important part of my research. I thank Dr. Joshep Ziller, Ryan Zarkesh, and Jordan Corbey for helping me with the X-ray diffraction and determination of my crystal structures. I would also like to thank Dr. John Greaves and Dr. Beniam Berhane for the MS assistance. Thanks to the Shea lab members, Ruobing Zhao and Dr. Eduardo Baez for their GPC assistance.

I would like to thank all my friends in Spain, especially Oscar Cordovilla, Antonio Dominguez (Homer), Juan Maria Alcaide, Ruben Trapero, Jose Antonio Huertas (Rubio), and to all those with whom I have had the pleasure of sharing a few moments in life.

I must thank Pat Morgan, Carol Willis, Devon Shay, David Slater, Craig Barto, Tom Shollin, Brandon Bridgman, and everyone else at Signal Hill Petroleum for their support.

I also would like to thank my brother Hilario Camacho Fernandez for his support and advice, te quiero hermano. I also would like to thank my brother Dimas Camacho Fernandez who passed away during my graduate studies at UCI, you are deeply missed. My parents Felicidad and Angel, thank you for being the best guide in the world, os quiero y admiro. Muchas gracias por todo lo que habéis hecho por mí.

I want to give thanks to the most important person in my life, my wife Manuela, you mean everything to me. Muchas gracias Chiqui por estar a mi lado, sin tu ayuda y apoyo no lo habría logrado.

CURRICULUM VITAE

Miguel Angel Camacho Fernandez

Education

2014	Ph.D. in Organic Chemistry, University of California, Irvine
2010	M.S. in Chemistry, California State University Long Beach
2000	B.S. in Chemistry, University of Granada, Spain

Professional Experience

20014-present	Chemical Specialist at Signal Hill Petroleum
2012-2014	Geochemical Tech at Signal Hill Petroleum
2004-2012	Engineering Technician at Signal Hill Petroleum
2003-2004	Petroleum Technician at Signal Hill Petroleum
2000-03	Voluntary work assisting handicapped people at O.N.C.E., Spain

AWARDS AND HONORS

2006	Graduate Dean's Honor List, Spring, CSULB
2006	Departmental (Chemistry and Biochemistry Department) Graduate Honor, Spring 2006, CSULB
2006	American Institute of Chemists Graduate Award, Spring, CSULB
2007	Hypercube (Computational Chemistry) Award, Spring, CSULB

PUBLICATIONS

Camacho-Fernandez, Miguel A.; Yen, Max; Ziller, Joseph W.; Guan, Zhibin "Direct observation of a cationic ruthenium complex for ethylene insertion polymerization" *Chem. Sci.* **2013**, *4*, 2902-2906.

Camacho-Fernandez, Miguel A.; Ziller, Joseph W.; Guan, Zhibin "Heteroatom Effect on η6-Arene Tethered Ru(II) Complexes for Ethylene Polymerization: Experimental and DFT Studies" in preparation.

Camacho-Fernandez, Miguel A.; Ziller, Joseph W.; Guan, Zhibin "Ethylene Polymerization with a Half-metallocene Dithiocarbamate Ruthenium (IV) Complex: An Experimental and Theoretical Study" in preparation.

Wang, Rongming; **Camacho-Fernandez, Miguel A.**; Xu, Wei; Zhang, Jian; Li, Lijuan " Neutral and reduced Roussin's red salt ester [Fe2(μ-RS)2(NO)4] (R = n-Pr, t-Bu, 6-methyl-2-pyridyl and 4,6-dimethyl-2-pyrimidyl): synthesis, X-ray crystal structures, spectroscopic, electrochemical and density functional theoretical investigations" *Dalton Trans.* **2009**, 777-786.

ABSTRACT OF THE DISSERTATION

η^6-Arene Tethered Ruthenium (II) Complexes and Half-metallocene Dithiocarbamate Ruthenium (IV) Complex for Olefin Polymerization: Experimental, Mechanistic, and DFT Studies

By

Miguel Angel Camacho Fernandez

Doctor of Philosophy in Chemistry

University of California, Irvine, 2014

Professor Zhibin Guan, Chair

There are very few reports of ruthenium complexes for olefin polymerization and the active species are unknown. In this dissertation we explore a series of new ruthenium II and IV complexes for olefin polymerization catalysis. We synthesized an arene-tethered ruthenium complex (η^6-$C_6H_5(CH_2)_3SCH_3RuCl_2$) capable of catalyzing ethylene polymerization using $AlMe_2Cl$ as cocatalyst. Homologous dimethylated η^6-$C_6H_5(CH_2)_3SCH_3Ru(CH_3)_2$ complex in the presence of ethylene also yielded polyethylene when activated with HBArF ($[H(Et_2O)_2]^+[BAr'_4]^-$ (where Ar'=3,5-$(CF_3)_2C_6H_3$)). Mechanistic studies by ^{1}H-NMR and mass spectrometry support a ruthenium cationic [η^6-$C_6H_5(CH_2)_3SCH_3Ru(oligomer)]^+$ complex as the polymerization active species. This has unambiguously demonstrated for the first time a ruthenium complex as the active species for catalyzing olefin insertion polymerization.

We also studied heteroatom effect η^6-Arene tethered ruthenium (II) complexes on polymerization activity. Complexes (η^6-$C_6H_5(CH_2)_3SCH_3RuCl_2$), ($\eta^6$-$C_6H_5(CH_2)_3N(CH_3)_2RuCl_2$), and $[(\eta^6$-$C_6H_5(CH_2)_3OCH_3RuCl_2)]_2$ with coordinating oxygen,

sulfur, and nitrogen heteroatoms in the tethered arms have been compared for olefin polymerization. Nitrogen and sulfur-containing complexes are active for olefin polymerization while oxygen-containing complex is inactive. The nitrogen-containing complex is 1.5-fold more active than the sulfur-containing complex. The polymers obtained are composed of two different fractions, a high molecular weight fraction (55-161 $kg \cdot mol^{-1}$) and a low molecular weight fraction (276-761 $g \cdot mol^{-1}$). The polydispersities of both fractions are narrow, indicating a single-site catalyst. DFT calculations were carried out on to determine the migratory insertion barriers. Nitrogen-containing complex was found to have a migratory insertion barrier of the chain propagation of 19.4 $kcal \cdot mol^{-1}$ while sulfur-containing was found to be 21.8 $kcal \cdot mol^{-1}$. Theoretical calculations are in agreement with the experimental polymerization activity results.

We hypothesize that a more electron deficient ruthenium complex will be more active. We synthesized Ru(IV) dimethyl complex [$Cp^*(\kappa^2\text{-}S_2CNMe_2)Ru^{IV}Me_2$] that polymerizes ethylene with higher activity. The polymers obtained were linear with high molecular weights (up to 322 $kg \cdot mol^{-1}$) and narrow monomodal molecular weight distributions (Mw/Mn=1.69–2.50). Pronounced counterion effects were observed: the methylaluminoxane activator gave the highest productivities, whereas HBArF resulted in no activity. These results are further supported by DFT calculations, which indicate a low migratory insertion barrier for chain propagation (9.8 $kcal \cdot mol^{-1}$) but high ethylene uptake energies (15.6 $kcal \cdot mol^{-1}$).

Chapter 1

Ruthenium catalysts for Olefin Polymerization and Computational Modeling of Transition Metals for Polymerization Catalysis

1.1 Transition Metal Polymerization Catalysis

Polyolefins are the largest volume produced plastics and their production continues to grow progressively.[1-3] Polyolefins is the general name of polymers based on ethylene and α-olefins and over 70 billion kilograms are produced every year.[4] Polyolefins physical properties vary from waxes to flexible elastomers to rigid thermoplastics and are used in a wide range of applications. Industrial olefin polymerization was traditionally carried out at high pressures and high temperatures initiated by radicals.[5] These polymerization conditions did not allow control over polymer stereochemistry, molecular weight, and polydispersity and it has been displaced by the use of early transition metal (ETM) catalysis. It was not until the 1950's when Ziegler made the groundbreaking discovery in which activation of heterogeneous $TiCl_3$ with alkyl-aluminum cocatalyst ($AlEt_3$) achieved polyethylene with great turnover frequencies.[6] This was immediately followed by Natta's α-olefins (propylene) polymerization studies using Ziegler's catalytic system.[7] Both scientists were awarded the Nobel prize in chemistry in 1963 "for their discoveries in the field of the chemistry and technology of high polymers". Many other heterogeneous catalyst based on early transition metals, such as chromium, with great activities have been

discovered since.[8-10]

Homogenous catalysis for olefin polymerization have been also developed and made it to industrial scale. Moreover, some of these homogeneous catalysts are attached to solid substrate becoming heterogeneous and enhancing their activity and stability.[5] Homogeneous catalysts offer the advantage of rapid rates of diffusion of reagents and heat in solution, but also a better stereo- and regio-control of polymers. The most important feature of homogeneous catalysts is that active species can be studied in solution-phase, such as nuclear magnetic resonance (NMR) spectroscopy, which offers valuable information on olefin polymerization mechanism.[5,11,12] Many homogeneous catalysts based on early transition metals have been discovered based on different ligand frameworks as depicted on Chart 1.1. Structures **1.1** and **1.2** are based on the metallocene ligand framework. Complexes based on **1.2** structure are also known as ansa-metallocene complexes that allow for rigorous stereocontrol of polymerization. Complexes based on structure **1.3** are known as halfmetallocene constratined geometry catalysts (CGC). In all cases very active species are obtained upon activation with alkyl-aluminum cocatalysts or by activation with borane-based cocatalysts of their dimethylated versions. [5,13-29]

Chart 1.1. Representative homogeneous ETM catalysts for olefin polymerization.

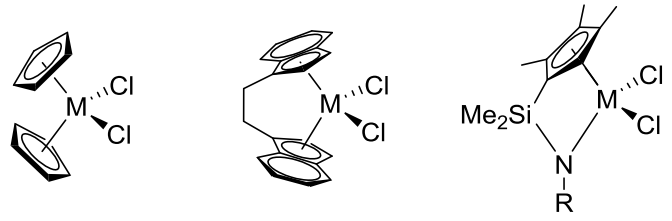

1.1 **1.2** **1.3**

M=Ti, Zr, Hf

Whereas ETM catalysts generally possess high activity for olefin polymerization, their oxophilicity hampers their ability to copolymerize ethylene with polar olefin monomers.[1-3] Copolymerization of ethylene with polar monomers will significantly improve properties such as dye retention, printability, and adhesion.[30-32]

In contrast, late transition metal (LTM) catalysts based on Ni(II) and Pd(II) (Chart 1.2) metals are more tolerant to polar groups and are active for ethylene polymerization, albeit with lower activities. Brookhart was the first one to report a series of α-diimine Ni(II) and Pd(II) complexes (**1.4**)(Chart 1.1).[33-37] Nickel complexes only incorporate methyl acrylate (MA) monomers at the chain ends, while palladium complexes are capable of within chain incorporation. Our group has also contributed to α-diimine LTM catalysis by the synthesis of cyclophane complex **1.5** that it is capable of incorporate high percentages of MA and displays high thermal stability.[38,39]

Complexes based on Pd(II)-ortho-phosphino-arenesulfonate **1.6**, the so called Drent's system, have been successfully shown to copolymerize ethylene with a wide range of polar monomers.[40] To this date only Pd(II)-α-diimine (**1.4**) and Pd(II)-ortho-phosphino-arenesulfonate (**1.6**) have been successfully shown to copolymerize ethylene with a wide range of polar monomers.[33,34,36,37,40-42] A number of research groups have contributed by the design of new catalysts and polymer synthesis.[43-52] While polar monomer incorporation is high in some cases, polymerization activities and molecular weights are low and make these catalysts unfit for industrial scale production. Consequently the search for a catalyst that incorporates polar monomers without sacrificing activity still remains the greatest challenge in olefin polymerization catalysis.

Chart 1.2. Representative LTM catalysts for olefin polymerization and copolymerization.

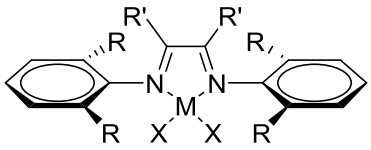

1.4, M = Ni, Pd
X = Br or Me
X= Br and Me

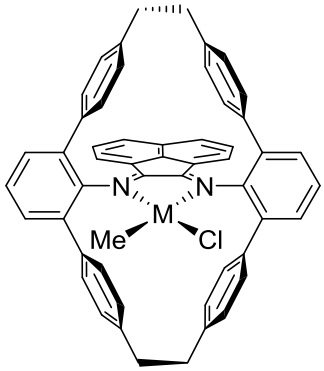

1.5, M = Ni, Pd

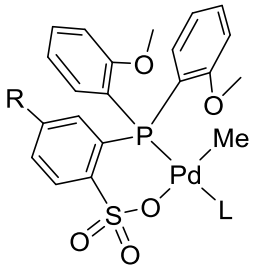

1.6
R = H, Me
L = 1/2 $Me_2NCH_2CH_2NMe_2$,
Pyridin, 2,6-Lutidine, PPh_3,
DMSO

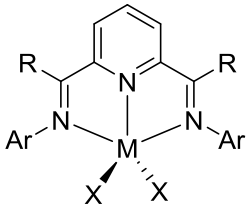

1.7, M = Fe, Co
X = Cl, Br

Catalysts based on middle-late transition metals such as Fe and Co (**1.7**, Chart 1.1) have also been found to display high activity but they are not able to incorporate polar monomers.[53,54] Ruthenium, which is in the same group as Fe and in the same row (i.e., second) as Pd, displays varied chemistry and tolerance to the presence of polar groups in other catalytic reactions.[55-58] Despite its success in other areas of catalysis, there have been very few reports in the last four decades of the use of ruthenium for ethylene polymerization.

1.2 Ruthenium Catalysts for Olefin Polymerization

The first report regarding ruthenium as an olefin polymerization catalyst was published in 1972 by Markham et al.[59] A hydridochlorotirs(triphenylphosphine)ruthenium(II) (**1.8**, Chart 1.3) complex – $HRuCl(PPh_3)_3$ – was capable of homopolymerize ethylene and butadiene in *N*,*N*-dimethylacetamide (DMA) solutions at 50-85 °C. This complex was already studied for homogenous catalytic hydrogenation of 1-alkenes, in addition, it was noticed the continuous consumption of ethylene and butadiene in DMA even in the absence of hydrogen.[60] Markham et al. studied the kinetics of ethylene and butadiene polymerization and found that reaction rates were first order for the catalyst and ethylene, while for butadiene was independent. Polymerization studies were carried out in the absence of cocatalyst which implies that either one of the coordinated phosphines or the chloride atom have to be replaced by the olefin to proceed with hydride insertion into the olefin to continue with polymerization by a coordination-insertion mechanism. Although phosphine displacement by ethylene is a possibility, chloride displacement by ethylene is very unlikely. Markham et al. interpreted that ethylene polymerization mechanism for the active species was analogous to Ziegler ($TiCl_3$) catalysts. However, copolymerization studies were not attempted even though active species seemed to be tolerant to the presence of polar groups since polymerization were carried out in DMA. Molecular weights of the polymers obtained were not measured in this report and no follow up work was published. In 1975 another report on ruthenium for olefin polymerization was published by Ikeda et al.[61] In this case a dihydridotetrakis-(triphenylphosphine) ruthenium(II) complex (**1.9**) –

$Ru(H)_2(PPh_3)_4$ - and other phosphine ligands was employed for the polymerization of ethylene, *α*-olefins, polar α-olefins such as acrylonitrile (AN) or methyl methacrylate (MMA), and copolymerizations of methacrylate (MA) with vinyl monomers in dimethylformamide (DMF). Copolymers were analyzed by elemental analysis to determine fraction of MA. Only polyacrylonitrile molecular weights were determined and resulted in high molecular weights. Activation was also carried out in the absence of cocatalyst. The proposed mechanism implies the displacement of triphenylphosphine by DMF followed by displacement of DMF by AN. The $Ru(H)_2(PPh_3)_3(AN)$ is suggested to proceed with insertion and chain propagation. In both reports, for **1.8** and **1.9**, it is not clear what the active species are and what mechanism is responsible for achieving active species and olefin polymerization. Due to the lack of experimental evidence it is not clear that a coordination insertion mechanism operates in these catalytic systems, but it is more likely that a cationic or anionic mechanism is responsible for the observed activity. Surprisingly, no more reports regarding ruthenium for olefin polymerization have been published in almost three decades.

Nomura in 1999 and 2000 reported a series of $(Pybox)RuX_2(ethylene)$ complexes (**1.10**) that were able to polymerize ethylene when activated by MAO mainly, MMAO, $AlEt_3/Ph_3CB(C_6F_5)_4$, and $AlEt_3/ Ph_3CB(C_6F_5)_4$.[62,63] In their reports they only analyzed a very limited amount of the polymers obtained. Molecular weights reported were very high (208 x 10^4 $kgmol^{-1}$) with a PDI of 2.93. Brookhart in 2000 reported a similar ruthenium complex (**1.11**).[64] Brookhart's complex has very similar ligand framework than Nomura's complex in which an analogous 2,6-diketiminoylpiridine-iron complex was found to be very active for ethylene oligomerization and polymerization.[53,54,65]

Chart 1.3. Early ruthenium (**1.8** and **1.9**), Nomura's (**1.10**), Brookhart's (**1.11**), and Claverie's (**1.12**) complexes.

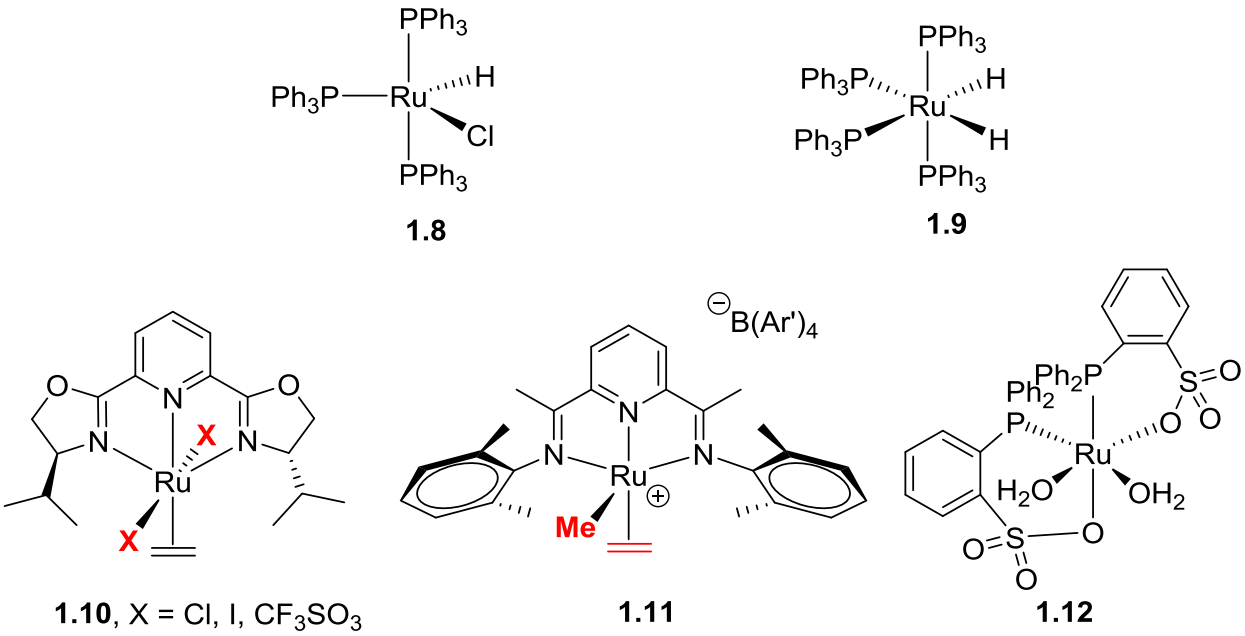

Complex **1.11** is a mono-cationic complex in which it has bound one ethylene and a methyl groups, this complex is in the active form and therefore it could proceed with methyl migration to ethylene. On the contrary, complex **1.11** is stable at room temperature and did not make any polymer under ethylene pressure. To the authors surprise, when complex **1.11** was heated at 70-80 °C and an ethylene pressure of 400 psi in DCM for hours decomposition of the complex was observed without polymer formation. Brookhart et al. observed production of 1-butene even after complex decomposition, which indicates that even oligomers might not be formed by original complex **1.11**. Other non-polar solvents and non-halogenated solvents were also tried giving yield to intractable oil formation but never solid polymer. Copolymerizations of ethylene with carbon monoxide (CO) were also tried without any results. Finally, the most compelling evidence that **1.11** is not active was the NMR studies in which methyl migration to ethylene was not observed, therefore

questioning whether Nomura's complex **1.10** was the catalyst precursor for the observed activity when MAO was used as cocatalyst.

Brookhart et al. attributed the inactivity to the coordination geometry of Ru complex. The distorted square pyramidal coordination of **1.11** results in non-degenerate (non-equivalent sites) coordination sites (Figure 1.1) of olefin and alkyl groups relative to the tridentate ligand, resulting in prohibitively high energetic barrier for migratory insertion. Indeed, a recent computational study calculated that the barriers for migratory insertion of the coordinated olefin into the Ru alkyl bond in **1.10** and **1.11** are larger than 25 kcal·mol^{-1}, too high for olefin insertion polymerization.[66] The authors used density functional theory (DFT) to study Nomura's (**1.10**) and Brookhart's (**1.11**) complexes in order to elucidate if migratory insertion was possible and which are the active species. DFT studies were carried out assuming a Cossee-Arlman coordination-insertion mechanism. As mentioned earlier, the calculated insertion barriers for **1.10** (25.2 kcal·mol^{-1}) and **1.11** (26.0 kcal·mol^{-1}) resulted to be very high and the difference of activation energy between complex **1.10** and **1.11** was found to be less than 1 kcal·mol^{-1} which does not explain the difference in the observed activity. Several oxidation and spin states were also investigated by DFT without any significant reduction in the migratory insertion barrier. Only in the case of quartet dicationic complex the calculated insertion barrier was considerably low (18.2 kcal·mol^{-1}) to achieve more active species. However, the energy to generate such dicationic species was found to be very high, therefore adding this to the activation energy to the insertion barrier will make it impossible to generate any polyethylene. These results suggest that the activity observed by Nomura is likely due to some other species generated by the activation of complex **1.10**. Very recently, Claverie et al.[67] reported a neutral

diaqua-Ru-di(phosphine-arenesulfonato) (**1.12**) complex that surprisingly made crosslinked polyethylene. No mechanistic study was carried out to identify the active species and the process for crosslinking.

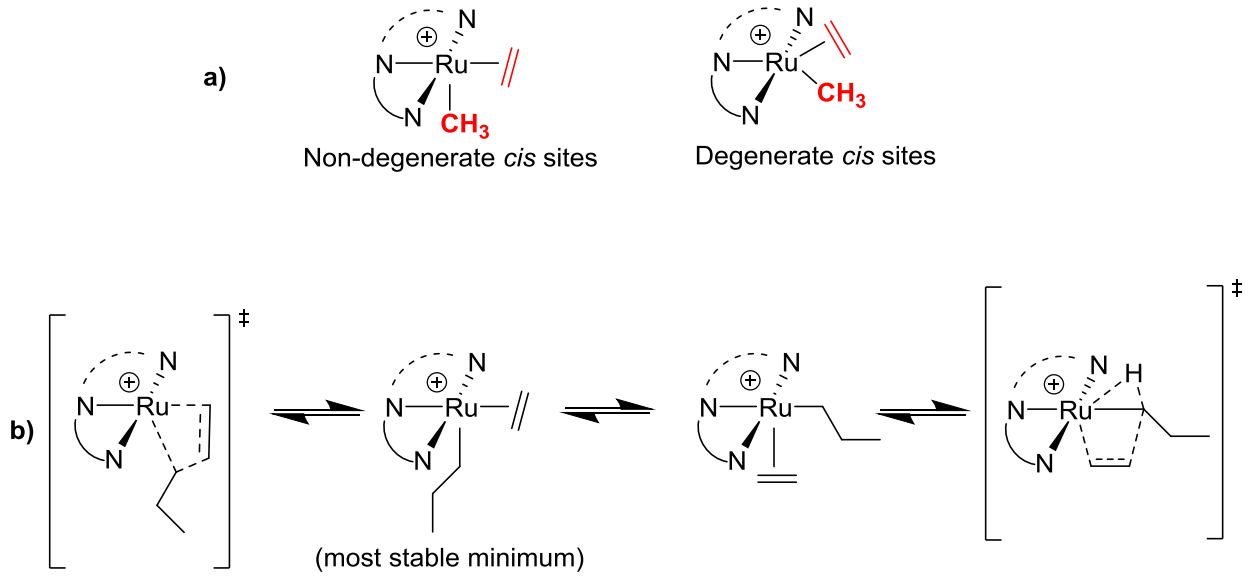

Figure 1.1. a) Non-degenerate (*cis* and *trans* to pyridine) and degenerate *cis* sites. b) The two proposed insertion mechanisms for non-degenerate *cis* and *trans* sites to pyridine.[66]

1.3 Olefin Insertion Evidence by Ruthenium and Piano Stool Complexes of Cobalt, Rhodium for Olefin Polymerization

For all of the aforementioned active Ru complexes, none has unambiguously established the active species responsible for olefin insertion polymerization in the system. Despite the examples above in which migratory insertion has not been fully demonstrated, there are a few examples in which olefin insertion into ruthenium hydride, alkyl, and aryl bonds has been proposed.[68-70] All these complexes are based on piano stool with or without a tethered arm. Chase et al. abstracted a bromide from complex non-tethered complex **1.13**

in the presence of ethylene and afforded styrene-hydride mixture of diastereomers (**1.14a** and **1.14b**) as a result of aryl-ethylene insertion followed by *β*-hydrogen elimination. X-Ray crystallography and NMR indicate that it is certainly a styrene-hydride complex and not a simple agostic interaction of the olefinic styrene protons.[68]

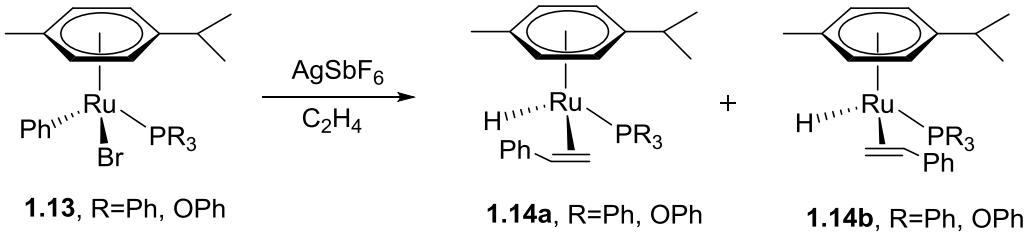

Figure 1.2. Aryl-ethylene migratory insertion reported by Chase et al.[68]

Lee et al. also studied a η^6-arene phosphine tethered ruthenium complex **1.15** by activation with strong boronic acid in the presence of CO, acetylene, ethylene, and norbornene (Scheme 1.1).[69] Reaction in the presence of CO resulted in the formation of stable complex **1.15a** that did not proceed with migratory insertion into CO. On the other hand when activated in the presence of norbornene or acetylene, polymers were obtained. In the case of norbornene polymerization Lee et al. proposed that polynorbornene was obtained by a ROMP mechanism presumably catalyzed by ruthenium. Acetylene polymerization was observed and proposed to occur via coordinative insertion of acetylene into the Ru-alkyl bonds. Another interesting observation under acetylene excess was the detection by NMR and single crystal X-ray crystallography of **1.15b** which is proposed to form through acetylene migratory insertion followed by two consecutive *cis* insertions of acetylene. Polyacetylene in this case is thought to be formed by consecutive *trans* propagations.

Scheme 1.1. Activation and reactivity of **1.15**.

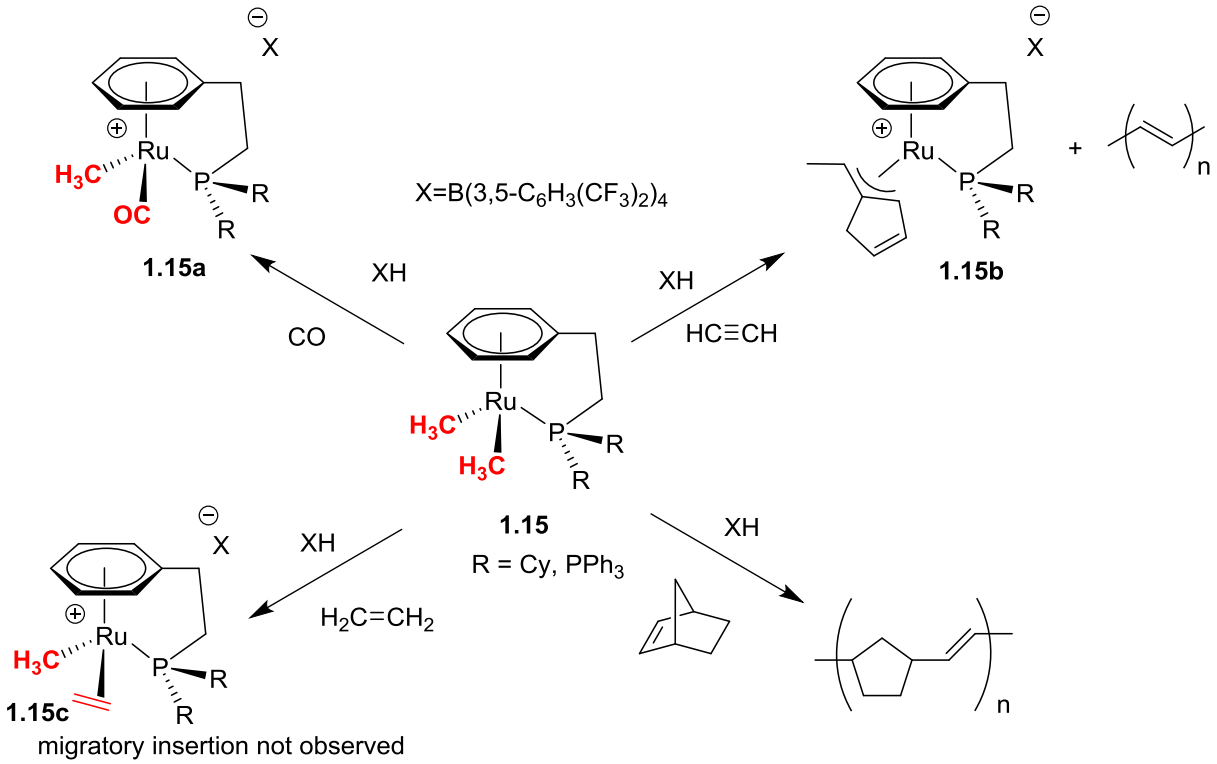

Finally, activation of complex **1.15** in the presence of ethylene was also studied. Ethylene monocationic complex **1.15c** was observed by NMR but ethylene migratory insertion was never observed. On the contrary, complex **1.15c** decomposes in CH_2Cl_2 after 48 hours forming dimeric ruthenium complex **1.15d** (Scheme 1.2). Formation of **1.15d** can be only explained by the reaction of complex **1.15c** with CH_2Cl_2 although authors could not provide any spectroscopy evidence. Other transition metals hydrides have been observed to react with haloalkanes to yield the corresponding metal-halides and reduction of the haloalkane.[71-75] Also radical pathways have been proposed for other organometallic complexes that decompose in the presence of CCl_4.[72,73]

Scheme 1.2. Decomposition pathway proposed for **1.15c**.

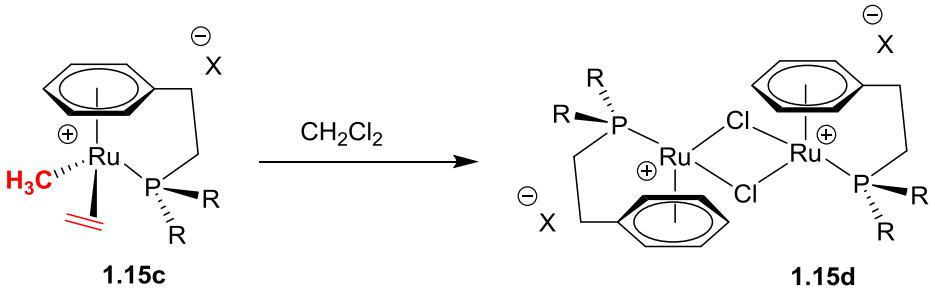

1.15c **1.15d**

R = Cy, Ph_3

X=$B(3,5\text{-}C_6H_3(CF_3)_2)_4$

Further studies were carried out on complex **1.15** by the same group in the presence of ethylene. In this case complex **1.15** was activated with Ph_3CPF_6 in the presence of ethylene. Surprisingly, one proton was abstracted rather than a methyl group, forming complex **1.15e** that by further methyl insertion produces complex **1.15f** forming reversibly complex **1.15g** by β-hydrogen elimination (Scheme 1.3).

Scheme 1.3. Activation and decomposition pathway for **1.15**.

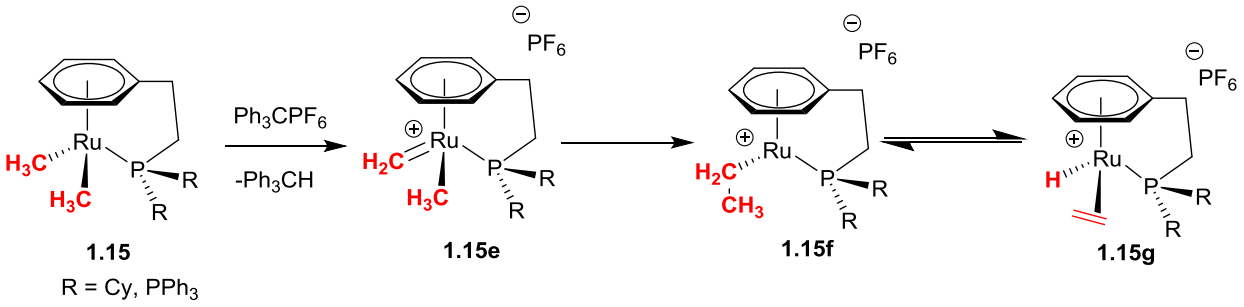

1.15 **1.15e** **1.15f** **1.15g**

R = Cy, PPh_3

All these studies indicate that olefin migratory insertion into Ru-alkyl or Ru-H bonds are possible and that acetylene polymerization is also possible. Despite all these spectroscopic results there is still no clear evidence that ruthenium cationic catalyst can

make polyethylene by a coordination insertion mechanism. The aforementioned ruthenium tethered complexes have the right *cis* geometry for migratory insertion, which it seems to be a necessary condition as proposed by Brookhart et al.[64] On the other hand, formation of the inactive cationic complex **1.15c** indicates that migratory insertion must have a very high energy to occur. Moreover, the observation of reversible hydride insertion of complex **1.15g** indicates that at least hydride migratory insertion is possible. The inactivity of ethylene polymerization of these types of complexes might have an electronic explanation. Olefin migratory insertion is strongly dependent on orbitals overlap.

Migratory insertion is proposed to happen through electron donation from the metal-alkyl bond to the π-antibonding orbital of the coordinated olefin. Early transition metal catalysts are completely oxidized (d^0) and therefore electron deficient. This electron deficiency makes back-donation to olefin π-antibonding orbital very poor and there is no competition for the orbital between metal *d*-orbitals and metal-alkyl bond, making formation of a new carbon-carbon bond possible. This is the reason why early transition metals insertion barriers are minimal or inexistent. On the contrary, late transition metals have higher insertion barriers because they are more electron rich than early transition metals. Late transition metals are more electron rich, since their *d*-orbitals are partially populated (d^8 for Pd(II) and Ni(II)), and participate in the back-bonding to the olefin π-antibonding orbital and therefore competing with the metal-alkyl bond. As a result, late transition metals present a higher migratory insertion barrier. In the case of the ruthenium tethered complexes described above we can infer that ethylene migratory insertion does not happen due to the electron rich nature of these Ru(II) (d^6) complexes. The fact that phosphine is a very good donor ligand also increases electron density in the metal center

and as a consequence back-bonding to the ethylene π-antibonding orbital is enhanced and forbids migratory insertion. Hydride insertion on the other hand seems to be tolerated, this can be explained by the fact that hydride insertion generally requires lower activation barriers,[33,76] but even in this case complete migratory insertion does not happen for ruthenium. One way to prove this hypothesis would be reducing electron density on complex **1.15** and activate it in the same manner to produce a more electron deficient complex. The best manner to make more electron deficient complex would be the substitution of the strong donating phosphine atom by a less donating heteroatom such as oxygen, nitrogen, or sulfur. Unfortunately, there are no reports of such complexes for olefin polymerization. Despite the lack of results, this type of arene-tetherd complexes have structural similarities with the so-called constrained geometry catalysts (CGC).

As described previously, metallocene and half-sandwich complexes of early transition metals show high activity towards ethylene polymerization. These complexes have in common a cyclopentadienyl ligand with functionalized tethered arm with a pendant coordinating hetereoatom making the tethered cyclopentadienyl ligand bidentate in nature. Besides early transition metal, other late transition metals with piano stool geometry of non-tethered and tethered half-metallocene cobalt[77-83] and tethered half-metallocene rhodium[84] have been found to be active for olefin polymerization.

In Chart 1.4 there are depicted several piano stool complexes of Co and Rh that have been tried for olefin polymerization. Cobalt complexes without tethered arm like complex **1.16** display living polymerization with narrow polydispersities and moderate molecular weights.[78-80,83] Cobalt complexes of this type have a phosphine coordinating ligand that does not stop completely ethylene polymerization. This is not the case for the ruthenium

complexes described above (vide supra) in which the phosphine ligand might have a negative effect on activity. Similar complexes with a tethered arm have also been tried, like in the case of complex **1.17** that when it is activated with MMAO (Al/Co 1000) under ethylene pressure (14-800 psi) yields to polyethylene with polydisperties above 2 and moderate to low molecular weights. Complex **1.17** displays greater activity than the non-tethered phosphine complexes described previously. There are significant differences besides possessing a tethered arm; complex **1.17** has a coordination thiol moiety instead of a phosphine. This might be the reason why complex **1.17** has higher activity, since sulfur is a less electron donating atom, and therefore making a more active catalyst. Complex **1.17** was also treated with HBArF in the presence of acetonitrile to afford cationic complex **1.18** that is already in its activated form. When complex **1.18** was exposed to ethylene at high pressures, it produced polyethylene with similar properties to those produced with complex **1.17** although with less activity due to acetonitrile coordination.[77] Surprisingly, complex **1.19** was reported to be significantly less active (only 14 psi polymerizations were tried) than complexes **1.17** and **1.18**. This can be due to differences in strength coordination of the different thioether arm. Also, the nitrogen coordinated complex **1.20** has been found to be active for olefin polymerization but once again much less active than complexes **1.17** and **1.18**.[81]

Also, similar rhodium complexes **1.21** and **1.22** were tested for olefin polymerization.[84] Rhodium, as a second row metal, displayed lower activities as expected. Complex **1.21** gave yield to high molecular weight (reported as Mw; polydispersities were not reported) polyethylene at 1 atm of ethylene and activated by 3000-5000 equivalents of aluminum co-catalyst (MAO) at 30-50 °C. Complex **1.22** was also tested for olefin

polymerization; maximum activation was achieved at 65 °C. Gou et al.[84] proposed that this high temperature might facilitate opening of dimeric species and as a result achieve active species. Complex **1.22** produces polymers with lower molecular weight (reported as Mw; polydispersities were not reported) than complex **1.21**. Surprisingly, activity of complex **1.22** decreases as ethylene pressure is increased 1-4 atm. For all aforementioned cobalt and rhodium complexes, copolymerizations with polar monomers were not reported.

Chart 1.4. Piano stool complexes of Co and Rh for olefin polymerization.

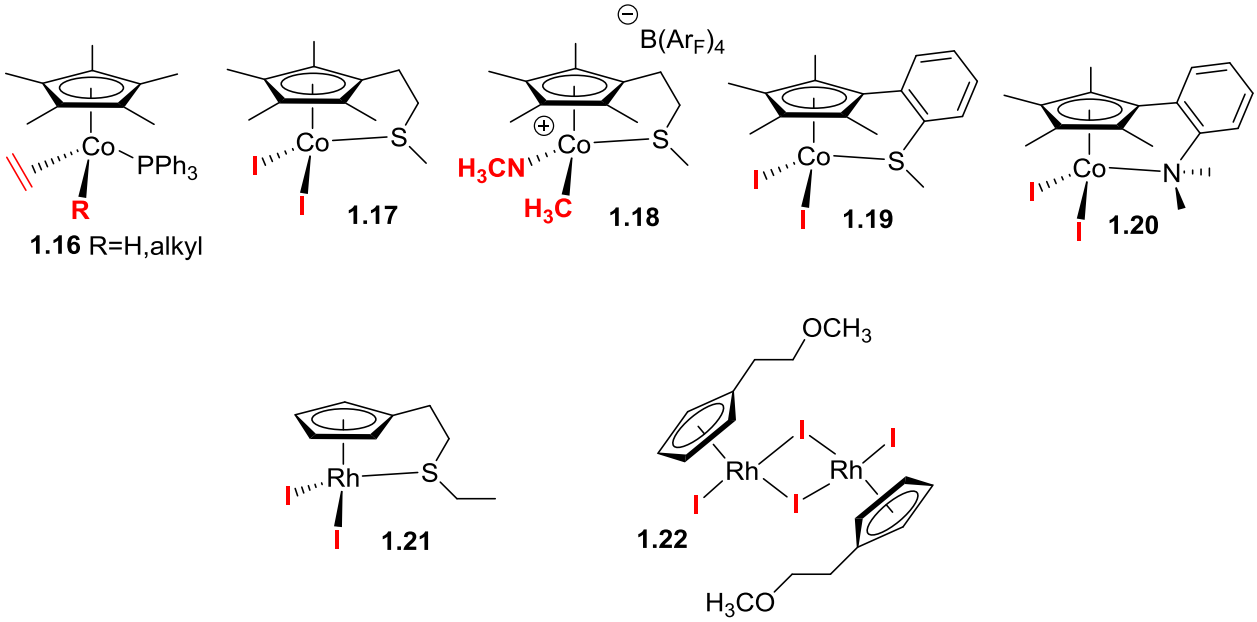

In conclusion, it seems obvious that η^6-arene tethered complexes might be candidates for olefin polymerization since reversible ethylene-hydride migratory insertion has been observed experimentally (**1.15f** ⇔ **1.15g**).[69] Also, structurally similar cobalt and rhodium complexes with sulfur, nitrogen, and oxygen heteroatoms on the tethered arm are capable of catalyzing olefin polymerization.[78-80,83,84] We proposed, that by changing the

heteroatom from phosphine to sulfur, nitrogen, or oxygen on tethered arm of η^6-arene tethered complexes we might obtain active complexes for ethylene polymerization.

1.4 Computational Modeling of Transition Metals for Polymerization Catalysis

Computational chemistry, also called theoretical chemistry or molecular modeling, has become an independent area of research. It is not only a supporting tool to explain experimentally observed results, but also used to predict chemical phenomena by the use of computers and the fundamental laws of physics. Although a great deal of computational resources are required to run calculations, the significant increase in the performance of computer hardware and the development of considerable amount of software packages have made computational chemistry reasonably affordable. Computational chemistry calculations can be divided into two main areas: molecular mechanics and electronic structure theory.[85-88] The main difference is that the first one uses the laws of classical physics to predict the properties of the molecules, and the second one uses the laws of quantum mechanics, which is not a classical physics approach. Molecular mechanics is less expensive than electronic structure methods and very useful for large systems such as proteins and macro-molecules, because it neglects electrons in the calculations. Therefore, it is harder to predict properties for which electronic effects are responsible.

The electronic structure methods use quantum mechanics to predict the physical and chemical properties of the system under study, by solving Schrödinger equation. Schrödinger equation cannot be exactly solved even for small systems therefore it is

impossible to solve for large systems. In order to obtain an approximate solution of the Schrödinger equation, certain mathematical approximations have to be made. The different electronic structure methods are characterized and classified by the approximations used.

Semi-empirical approximations use some parameters that are derived from experimental results and these are added to the theoretical calculations in order to simplify them. *Ab initio* approximations are electronic methods based on the laws of quantum mechanics. The third electronic method is Density Functional Theory (DFT). DFT it is similar to *ab initio* methods but less expensive speaking in computational terms. The main difference between DFT and other electronic structure methods is that DFT does not consider electrons as independent entities but rather a cloud of electron density spatially dependent on the three-dimensional coordinates. The main advantage of DFT is that requires less computational time than other *ab initio* methods and it makes it ideal for large systems and transition metal complexes. DFT also allows for the inclusion of relativistic effects and electron correlation which are essential for most transition metals. At the same time, DFT methods can be further classified depending on the approximations and inclusion of empirical parameters; however, this falls outside the scope of this thesis and we refer the reader to other works that explore DFT methods in-depth.[85-88]

What DFT offers is a reasonable balance between computational cost and the level of accuracy obtained. In addition, DFT is capable of predicting chemical properties that are derived for the electronic structure and therefore makes it ideal for the study of transition metal chemistry. Indeed, DFT has been used for the modeling of various chemical reactions involving transition metals.[89-95] Computational modeling can be used to examine elementary reaction steps of the catalytic cycle, which provides a fundamental

understanding on how the catalytic cycle operates. This knowledge from computational modeling can be used to explain not only the observed chemical properties, but also can be used for rational and engineering design of new catalysts. In the case of olefin polymerization, computational modeling has been used to describe many of the active catalytic systems.[96-98]

The generally accepted Cossee-Arlman mechanism for olefin coordination and migratory insertion is depicted on Scheme 1.4.[99-101] Cossee-Arlman mechanism can be divided into three steps. The first step is activation, in which a catalyst precursor and an activator generate a cationic active catalyst. The second step involves olefin uptake or bonding to the cationic active species, and third step includes migratory insertion of ethylene into the metal-alkyl bond. Olefin bonding to the metal center consists of olefin π-orbital donation to empty d-orbital on the metal and simultaneously back-donation of occupied d-orbitals to the π-antibonding orbital of olefin. In the case of ETM like Ti(IV) and Zr(IV) (d^0 metals) cannot contribute to back-bonding, thus olefin binding consists purely of olefin electron donation to the metal. On the other hand, LTM like Ni(II) and Pd(II) are considered d^8 metals and have d-electrons, therefore allowing LTM to participate in back-bonding. Olefin π-complexation has been calculated for ETM and LTM and values range from 5-45 kcal·mol^{-1} (exothermic) depending on the level of theory used.[102-118] All these results suggest that ethylene coordination is thermodynamically favored for cationic active metal catalysts.

Scheme 1.4. Cosee-Arlman mechanism for chain initiation and propagation.

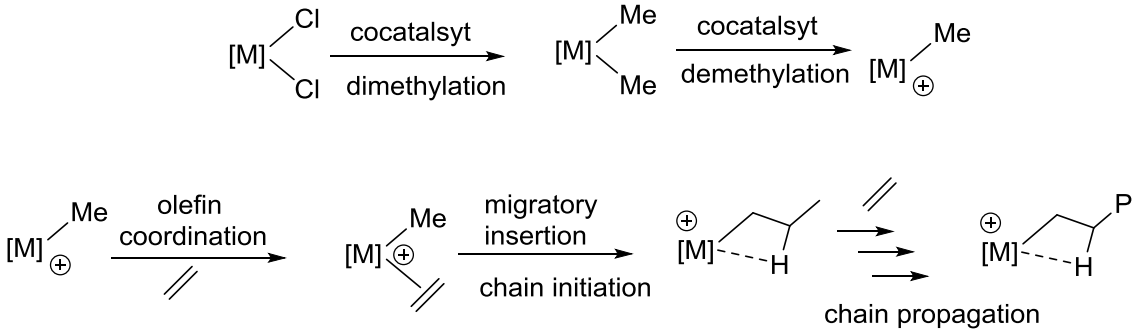

Theoretical results are similar for ETM and LTM which contradict experimental results. In the case of ETM, a greater first-order dependence on olefin concentration has been proposed.[119] For LTM (Ni and Pd) a zeroth-order olefin concentration dependence is proposed.[33,37] The discrepancy between experimental and theoretical results has been attributed to the limitations of electronic methods to accurately reproduce experimental results, or the effect that solvent and counterion can play with ETM and LTM respectively. The active species that are used to measure ethylene uptake are usually consider to be cationic alkyl metal M-CH_3, but this catalyst does not represent a growing polymer species and therefore neglects the effect of polymer chain interaction to the metal, such as β-agostic interaction. Some theoretical calculations with M-C_3H_7 as the active species, result in ethylene uptakes to be ~15 kcal·mol^{-1} higher in energy as a consequence of β-agostic interaction disruption by olefin coordination.[103,105,107,120]

Olefin insertion is the most important step on the mechanism, since it determines chain growth of the polymer. Chain initiation is considered to be migratory insertion of ethylene to a metal-CH_3, but this step is proposed not to be representative of chain growth.

The chain growth, or propagation, is migratory insertion of bounded ethylene to a metal-R bond in which R is a polymer chain. Modeling of a polymer chain attached to the metal center is computationally too expensive and an active cationic metal-C_3H_7 is considered instead to model chain propagation.[107] Migratory insertion is better described by the orbitals interactions that determine the step as depicted in Figure 1.3.

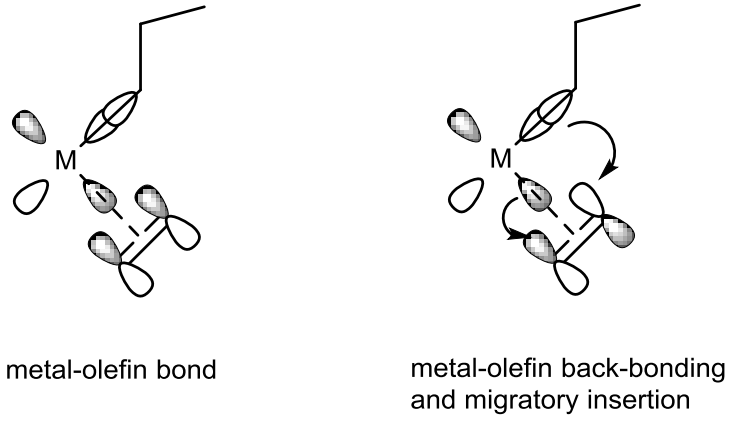

Figure 1.3. Molecar orbitals involved in olefin migratory insertion mechanism.

Molecular modeling is a unique tool that is capable of describing the molecular orbital involved in chemical transformation. Migratory olefin insertion barrier, among other factors, can be rationalized on metal d-electron density. Calculations have shown that ethylene binding to a metal center is through both π-donation into d-orbital on the metal, and back-donation from d-metal orbitals to π-antibonding of the bound ethylene.[76,107,121] This has two effects: first on ethylene free rotation, and second on the insertion barrier. Free rotation of ethylene is hindered if there is back-donation from the d-metal orbital to the π-antibonding orbital of ethylene. Ethylene rotation prior to migratory insertion has

been proposed for d-electron rich metals Ni and Pd, which makes their total insertion barrier higher.[105,107] This combination of π-donation and π-antibonding back-donation makes ethylene-metal bonding more double bond in character, hindering ethylene free rotation which is needed to proceed with insertion. The second effect is directly related to the insertion of the polymer chain. Insertion is proposed to happen through electron donation of the metal-alkyl σ-bond into the π-antibonding orbital of ethylene. If the metal is d^0 there is no back-bonding to this π-antibonding orbital and there is no competition with the metal-alkyl donating bond. If the metal has d-electrons, then some back-bonding to the π-antibonding orbital of ethylene occurs that competes with the metal-alkyl donating bond. This competitive effect raises the insertion barrier. Modeling of ETM with different d-electrons configuration (d^0, d^1, and d^2) resulted in a higher insertion barrier as d-electron count increases. If we consider these factors we should expect lower activity for LTM than the observed. One possible explanation is that for LTM d-orbitals are lower in energy so back-bonding is less pronounced. This might be the reason why Ni and Pd d^8 have reasonable insertion barriers and d^0 ETM very small insertion barriers. Jensen et. al also quantified the effect of back-bonding for LTM.[122] They found that LTM back-bonding increases polar group tolerance favoring ethylene insertion, which is explained by increased back-donation to ethylene. They also found increased insertion barrier energies which again can be attributed to competition between back-bonding of the metal and metal-alkyl bond donation into π-antibonding orbital of ethylene. All these results are in excellent agreement with experimental results in which ETM display greater active than LTM. The experimentally observed insertion barriers are between 0 and 15 kcal·mol^{-1}. Theoretical calculations vary depending on the level of theory used but DFT usually

reproduce experimental results satisfactorily.[33,76,105,107,123]

Besides ethylene coordination and migratory insertion, other interactions between the metal and the polymer chain can occur. Figure 1.4 depicts the general reaction coordinate which is sufficient to understand most olefin polymerization catalytic systems. Chain initiation generates β-agostic structure **A** that is opened by incoming ethylene to from olefin bonded structure **B**. Migratory insertion goes through transition state **C** to form the kinetically favored product of migratory insertion **D** that can be described as a γ-agotic complex. This is generally a weak agostic interaction and it relaxes to the β-agostic final product **F** through transition state **E**. The γ-agostic (**D**) chelate is easily opened by twisting the Cα-Cβ bond and reorganizes to form **E**. From this, another ethylene will coordinate repeating the process of chain propagation.

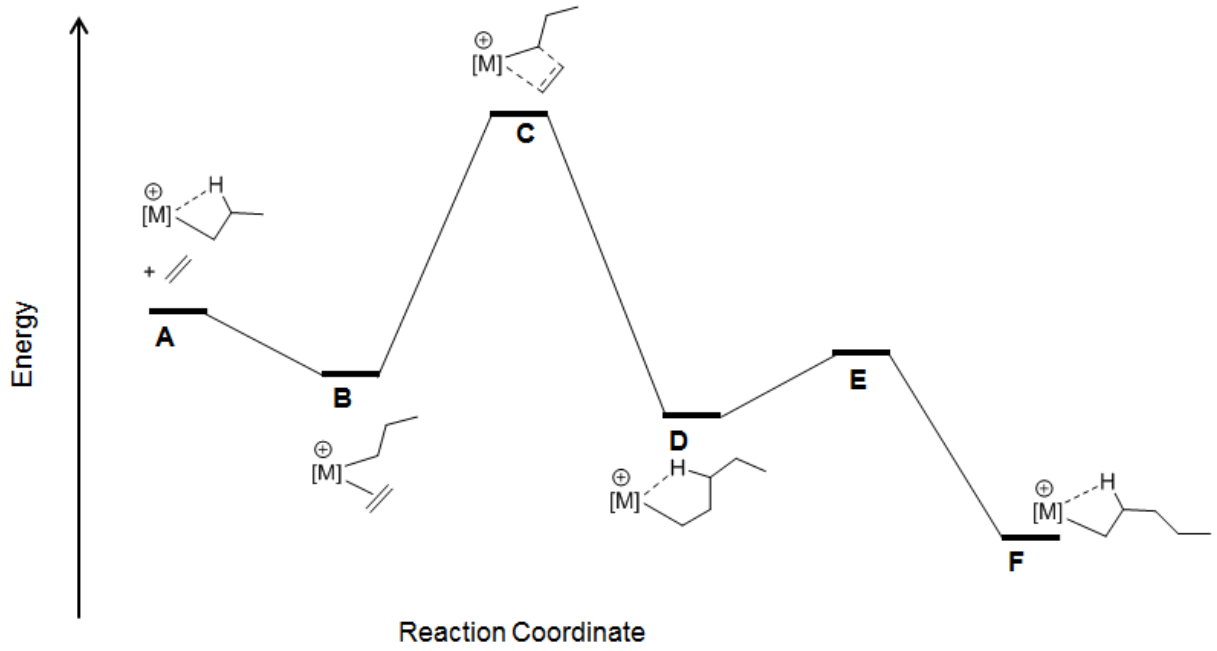

Figure 1.4. Chain propagation potential energy surface and reaction coordinate.

Other aspects such as solvent influence[5,33,107] and counterion effect[107,124,125] have not been study in depth because they are computationally challenging even though they play a significant role in activity and polymer characteristics.[5,33] In general, the great majority of calculations are in the gas phase and considered to be satisfactory to describe the catalytic pathway for olefin polymerization by transition metal catalysts.[107]

1.5 References

(1) *Topics in Organometallic Chemistry*; Springer: Berlin/Heidelberg, 2009; Vol. 29.
(2) *Transition Metal Polymerization Catalysts*; John Wiley & Sons, Inc.: New Yersey, 2009.
(3) *Organometallic Catalysts and Olefin Polymerization*; Springer: Berlin, 2009.
(4) Hustad, P. D. *Science* **2009**, *325*, 704-707.
(5) *Handbook of Transition Metal Polymerization Catalysts*; John Wiley & Sons, Inc.: Hoboken, New Yersey, 2010.
(6) Ziegler, K.; Holzkamp, E.; Breil, H.; Martin, H. *Angew. Chem.* **1955**, *67*, 541-547.
(7) Natta, G.; Pino, P.; Corradini, P.; Danusso, F.; Mantica, E.; Mazzanti, G.; Moraglio, G. *J. Am. Chem. Soc.* **1955**, *77*, 1708-1710.
(8) Kashiwa, N. *J. Polym. Sci., Part A: Polym. Chem.* **2004**, *42*, 1-8.
(9) Karol, F. J. W., B. E.; Levine, I. J.; Goeke, G. L.; Noshay, A. *Advances in Polyolefins*; Plenum: New York, 1987.
(10) Karol, F. K. C., K. J.; Wagner, B. E. *Transition Metals and Organometallics as Catalysts for Olefin Polymerization*; Springer-Verlag: Berlin, 1988.
(11) Kaminsky, W. *J. Chem. Soc., Dalton Trans.* **1998**, 1413-1418.
(12) Scheirs, J.; Kaminsky, W. *Merallocene-based Polyolefins, Preparation, Properties, and Technology*; Wiley, 2000; Vol. 2.
(13) Murad, A. F.; Kleinschroth, J.; Hopf, H. *Angew. Chem. Int. Ed.* **1980**, *19*, 389-390.
(14) Sinn, H.; Kaminsky, W. In *Adv. Organomet. Chem.*; Stone, F. G. A., Robert, W., Eds.; Academic Press: 1980; Vol. Volume 18, p 99-149.
(15) Wild, F. R. W. P.; Zsolnai, L.; Huttner, G.; Brintzinger, H. H. *J. Organomet. Chem.* **1982**, *232*, 233-247.
(16) Kaminsky, W.; Külper, K.; Brintzinger, H. H.; Wild, F. R. W. P. *Angew. Chem. Int. Ed.* **1985**, *24*, 507-508.
(17) Canich, J. A. M.; Exxon Chemical Patents, Inc., USA . 1991, p 30 pp.
(18) Canich, J. A. M.; Exxon Chemical Patents, Inc., USA . 1992, p 26 pp. Cont.-in-part of U.S. 25,055,438.
(19) Canich, J. M.; Hlatky, G. G.; Turner, H. W.; Exxon Chemical Patents, Inc., USA . 1992, p 45 pp.
(20) Canich, J. A. M.; Exxon Chemical Patents Inc., USA . 1996, p 60 pp.
(21) Canich, J. A. M.; Turner, H. W.; Hlatky, G. G.; Exxonmobil Chemical Patents Inc., USA . 2007, p 18pp., Cont.-in-part of U.S. Ser. No. 533,245.
(22) Santos, J. M.; Ribeiro, M. R.; Portela, M. F.; Cramail, H.; Deffieux, A.; Antiñolo, A.; Otero, A.; Prashar, S. *Macromol. Chem. Phys.* **2002**, *203*, 139-145.
(23) Marques, M. M.; Correia, S. G.; Ascenso, J. R.; Ribeiro, A. F. G.; Gomes, P. T.; Dias, A. R.; Foster, P.; Rausch, M. D.; Chien, J. C. W. *J. Polym. Sci., Part A: Polym. Chem.* **1999**, *37*, 2457-2469.
(24) Alt, H. G.; Föttinger, K.; Milius, W. *J. Organomet. Chem.* **1999**, *572*, 21-30.
(25) Alt, H. G.; Reb, A. *J. Mol. Catal. A: Chem.* **2001**, *175*, 43-50.
(26) Alt, H. G.; Reb, A.; Kundu, K. *J. Organomet. Chem.* **2001**, *628*, 211-221.
(27) Alt, H. G.; Reb, A.; Milius, W.; Weis, A. *J. Organomet. Chem.* **2001**, *628*, 169-182.

(28) Carpenetti, D. W.; Kloppenburg, L.; Kupec, J. T.; Petersen, J. L. *Organometallics* **1996**, *15*, 1572-1581.
(29) Ioku, A.; Hasan, T.; Shiono, T.; Ikeda, T. *Macromol. Chem. Phys.* **2002**, *203*, 748-755.
(30) Chung, T. C. *Functionalization of Polyolefins*; Academic Press: London, 2002.
(31) Dong, J.-Y.; Hu, Y. *Coord. Chem. Rev.* **2006**, *250*, 47-65.
(32) Yanjarappa, M. J.; Sivaram, S. *Prog. Polym. Sci.* **2002**, *27*, 1347-1398.
(33) Ittel, S. D.; Johnson, L. K.; Brookhart, M. *Chem. Rev.* **2000**, *100*, 1169-1203.
(34) Svejda, S. A.; Johnson, L. K.; Brookhart, M. *J. Am. Chem. Soc.* **1999**, *121*, 10634-10635.
(35) Mecking, S.; Johnson, L. K.; Wang, L.; Brookhart, M. *J. Am. Chem. Soc.* **1998**, *120*, 888-899.
(36) Johnson, L. K.; Mecking, S.; Brookhart, M. *J. Am. Chem. Soc.* **1996**, *118*, 267-268.
(37) Johnson, L. K.; Killian, C. M.; Brookhart, M. *J. Am. Chem. Soc.* **1995**, *117*, 6414-6415.
(38) Camacho, D. H.; Salo, E. V.; Ziller, J. W.; Guan, Z. *Angew. Chem. Int. Ed.* **2004**, *43*, 1821-1825.
(39) Popeney, C. S.; Camacho, D. H.; Guan, Z. *J. Am. Chem. Soc.* **2007**, *129*, 10062-10063.
(40) Drent, E.; van Dijk, R.; van Ginkel, R.; van Oort, B.; Pugh, R. I. *Chem. Commun.* **2002**, 744-745.
(41) Boffa, L. S.; Novak, B. M. *Chem. Rev.* **2000**, *100*, 1479-1494.
(42) Nakamura, A.; Ito, S.; Nozaki, K. *Chem. Rev.* **2009**, *109*, 5215-5244.
(43) Carrow, B. P.; Nozaki, K. *J. Am. Chem. Soc.* **2012**, *134*, 8802-8805.
(44) Anselment, T. M. J.; Wichmann, C.; Anderson, C. E.; Herdtweck, E.; Rieger, B. *Organometallics* **2011**, *30*, 6602-6611.
(45) Berkefeld, A.; Drexler, M.; Möller, H. M.; Mecking, S. *J. Am. Chem. Soc.* **2009**, *131*, 12613-12622.
(46) Guironnet, D.; Caporaso, L.; Neuwald, B.; Göttker-Schnetmann, I.; Cavallo, L.; Mecking, S. *J. Am. Chem. Soc.* **2010**, *132*, 4418-4426.
(47) Berkefeld, A.; Mecking, S. *Angew. Chem. Int. Ed.* **2008**, *47*, 2538-2542.
(48) Kochi, T.; Noda, S.; Yoshimura, K.; Nozaki, K. *J. Am. Chem. Soc.* **2007**, *129*, 8948-8949.
(49) Luo, S.; Vela, J.; Lief, G. R.; Jordan, R. F. *J. Am. Chem. Soc.* **2007**, *129*, 8946-8947.
(50) Weng, W.; Shen, Z.; Jordan, R. F. *J. Am. Chem. Soc.* **2007**, *129*, 15450-15451.
(51) Wu, F.; Foley, S. R.; Burns, C. T.; Jordan, R. F. *J. Am. Chem. Soc.* **2005**, *127*, 1841-1853.
(52) Leung, D. H.; Ziller, J. W.; Guan, Z. *J. Am. Chem. Soc.* **2008**, *130*, 7538-7539.
(53) Small, B. L.; Brookhart, M.; Bennett, A. M. A. *J. Am. Chem. Soc.* **1998**, *120*, 4049-4050.
(54) Britovsek, G. J. P.; Bruce, M.; Gibson, V. C.; Kimberley, B. S.; Maddox, P. J.; Mastroianni, S.; McTavish, S. J.; Redshaw, C.; Solan, G. A.; Strömberg, S.; White, A. J. P.; Williams, D. J. *J. Am. Chem. Soc.* **1999**, *121*, 8728-8740.
(55) Noyori, R.; Takaya, H. *Acc. Chem. Res.* **1990**, *23*, 345-350.
(56) Grubbs, R. H.; Miller, S. J.; Fu, G. C. *Acc. Chem. Res.* **1995**, *28*, 446-452.
(57) Trnka, T. M.; Grubbs, R. H. *Acc. Chem. Res.* **2001**, *34*, 18-29.
(58) Ueda, J.; Matsuyama, M.; Kamigaito, M.; Sawamoto, M. *Macromolecules* **1998**, *31*, 557-562.
(59) James, B. R.; Markham, L. D. *J. Catal.* **1972**, *27*, 442-451.
(60) Hallman, P. S.; McGarvey, B. R.; Wilkinson, G. *Journal of the Chemical Society A: Inorganic, Physical, Theoretical* **1968**, 3143-3150.
(61) Komiya, S.; Yamamoto, A.; Ikeda, S. *Bull. Chem. Soc. Jpn.* **1975**, *48*, 101-107.
(62) Nomura, K.; Warit, S.; Imanishi, Y. *Macromolecules* **1999**, *32*, 4732-4734.

(63) Nomura, K.; Sidokmai, W.; Imanishi, Y. *Bull. Chem. Soc. Jpn.* **2000**, *73*, 599-605.
(64) Dias, E. L.; Brookhart, M.; White, P. S. *Organometallics* **2000**, *19*, 4995-5004.
(65) J. P. Britovsek, G.; C. Gibson, V.; J. McTavish, S.; A. Solan, G.; J. P. White, A.; J. Williams, D.; J. P. Britovsek, G.; S. Kimberley, B.; J. Maddox, P. *Chem. Commun.* **1998**, 849-850.
(66) Heyndrickx, W.; Occhipinti, G.; Minenkov, Y.; Jensen, V. R. *J. Mol. Catal. A: Chem.* **2010**, *324*, 64-74.
(67) Piche, L.; Daigle, J.-C.; Claverie, J. P. *Chem. Commun.* **2011**, *47*, 7836-7838.
(68) Faller, J. W.; Chase, K. J. *Organometallics* **1995**, *14*, 1592-1600.
(69) Umezawa-Vizzini, K.; Lee, T. R. *Organometallics* **2004**, *23*, 1448-1452.
(70) Foley, N. A.; Lee, J. P.; Ke, Z.; Gunnoe, T. B.; Cundari, T. R. *Acc. Chem. Res.* **2009**, *42*, 585-597.
(71) Booth, B. L.; Haszeldine, R. N. *J. Chem. Soc. A* **1966**, 157-160.
(72) Booth, B. L.; Shaw, B. L. *J. Organomet. Chem.* **1972**, *43*, 369-375.
(73) Carter, W. J.; Kelland, J. W.; Okrasinski, S. J.; Warner, K. E.; Norton, J. R. *Inorg. Chem.* **1982**, *21*, 3955-3960.
(74) Green, M. L. H.; Wong, L.-L. *J. Chem. Soc., Chem. Commun.* **1984**, 1442-1443.
(75) Wache, S. *J. Organomet. Chem.* **1995**, *494*, 235-240.
(76) Margl, P.; Deng, L.; Ziegler, T. *J. Am. Chem. Soc.* **1998**, *120*, 5517-5525.
(77) Daugulis, O.; Brookhart, M.; White, P. S. *Organometallics* **2003**, *22*, 4699-4704.
(78) Cracknell, R. B.; Orpen, A. G.; Spencer, J. L. *J. Chem. Soc., Chem. Commun.* **1984**, 326-328.
(79) Schmidt, G. F.; Brookhart, M. *J. Am. Chem. Soc.* **1985**, *107*, 1443-1444.
(80) Brookhart, M.; Volpe, A. F.; Lincoln, D. M.; Horvath, I. T.; Millar, J. M. *J. Am. Chem. Soc.* **1990**, *112*, 5634-5636.
(81) Enders, M.; Ludwig, G.; Pritzkow, H. *Organometallics* **2001**, *20*, 827-833.
(82) Sujith, S.; Lee, B. Y.; Han, A. W. *Bull. Korean Chem. Soc.* **2007**, *28*, 1299-1304.
(83) Brookhart, M.; DeSimone, J. M.; Grant, B. E.; Tanner, M. J. *Macromolecules* **1995**, *28*, 5378-5380.
(84) Hou, X.-F.; Cheng, Y.-Q.; Wang, X.; Jin, G.-X. *J. Organomet. Chem.* **2005**, *690*, 1855-1860.
(85) Christopher, J. C. *Essential of Computational Chemistry: Theories and Models*; Wiley and Sons, Inc., 2004.
(86) Leach, A. R. *Molecular Modeling: Principles and Apllications*; 2nd ed.; Prentice Hall: Englewood Hills, NJ, 2001.
(87) Jensen, F. *Introduction to Computational Chemistry*; 2nd ed.; Wiley: New York, 2006.
(88) Piela, L. *Ideas of Quantum Chemistry*; Elsevier: New York, 2006.
(89) Ziegler, T.; Autschbach, J. *Chem. Rev.* **2005**, *105*, 2695-2722.
(90) Musaev, D.; Morokuma, K. In *Theoretical Aspects of Transition Metal Catalysis*; Frenking, G., Ed.; Springer Berlin Heidelberg: 2005; Vol. 12, p 1-30.
(91) Sakaki, S. In *Theoretical Aspects of Transition Metal Catalysis*; Frenking, G., Ed.; Springer Berlin Heidelberg: 2005; Vol. 12, p 31-78.
(92) Drudis-Solé, G.; Ujaque, G.; Maseras, F.; Lledós, A. In *Theoretical Aspects of Transition Metal Catalysis*; Frenking, G., Ed.; Springer Berlin Heidelberg: 2005; Vol. 12, p 79-107.
(93) Deubel, D.; Loschen, C.; Frenking, G. In *Theoretical Aspects of Transition Metal*

Catalysis; Frenking, G., Ed.; Springer Berlin Heidelberg: 2005; Vol. 12, p 109-144.
(94) Tobisch, S. In *Theoretical Aspects of Transition Metal Catalysis*; Frenking, G., Ed.; Springer Berlin Heidelberg: 2005; Vol. 12, p 187-218.
(95) Staemmler, V. In *Theoretical Aspects of Transition Metal Catalysis*; Frenking, G., Ed.; Springer Berlin Heidelberg: 2005; Vol. 12, p 219-256.
(96) Angermund, K.; Fink, G.; Jensen, V. R.; Kleinschmidt, R. *Macromol. Rapid Commun.* **2000**, *21*, 91-97.
(97) Angermund, K.; Fink, G.; Jensen, V. R.; Kleinschmidt, R. *Chem. Rev.* **2000**, *100*, 1457-1470.
(98) Michalak, A.; Ziegler, T. In *Theoretical Aspects of Transition Metal Catalysis*; Frenking, G., Ed.; Springer Berlin Heidelberg: 2005; Vol. 12, p 145-186.
(99) Arlman, E. J. *J. Catal.* **1964**, *3*, 89-98.
(100) Cossee, P. *J. Catal.* **1964**, *3*, 80-88.
(101) Arlman, E. J.; Cossee, P. *J. Catal.* **1964**, *3*, 99-104.
(102) Jolly, C. A.; Marynick, D. S. *J. Am. Chem. Soc.* **1989**, *111*, 7968-7974.
(103) Musaev, D. G.; Froese, R. D. J.; Svensson, M.; Morokuma, K. *J. Am. Chem. Soc.* **1997**, *119*, 367-374.
(104) Musaev, D. G.; Svensson, M.; Morokuma, K.; Strömberg, S.; Zetterberg, K.; Siegbahn, P. E. M. *Organometallics* **1997**, *16*, 1933-1945.
(105) Deng, L.; Margl, P.; Ziegler, T. *J. Am. Chem. Soc.* **1997**, *119*, 1094-1100.
(106) A. H. Griffiths, E.; J. P. Britovsek, G.; C. Gibson, V.; R. Gould, I. *Chem. Commun.* **1999**, 1333-1334.
(107) Rappé, A. K.; Skiff, W. M.; Casewit, C. J. *Chem. Rev.* **2000**, *100*, 1435-1456.
(108) Froese, R. D. J.; Musaev, D. G.; Morokuma, K. *Organometallics* **1999**, *18*, 373-379.
(109) Woo, T. K.; Fan, L.; Ziegler, T. *Organometallics* **1994**, *13*, 432-433.
(110) Woo, T. K.; Fan, L.; Ziegler, T. *Organometallics* **1994**, *13*, 2252-2261.
(111) Fujimoto, H.; Yamasaki, T.; Mizutani, H.; Koga, N. *J. Am. Chem. Soc.* **1985**, *107*, 6157-6161.
(112) Kawamura-Kuribayashi, H.; Koga, N.; Morokuma, K. *J. Am. Chem. Soc.* **1992**, *114*, 2359-2366.
(113) Kawamura-Kuribayashi, H.; Koga, N.; Morokuma, K. *J. Am. Chem. Soc.* **1992**, *114*, 8687-8694.
(114) Yoshida, T.; Koga, N.; Morokuma, K. *Organometallics* **1995**, *14*, 746-758.
(115) Jensen, V. R.; Børve, K. J. *Organometallics* **1997**, *16*, 2514-2522.
(116) Bernardi, F.; Bottoni, A.; Miscione, G. P. *Organometallics* **1998**, *17*, 16-24.
(117) Castonguay, L. A.; Rappe, A. K. *J. Am. Chem. Soc.* **1992**, *114*, 5832-5842.
(118) Fusco, R.; Longo, L.; Masi, F.; Garbassi, F. *Macromolecules* **1997**, *30*, 7673-7685.
(119) Yu, Z.; Chien, J. C. W. *J. Polym. Sci., Part A: Polym. Chem.* **1995**, *33*, 125-135.
(120) Deng, L.; Ziegler, T.; Woo, T. K.; Margl, P.; Fan, L. *Organometallics* **1998**, *17*, 3240-3253.
(121) Margl, P.; Deng, L.; Ziegler, T. *Organometallics* **1998**, *17*, 933-946.
(122) Heyndrickx, W.; Occhipinti, G.; Bultinck, P.; Jensen, V. R. *Organometallics* **2012**, *31*, 6022-6031
(123) Deng, L.; Woo, T. K.; Cavallo, L.; Margl, P. M.; Ziegler, T. *J. Am. Chem. Soc.* **1997**, *119*, 6177-6186.
(124) Mason, M. R.; Smith, J. M.; Bott, S. G.; Barron, A. R. *J. Am. Chem. Soc.* **1993**, *115*,

4971-4984.
(125) Harlan, C. J.; Bott, S. G.; Barron, A. R. *J. Am. Chem. Soc.* **1995**, *117*, 6465-6474.

Chapter 2

First Direct Observation of a Cationic Ruthenium Complex for Ethylene Insertion Polymerization

2.1 Introduction

Polyolefin industry continues to grow steadily because of continuous discoveries of new catalysts, processes, and polyolefin materials with new properties. While early transition metal catalysts generally have high activity for olefin polymerization, their oxophilicity has largely prevented them from incorporation of polar olefins.[1,2] During the last two decades, significant advances have been made in the development of late-transition-metal polymerization catalysts. A few notable examples include the Ni(II)- and Pd(II)-α-diimine systems discovered by Brookhart and coworkers[3-5] and the Pd(II)-ortho-phosphino-arenesulfonate system initially introduced by Drent and coworkers.[6] Excitingly, some of the late transition metal catalysts are able to copolymerize functional olefins such as methyl acrylate (MA).[4,6-11] Following these pioneering studies, a number of groups have made important contributions to this area both in new catalyst design and new polymer synthesis.[10,12-23] Despite their promising attributes, late transition metal catalysts are generally less active than early transition metal catalysts, warranting the search of other transition metal complexes for olefin polymerization.

An ideal catalyst system should combine the functional group tolerance of late

transition metals with the high activities of early transition metals. Group 8 metals, located right in the center of the transition metal block in the periodic table, may offer a possibility to combine such good attributes. Particularly, ruthenium complexes have proven to be very versatile in various types of catalytic reactions and show excellent functional group tolerance.[24-27] Although best known for metathesis polymerization,[26] ruthenium has also been sporadically investigated for olefin insertion polymerization.[28-32] In early 1970's, hydridoruthenium species – $HRuCl(PPh_3)_3$ or $(H)_2Ru(PPh_3)_4$ – were reported for insertion polymerization of ethylene or polar olefins.[28,29] In addition, there are reports of ethylene-arene and hydride-olefin inserions by Ru(II) complexes although no olefin polymerization or chain growth has been reported.[33-35] Later, Nomura et al.[30,31] reported a ruthenium-pybox complex (**2.1**) (Chart 2.1), which in combination with MAO could polymerize ethylene. However, in a detailed study by Brookhart and coworkers,[32] a similar Ru-diiminopyridine complex (**2.2**) was shown to be completely inactive despite the fact that the analogous Fe(II)-diiminopyridine complexes show excellent activity toward ethylene insertion polymerization.[36,37] The authors attributed the inactivity to the coordination geometry of Ru complex. The distorted square pyramidal coordination of the Ru complex **2.2** results in non-degenerate coordination sites of olefin and alkyl groups relative to the tridentate ligand, resulting in prohibitively high energetic barrier for migratory insertion. Indeed, a recent computational study calculated that the barriers for migratory insertion of the coordinated olefin into the Ru alkyl bond in **2.1** and **2.2** are larger than 25 kcal/mol, too high for olefin insertion polymerization.[38] Very recently, Claverie et al.[39] reported a Ru-di(phosphine-arenesulfonato) complex that surprisingly made cross-linked polyethylene. Notably, for all of the aforementioned active Ru

complexes, none has unambiguously established the active species responsible for olefin insertion polymerization in the system.

Chart 2.1 Nomura's (**2.1**), Brookhart's (**2.2**), and our proposed complex **2.3**

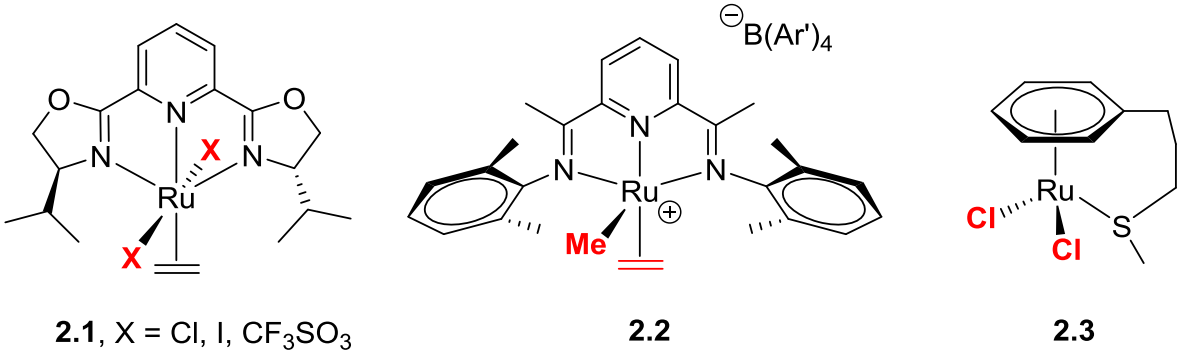

2.1, X = Cl, I, CF_3SO_3 **2.2** **2.3**

On the basis of these previous studies, we hypothesize that it would be possible to achieve active Ru(II) complexes for insertion polymerization if they are designed in such a manner that the alkyl and olefin occupy equivalent coordination sites in *cis* geometry for the active intermediates. To test this hypothesis, herein we designed a Ru(II) η^6–arene complex containing a tethered sulfur ligand (**2.3**) (Chart 2.1). Complex **2.3** adopts a "piano stool" type of coordination geometry, which upon activation should generate two equivalent coordination sites for active migratory insertion. An analogous dialkylruthenium(II) η^6–arene complex with a tethered phosphine ligand was reported previously, which was inactive for ethylene polymerization.[40,41]

2.2 Synthesis, Characterization, and Polymerization Results

Complex **2.3** was synthesized by following a similar procedure reported in literature

for other tethered Ru(II) η^6–arene complexes.[42] First, methyl 3-phenylpropyl sulfide (**2.3a**) was prepared with a literature procedure[43] followed by Birch reduction[44] to afford the ligand **2.3b**. For complexation, $RuCl_3$(hydrate) and **2.3b** were heated to reflux in ethanol to form **2.3** as an air stable orange powder (Scheme 2.1). Complex **2.3** was fully characterized by $^1H/^{13}C$ NMR including COSY and NOE experiments, electrospray ionization mass spectrometry (ESI-MS), elemental analysis, and single crystal X-Ray crystallography.

Scheme 2.1. Synthesis of complex **2.3**.

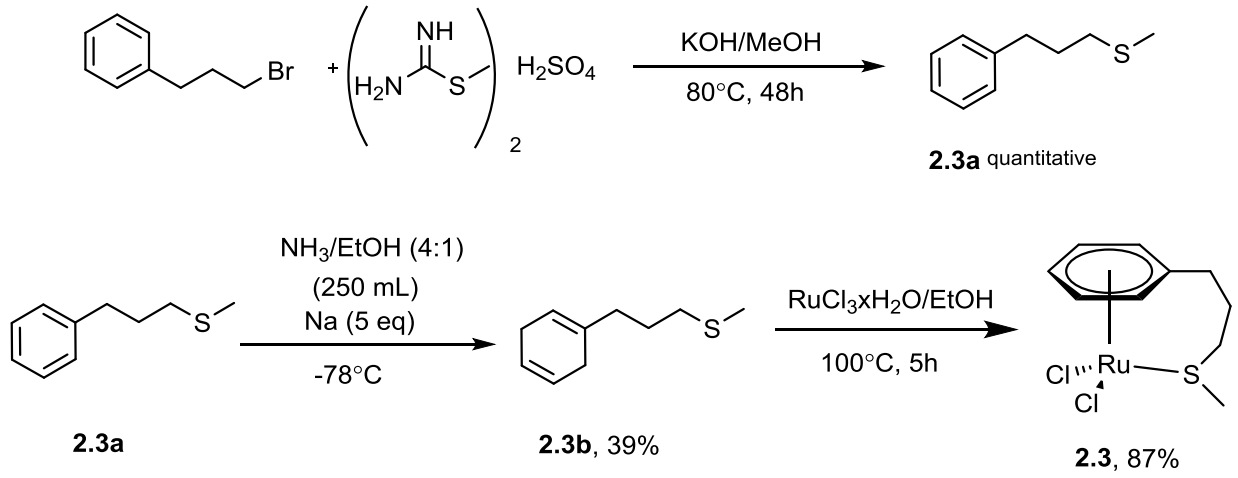

Single crystal of complex **2.3** suitable for X-ray diffraction was obtained by slow diffusion of hexanes into a saturated solution of **2.3** in dichloromethane (DCM) at 4 ºC. The X-ray structure of **2.3** in ORTEP is shown in Figure 2.1. Due to chirality on the sulfur atom, complex **2.3** exists as a mixture of two enantiomers as can be seen in the unit cell (Figure 2.2). X-ray confirms a three-legged half-sandwich (piano stool) in which the sulfur is coordinated with ruthenium to form an 18 electron complex. Sulfur atom is in a

pseudo-tetrahedral conformation with a non-bonding pair of electrons occupying one coordination site. Ruthenium metal center is centered below the arene moiety. The tethered chain is coordinated to the metal in a zigzag fashion. The bond length of Ru-S is 2.367 Å which is slightly shorter than for Ru-Cl(1) 2.403 Å, or Ru-Cl(2) 2.423 Å, due to the difference in size between chlorine and sulfur atoms. The arene moiety is not tilted; the arene carbon-ruthenium distances are all very similar ranging from 2.173 to 2.207 Å. The Cl(1)-Ru(1)-Cl(2) biting angle is 86.88°.

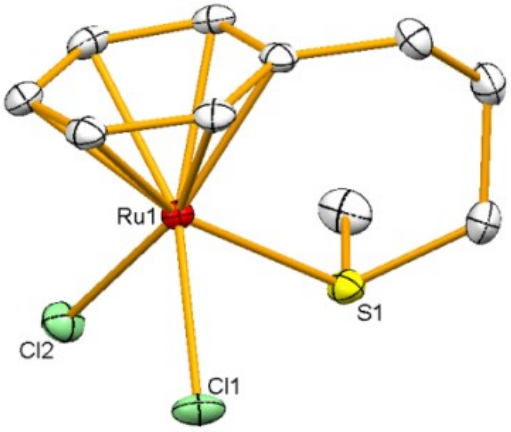

Figure 2.1. X-Ray crystal structure of complex **2.3**. ORTEP drawing, ellipsoids at 60% probability radius, hydrogens omitted for clarity. Selected interatomic distances (Å) and angles (deg): Cl(1)-Ru(1)=2.4032(1), Cl(2)-Ru(1)=2.4228(1), S(1)-Ru(1)=2.3670(1), Cl(1)-Ru(1)-Cl(2)=86.88(0).

Complex **2.3** was also characterized by NMR. Complex **2.3** displays poor solubility, being DCM the best choice for NMR studies since more polar solvents such as DMSO might coordinate and displace the S-Me moiety. Room temperature ^{1}H NMR displays very broad peaks due to slow interconversion between the two isomers (A and B, Figure 2.2) characterized by X-ray diffraction. In order to characterize the complex by ^{1}H NMR variable

temperature experiments were carried out as depicted in Figure 2.3. The sulfide arm remains coordinated to ruthenium in solution as evidenced by the diastereotopic arene and tethered arm protons observed in ^1H NMR spectra. When a CD_2Cl_2 solution of complex **3** is heated at 323 K peaks are still broad but allows for protons assignment. When temperature is lowered to 203 K almost all protons can be assigned unambiguously by HMQC/COSY-NMR, except for the tethered arm protons due to signals overlap (Figure 2.3). At higher temperatures (233-293 K) the slow interconversion between isomers broadens most proton signals except for protons "g" and "a" whose shifts are not affected by inversion at sulfur. At 203 K there is only one isomer present and COSY and NOESY NMR allow to assign aromatic protons relatively to S-Me proton (Figures 2.4 and 2.5).

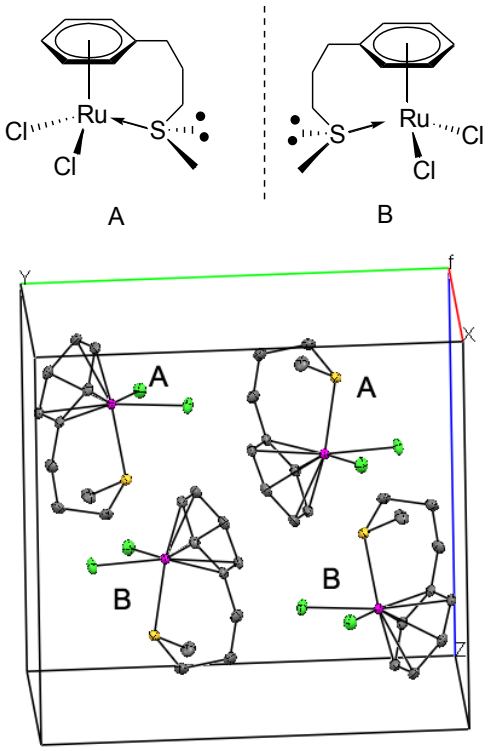

Figure 2.2. Unit cell for $RuCl_2(Ph(CH_3)_3SCH_3)$ **(2.3)** showing two different isomers A and B. Hydrogens are omitted for clarity.

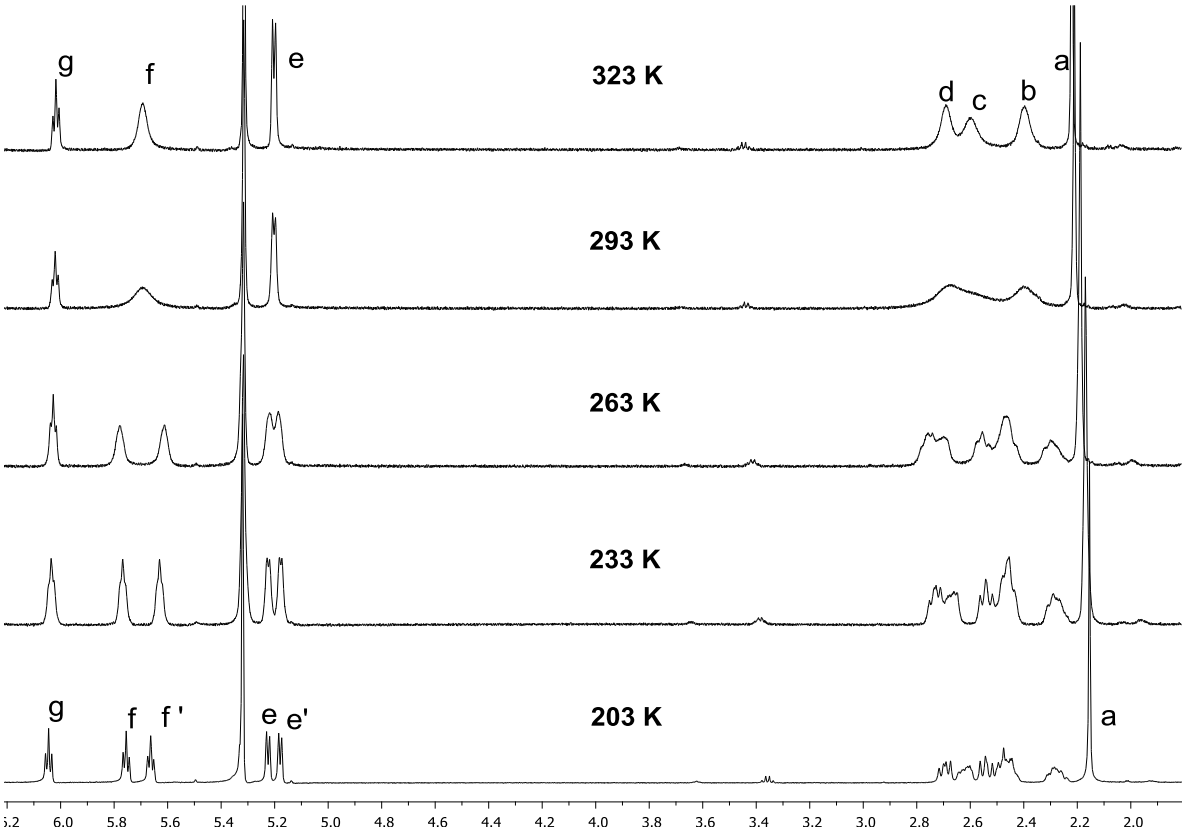

Figure 2.3. Variable temperature ^{1}H-NMR spectrum for complex **2.3** at different temperatures in CD_2Cl_2. Coalescence of peaks "f" and "f'" is used for sulfur inversion barrier calculation.

On the basis of variable temperature ^{1}H NMR data in Figure 2.3, the inversion barrier on sulfur was estimated to be 14.4±0.1 kcal·mol^{-1}, which is close to the inversion barrier for a tetramethylcyclopentadienyl-S-tethered cobalt complex reported previously.[45] Inversion Barrier was calculated from NMR by using the equations 1 and 2. Coalescence of "f" peak was used ($\Delta\nu = 50Hz$) and T_c=293 K to calculate the inversion barrier.

$$k_c = \frac{\pi\Delta\nu}{\sqrt{2}} \cong 2.22\Delta\nu \quad rate\ constant\ at\ coalescence\ \Delta\nu(Hz) \qquad (1)$$

$$\Delta G_c^{\neq} = RT\left[23.76 - \ln\left(\frac{k_c}{T_c}\right)\right] \quad \Delta G_c^{\neq}\ at\ coalescence\ T_c = 293\ K \qquad (2)$$

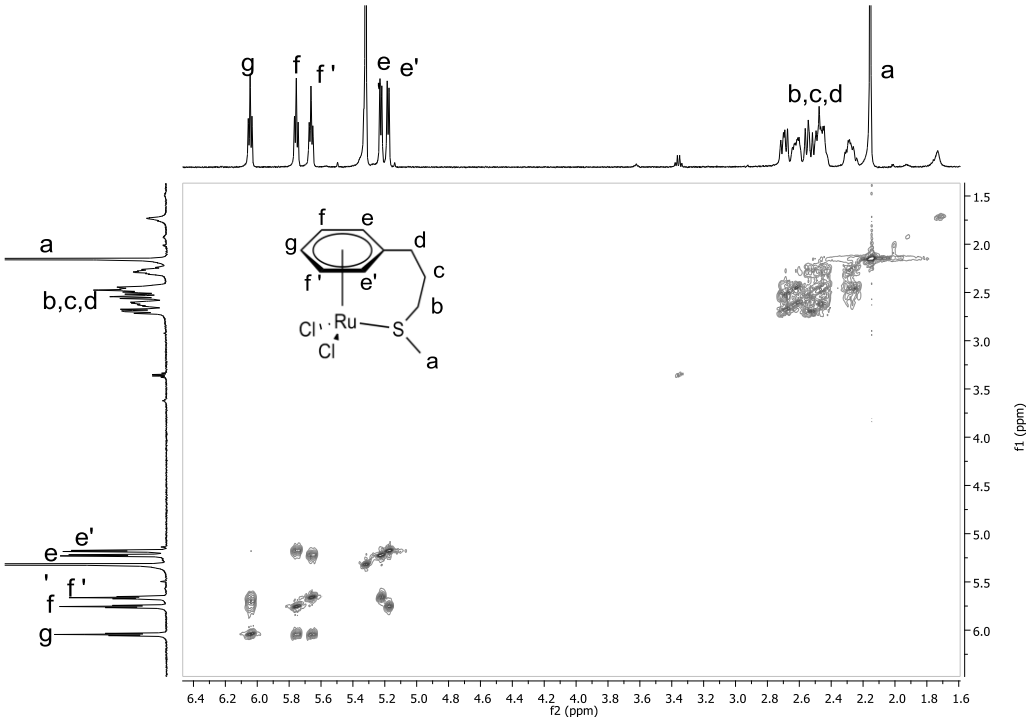

Figure 2.4. Complex **2.3** COSY-NMR at 203K in CD_2Cl_2.

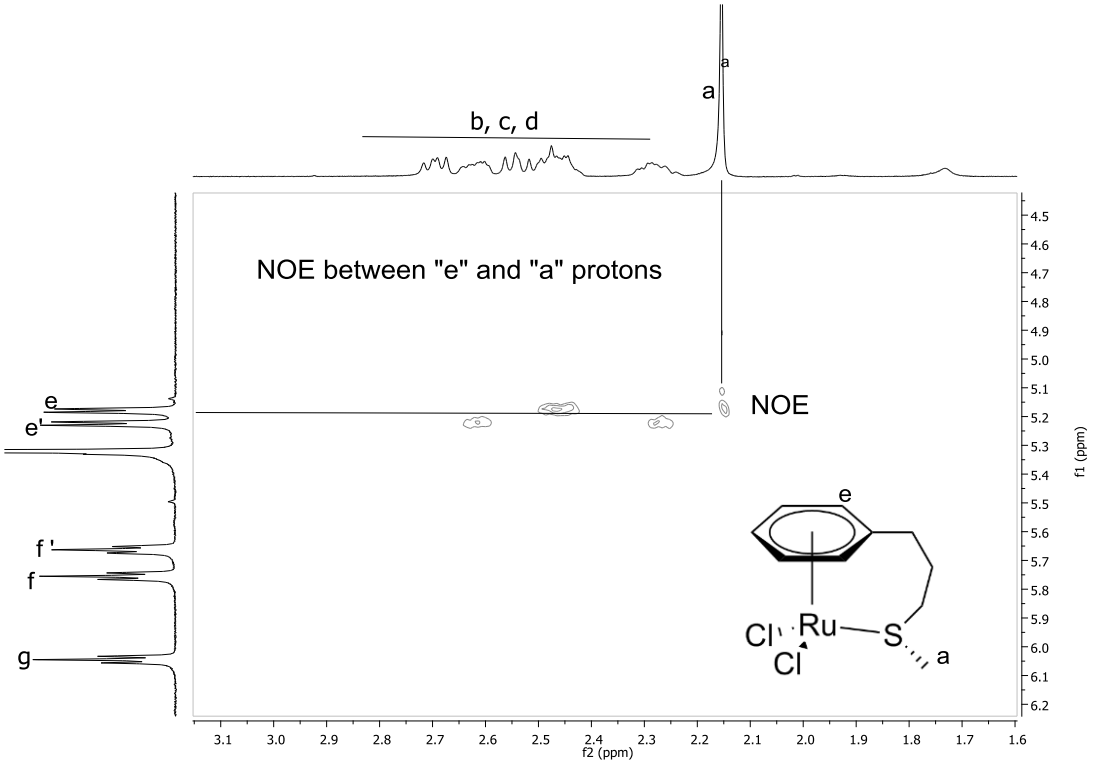

Figure 2.5. Complex **2.3** NOESY-NMR at 203 K in CD_2Cl_2.

Complex **2.3** was tested for ethylene polymerization using different alkyl-aluminum cocatalysts ($AlMe_3$ and MAO) with no activity. Encouragingly, when $AlMe_2Cl$ was used as the coctalyst (Table 2.1) for activation complex 3 exhibited moderate activity for producing high molecular weight (Mn> $2x10^5$ g/mol) linear polyethylene. The polymerization result is reproducible (entries 1 and 2 in Table 2.1). Increasing ethylene pressure resulted in an increase in molecular weight and a decrease in branching density (entry 3). The polyethylene samples obtained are semicrystalline with melting temperature (Tm) around 130 °C. Gel permeation chromatography (GPC) reveals bimodal molecular weight distribution with a high molecular weight fraction (Mn > $2 \cdot 10^5$ g/mol) and a significantly lower molecular weight fraction (Mn ~ 600-850 g/mol), suggesting the presence of two different active species. As a negative control, a blank polymerization with only $AlMe_2Cl$ cocatalyst did not produce any polyethylene (entry 4), indicating that the ruthenium complex is critical for the active polymerization.

Although polymerization results with complex **2.3** were successful, mechanistic studies of active species with **2.3** are not trivial due to the large excess of cocatalyst ($AlMe_2Cl$) needed. One method to study active species is the use of methylated complexes that can be activated by the use of one equivalent of a strong Brønsted-Lowry acid in the presence of ethylene to generate active catalyst resting states. To further probe the active species for the polymerization, we synthesized a dimethylated complex **2.4** via direct methylation of **2.3** with MeLi (Scheme 2.2).

Table 2.1. Ethylene polymerization results.[a]

Entry	Cat	Co-cat	Yield (mg)	Time[b] (h)	Press[c] (psi)	M_n[d] (10^{-5})	PDI[e]	T_m (°C)[f]	Branch.[g]	Act[h]
1[i]	**2.3**	$AlMe_2Cl$	15	4	400	1.98	2.03	129	18	625
2[i]	**2.3**	$AlMe_2Cl$	17	4	400	2.14	3.01	130	20	708
3[i]	**2.3**	$AlMe_2Cl$	93	12	800	2.62	3.03	131	8	1292
4	-	$AlMe_2Cl$	0	4	400	n/a	n/a	n/a	n/a	0
5[k]	**2.4**	HBArF[m]	28	12	400	610[l]	1.19	61	36	42
6[k]	**2.4**	HBArF[m]	55	12	800	656[l]	1.23	75	27	83
7[k]	**2.4**	HBArF[m]	51	12	800	657[l]	1.17	69	26	77
8	-	HBArF[m]	0	12	800	n/a	n/a	n/a	n/a	0

[a]General conditions: all polymerizations run in a 600 mL Parr reactor with 100 mL of dichloromethane (DCM) as the solvent. Temperature was kept 45-50 °C. [b]Hours. [c]Ethylene pressure. [d]Determine by GPC in 1,2,4-trichlorobenzene vs polyethylene standards. [e]PDI=Mw/Mn. [f]Determine by DSC in ºC. [g]Determined by 1H-NMR and expressed as the number of Me's per 1000 carbons. [h]Activity (gPE/mol of catalyst per hour).[i]6 µmol of complex **3** and 1000 equivalents of $AlMe_2Cl$ (1.0M solution in hexanes) as cocatalyst. [k]55 µmol of complex **4** and $([H(Et2O)2]^+ [BAr'4]^-)$ (1 eq) as cocatalyst. [l]Mn in g/mol. [m]HBArF = $([H(Et_2O)_2]^+ [BAr'_4]^-)$ Entries 4 and 8 are negative control polymerizations with only $AlMe_2Cl$ and HBAeF respectively.

Scheme 2.2. Synthesis of complex **2.4**

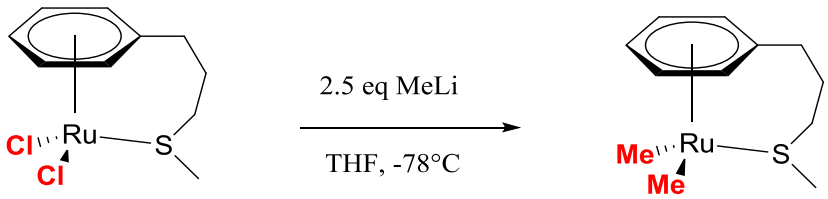

2.3 **2.4**, y 20%

Complex **2.4** was fully characterized single crystal X-ray crystallography and NMR. Single crystal of complex **2.4** suitable for X-ray diffraction was obtained by slow

evaporation of a pentanes solution at room temperature inside a glove box. The X-ray structure of **2.4** in ORTEP is shown in Figure 2.6. Similarly to **2.3**, complex **2.4** also exists as a mixture of two enantiomers in the unit cell confirmed by single crystal X-ray diffraction (Figure 2.7). Coordination around the ruthenium metal in complex **2.4** is analogous to complex **2.3**. The bond length of Ru-S is 2.319 Å slightly shorter than for dichloride complex **2.3**. Ruthenium-carbon methyl bond distances (Ru-C(12) 2.204 Å and Ru-C(11) 2.141 Å) are shorter than Ru-Cl due to chlorides being larger compared to methyl groups. The bond distance in Ru-C(12) is larger than Ru-C(11) by 0.063 Å due to sterics of the S-Methyl group that is on the same side of C(12). The arene carbon-ruthenium distances are all very similar ranging from 2.200 to 2.253 Å and are slightly larger than for complex **2.3**. The Cl(12)-Ru(1)-Cl(11) bite angle is 81.97°, significantly smaller than for Cl(1)-Ru-Cl(2) (86.88°) complex **2.3**, this is due once again to chlorides larger size.

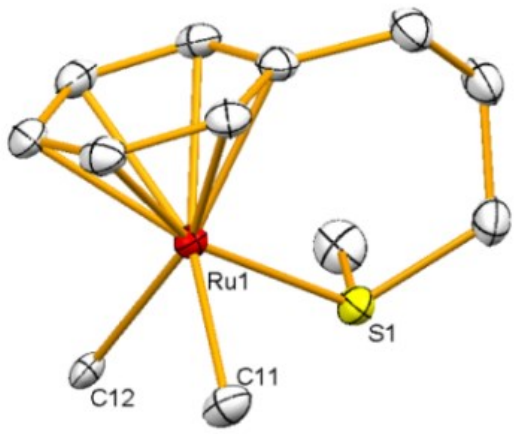

Figure 2.6. X-Ray crystal structure of **2.4**. ORTEP drawing, ellipsoids at 60% probability radius, hydrogens omitted for clarity. Selected interatomic distances (Å) and angles (°): C(12)-Ru(1)=2.204(1), S(1)-Ru(1)=2.3187(4), C(11)-Ru(1)=2.141(2).

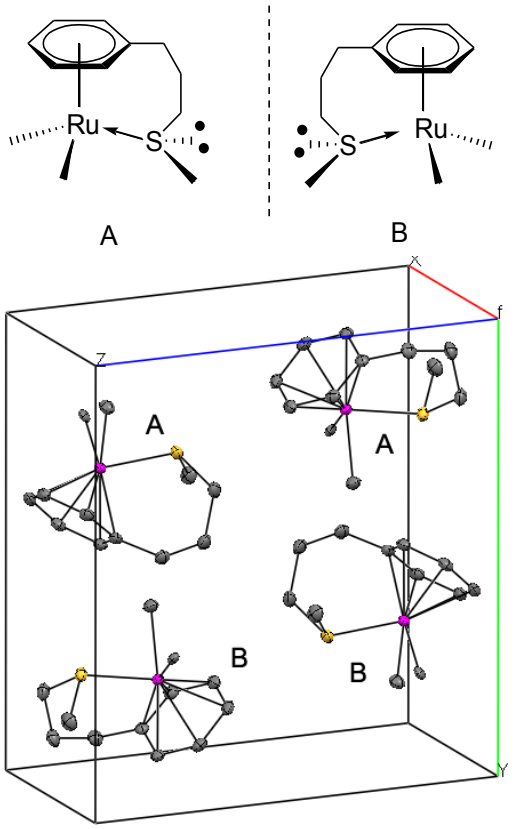

Figure 2.7. Unit cell for $Ru(CH_3)_2(Ph(CH_3)_3SCH_3)$ **(2.4)** showing two different stereoisomers A and B. Hydrogens omitted for clarity.

Also, for complex **2.4** the sulfide arm remains coordinated to ruthenium in solution as evidenced once again by the diastereotopic arene and tethered arm protons and carbons in $^{1}H/^{13}C$-NMR spectra al low temperature (Figure 2.8 and 2.9). Low temperature ^{1}H, ^{13}C, NOE, and 2D-NMR were necessary to completely assigned all proton and carbon signals for complex **2.4** in solution (Figures 2.8-2.13). Inversion barrier at sulfur can also be calculated for this complex using equations (1) and (2). Coalescence of methyl peaks at 298 K were used to determine an inversion barrier in sulfur that was calculated to be 14.6±0.1 $kcal \cdot mol^{-1}$, almost identical to complex **2.3** inversion barrier.

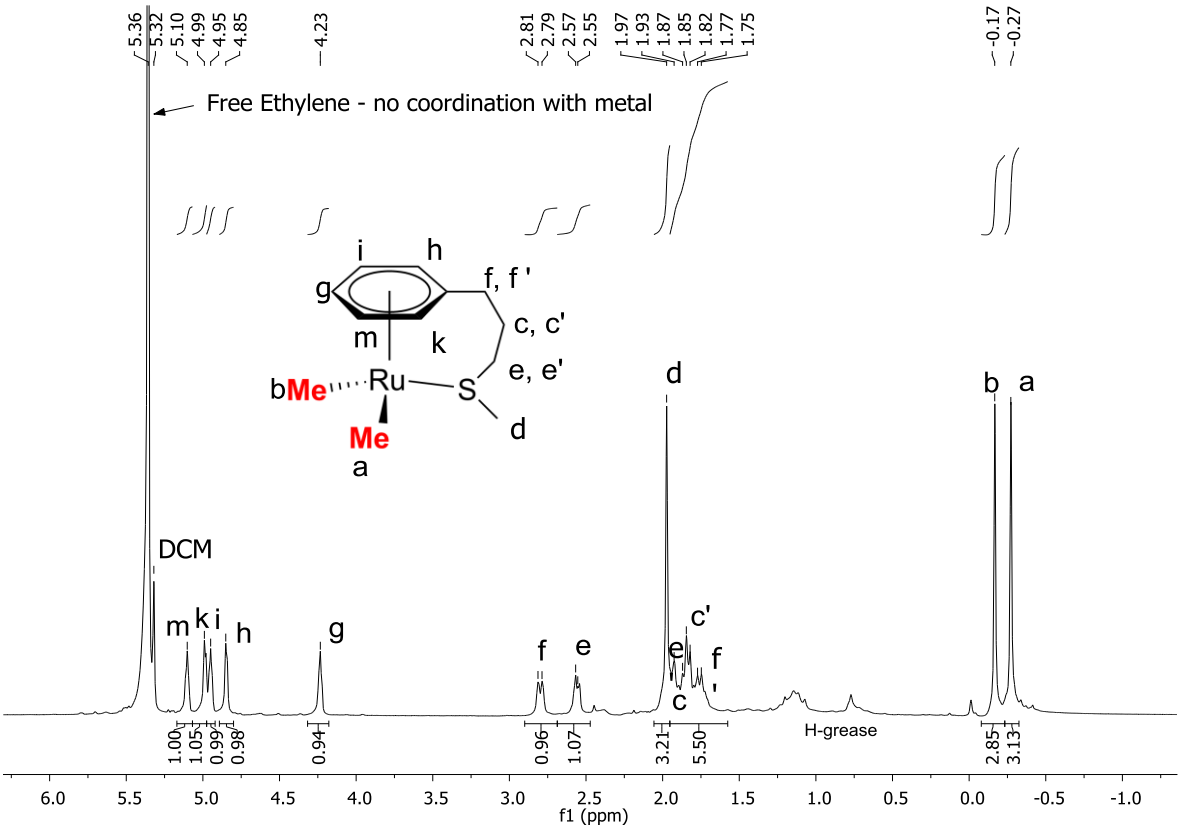

Figure 2.8. ^{1}H-NMR spectrum of complex **2.4** at 183 K in CD_2Cl_2.

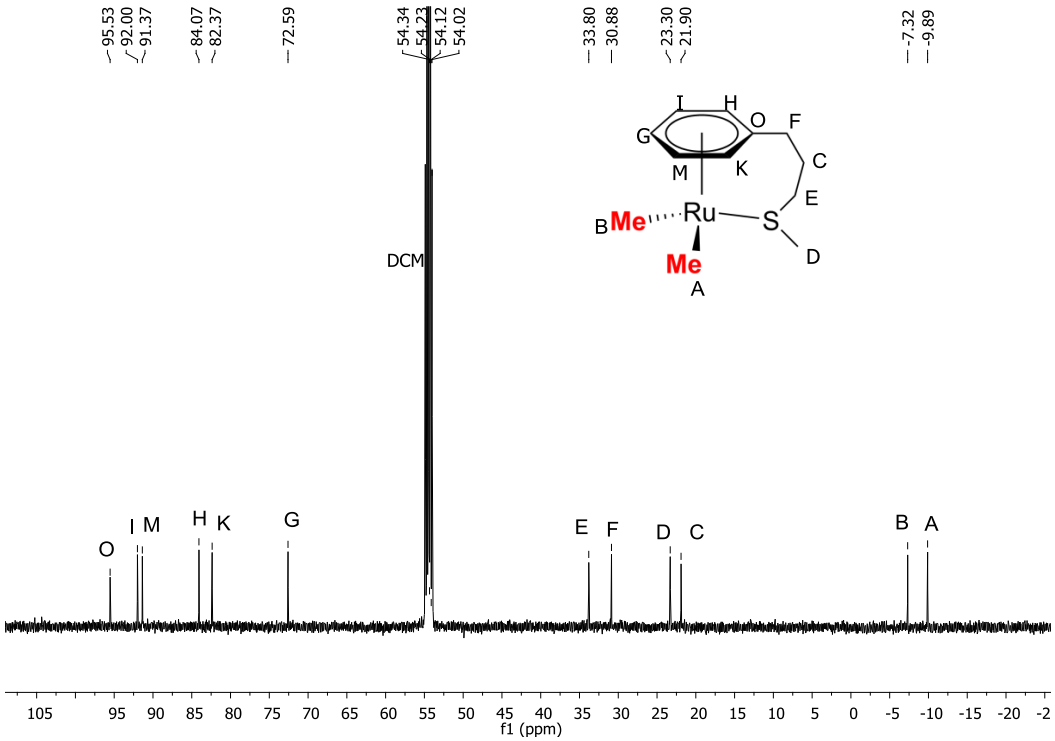

Figure 2.9. ^{13}C-NMR spectrum of complex **2.4** at 183 K in CD_2Cl_2.

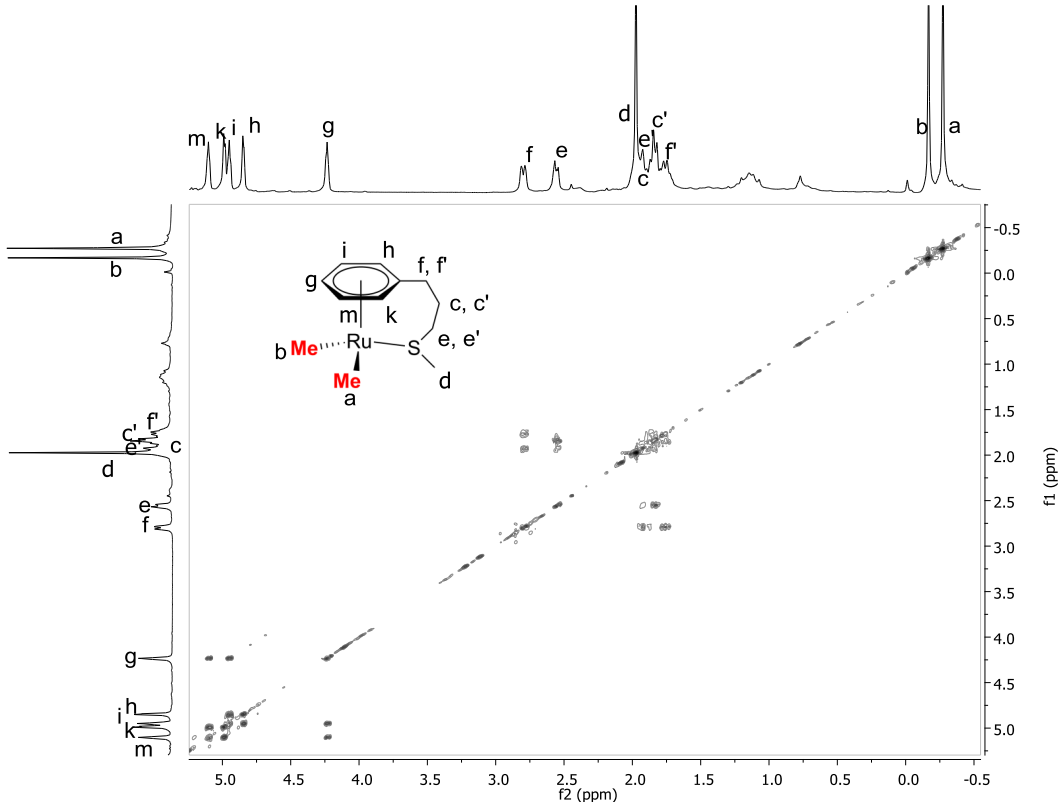

Figure 2.10. COSY-NMR spectrum of complex **2.4** at 183 K in CD_2Cl_2.

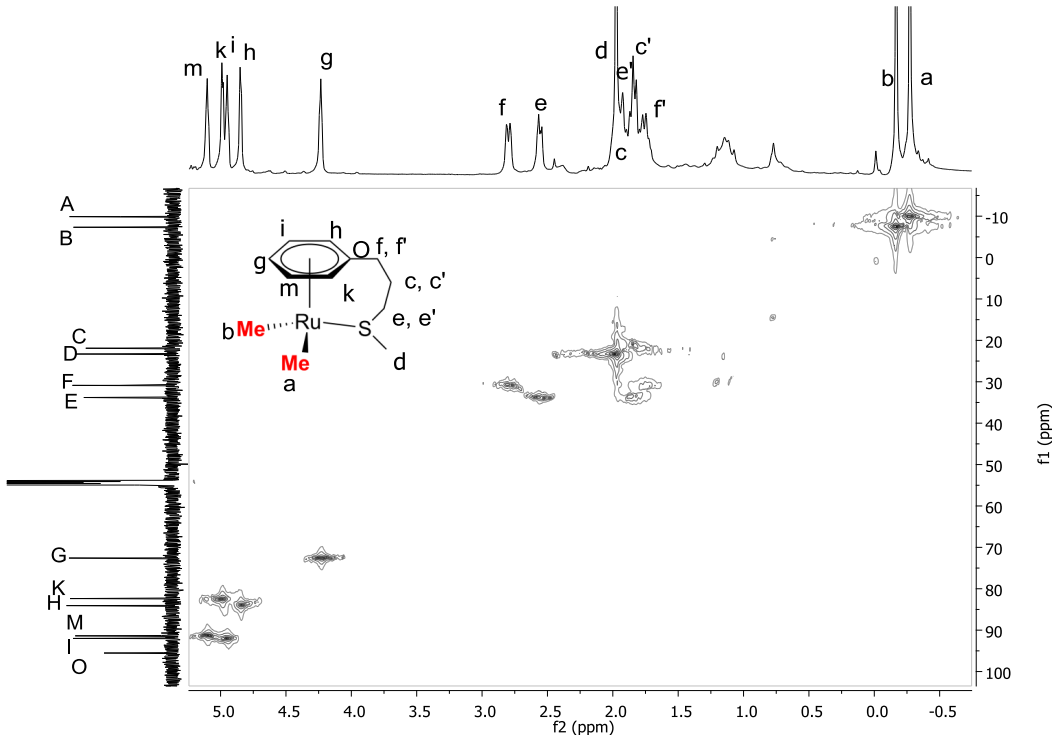

Figure 2.11. HMQC-NMR spectrum of complex **2.4** at 183 K in CD_2Cl_2.

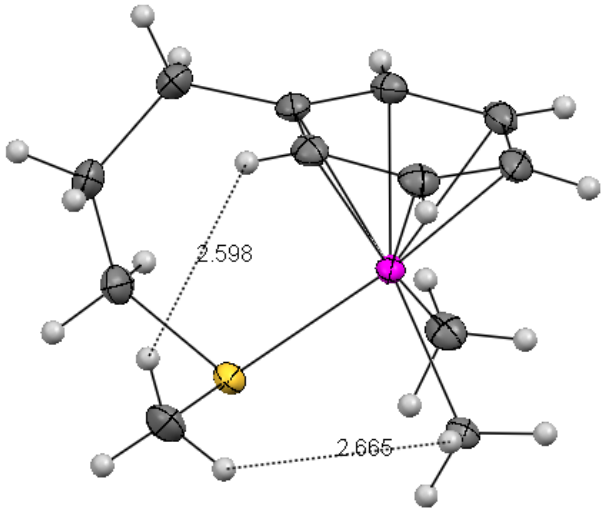

Figure 2.12. X-Ray crystal structure of complex **2.4** with selected atom distances for NOE identification.

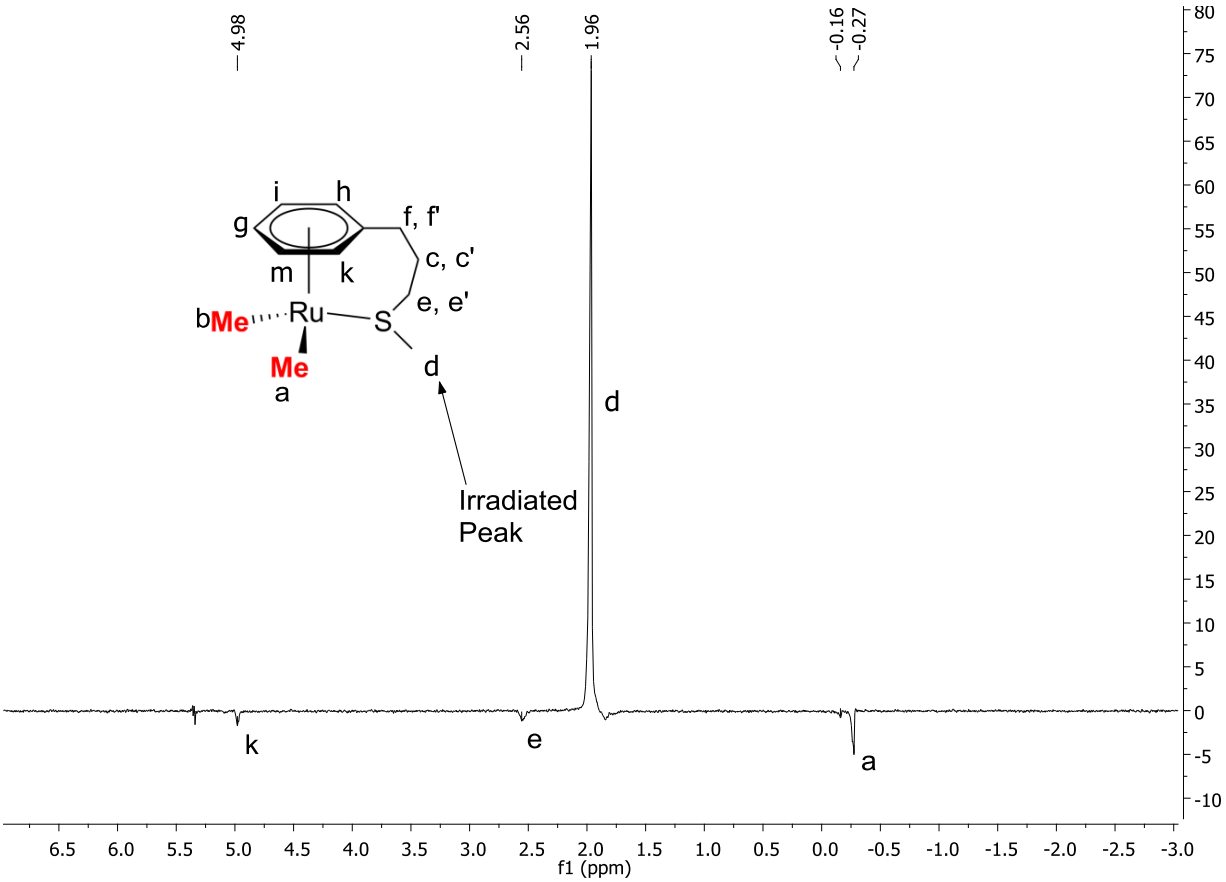

Figure 2.13. NOE-NMR spectrum of complex **2.4** at 183 K in CD_2Cl_2.

Complex **2.4** can be mono-demethylated by treating it with a stoichiometric amount of a strong acid to generate the proposed cationic active species. In our study, we used 1 eq. of the Brookhart oxonium acid,[3,46] $[H(Et_2O)_2]^+$ $[BAr'_4]^-$ (where Ar'= 3,5-$(CF_3)_2C_6H_3$)), to protonate complex **2.4** for removing one methyl group. Upon exposure to ethylene, the mono-demethylated complex exhibited activity for polymerizing ethylene (Table 2.1, entries 5-7). Similar to polymerization with **2.3**/$AlMe_2Cl$ system, higher ethylene pressure resulted in higher activity and lower branching density. For control, exposure of only ($[[H(Et_2O)_2]^+$ $[BAr'_4]^-$) to ethylene in the absence of complex **2.4** did not yield any polymer (Table 2.1, entry 8), proving again that the ruthenium complex is the active species responsible for ethylene polymerization. The structure of the polymer obtained with **2.4**/($[H(Et_2O)_2]^+$ [BAr'4]$^-$) was identified as polyethylene by ^{1}H NMR analysis. GPC traces of polymers made by **2.4**/($[H(Et_2O)_2]^+$ $[BAr'_4]^-$) system are monomodal with molecular weights and PDIs very similar to the low molecular weight fraction of polyethylene obtained with **2.3**/$AlMe_2Cl$ system (Table 2.1, entries 5-7), suggesting that the low molecular weight polyethylene could be produced by the same active species for **2.3**/$AlMe_2Cl$ and **2.4**/($[H(Et_2O)_2]^+$ $[BAr'_4]^-$) systems. The relatively low molecular weight of polyethylene could be due to the low activity and facile chain transfer of this catalyst that lacks steric bulkiness. In the case of polymerizations with **2.3**/$AlMe_2Cl$ system, a much high molecular weight polyethylene was also formed, presumably by a different active species with unknown structure. The elucidation of active species in such aluminum alkyl activated systems remains an unsolved challenge in coordination polymerization field. Similar to our observation, large discrepancies for activity and molecular weight were also observed in early transition metal polymerization catalysts between well-defined cationic species and

aluminum alkyl activated systems. For example, in Jordan's seminal work of a well-defined $Cp_2ZrMe(THF)^+$ system for ethylene polymerization, the activity is ~ 430 turnovers/hr and Mn is ~ 7130 g/mol,[47] both orders of magnitude lower than Cp_2ZrCl_2/aluminum alkyl activated polymerization.[48] Other studies have also shown that both polymerization activity and polyolefin molecular weight significantly depend on cocatalyst used.[49] One possibility for our **2.3**/$AlMe_2Cl$ system is the formation of a small amount of highly active Cl-bridged or clustered species contributing to the formation of high molecular weight polyethylene. Similar halogen-bridged species of this type have been previously reported.[50-53]

2.3 Variable Temperature NMR Mechanistic Studies of Ethylene Migratory Insertion

To further investigate the active species contributing to ethylene polymerization, using low temperature ^1H NMR we monitored the initial ethylene binding and subsequent migratory insertion to the in situ generated cationic Ru species. For this purpose, the dimethylated complex **2.4** was added to ethylene-saturated CD_2Cl_2 solution at – 78°C. Addition of one equivalent of $[H(Et_2O)_2]^+ [BAr'_4]^-$ (Scheme 2.3) cleaves one methyl group to generate the active cationic species, complex **2.5**. Low temperature ^1H NMR at – 90 °C (Figures 2.14-2.16) shows that complex **2.5** exists in two different diastereomers (**2.5A** major and **2.5B** minor, Scheme 2.3) due to the chirality of the sulfur atom. Based on NMR integrations, the two species are present in a 4:1 ratio at –90 °C. Complex **2.5A** is the major

species because it has less steric repulsion between the S-CH_3 methyl group and the ethylene bound to Ru. In the minor complex (**2.5B**), ethylene coordinates on the same side of the methyl group, resulting in slightly higher steric repulsion. A number of NMR techniques, including COSY, HMQC, and NOE experiments, were employed to investigate the active species (Figures 2.14-2.26). The ethylene coordinated to the cationic Ru species in complex **2.5** was observed at – 90 °C with no free rotation, affording four proton signals from 4.0 ppm to 1.5 ppm (Figures 2.14-2.20). At – 10 °C, the two diastereomers re-equilibrated to a ratio of **2.5A:2.5B** ~ 2:1. Upon further warming, the ethylene proton signals coalesced to give two doublets centered at 2.9 ppm (Figures 2.21-2.26). At 25 °C, the two sets of peaks from the two diastereomers coalesced into one set of broad peaks due to dynamic exchange, precluding detailed structural analysis. At 45 ºC, the Ru-Me peaks started to disappear and the ^{1}H NMR spectrum became more complex (Figure 2.27).

Scheme 2.3. In situ activation of **2.4** to form active catalyst **2.5** (**2.5A** and **2.5B** isomers).

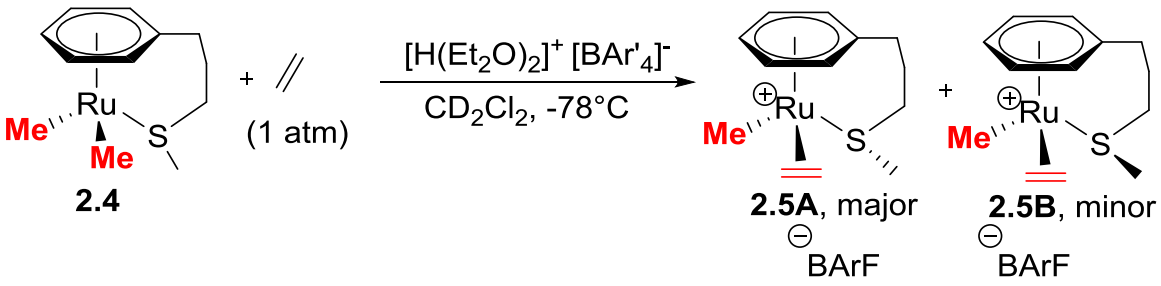

The initial migratory insertion barrier was determined by monitoring Ru-Me peak disappearance.[5] The first insertion was observed at 288 K at a very slow rate (Figure 2.28). As mentioned above, complex **2.5** exists in two diastereomers, **2.5A** and **2.5B**. The Ru-Me peak for the major **2.5** isomer, **2.5A**, significantly overlaps with growing oligomers,

precluding quantitative integration of the signal (Figures 2.28 and 2.29). Therefore, the Ru-Me peak of the minor isomer, **2.5B**, was chosen for kinetic analysis. We determined the initial migratory insertion barrier by monitoring Ru-Me first-order disappearance for **2.5B** at 301 K for a period of 6 hr. Insertion barriers in the same manner Brookhart did for late transition metals.[12] Ru-Me peak disappearance follows a first-order kinetics (Figure 2.30) with a rate constant $k_{\mathbf{2.5B}}$=1.9x10^{-4}s^{-1} at 301 K. The initial migratory insertion barrier was calculated to be 22.8±0.1 kcal·mol^{-1} at 301 K (Figures 2.29 and 2.30), which is significantly lower than the theoretically calculated barriers for complexes **2.1** and **2.2**.[38] Free ethylene consumption was also monitored, which correlates well with Ru-Me disappearance (Figures 2.31 and 2.32). Monitoring the growth of oligomers was complicated by rapid β-hydogen elimination and chain transfer as well as by peak overlaps.

The same solution used for these aforementioned NMR studies was heated to 45 °C for 15 minutes and then subjected to electrospray mass spectrometry (ESI-MS) analysis of species existing in the solution (Figure 2.33). The ESI-MS spectrum unambiguously confirmed that migratory insertion indeed occurred on the cationic ruthenium species **2.5**. Two series of growing oligomers were observed in the spectrum with increasing numbers of ethylene insertion. In one series of peaks, the number of carbons in the alkyl chain is odd (n = 1, 3, 5, 7, Figure 2.33, blue dots), which resulted from primary ethylene insertion to complex **2.5**. In another series of peaks, the number of carbons in the alkyl chain is even (n = 0, 2, 4, 6, Figure 2.33, red dots), which presumably formed by ethylene insertion after chain transfer occurred to the Ru center. The isotopic pattern for each peak agrees well with the molecular formula for each oligomeric species (Figures 2.34-2.35). Interestingly, an almost identical ESI-MS spectrum was obtained when **2.3**/AlMe2Cl system was exposed

to ethylene (1 atm at 45 ºC for 5 minutes, Figure 2.36), confirming that the active species are the same in both cases. Both our NMR and ESI-MS data confirm that the ruthenium is the active center where polymer chain grows.

2.4 Conclusions

In conclusion, we have designed and synthesized a novel ruthenium η^6-arene complex with a tethered sulfur ligand that is capable of catalyzing ethylene insertion polymerization. The structures of the Ru complexes were fully characterized by NMR, ESI-MS, elemental analysis, and X-ray crystallography. The complexes **2.3** and **2.4** adopt a "piano stool" type of coordination geometry, which upon activation generates two equivalent coordination sites for active migratory insertion. The active catalytic species was investigated by low temperature ^{1}H NMR and mass spectrometry. Our results have unambiguously established that the cationic ruthenium complex **2.5** is the active species for ethylene insertion polymerization. To the best of our knowledge, this is first direct observation of a cationic Ru complex responsible for olefin insertion polymerization. The initial migratory insertion barrier was determined to be ~ 22.8±0.1 kcal·mol^{-1} at 301 K, a barrier significantly higher than that for the nickel- and palladium-α-diimine system [3-5,9] but lower than the calculated barriers for previous ruthenium complexes **2.1** and **2.2**.[38]

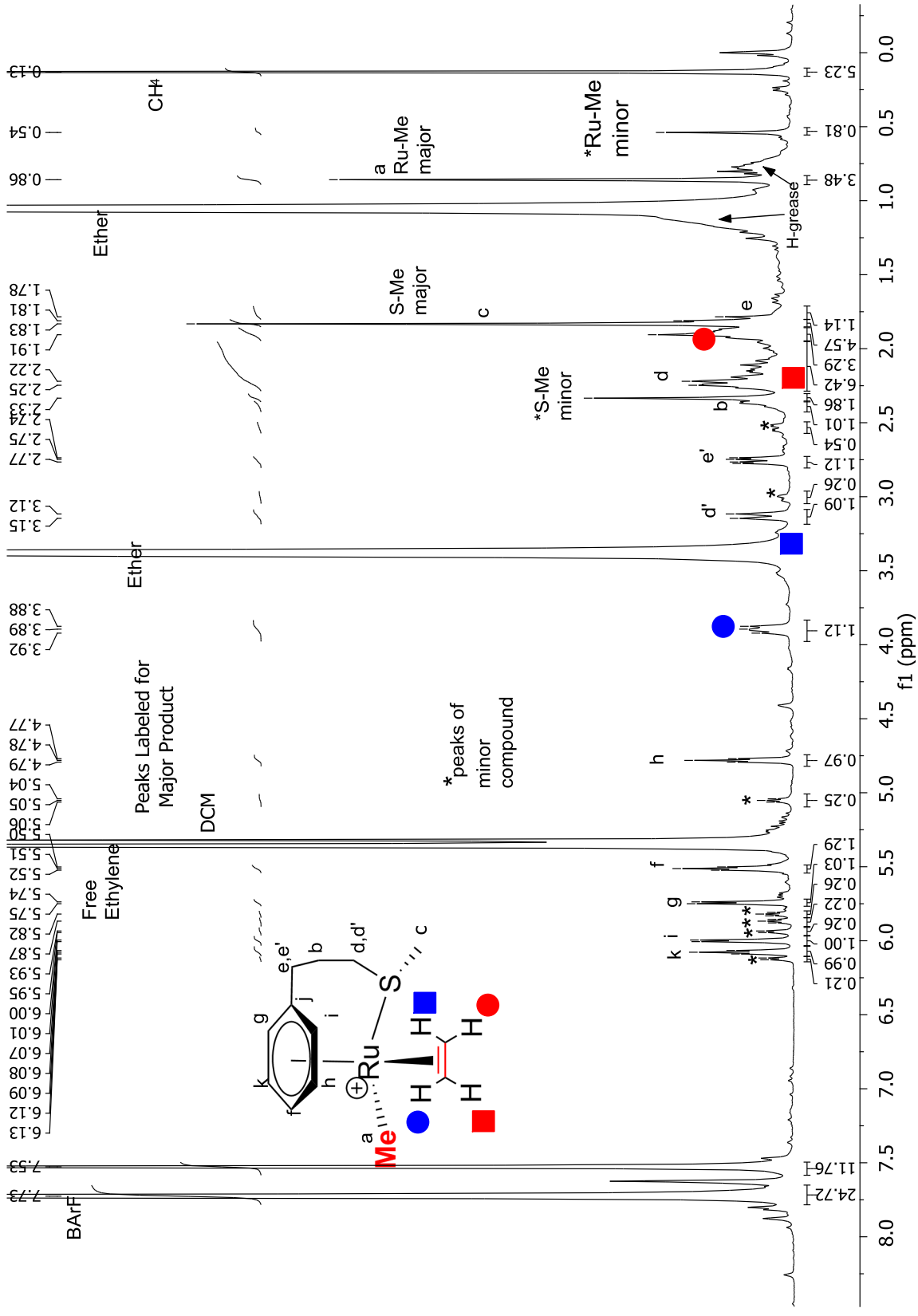

Figure 2.14. ^{1}H-NMR spectrum of complex **2.5** at 183 K in CD_2Cl_2. Only peaks for major product **2.5A** are labeled.

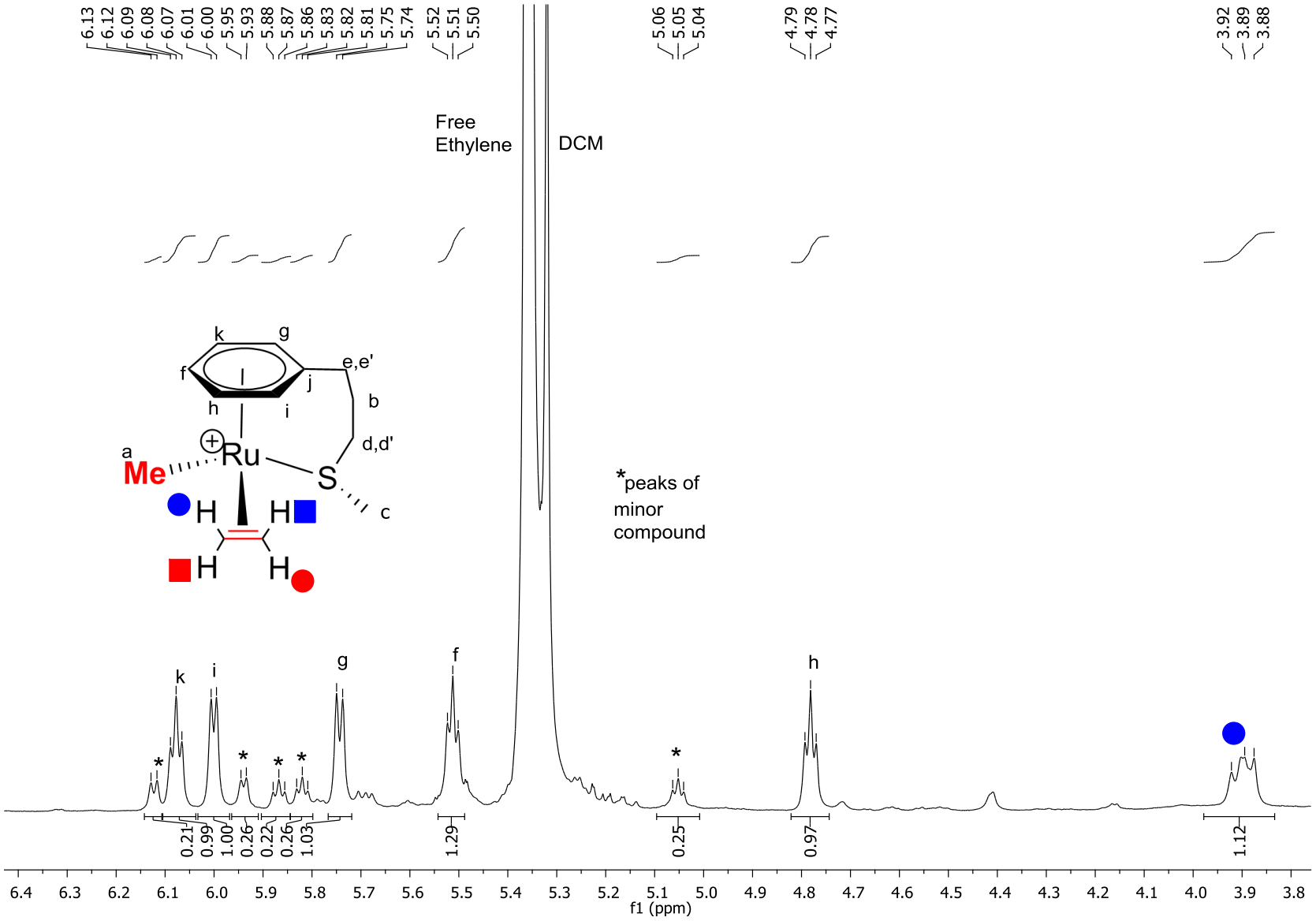

Figure 2.15. ^{1}H-NMR spectrum of complex **2.5** (with aromatic region expanded) at 183 K in CD_2Cl_2.

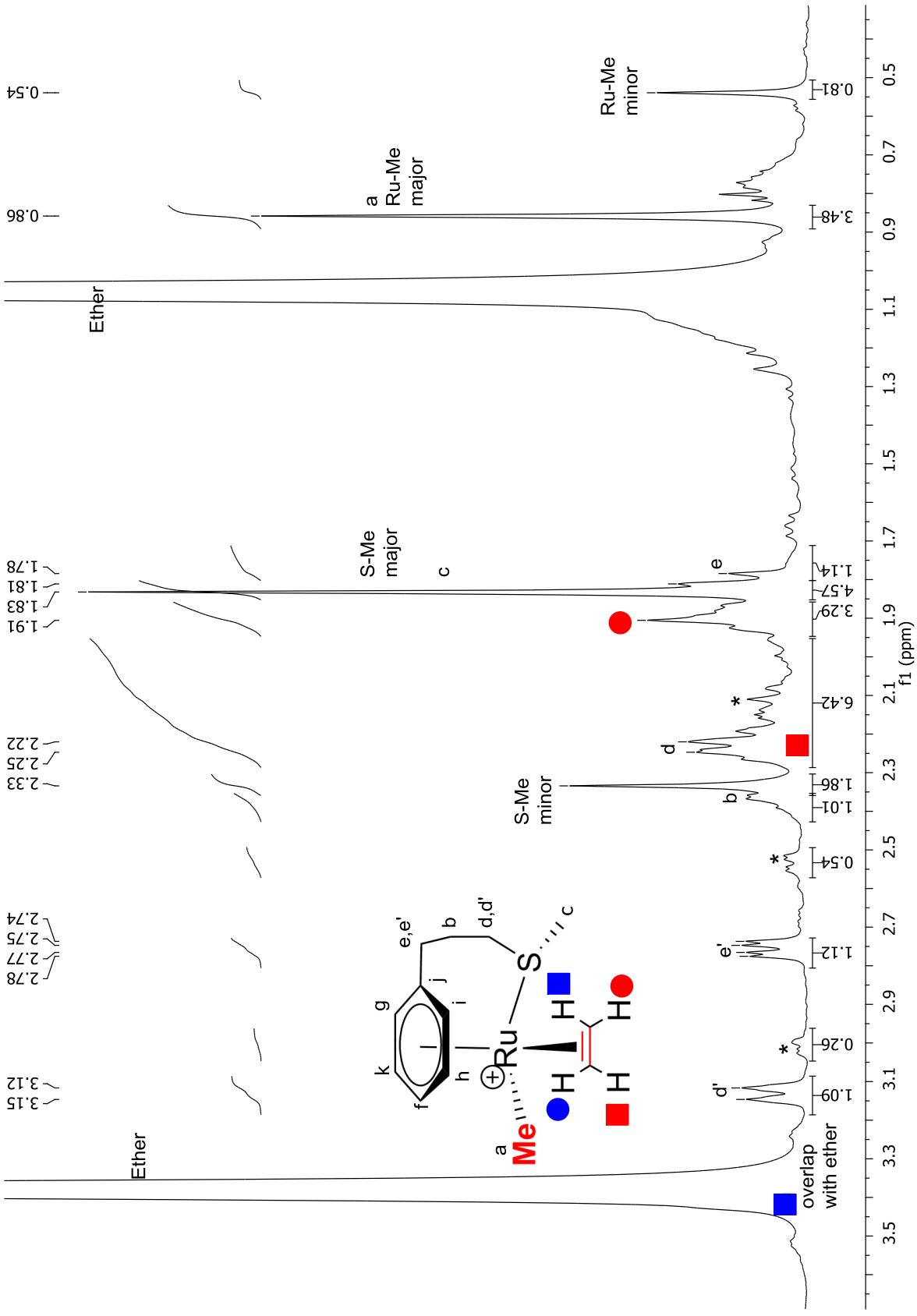

Figure 2.16. ^{1}H-NMR spectrum of complex **2.5** (with aliphatic region expanded) at 183 K in CD_2Cl_2.

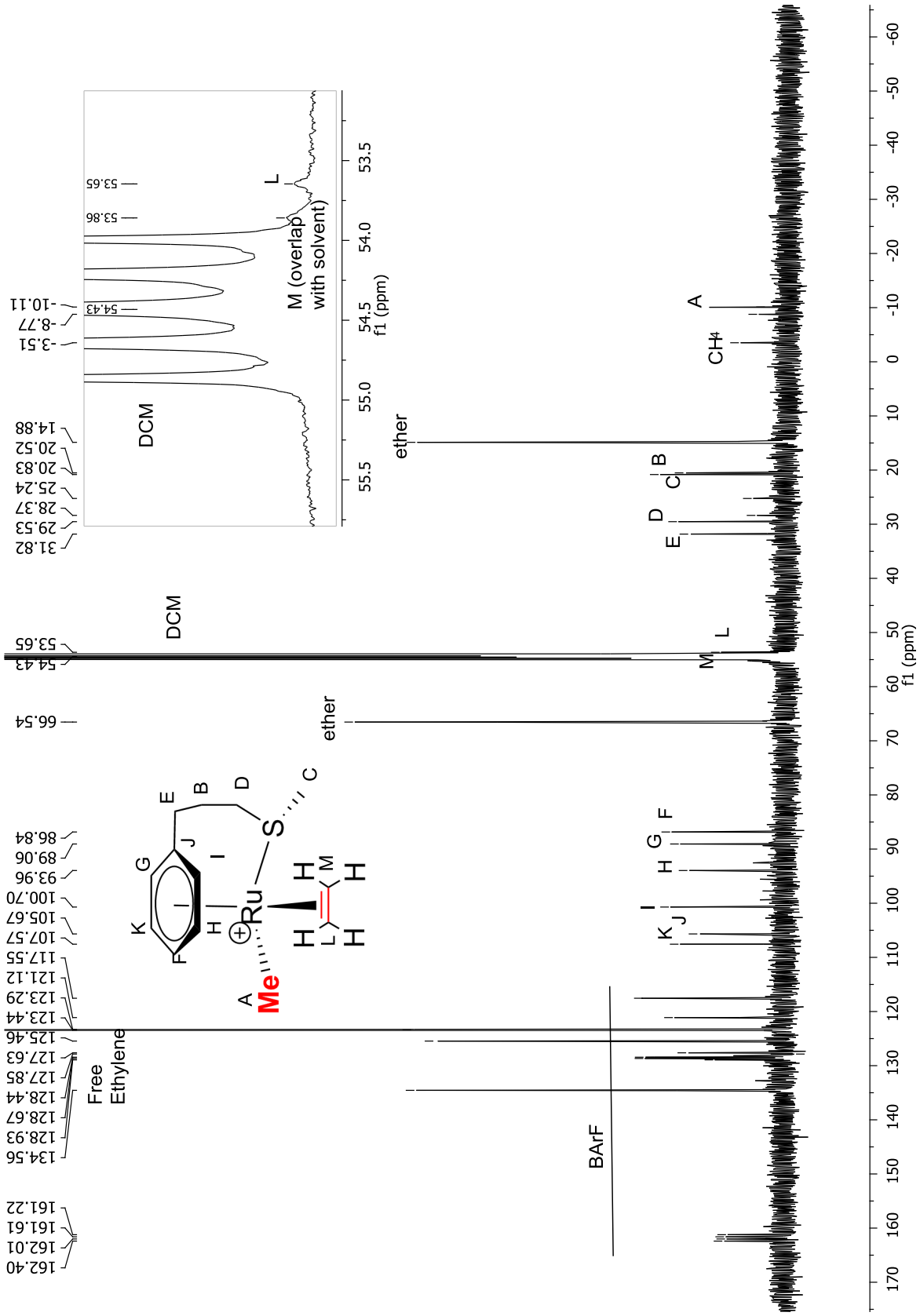

Figure 2.17. ^{13}C-NMR spectrum of complex **2.5** at 183 K in CD_2Cl_2.

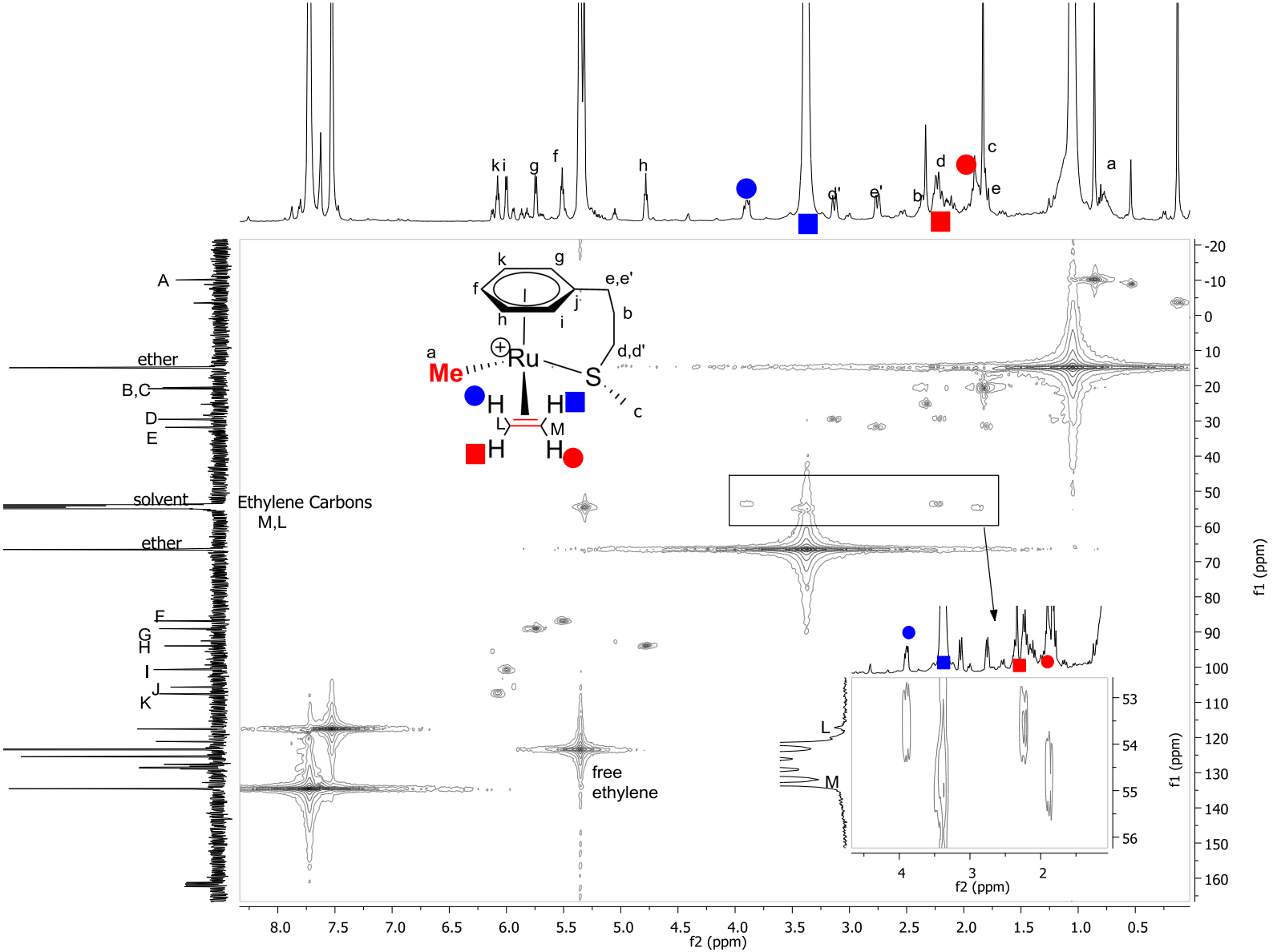

Figure 2.18. HMQC-NMR spectrum of complex **2.5** at 183 K in CD_2Cl_2.

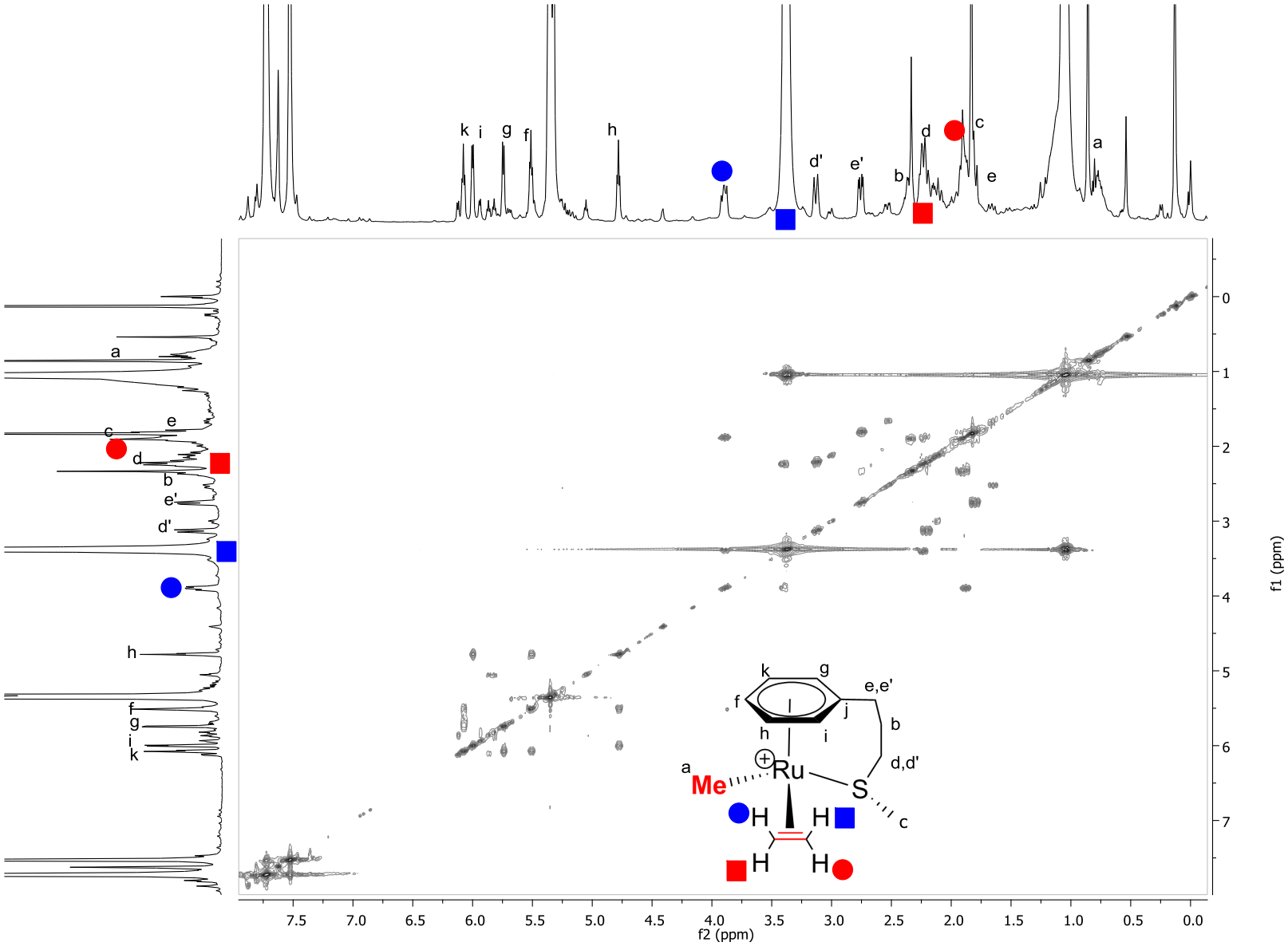

Figure 2.19. COSY-NMR spectrum of complex **2.5** at 183 K in CD_2Cl_2.

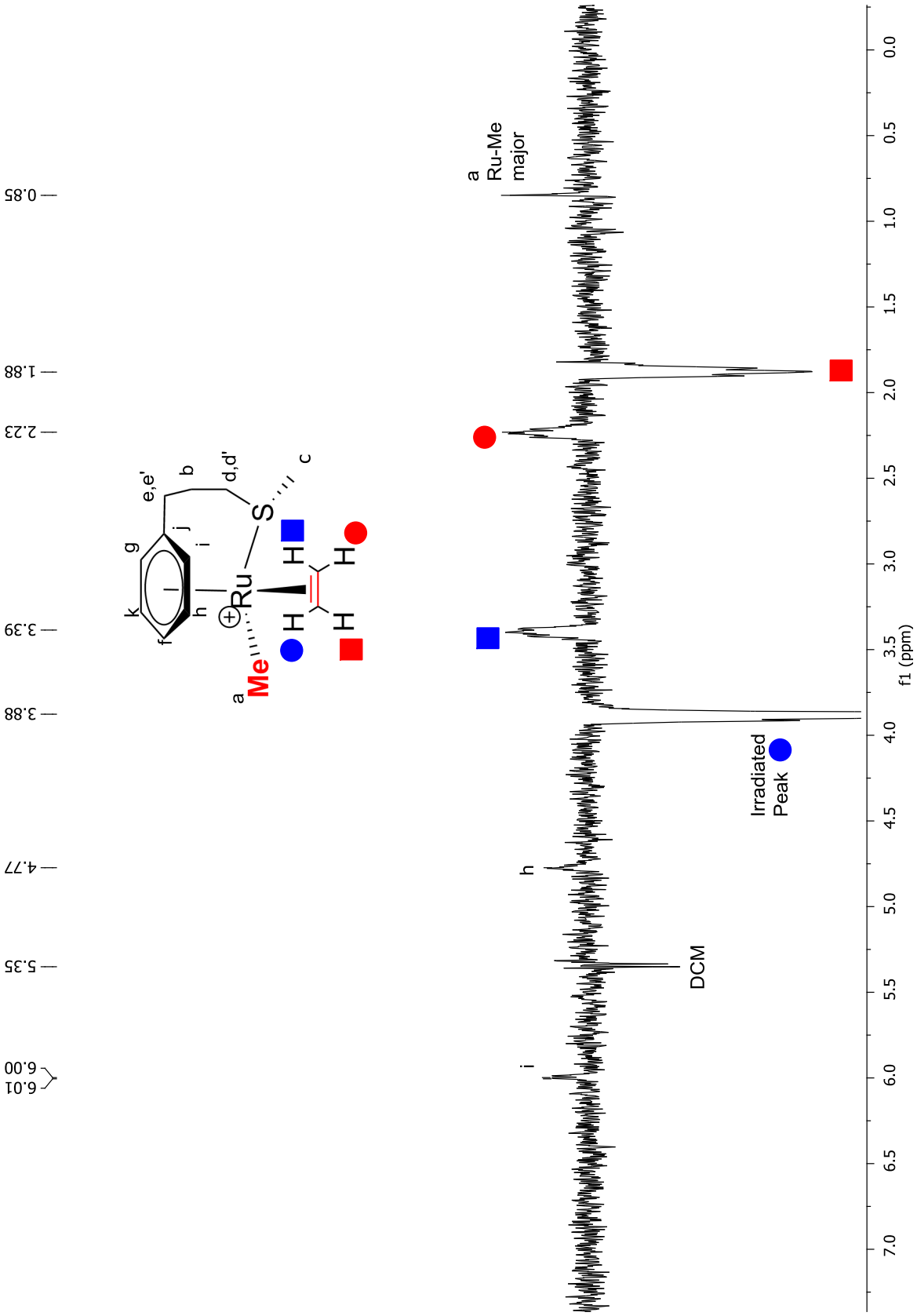

Figure 2.20. NOE-NMR spectrum of complex **2.5** at 183 K in CD_2Cl_2.

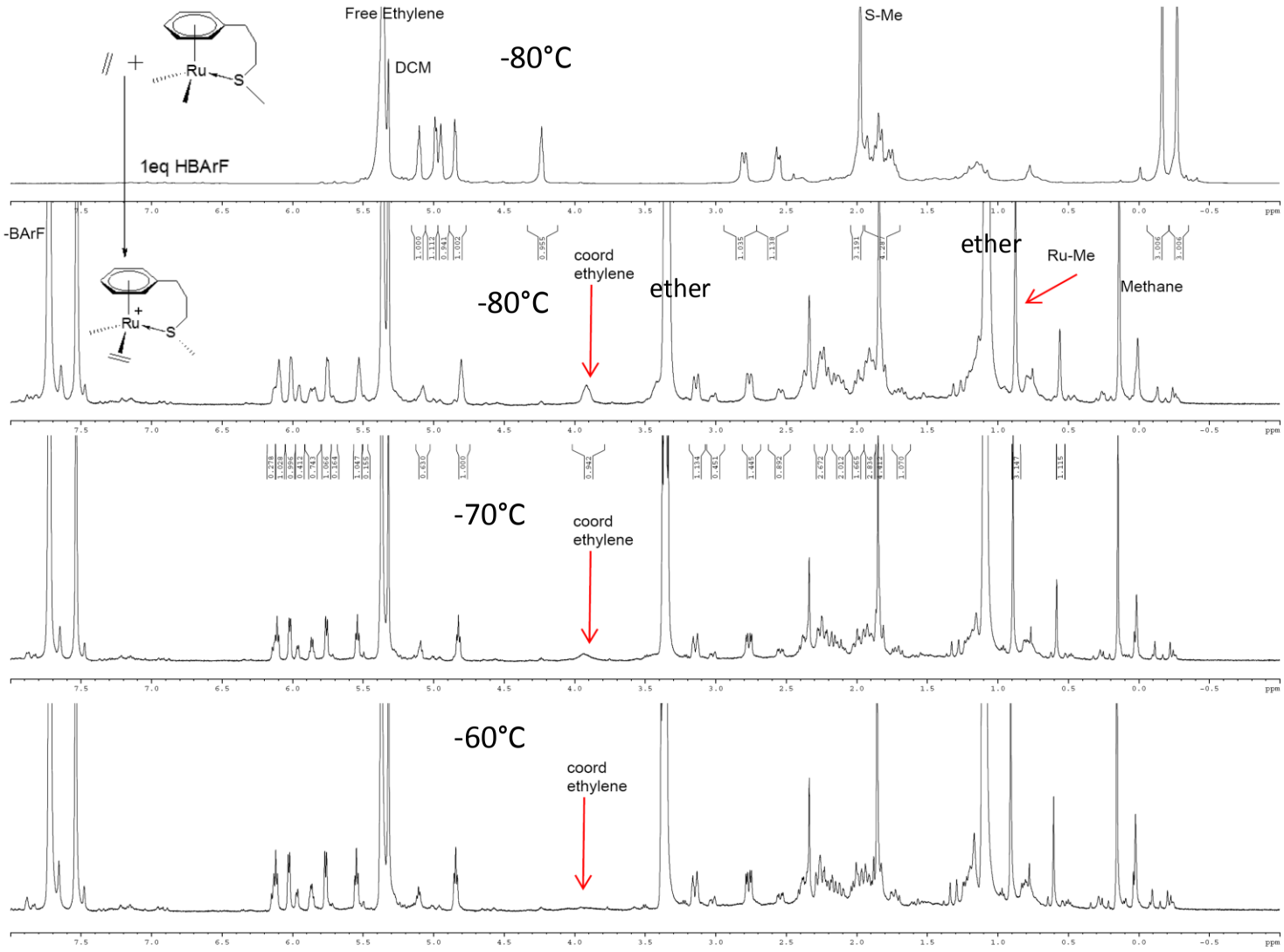

Figure 2.21. Variable temperature (193-213K) ^{1}H-NMR spectrum of complex **2.5** in CD_2Cl_2.

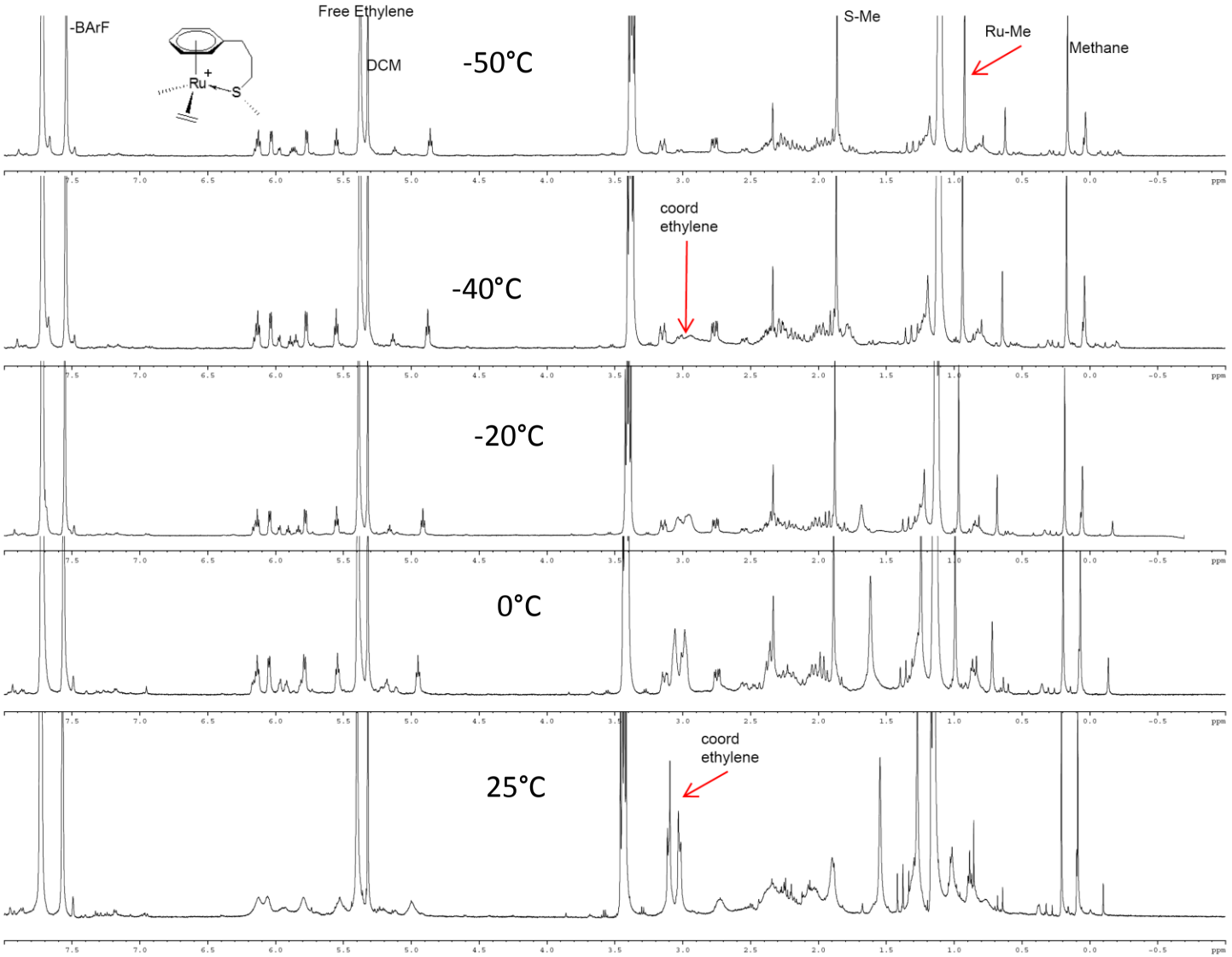

Figure 2.22. Variable temperature (223-298K) ^{1}H-NMR spectrum of complex **2.5** in CD_2Cl_2.

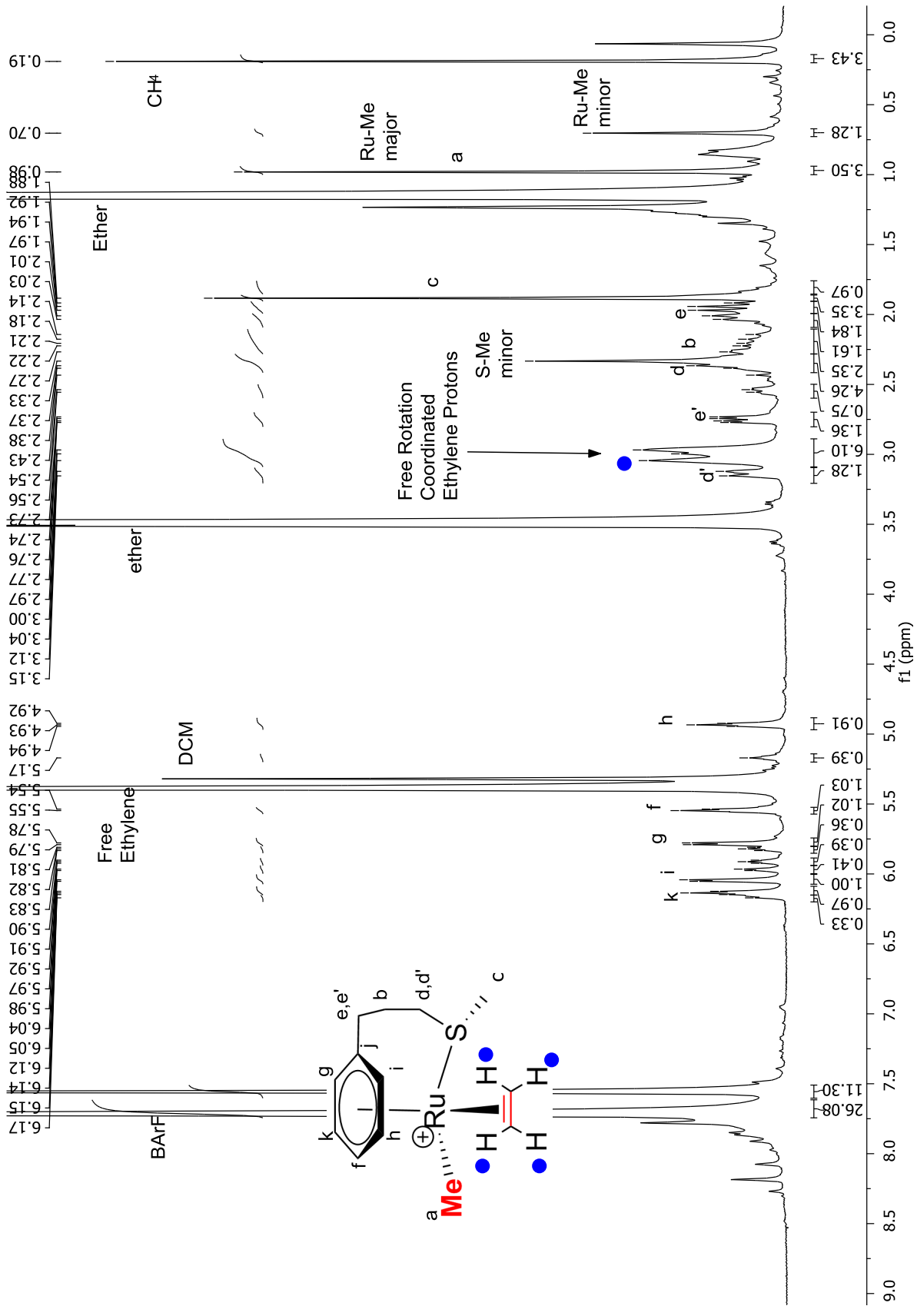

Figure 2.23. ^{1}H-NMR spectrum of complex **2.5** at 263 K in CD_2Cl_2.

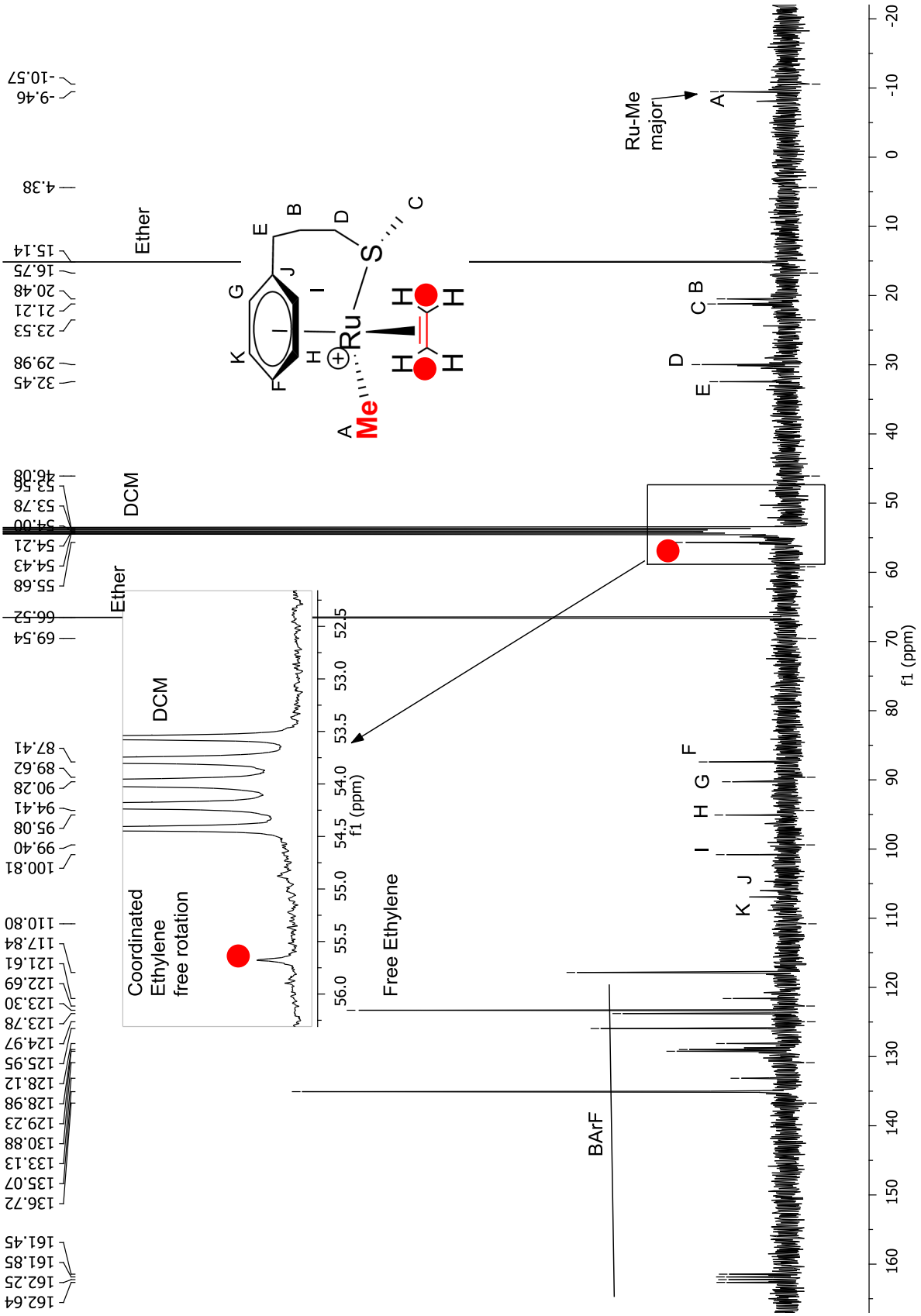

Figure 2.24. ^{13}C-NMR spectrum of complex **2.5** 263 K in CD_2Cl_2.

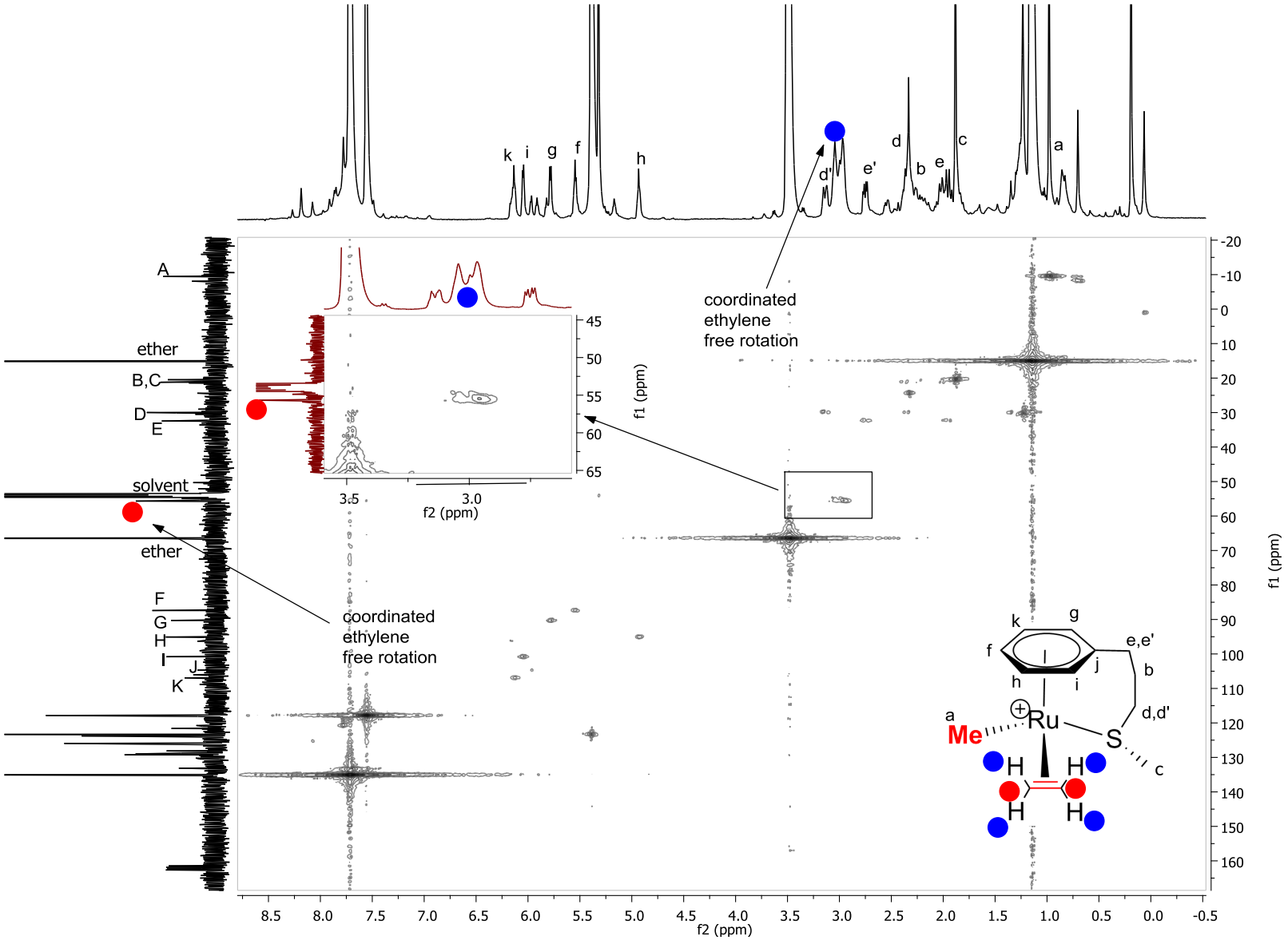

Figure 2.25. HMQC-NMR spectrum of complex **2.5** at 263 K in CD_2Cl_2.

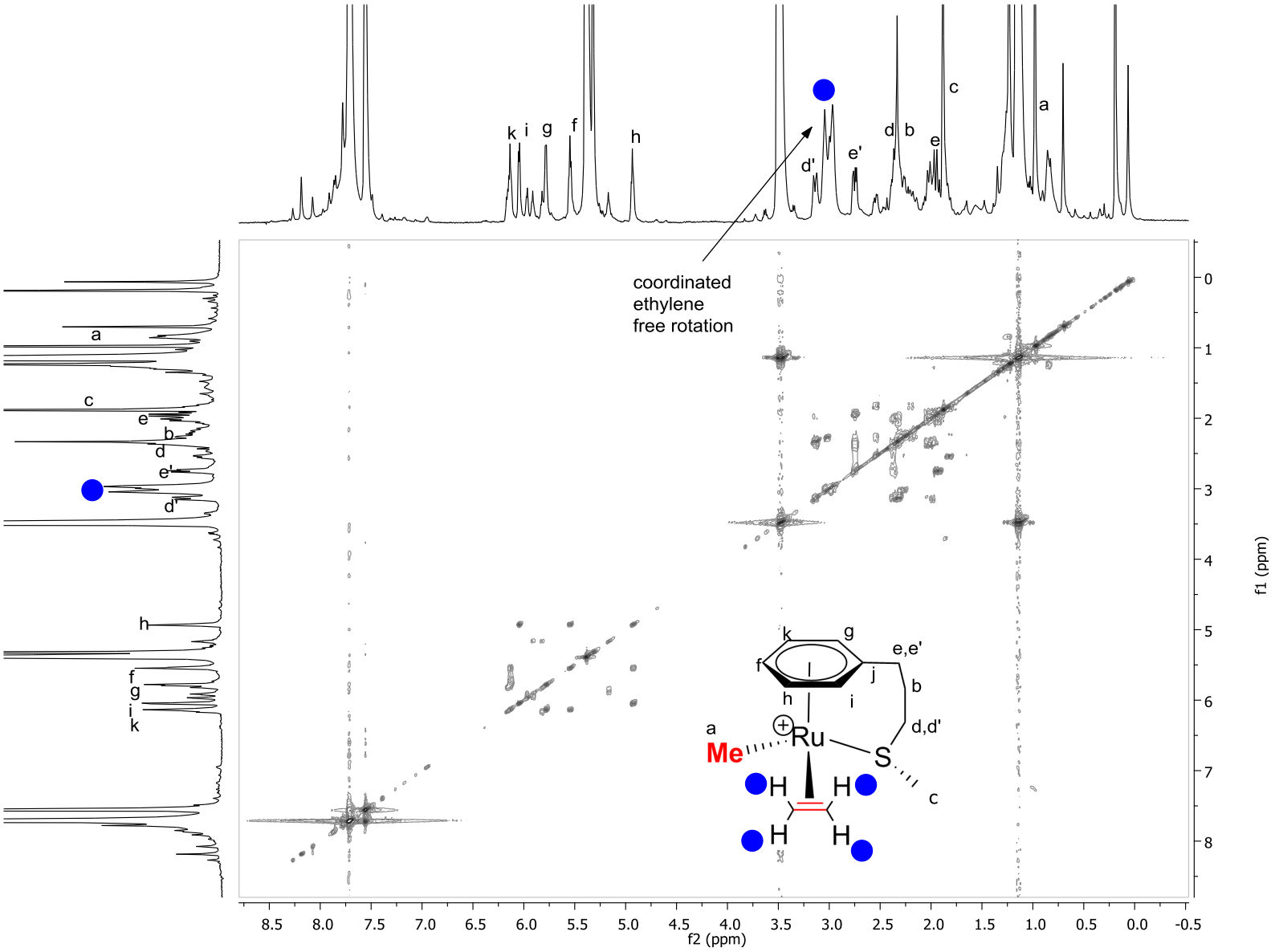

Figure 2.26. COSY-NMR spectrum of complex **2.5** at 263 K in CD_2Cl_2.

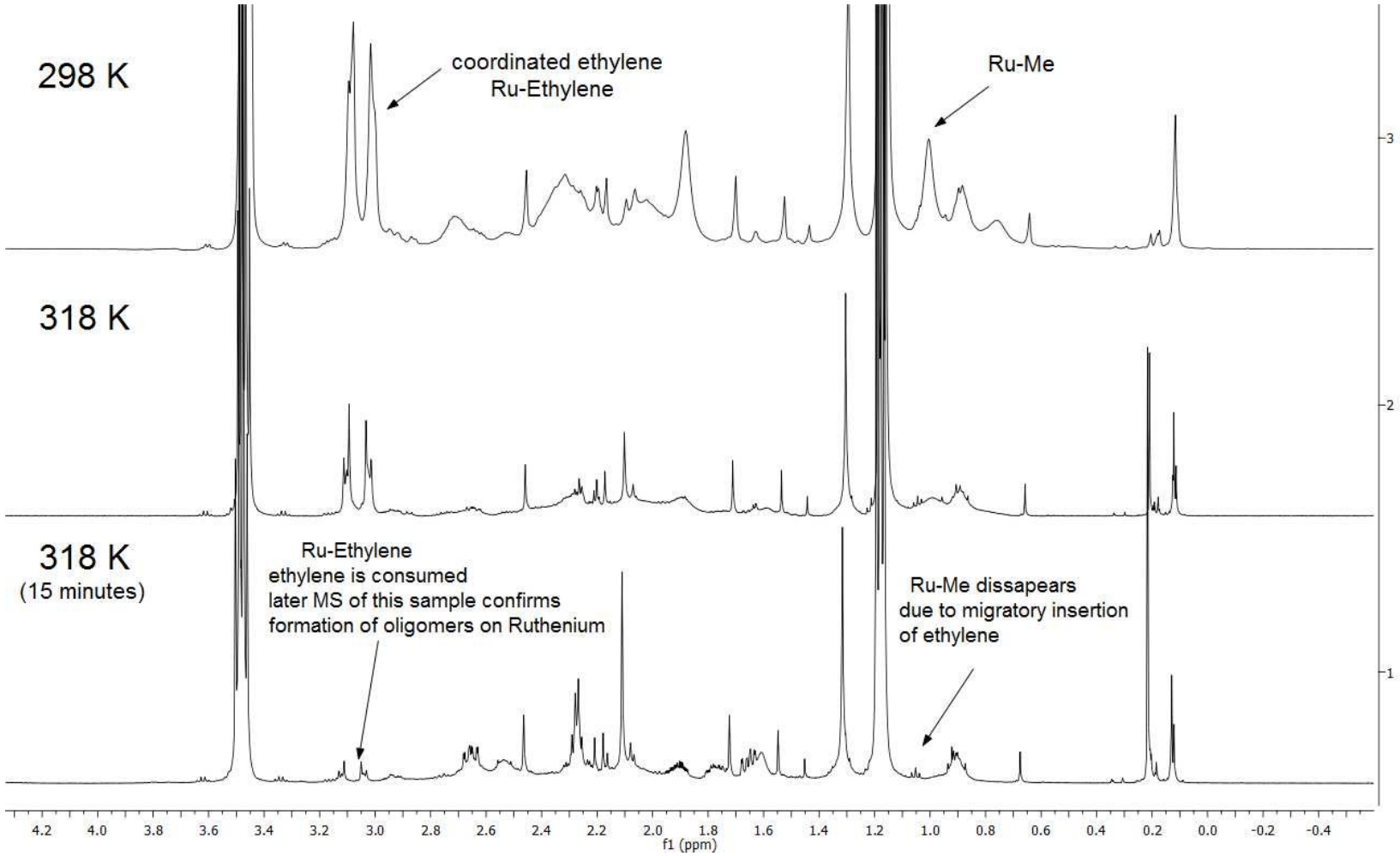

Figure 2.27. ^{1}H-NMR spectra of complex **2.5** running at different temperature (in CD_2Cl_2 from 298 K to 318 K, and then hold at 318 K for 15 minutes). Ethylene consumption and Ru-Me peak disappearance provide direct evidence for ethylene migratory insertion on Ru center. ESI-MS spectrum in the subsequent figure is from this sample probing growing oligomers bound on Ru center.

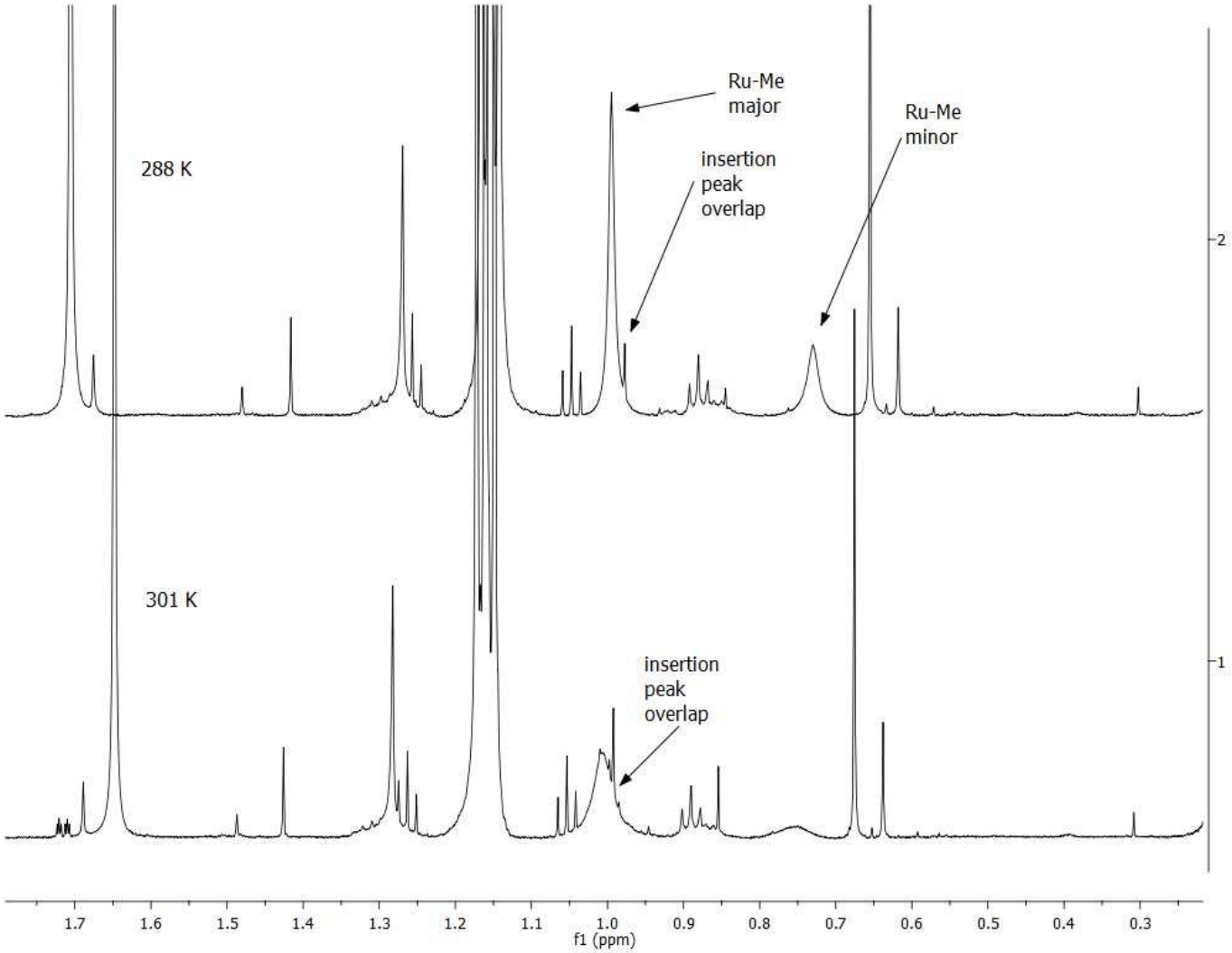

Figure 2.28. Ru-Me peak monitoring of complexes **2.5A** and **2.5B** for insertion barrier calculation. First insertion is observed at 288 K. Peaks overlaps of major isomer (**2.5A**) avoids insertion barrier calculation, we used minor isomer peak (**2.5B**) instead. Increasing temperature to 301 K broadens peaks due to faster isomers exchange but at this temperature insertion can be monitored in reasonable time (7 hours).

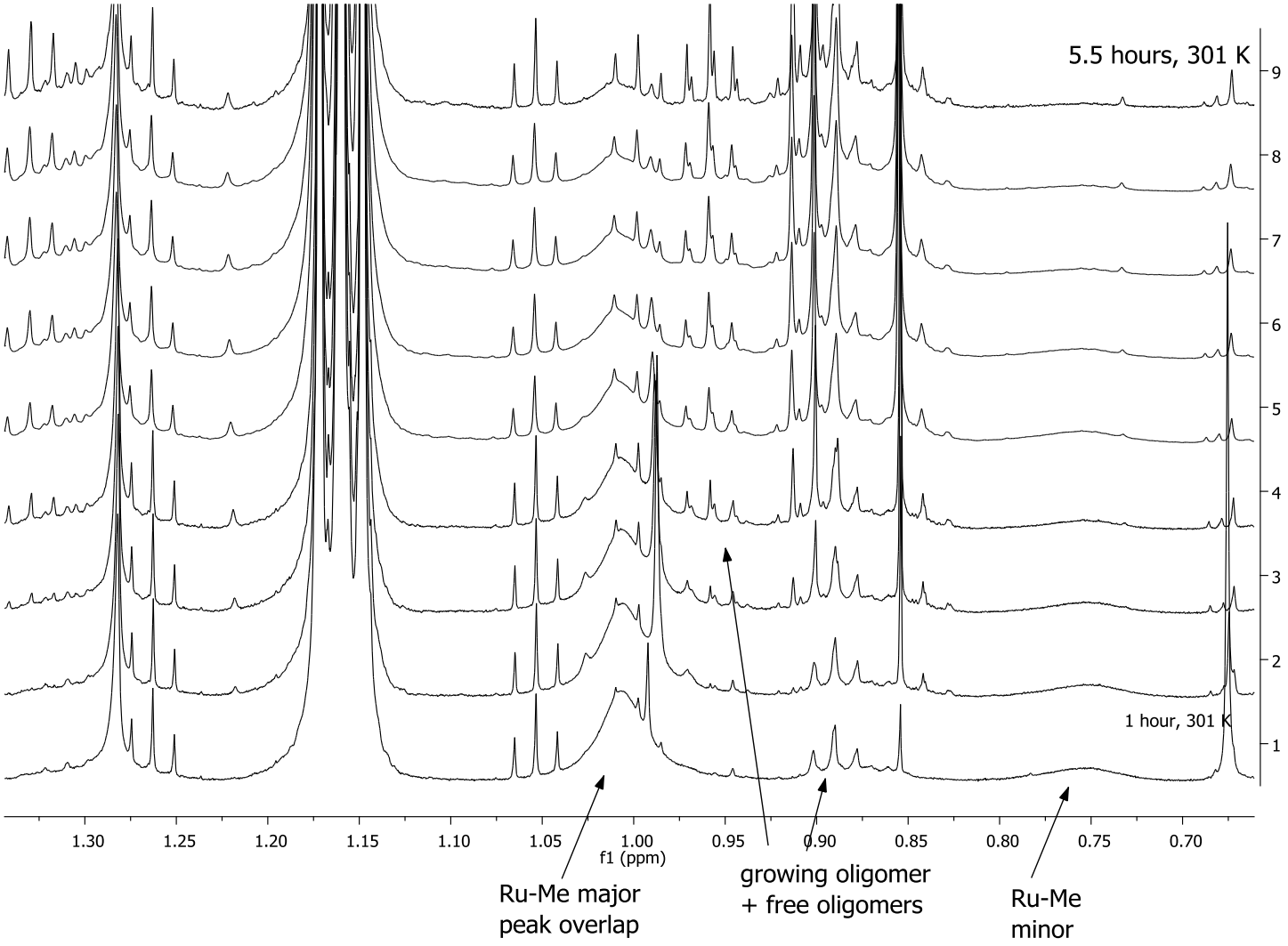

Figure 2.29. Ru-Me peak monitoring of complex **2.5**. Ru-Me major peaks overlaps with oligomers, Ru-Me minor has not significant overlap and it is used to calculate insertion barrier.

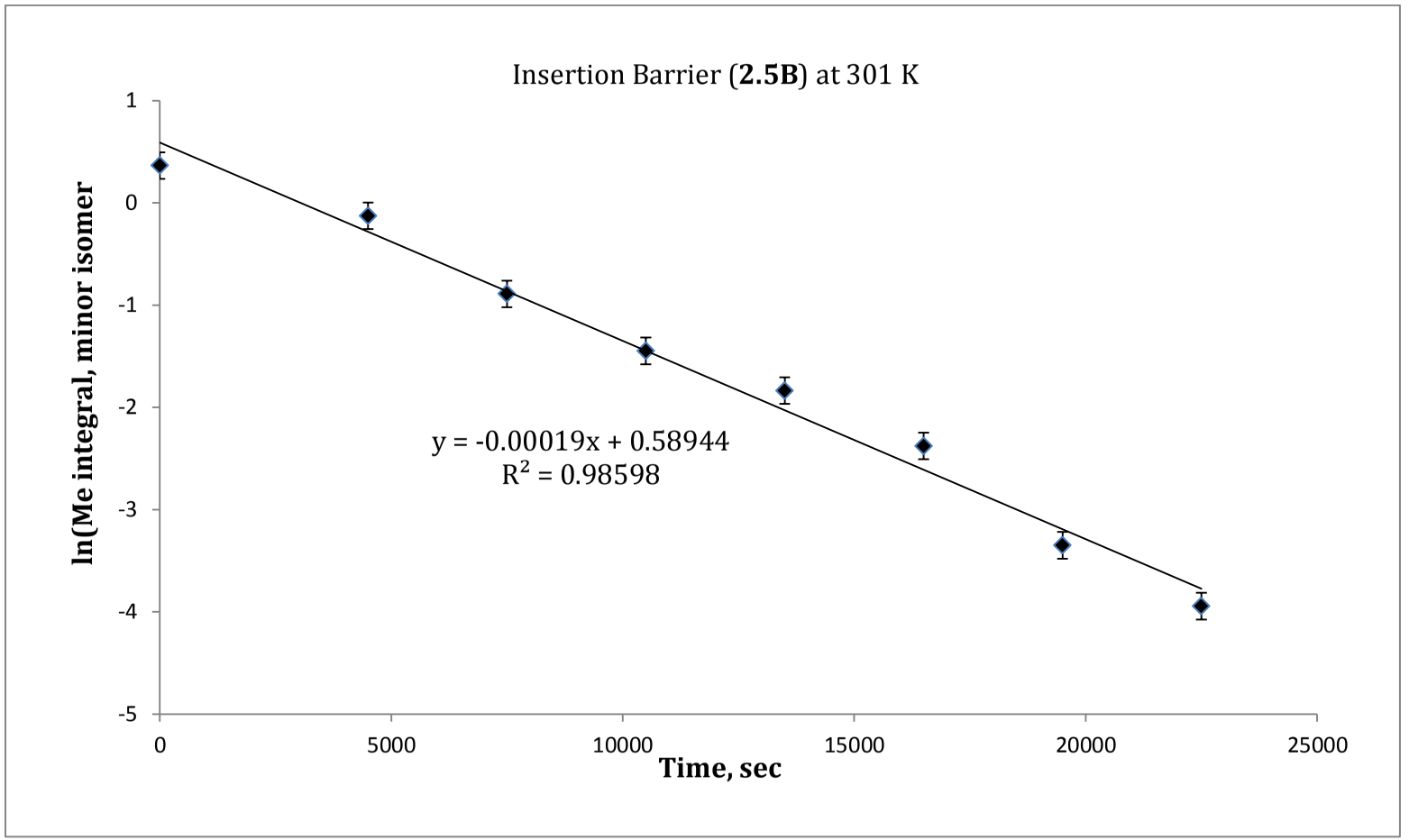

Figure 2.30. First order consumption of Ru-Me (**2.5B**) at 301 K.

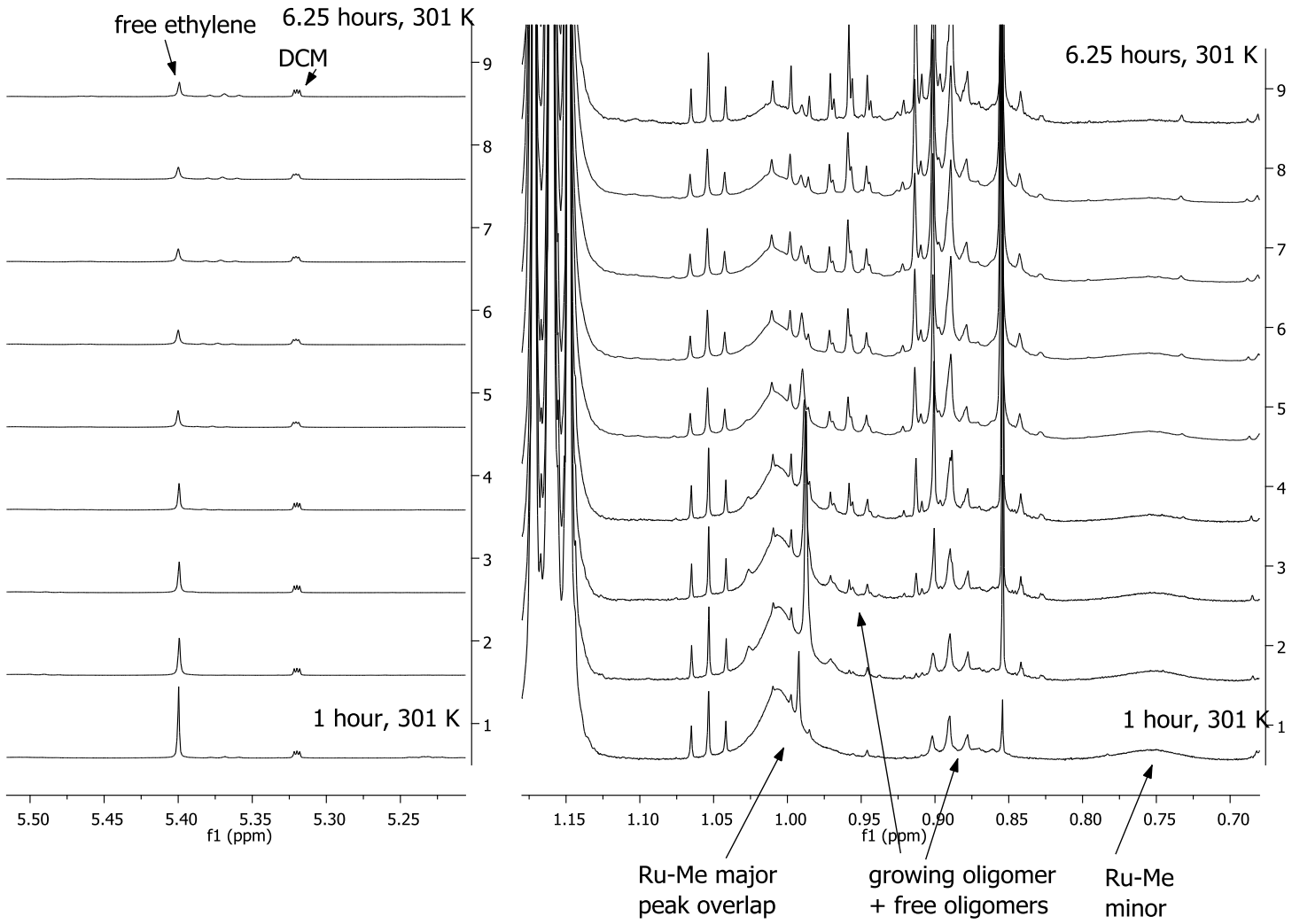

Figure 2.31. Monitoring correlation of free ethylene consumption and Ru-Me peak disappearance complex **2.5** (not at same vertical scale for easiness of comparison). Ethylene is consumed by both isomers **2.5A** and **2.5B**.

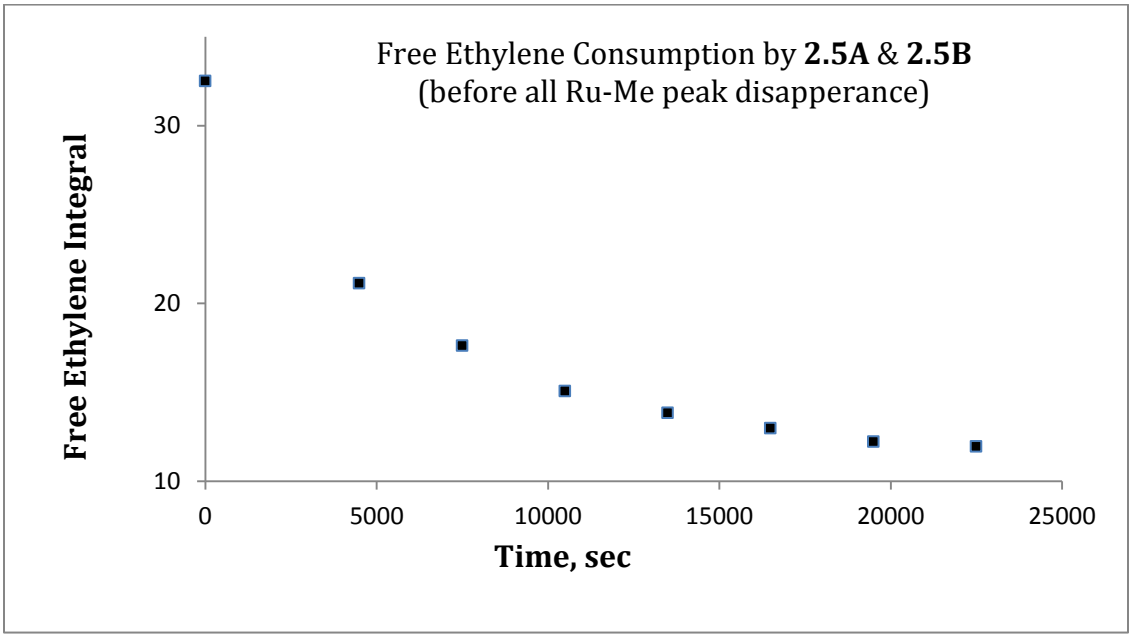

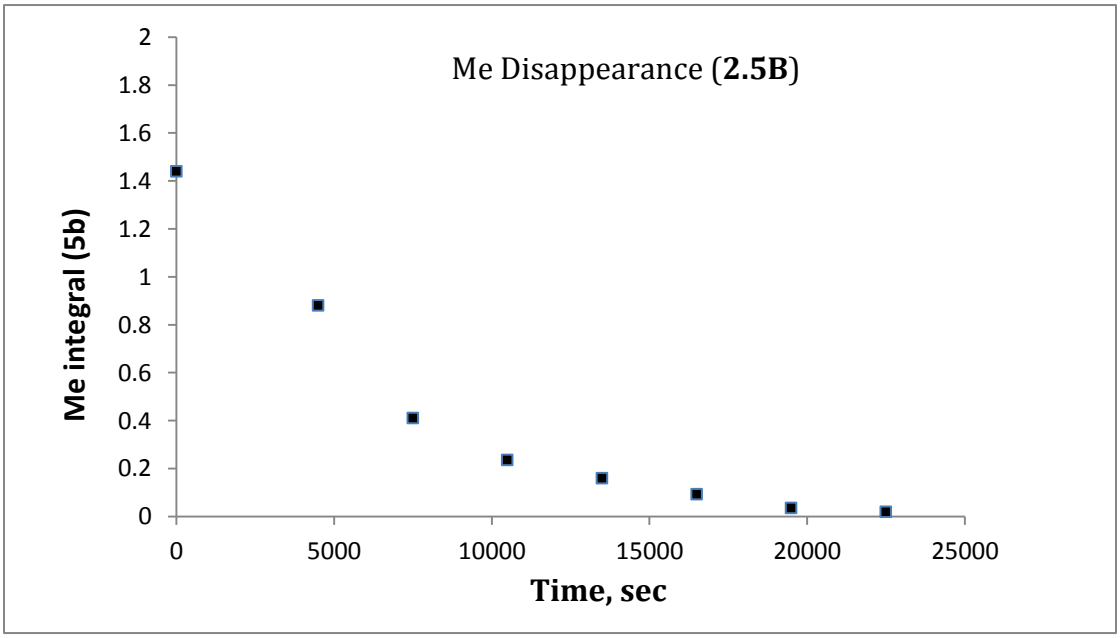

Figure 2.32. Top, free ethylene consumption by **2.5A** and **2.5B** monitoring, 301 K. Bottom, Ru-Me disappearance of **2.5B**, 301 K.

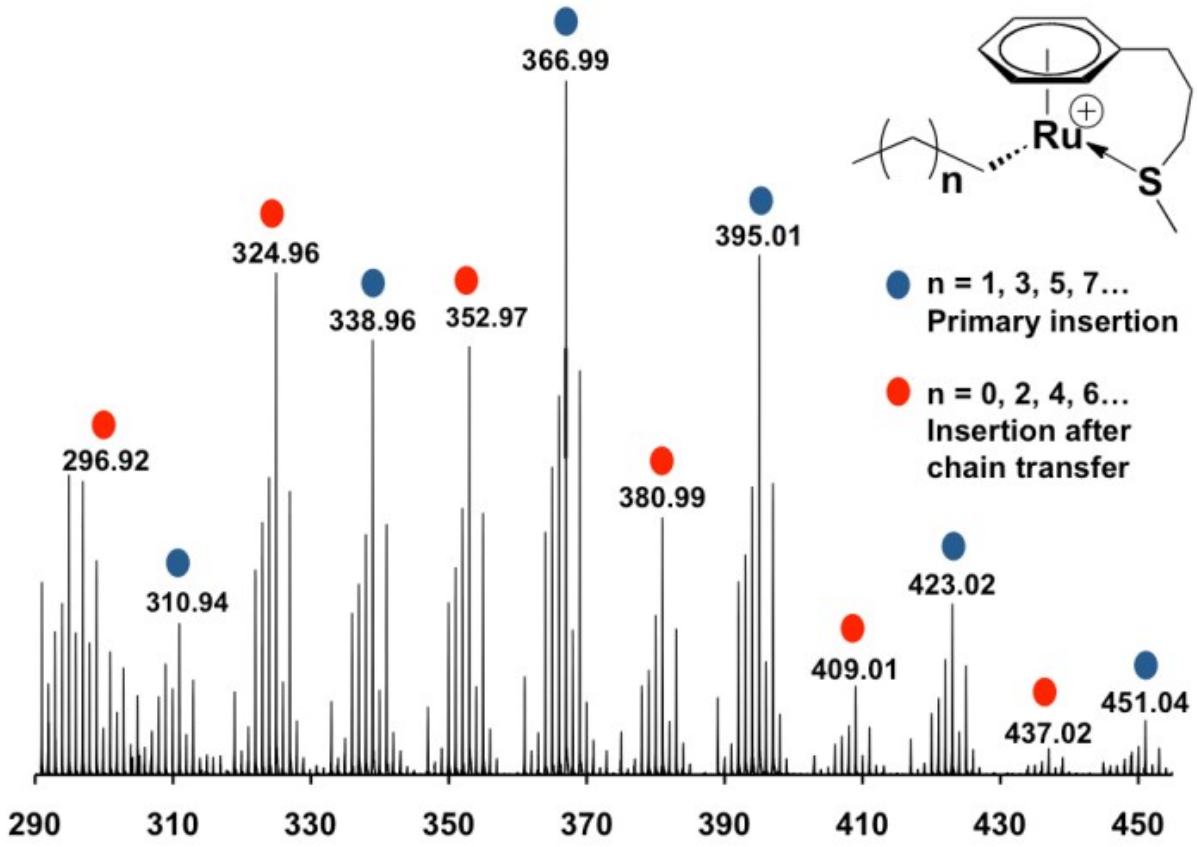

Figure 2.33. ESI-MS spectrum of the in situ polymerization sample. Several growing oligomeric species were identified due to successive ethylene insertion to the cationic Ru center. Blue circles indicate oligomers resulted from primary ethylene insertion to complex **2.5**. Red circles indicate oligomers formed from ethylene insertion to $Ru(H)^+$ species generated from chain transfer.

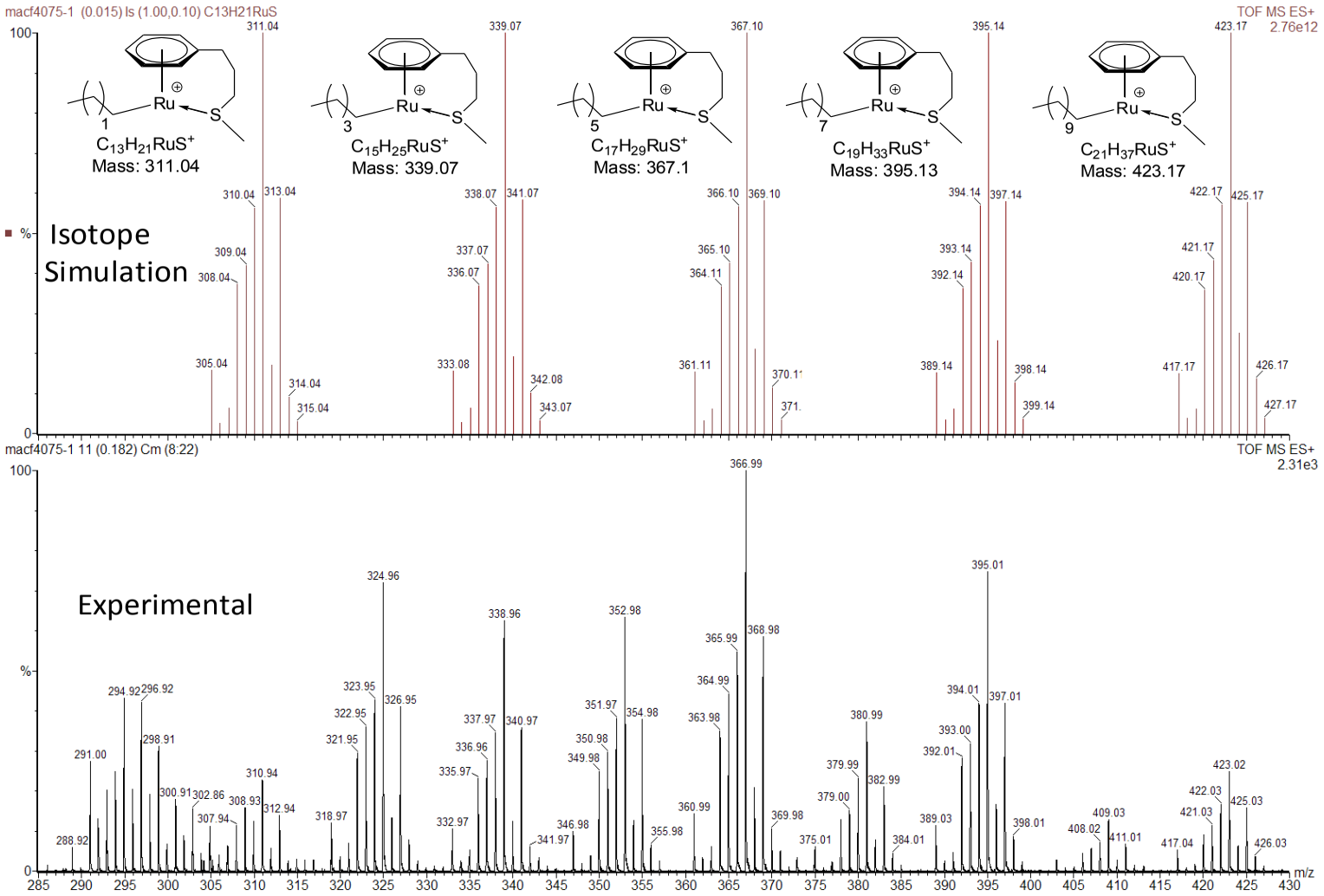

Figure 2.34. ESI-MS of ethylene oligomers bound to cationic Ru center formed by primary ethylene insertion (oligomers with odd number of carbons). Comparison between isotope modeling (top) and experimental data (bottom).

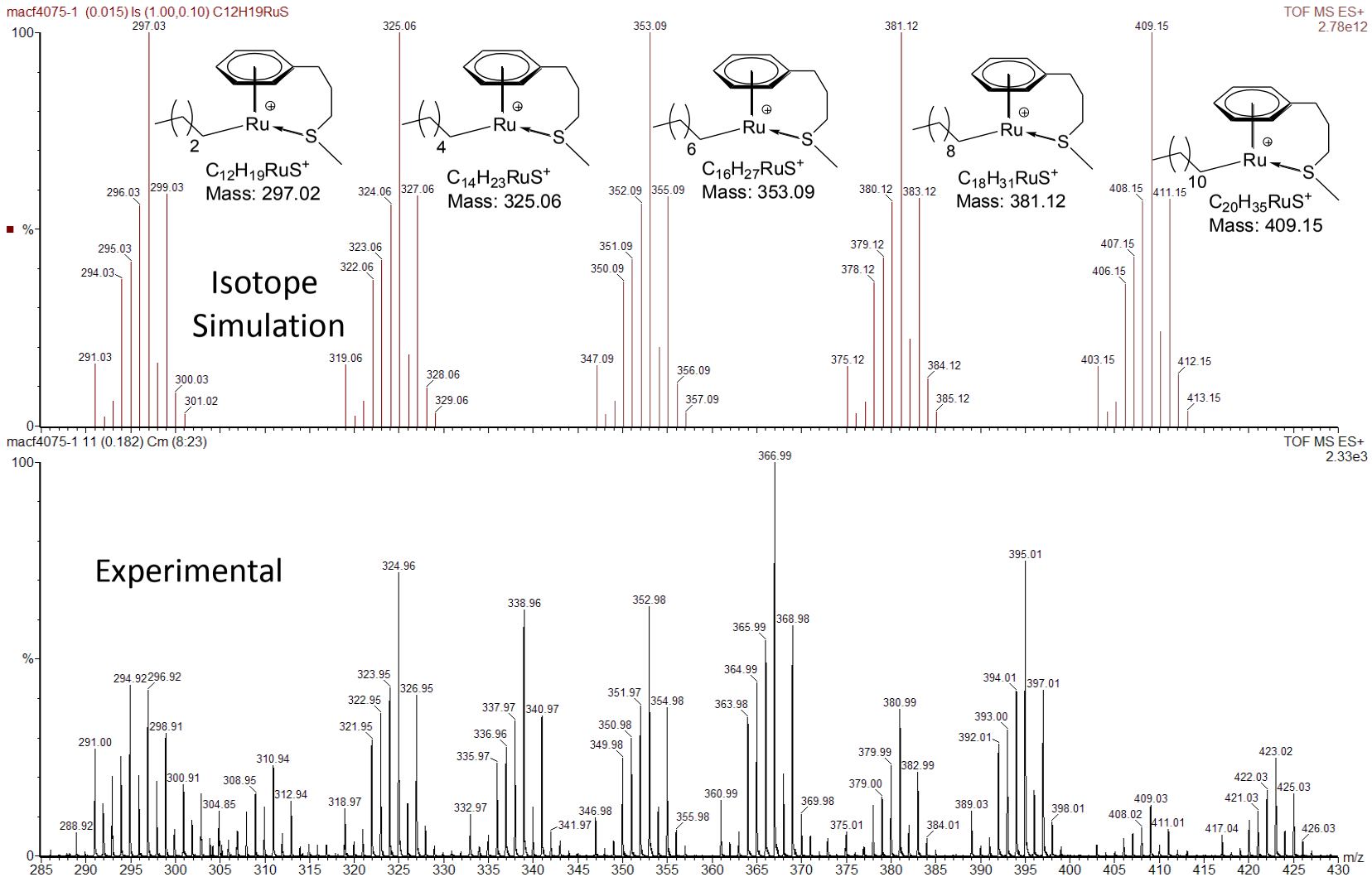

Figure 2.35. ESI-MS of ethylene oligomers bound to cationic Ru center formed by ethylene insertion after chain transfer (oligomers with even number of carbons). Comparison between isotope modeling (top) and experimental data (bottom).

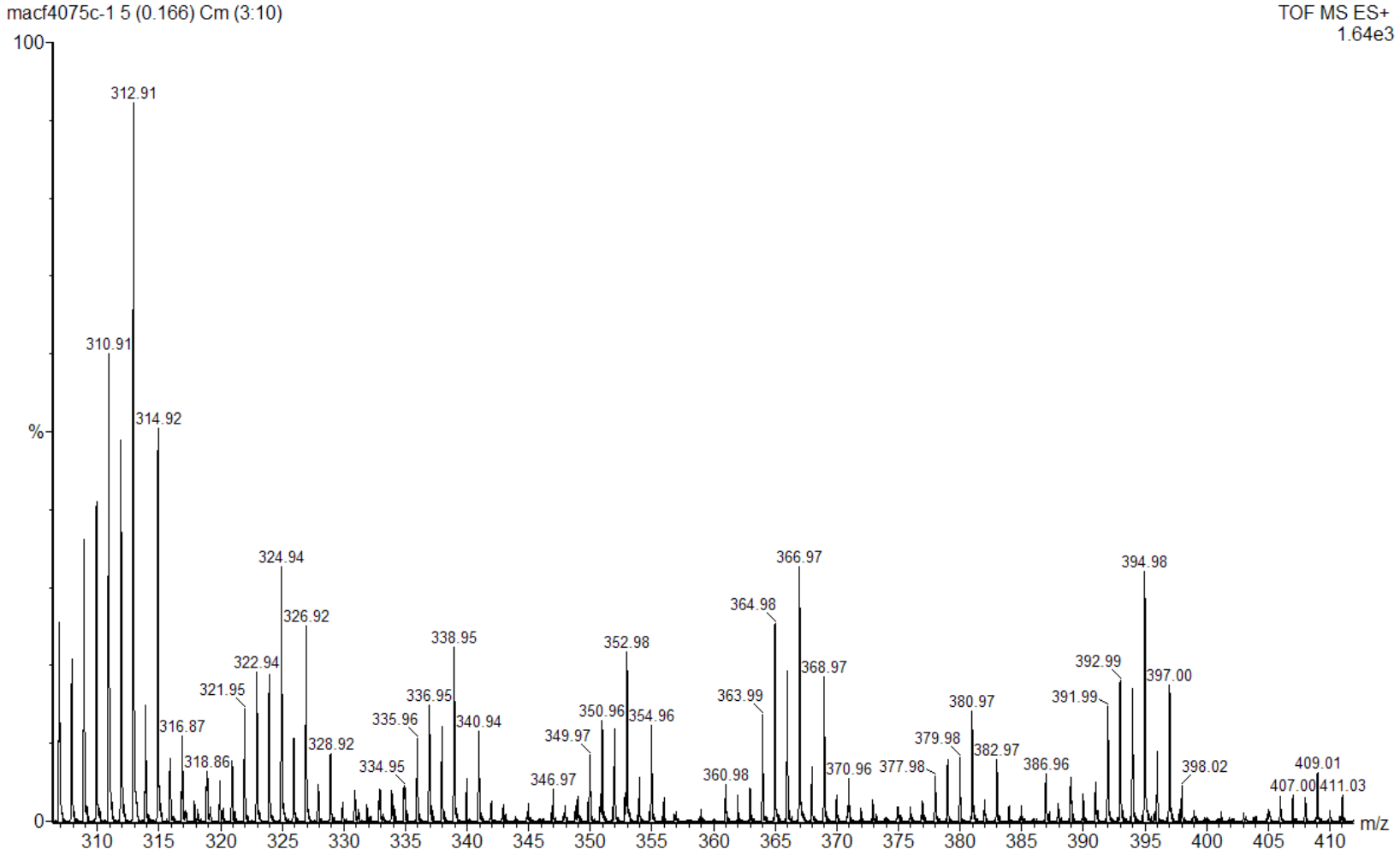

Figure 2.36. ESI-MS spectrum of ethylene oligomers bound to cationic Ru center formed *in situ* with **2.3**/$AlMe_2Cl$ system.

2.5 References

(1) *Topics in Organometallic Chemistry*; Springer: Berlin/Heidelberg, 2009; Vol. 29.
(2) *Organometallic Catalysts and Olefin Polymerization*; Springer: Berlin, 2009.
(3) Johnson, L. K.; Killian, C. M.; Brookhart, M. *J. Am. Chem. Soc.* **1995**, *117*, 6414-6415.
(4) Johnson, L. K.; Mecking, S.; Brookhart, M. *J. Am. Chem. Soc.* **1996**, *118*, 267-268.
(5) Svejda, S. A.; Johnson, L. K.; Brookhart, M. *J. Am. Chem. Soc.* **1999**, *121*, 10634-10635.
(6) Drent, E.; van Dijk, R.; van Ginkel, R.; van Oort, B.; Pugh, R. I. *Chem. Commun.* **2002**, 744-745.
(7) Mecking, S.; Johnson, L. K.; Wang, L.; Brookhart, M. *J. Am. Chem. Soc.* **1998**, *120*, 888-899.
(8) Boffa, L. S.; Novak, B. M. *Chem. Rev.* **2000**, *100*, 1479-1494.
(9) Ittel, S. D.; Johnson, L. K.; Brookhart, M. *Chem. Rev.* **2000**, *100*, 1169-1203.
(10) Carrow, B. P.; Nozaki, K. *J. Am. Chem. Soc.* **2012**, *134*, 8802-8805.
(11) Nakamura, A.; Ito, S.; Nozaki, K. *Chem. Rev.* **2009**, *109*, 5215-5244.
(12) Rose, J. M.; Cherian, A. E.; Coates, G. W. *J. Am. Chem. Soc.* **2006**, *128*, 4186-4187.
(13) Berkefeld, A.; Drexler, M.; Möller, H. M.; Mecking, S. *J. Am. Chem. Soc.* **2009**, *131*, 12613-12622.
(14) Guironnet, D.; Caporaso, L.; Neuwald, B.; Göttker-Schnetmann, I.; Cavallo, L.; Mecking, S. *J. Am. Chem. Soc.* **2010**, *132*, 4418-4426.
(15) Berkefeld, A.; Mecking, S. *Angew. Chem. Int. Ed.* **2008**, *47*, 2538-2542.
(16) Ito, S.; Kanazawa, M.; Munakata, K.; Kuroda, J.-i.; Okumura, Y.; Nozaki, K. *J. Am. Chem. Soc.* **2011**, *133*, 1232-1235.
(17) Kochi, T.; Noda, S.; Yoshimura, K.; Nozaki, K. *J. Am. Chem. Soc.* **2007**, *129*, 8948-8949.
(18) Luo, S.; Vela, J.; Lief, G. R.; Jordan, R. F. *J. Am. Chem. Soc.* **2007**, *129*, 8946-8947.
(19) Weng, W.; Shen, Z.; Jordan, R. F. *J. Am. Chem. Soc.* **2007**, *129*, 15450-15451.
(20) Wu, F.; Foley, S. R.; Burns, C. T.; Jordan, R. F. *J. Am. Chem. Soc.* **2005**, *127*, 1841-1853.
(21) Anselment, T. M. J.; Wichmann, C.; Anderson, C. E.; Herdtweck, E.; Rieger, B. *Organometallics* **2011**, *30*, 6602-6611.
(22) Camacho, D. H.; Salo, E. V.; Ziller, J. W.; Guan, Z. *Angew. Chem. Int. Ed.* **2004**, *43*, 1821-1825.
(23) Leung, D. H.; Ziller, J. W.; Guan, Z. *J. Am. Chem. Soc.* **2008**, *130*, 7538-7539.
(24) Noyori, R.; Takaya, H. *Acc. Chem. Res.* **1990**, *23*, 345-350.
(25) Grubbs, R. H.; Miller, S. J.; Fu, G. C. *Acc. Chem. Res.* **1995**, *28*, 446-452.
(26) Trnka, T. M.; Grubbs, R. H. *Acc. Chem. Res.* **2001**, *34*, 18-29.
(27) Ueda, J.; Matsuyama, M.; Kamigaito, M.; Sawamoto, M. *Macromolecules* **1998**, *31*, 557-562.
(28) James, B. R.; Markham, L. D. *J. Catal.* **1972**, *27*, 442-451.
(29) Komiya, S.; Yamamoto, A.; Ikeda, S. *Bull. Chem. Soc. Jpn.* **1975**, *48*, 101-107.
(30) Nomura, K.; Warit, S.; Imanishi, Y. *Macromolecules* **1999**, *32*, 4732-4734.
(31) Nomura, K.; Sidokmai, W.; Imanishi, Y. *Bull. Chem. Soc. Jpn.* **2000**, *73*, 599-605.
(32) Dias, E. L.; Brookhart, M.; White, P. S. *Organometallics* **2000**, *19*, 4995-5004.
(33) Faller, J. W.; Chase, K. J. *Organometallics* **1995**, *14*, 1592-1600.

(34) Umezawa-Vizzini, K.; Lee, T. R. *Organometallics* **2004**, *23*, 1448-1452.
(35) Foley, N. A.; Lee, J. P.; Ke, Z.; Gunnoe, T. B.; Cundari, T. R. *Acc. Chem. Res.* **2009**, *42*, 585-597.
(36) Small, B. L.; Brookhart, M.; Bennett, A. M. A. *J. Am. Chem. Soc.* **1998**, *120*, 4049-4050.
(37) Britovsek, G. J. P.; Bruce, M.; Gibson, V. C.; Kimberley, B. S.; Maddox, P. J.; Mastroianni, S.; McTavish, S. J.; Redshaw, C.; Solan, G. A.; Strömberg, S.; White, A. J. P.; Williams, D. J. *J.Am. Chem. Soc.* **1999**, *121*, 8728-8740.
(38) Heyndrickx, W.; Occhipinti, G.; Minenkov, Y.; Jensen, V. R. *J. Mol. Catal. A: Chem.* **2010**, *324*, 64-74.
(39) Piche, L.; Daigle, J.-C.; Claverie, J. P. *Chem. Commun.* **2011**, *47*, 7836-7838.
(40) Umezawa-Vizzini, K.; Guzman-Jimenez, I. Y.; Whitmire, K. H.; Lee, T. R. *Organometallics* **2003**, *22*, 3059-3065.
(41) Abele, A.; Wursche, R.; Klinga, M.; Rieger, B. *J. Mol. Catal. A: Chem.* **2000**, *160*, 23-33.
(42) Therrien, B. *Coord. Chem. Rev.* **2009**, *253*, 493-519.
(43) Shevchenko, N. E.; Nenajdenko, V. G.; Balenkova, E. S. *Synthesis* **2003**, *2003*, 1191-1200.
(44) Birch, A. J. *Journal of the Chemical Society (Resumed)* **1944**, *0*, 430-436.
(45) Daugulis, O.; Brookhart, M.; White, P. S. *Organometallics* **2003**, *22*, 4699-4704.
(46) Brookhart, M.; Grant, B.; Volpe, A. F. *Organometallics* **1992**, *11*, 3920-3922.
(47) Jordan, R. F.; Bajgur, C. S.; Willett, R.; Scott, B. *J. Am. Chem. Soc.* **1986**, *108*, 7410-7411.
(48) *Polymeriz Materials Encyclopedia*; Taylor & Francis, 1996; Vol. 6.
(49) Chen, E. Y.-X.; Marks, T. J. *Chem. Rev.* **2000**, *100*, 1391-1434.
(50) Corker, J. M.; Evans, J. *J. Chem. Soc., Chem. Commun.* **1991**, 1104-1106.
(51) de Souza, C. G.; de Souza, R. F.; Bernardo-Gusmão, K. *Applied Catalysis A: General* **2007**, *325*, 87-90.
(52) Bryliakov, K. P.; Talsi, E. P.; Semikolenova, N. V.; Zakharov, V. A. *Organometallics* **2009**, *28*, 3225-3232.
(53) Evans, W. J.; Champagne, T. M.; Giarikos, D. G.; Ziller, J. W. *Organometallics* **2005**, *24*, 570-579.

2.5 Experimental Section

General. All organic synthesis and organometallic complexations were conducted under inert atmosphere by using standard Schlenk, vacuum, or glove box (N_2) techniques. Ethanol was degassed with N_2 prior to use. The strong acid $[H(Et_2O)_2]^+$ $[BArF]^-$ (where Ar'= 3,5-$(CF_3)_2C_6H_3$)) was synthesized following Brookhart's procedure.[1]

^{1}H NMR, ^{13}C-NMR, NOE, and 2D-NMR spectra were recorded on a 500 MHz Bruker Avance GN-500, CRYO-500, or a Bruker Avance 600 MHz (for some insertion studies) spectrometer. All NMR chemical shifts are reported as δ in parts per million (ppm). ^{1}H and ^{13}C NMR spectra are relative to residual solvent. Coupling constants are reported in Hz. Electrospray Ionization Mass Spectrometric analyses (ESI-MS) were obtained on a Waters Micromass LCT ESI-MS. ESI-MS spectra analysis and isotope pattern simulations were carried out with MassLynx Mass Spectrometry software. Elemental analysis was performed by Atlantic Microlab, Inc.

All reagents were used as received from commercial suppliers unless otherwise noted. Anhydrous solvents were passed through a column of activated alumina (type A2, size 12x32, Purify) under argon pressure. Deuterated solvents were purchased from Cambridge Isotope Laboratories and were placed over activated 4Å molecular sieves. CD_2Cl_2 was dried over CaH_2 and distilled. Ultrahigh pure grade ethylene gas was purchased from Praxair and used without further purification.

Polyethylene molecular weight (Mw and Mn) was determined by High Temperature Gel Permeation Chromatography (HT-GPC) with polystyrene standards. Branching was determined by ^{1}H-NMR and expressed as the number of Me's per 1000 carbons.[2]

General procedure for ethylene polymerization. A 600 mL autoclave was heated under high vacuum to 120 °C for two hours then twice purged with ethylene and cooled to 0ºC. Two Schlenk flasks of 50 and 100 mL respectively were kept in an oven overnight and introduced in the glove box. 100 mL of dry methylene chloride (DCM) solvent was measured. 10 mL of the solvent were used to dissolve the desired amount of complex **2.3** in the 50 mL flask. Another 10 mL were loaded into a syringe for later rising of the flask. The left 80 ml solution (DCM) was loaded with the desired amount of cocatalyst (1.0M solution of $AlMe_2Cl$ in Hexanes). The cocatalyst solution was then transferred into the reactor through cannula under inert atmosphere. The reactor was then filled with ethylene at 200 psi for 10 minutes. Solution of complex **2.3** was introduced through cannula under inert atmosphere and the flask was rinsed with the previously loaded syringe. Parr reactor was closed and pressurized and heated up to the desire values. Polymerization was quenched with a methanol-acidic solution (100 mL). Polyethylene was filtrated and washed with MeOH and acetone. Polyethylene was dried under high vacuum overnight.

Polymerizations with complex 2.4 ($[H(Et_2O)_2]^+$ $[BAr'_4]^-$) as activator). A 600 mL autoclave was heated under high vacuum to 120 °C for two hours then twice purged with ethylene and cooled to 0 ºC. A Schlenk flask (100 ml) was dried overnight and introduced in a glove box. The desired amount of complex **2.4** is measured from a stock solution in DCM and loaded into the 100 mL flask. The flask containing complex **2.4** is filled with DCM to complete a total volume of 100 mL. A 15 mL vial, previously dried overnight, is used to weight 1 equivalent of ($[H(Et_2O)_2]^+$ $[BAr'_4]^-$) and dissolved in a small amount of DCM (10 mL) and loaded in a 12 mL syringe. The solution containing complex **2.4** is taken out of the glove box and flushed with ethylene at -78 °C for 15 minutes. ($[H(Et_2O)_2]^+$

$[BAr'_4]^-$) solution in the above mention 12 mL syringe is added, this will make complex **2.5** in situ. Solution containing complex **2.5** is then loaded in the Parr reactor through cannula under ethylene atmosphere. Reactor is closed, pressurized with ethylene to the desired pressure, and heated up to the polymerization temperature. Polymerization is stopped by the addition of methanol (200ml). Polyethylene is purified by centrifuging at 8000 rpm for 10 minutes and dried overnight under high vacuum.

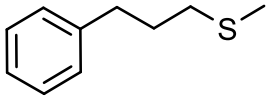

2.3a

Synthesis of methyl(3-phenylpropyl)sulfide (2.3a). Similar to previously reported procedure.[43] 5.0336 g of 2-methyl thiopseudourea sulfate (0.018 mol, 1.8 eq) and 3.92770g (0.07 mol, 7 eq) of potassium hydroxide were dissolved in MeOH (50 mL), in a 100 mL round bottom flask. After 30 minutes of stirring, 2.0000g of 1-(3-bromopropyl)benzene (0.01 mol, 1 eq) was charged through a needle into the solution. The reaction mixture was heated at reflux for 2 days and monitored by TLC. Yellowish oil was obtained. Purification by high vacuum distillation afforded a colorless oil Yield: quantitative. ^{1}H NMR (500 MHz, $CDCl_3$): δ 7.21 (m, 2H), 7.12 (m, 3H), 2.65 (t, *J* = 7.5 Hz, 2H), 2.44 (t, *J* = 7.0 Hz, 2H), 2.03 (s, 2H), 2.22 (s, 3H), 1.85 (tt, *J* = 7.0, 7.5 Hz, 2H). ^{13}C NMR (500 MHz, $CDCl_3$): δ 141.8, 128.7, 128.6, 126.1, 35.0, 33.8, 30.9, 15.7.

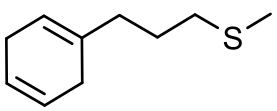

2.3b

Synthesis of (3-(cyclohexa-1,4-dienyl)propyl)(methyl)sulfide (2.3b). Birch Reduction.[44] A two neck 500 mL round bottom flask was flame dried, cooled down in a dry ice/acetone bath (-78 °C) which was kept all the time. 60 mL of degassed ethanol were added and 2.3420 g (0.014 mol, 1 eq) of **2.3a** was added. Gaseous NH_3 (~240 mL) was liquefied into the flask with the help of dry ice/acetone mixture in a cold finger apparatus, and stirred for 10 minutes. Metal Sodium 1.5100 g (0.070 mol, 5 eq) was added portion wise. A 500 mL saturated solution of Ammonium Chloride (NH_4Cl) is added to the reaction flask. Product was isolated by repeated extractions with Ether (3 x 500 mL) and drying of the organic phase over Magnesium Sulfate. High vacuum distillation afforded a colorless oil. Yield: 0.6408g, 39%. ^{1}H NMR (500 MHz, $CDCl_3$): δ 5.70 (b, 2H), 5.44 (b, 1H), 2.68 (m, 2H), 2.59 (m, 2H), 2.49 (t, *J* = 6.5 Hz, 2H), 2.10 (s, 3H), 2.07 (t, *J* = 7.5 Hz, 2H), 1.85 (tt, *J* = 6.5, 7.5 Hz, 2H). ^{13}C NMR (500 MHz, $CDCl_3$): δ 134.3, 124.5, 124.4, 119.1, 36.6, 36.2, 34.0, 29.0, 26.9, 15.7.

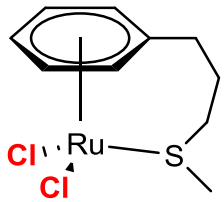

2.3

Synthesis of [Ru(η^6- Ph$(CH_2)_3$S$(CH_3)_2Cl_2$] (2.3). A total of 0.6408 g (0.0038 mol, 2 eq) of **2.3b** were added to degassed ethanol (10 mL) and stirred for 10 minutes. 0.4968 g (0.0019 mol, 1 eq) of $RuCl_3(H_2O)_x$ were added to the solution (calculations with x=3). The mixture was heated under reflux for 5 hours. The solution was left to reach room temperature and filtered to obtain an orange powder. The solid was washed with ether and hexanes under filtration and dried *in vacuo*. Red crystals suitable for analysis were

obtained at 4°C from a solution in DCM/hexanes by slow diffusion. Yield: 0.5635 g, 87%. ^{1}H NMR (500 MHz, CD_2Cl_2, 298K): δ 6.03 (dd, 5.5, 5.5 Hz, 1H,), 5.00-5.40 (b, 2H), 5.20 (d, 5.5 Hz, 2H), 3.00-2.20 (b, 6H), 2.18 (s, 3H). ^{1}H NMR (500 MHz, CD_2Cl_2, 323K): δ 6.02 (dd, 5.0 Hz, 1H), 5.68 (b, 2H), 5.20 (d, 5.0 Hz, 2H), 2.70 (b, 2H), 2.60 (b, 2H), 2.40 (b, 2H), 2.22 (s, 3H). ^{1}H NMR (500 MHz, CD_2Cl_2, 203K): δ 6.05 (dd, 5.5, 6.0 Hz, 1H), 5.76 (dd, 5.5, 6.0 Hz, 1H), 5.66 (dd, 5.5, 5.5 Hz, 1H), 5.21 (d, 5.5 Hz, 1H), 5.18 (d, 5.5 Hz, 1H), 2.72-2.37 (m, 5H), 2.28 (m, 1H), 2.15 (s, 3H). ^{13}C NMR (500 MHz, CD_2Cl_2, 298K): δ 91.2, 89.6, 34.9, 30.5, 24.4, 18.6, carbon signals corresponding to carbons "E" and "F" are not seen due to slow inversion at 298K. ESI-MS (ESI+, CH_2Cl_2) *m/z* calcd for $C_{10}H_{14}Cl_2SRu$ $[M]^+$, 338.26; found $[M\text{-}Cl]^+$, 302.95. Elemental Analysis: Anal. Calcd for C10H14Cl2RuS: C, 35.51; H, 4.17; Cl, 20.96; Ru, 29.88; S, 9.48. Found: C, 35.74; H, 4.19; S, 9.82.

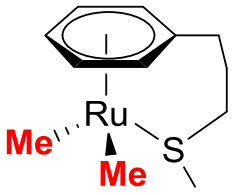

2.4

Synthesis of [Ru(η^6- Ph$(CH_2)_3$S$(CH_3)_2(CH_3)_2$] (2.4). A total of 0.2000 g (0.591 mmol, 1 eq) of **2.3** were suspended on 20ml of THF (in glove box) sonicated and stirred for 10 minutes. Outside glove box the solution was cooled down to -78°C. MeLi was added from a 1.6M solution in ether 0.94 ml (1.5 mmol, 2.5 eq). MeLi solution was added through needle dropwise. Solution was allowed to reach 10°C but not higher. Solution turns dark red when it reaches 10°C and then it is dried under high vacuum to eliminate THF keeping temperature under 10°C. Flask was introduced in the glove box and red dark solid was dissolved in ether. Ether solution was filtrated through celite and Florisyl (plug). Drying of

solution afforded yellow crystalline material. Golden crystals suitable for analysis were obtained from a DCM solution by slow evaporation. Complex **2.4** is very unstable and must be kept under inert atmosphere. Yield: 0.0352 g, 20%. ^{1}H NMR (500 MHz, CD_2Cl_2, 183K): δ 5.10 (b, 1H,), 4.99 (b, 1H), 4.95 (b, 1H), 4.85 (b, 1H), 4.23 (b, 1H). 2.80 (d, 7.0 Hz, 1H), 2.56 (m, 1H), 1.97 (s, 3H), 1.95-1.58 (m, 6H), -0.17 (s, 3H), -0.27 (s, 3H). ^{13}C NMR (500 MHz, $CDCl_3$, 183K): δ 95.3, 92.0, 91.4, 84.1, 82.4, 72.6, 33.8, 30.9, 23.3, 21.9, -7.32, -9.89.HRMS (ESI+, CH_2Cl_2) *m/z* calcd for $C_{12}H_{20}SRu$ $[M]^+$, 297.42; found $[M\text{-}CH_3]^+$, 283.01.

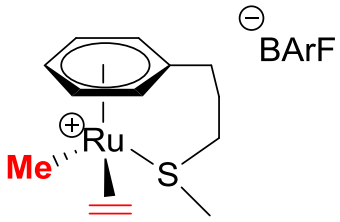

2.5

Synthesis of [Ru(η^6- Ph$(CH_2)_3$S$(CH_3)_2$(CH_2=CH_2)] (2.5). In a 2 mL vial 0.0300 g (0.101 mmol, 1 eq) of **2.4** were dissolved in 1ml of CD_2Cl_2 and transferred to a NMR tube. The solution was flushed with ethylene at 1atm to saturate solution and cooled down to -78°C. ($[H(Et_2O)_2]^+$ $[BAr'_4]^-$) 0.1006 g (0.101 mmol, 1 eq) were dissolved in 2ml of CD_2Cl_2. Addition of ($[H(Et_2O)_2]^+$ $[BAr'_4]^-$) solution was added through needle to complex **2.4** solution at -78°C. This solution is used for complex characterization and insertion studies. Two isomers are formed as depicted on the scheme above, reported only the peaks for the major compound. Poor stability forbids complex isolation and needs to be prepared in-situ for NMR or polymerization studies. NMR (500 MHz, CD_2Cl_2, 183K): δ 6.08 (dd, 5.5, 5.5 Hz, 1H), 6.00 (d, 5.5 Hz, 1H), 5.74 (d, 5.5 Hz, 1H), 5.51 (dd, 5.5, 5.5 Hz, 1H), 4.78 (dd, 5.5, 5.5 Hz, 1H), 3.89 (m, 1H), 3.14 (d, 6.0 Hz, 1H), 2.76 (dd, 5.5, 12.5 Hz 1H), 2.36-1.72 (m, 7H), 1.83 (s, 3H). ^{13}C NMR (500 MHz, $CDCl_3$, 183K): δ157.6, 105.7, 100.7, 93.9, 89.1, 86.8, 53.6, 31.8,

29.5, 20.8, 20.5, -10.1. HRMS (ESI+, CH_2Cl_2) *m/z* calcd for $C_{15}H_{26}SRu$ $[M]^+$, 339.5; found $[M]^+$, 339.07.

X-ray Data Collection, Structure Solution and Refinement for $RuCl_2(Ph(CH_3)_3SCH_3)$ (2.3). A red crystal of approximate dimensions 0.23 x 0.25 x 0.33 mm was mounted on a glass fiber and transferred to a Bruker SMART APEX II diffractometer. The APEX2[5] program package was used to determine the unit-cell parameters and for data collection (10 sec/frame scan time for a sphere of diffraction data). The raw frame data was processed using SAINT[6] and SADABS[7] to yield the reflection data file. Subsequent calculations were carried out using the SHELXTL[8] program. The diffraction symmetry was 2/*m* and the systematic absences were consistent with the monoclinic space group $P2_1/n$ that was later determined to be correct.

The structure was solved by direct methods and refined on F^2 by full-matrix least-squares techniques. The analytical scattering factors[9] for neutral atoms were used throughout the analysis. Hydrogen atoms were located from a difference-Fourier map and refined (x,y,z and U_{iso}).

At convergence, wR2 = 0.0413 and Goof = 1.090 for 183 variables refined against 2627 data (0.74Å), R1 = 0.0159 for those 2580 data with $I > 2.0\sigma(I)$.

Table 2.2. Crystal data and structure refinement for **2.3**.

Identification code	zg29 (Miguel Camacho)	
Empirical formula	C_{10} H_{14} Cl_2 Ru S	
Formula weight	338.24	
Temperature	143(2) K	
Wavelength	0.71073 Å	
Crystal system	Monoclinic	
Space group	$P2_1/n$	
Unit cell dimensions	a = 7.0069(4) Å	α= 90°.
	b = 12.8404(7) Å	β= 92.9276(5)°.
	c = 12.4298(7) Å	γ = 90°.
Volume	1116.87(11) $Å^3$	
Z	4	
Density (calculated)	2.012 Mg/m^3	
Absorption coefficient	2.024 mm^{-1}	
F(000)	672	
Crystal color	red	
Crystal size	0.33 x 0.25 x 0.23 mm^3	
Theta range for data collection	2.28 to 28.56°	
Index ranges	$-8 \le h \le 8$, $-16 \le k \le 17$, $-16 \le l \le 15$	
Reflections collected	12519	
Independent reflections	2627 [R(int) = 0.0185]	
Completeness to theta = 25.50°	100.0 %	
Absorption correction	Numerical	
Max. and min. transmission	0.6521 and 0.5521	
Refinement method	Full-matrix least-squares on F^2	
Data / restraints / parameters	2627 / 0 / 183	
Goodness-of-fit on F^2	1.090	
Final R indices [I>2sigma(I) = 2580 data]	R1 = 0.0159, wR2 = 0.0410	
R indices (all data, 0.74Å)	R1 = 0.0163, wR2 = 0.0413	
Largest diff. peak and hole	0.437 and -0.464 e.$Å^{-3}$	

Table 2.3. Atomic coordinates ($x10^4$) and equivalent isotropic displacement parameters ($Å^2 x\ 10^3$) for **2.3**. U(eq) is defined as one third of the trace of the orthogonalized U^{ij} tensor.

	x	y	z	U(eq)
Ru(1)	1801(1)	1824(1)	8379(1)	9(1)
Cl(1)	616(1)	3575(1)	8492(1)	17(1)
Cl(2)	4904(1)	2585(1)	8110(1)	17(1)
S(1)	1327(1)	2126(1)	6506(1)	14(1)
C(1)	-594(2)	1208(1)	9225(1)	14(1)
C(2)	903(2)	1445(1)	10010(1)	15(1)
C(3)	2741(2)	1056(1)	9894(1)	16(1)
C(4)	3107(2)	397(1)	9002(1)	15(1)
C(5)	1616(2)	121(1)	8255(1)	14(1)
C(6)	-264(2)	539(1)	8354(1)	13(1)
C(7)	-1848(2)	290(1)	7531(1)	16(1)
C(8)	-1371(2)	449(1)	6357(1)	18(1)
C(9)	-971(2)	1576(1)	6065(1)	19(1)
C(10)	2926(3)	1292(1)	5816(1)	21(1)

Table 2.4. Bond lengths [Å] and angles [°] for **2.3**.

Ru(1)-Cnt	1.670
Ru(1)-C(4)	2.1729(14)
Ru(1)-C(1)	2.1738(14)
Ru(1)-C(6)	2.1941(14)
Ru(1)-C(5)	2.1952(15)
Ru(1)-C(3)	2.1975(15)
Ru(1)-C(2)	2.2073(14)
Ru(1)-S(1)	2.3670(4)
Ru(1)-Cl(1)	2.4032(4)
Ru(1)-Cl(2)	2.4228(4)
S(1)-C(10)	1.7987(17)
S(1)-C(9)	1.8165(17)
C(1)-C(6)	1.411(2)
C(1)-C(2)	1.428(2)
C(2)-C(3)	1.396(2)
C(3)-C(4)	1.428(2)
C(4)-C(5)	1.408(2)
C(5)-C(6)	1.433(2)
C(6)-C(7)	1.505(2)
C(7)-C(8)	1.527(2)
C(8)-C(9)	1.522(2)
Cnt-Ru(1)-Cl(1)	128.2
Cnt-Ru(1)-Cl(2)	129.0
Cnt-Ru(1)-S(1)	130.5
C(4)-Ru(1)-C(1)	80.94(6)
C(4)-Ru(1)-C(6)	68.67(6)
C(1)-Ru(1)-C(6)	37.69(5)
C(4)-Ru(1)-C(5)	37.59(5)
C(1)-Ru(1)-C(5)	68.14(5)
C(6)-Ru(1)-C(5)	38.12(5)
C(4)-Ru(1)-C(3)	38.15(6)
C(1)-Ru(1)-C(3)	68.11(6)
C(6)-Ru(1)-C(3)	80.97(6)
C(5)-Ru(1)-C(3)	68.12(6)

C(4)-Ru(1)-C(2)	67.74(6)
C(1)-Ru(1)-C(2)	38.03(5)
C(6)-Ru(1)-C(2)	68.18(5)
C(5)-Ru(1)-C(2)	79.99(5)
C(3)-Ru(1)-C(2)	36.94(6)
C(4)-Ru(1)-S(1)	121.62(4)
C(1)-Ru(1)-S(1)	117.54(4)
C(6)-Ru(1)-S(1)	92.87(4)
C(5)-Ru(1)-S(1)	95.12(4)
C(3)-Ru(1)-S(1)	159.66(4)
C(2)-Ru(1)-S(1)	155.12(4)
C(4)-Ru(1)-Cl(1)	155.28(4)
C(1)-Ru(1)-Cl(1)	91.98(4)
C(6)-Ru(1)-Cl(1)	118.38(4)
C(5)-Ru(1)-Cl(1)	156.44(4)
C(3)-Ru(1)-Cl(1)	117.33(4)
C(2)-Ru(1)-Cl(1)	92.14(4)
S(1)-Ru(1)-Cl(1)	82.683(13)
C(4)-Ru(1)-Cl(2)	91.42(4)
C(1)-Ru(1)-Cl(2)	159.03(4)
C(6)-Ru(1)-Cl(2)	153.82(4)
C(5)-Ru(1)-Cl(2)	116.25(4)
C(3)-Ru(1)-Cl(2)	93.87(4)
C(2)-Ru(1)-Cl(2)	121.05(4)
S(1)-Ru(1)-Cl(2)	83.103(13)
Cl(1)-Ru(1)-Cl(2)	86.879(13)
C(10)-S(1)-C(9)	100.89(8)
C(10)-S(1)-Ru(1)	108.14(6)
C(9)-S(1)-Ru(1)	108.09(5)
C(6)-C(1)-C(2)	120.70(13)
C(6)-C(1)-Ru(1)	71.94(8)
C(2)-C(1)-Ru(1)	72.26(8)
C(3)-C(2)-C(1)	120.22(14)
C(3)-C(2)-Ru(1)	71.14(9)
C(1)-C(2)-Ru(1)	69.71(8)
C(2)-C(3)-C(4)	119.65(14)

C(2)-C(3)-Ru(1)	71.91(8)
C(4)-C(3)-Ru(1)	69.99(8)
C(5)-C(4)-C(3)	120.32(14)
C(5)-C(4)-Ru(1)	72.06(8)
C(3)-C(4)-Ru(1)	71.86(8)
C(4)-C(5)-C(6)	120.24(13)
C(4)-C(5)-Ru(1)	70.34(9)
C(6)-C(5)-Ru(1)	70.90(8)
C(1)-C(6)-C(5)	118.75(13)
C(1)-C(6)-C(7)	120.46(13)
C(5)-C(6)-C(7)	120.77(13)
C(1)-C(6)-Ru(1)	70.37(8)
C(5)-C(6)-Ru(1)	70.98(8)
C(7)-C(6)-Ru(1)	129.22(10)
C(6)-C(7)-C(8)	115.54(12)
C(9)-C(8)-C(7)	114.03(13)
C(8)-C(9)-S(1)	117.99(11)

Table 2.5. Anisotropic displacement parameters ($Å^2$x 10^3) for **2.3**. The anisotropic displacement factor exponent takes the form: $-2\pi^2[h^2 a^{*2} U^{11} + ... + 2 h k a^* b^* U^{12}]$

	U^{11}	U^{22}	U^{33}	U^{23}	U^{13}	U^{12}
Ru(1)	10(1)	8(1)	10(1)	1(1)	1(1)	0(1)
Cl(1)	19(1)	10(1)	22(1)	2(1)	8(1)	3(1)
Cl(2)	12(1)	16(1)	23(1)	1(1)	2(1)	-2(1)
S(1)	20(1)	12(1)	11(1)	1(1)	1(1)	-1(1)
C(1)	15(1)	12(1)	14(1)	2(1)	4(1)	-1(1)
C(2)	23(1)	11(1)	11(1)	1(1)	2(1)	-2(1)
C(3)	21(1)	13(1)	15(1)	4(1)	-3(1)	-1(1)
C(4)	15(1)	12(1)	18(1)	5(1)	1(1)	3(1)
C(5)	18(1)	9(1)	14(1)	2(1)	4(1)	1(1)
C(6)	16(1)	10(1)	13(1)	2(1)	2(1)	-2(1)
C(7)	14(1)	16(1)	17(1)	-2(1)	0(1)	-4(1)
C(8)	19(1)	18(1)	15(1)	-3(1)	-2(1)	-3(1)
C(9)	22(1)	19(1)	14(1)	2(1)	-5(1)	0(1)
C(10)	28(1)	20(1)	17(1)	-3(1)	10(1)	-2(1)

Table 2.6. Hydrogen coordinates (x 10^4) and isotropic displacement parameters ($Å^2$x 10 ^{3}) for **2.3**.

	x	y	z	U(eq)
H(1)	-1790(30)	1526(16)	9281(16)	21(5)
H(2)	640(30)	1907(15)	10567(17)	18(5)
H(3)	3740(30)	1282(17)	10339(17)	24(5)
H(4)	4270(30)	180(16)	8892(16)	18(5)
H(5)	1920(30)	-304(16)	7667(15)	18(5)
H(7A)	-2210(30)	-444(16)	7629(15)	18(5)
H(7B)	-2940(30)	700(15)	7670(15)	18(5)
H(8A)	-370(30)	16(15)	6164(15)	16(4)
H(8B)	-2510(30)	246(16)	5935(16)	19(5)
H(9A)	-1890(30)	2024(17)	6390(17)	21(5)
H(9B)	-1000(30)	1665(16)	5308(18)	24(5)
H(10A)	2770(30)	1425(18)	5080(19)	29(5)
H(10B)	2710(30)	580(17)	5969(16)	23(5)
H(10C)	4160(30)	1470(18)	6075(18)	30(6)

Table 2.7. Torsion angles [°] for **2.3**.

C(4)-Ru(1)-S(1)-C(10)	-20.74(8)
C(1)-Ru(1)-S(1)-C(10)	-117.19(7)
C(6)-Ru(1)-S(1)-C(10)	-87.36(7)
C(5)-Ru(1)-S(1)-C(10)	-49.21(7)
C(3)-Ru(1)-S(1)-C(10)	-15.83(14)
C(2)-Ru(1)-S(1)-C(10)	-126.42(11)
Cl(1)-Ru(1)-S(1)-C(10)	154.39(6)
Cl(2)-Ru(1)-S(1)-C(10)	66.67(6)
C(4)-Ru(1)-S(1)-C(9)	87.70(8)
C(1)-Ru(1)-S(1)-C(9)	-8.76(7)
C(6)-Ru(1)-S(1)-C(9)	21.07(7)
C(5)-Ru(1)-S(1)-C(9)	59.22(7)
C(3)-Ru(1)-S(1)-C(9)	92.60(13)
C(2)-Ru(1)-S(1)-C(9)	-17.99(11)
Cl(1)-Ru(1)-S(1)-C(9)	-97.18(6)
Cl(2)-Ru(1)-S(1)-C(9)	175.10(6)
C(4)-Ru(1)-C(1)-C(6)	-66.67(9)
C(5)-Ru(1)-C(1)-C(6)	-29.86(8)
C(3)-Ru(1)-C(1)-C(6)	-104.10(9)
C(2)-Ru(1)-C(1)-C(6)	-131.92(13)
S(1)-Ru(1)-C(1)-C(6)	54.36(9)
Cl(1)-Ru(1)-C(1)-C(6)	137.14(8)
Cl(2)-Ru(1)-C(1)-C(6)	-136.41(10)
C(4)-Ru(1)-C(1)-C(2)	65.25(9)
C(6)-Ru(1)-C(1)-C(2)	131.92(13)
C(5)-Ru(1)-C(1)-C(2)	102.07(9)
C(3)-Ru(1)-C(1)-C(2)	27.83(8)
S(1)-Ru(1)-C(1)-C(2)	-173.72(7)
Cl(1)-Ru(1)-C(1)-C(2)	-90.94(8)
Cl(2)-Ru(1)-C(1)-C(2)	-4.49(16)
C(6)-C(1)-C(2)-C(3)	3.2(2)
Ru(1)-C(1)-C(2)-C(3)	-52.12(12)
C(6)-C(1)-C(2)-Ru(1)	55.35(12)
C(4)-Ru(1)-C(2)-C(3)	29.59(9)

C(1)-Ru(1)-C(2)-C(3)	133.89(13)
C(6)-Ru(1)-C(2)-C(3)	104.55(10)
C(5)-Ru(1)-C(2)-C(3)	66.73(9)
S(1)-Ru(1)-C(2)-C(3)	147.23(9)
Cl(1)-Ru(1)-C(2)-C(3)	-135.62(8)
Cl(2)-Ru(1)-C(2)-C(3)	-47.98(10)
C(4)-Ru(1)-C(2)-C(1)	-104.30(9)
C(6)-Ru(1)-C(2)-C(1)	-29.34(8)
C(5)-Ru(1)-C(2)-C(1)	-67.16(9)
C(3)-Ru(1)-C(2)-C(1)	-133.89(13)
S(1)-Ru(1)-C(2)-C(1)	13.34(15)
Cl(1)-Ru(1)-C(2)-C(1)	90.48(8)
Cl(2)-Ru(1)-C(2)-C(1)	178.13(7)
C(1)-C(2)-C(3)-C(4)	-1.7(2)
Ru(1)-C(2)-C(3)-C(4)	-53.12(12)
C(1)-C(2)-C(3)-Ru(1)	51.47(12)
C(4)-Ru(1)-C(3)-C(2)	-132.28(13)
C(1)-Ru(1)-C(3)-C(2)	-28.58(9)
C(6)-Ru(1)-C(3)-C(2)	-65.48(9)
C(5)-Ru(1)-C(3)-C(2)	-102.86(10)
S(1)-Ru(1)-C(3)-C(2)	-139.06(11)
Cl(1)-Ru(1)-C(3)-C(2)	51.88(9)
Cl(2)-Ru(1)-C(3)-C(2)	140.36(8)
C(1)-Ru(1)-C(3)-C(4)	103.70(10)
C(6)-Ru(1)-C(3)-C(4)	66.80(9)
C(5)-Ru(1)-C(3)-C(4)	29.43(9)
C(2)-Ru(1)-C(3)-C(4)	132.28(13)
S(1)-Ru(1)-C(3)-C(4)	-6.77(18)
Cl(1)-Ru(1)-C(3)-C(4)	-175.84(7)
Cl(2)-Ru(1)-C(3)-C(4)	-87.35(9)
C(2)-C(3)-C(4)-C(5)	-1.4(2)
Ru(1)-C(3)-C(4)-C(5)	-55.45(12)
C(2)-C(3)-C(4)-Ru(1)	54.02(12)
C(1)-Ru(1)-C(4)-C(5)	65.74(9)
C(6)-Ru(1)-C(4)-C(5)	28.68(8)
C(3)-Ru(1)-C(4)-C(5)	131.64(13)

C(2)-Ru(1)-C(4)-C(5)	102.93(9)
S(1)-Ru(1)-C(4)-C(5)	-51.11(9)
Cl(1)-Ru(1)-C(4)-C(5)	140.51(9)
Cl(2)-Ru(1)-C(4)-C(5)	-133.88(8)
C(1)-Ru(1)-C(4)-C(3)	-65.91(9)
C(6)-Ru(1)-C(4)-C(3)	-102.97(10)
C(5)-Ru(1)-C(4)-C(3)	-131.65(13)
C(2)-Ru(1)-C(4)-C(3)	-28.72(9)
S(1)-Ru(1)-C(4)-C(3)	177.24(7)
Cl(1)-Ru(1)-C(4)-C(3)	8.86(16)
Cl(2)-Ru(1)-C(4)-C(3)	94.47(9)
C(3)-C(4)-C(5)-C(6)	3.0(2)
Ru(1)-C(4)-C(5)-C(6)	-52.38(12)
C(3)-C(4)-C(5)-Ru(1)	55.35(12)
C(1)-Ru(1)-C(5)-C(4)	-104.06(9)
C(6)-Ru(1)-C(5)-C(4)	-133.60(12)
C(3)-Ru(1)-C(5)-C(4)	-29.83(9)
C(2)-Ru(1)-C(5)-C(4)	-66.34(9)
S(1)-Ru(1)-C(5)-C(4)	138.28(8)
Cl(1)-Ru(1)-C(5)-C(4)	-138.29(9)
Cl(2)-Ru(1)-C(5)-C(4)	53.46(9)
C(4)-Ru(1)-C(5)-C(6)	133.60(12)
C(1)-Ru(1)-C(5)-C(6)	29.54(8)
C(3)-Ru(1)-C(5)-C(6)	103.77(9)
C(2)-Ru(1)-C(5)-C(6)	67.26(9)
S(1)-Ru(1)-C(5)-C(6)	-88.12(8)
Cl(1)-Ru(1)-C(5)-C(6)	-4.69(15)
Cl(2)-Ru(1)-C(5)-C(6)	-172.94(7)
C(2)-C(1)-C(6)-C(5)	-1.7(2)
Ru(1)-C(1)-C(6)-C(5)	53.82(11)
C(2)-C(1)-C(6)-C(7)	179.81(13)
Ru(1)-C(1)-C(6)-C(7)	-124.68(13)
C(2)-C(1)-C(6)-Ru(1)	-55.50(12)
C(4)-C(5)-C(6)-C(1)	-1.4(2)
Ru(1)-C(5)-C(6)-C(1)	-53.53(11)
C(4)-C(5)-C(6)-C(7)	177.10(13)

Ru(1)-C(5)-C(6)-C(7)	124.97(13)
C(4)-C(5)-C(6)-Ru(1)	52.13(12)
C(4)-Ru(1)-C(6)-C(1)	103.23(9)
C(5)-Ru(1)-C(6)-C(1)	131.54(12)
C(3)-Ru(1)-C(6)-C(1)	65.68(9)
C(2)-Ru(1)-C(6)-C(1)	29.59(8)
S(1)-Ru(1)-C(6)-C(1)	-133.82(8)
Cl(1)-Ru(1)-C(6)-C(1)	-50.59(9)
Cl(2)-Ru(1)-C(6)-C(1)	146.00(8)
C(4)-Ru(1)-C(6)-C(5)	-28.31(8)
C(1)-Ru(1)-C(6)-C(5)	-131.54(12)
C(3)-Ru(1)-C(6)-C(5)	-65.86(9)
C(2)-Ru(1)-C(6)-C(5)	-101.95(9)
S(1)-Ru(1)-C(6)-C(5)	94.64(8)
Cl(1)-Ru(1)-C(6)-C(5)	177.87(7)
Cl(2)-Ru(1)-C(6)-C(5)	14.47(14)
C(4)-Ru(1)-C(6)-C(7)	-142.96(14)
C(1)-Ru(1)-C(6)-C(7)	113.81(16)
C(5)-Ru(1)-C(6)-C(7)	-114.65(16)
C(3)-Ru(1)-C(6)-C(7)	179.49(14)
C(2)-Ru(1)-C(6)-C(7)	143.40(14)
S(1)-Ru(1)-C(6)-C(7)	-20.01(13)
Cl(1)-Ru(1)-C(6)-C(7)	63.22(14)
Cl(2)-Ru(1)-C(6)-C(7)	-100.19(14)
C(1)-C(6)-C(7)-C(8)	128.62(15)
C(5)-C(6)-C(7)-C(8)	-49.85(19)
Ru(1)-C(6)-C(7)-C(8)	39.94(19)
C(6)-C(7)-C(8)-C(9)	-64.58(18)
C(7)-C(8)-C(9)-S(1)	76.13(17)
C(10)-S(1)-C(9)-C(8)	61.47(14)
Ru(1)-S(1)-C(9)-C(8)	-51.88(13)

X-ray Data Collection, Structure Solution and Refinement for $Ru(CH_3)_2(Ph(CH_3)_3SCH_3)$ (2.4). A gold crystal of approximate dimensions 0.17 x 0.20 x 0.22 mm was mounted on a glass fiber and transferred to a Bruker SMART APEX II diffractometer. The APEX2[5] program package was used to determine the unit-cell parameters and for data collection (20 sec/frame scan time for a sphere of diffraction data). The raw frame data was processed using SAINT[6] and SADABS[7] to yield the reflection data file. Subsequent calculations were carried out using the SHELXTL[8] program. The diffraction symmetry was $2/m$ and the systematic absences were consistent with the monoclinic space group $P2_1/n$ that was later determined to be correct.

The structure was solved by direct methods and refined on F^2 by full-matrix least-squares techniques. The analytical scattering factors[9] for neutral atoms were used throughout the analysis. Hydrogen atoms were either located from a difference-Fourier map and refined (x,y,z and U_{iso}) or were included using a riding model.

At convergence, wR2 = 0.0422 and Goof = 1.092 for 196 variables refined against 2930 data (0.74Å), R1 = 0.0171 for those 2831 data with $I > 2.0\sigma(I)$.

Table 2.8. Crystal data and structure refinement for $Ru(CH_3)_2(Ph(CH_3)_3SCH_3)$ (**2.4**).

Empirical formula	C_{12} H_{20} Ru S	
Formula weight	297.41	
Temperature	88(2) K	
Wavelength	0.71073 Å	
Crystal system	Monoclinic	
Space group	$P2(_1)/n$	
Unit cell dimensions	a = 6.8375(3) Å	α= 90°.
	b = 13.5463(5) Å	β= 93.8780(4)°.
	c = 12.8712(5) Å	γ = 90°.
Volume	1189.44(8) $Å^3$	
Z	4	
Density (calculated)	1.661 Mg/m^3	
Absorption coefficient	1.454 mm^{-1}	
F(000)	608	
Crystal color	gold	
Crystal size	0.22 x 0.20 x 0.17 mm^3	
Theta range for data collection	2.19 to 28.77°	
Index ranges	$-9 \le h \le 9$, $-18 \le k \le 17$, $-16 \le l \le 17$	
Reflections collected	13876	
Independent reflections	2930 [R(int) = 0.0130]	
Completeness to theta = 25.50°	100.0 %	
Absorption correction	Numerical	
Max. and min. transmission	0.7944 and 0.7452	
Refinement method	Full-matrix least-squares on F^2	
Data / restraints / parameters	2930 / 0 / 196	
Goodness-of-fit on F^2	1.092	
Final R indices [I>2sigma(I) = 2831 data]	R1 = 0.0171, wR2 = 0.0418	
R indices (all data, 0.74Å)	R1 = 0.0179, wR2 = 0.0422	
Largest diff. peak and hole	0.731 and -0.339 $e.Å^{-3}$	

Table 2.9. Atomic coordinates (x 10^4) and equivalent isotropic displacement parameters ($Å^2$x 10^3) for $Ru(CH_3)_2(Ph(CH_3)_3SCH_3)$ (**2.4**). U(eq) is defined as one third of the trace of the orthogonalized U^{ij} tensor.

	x	y	z	U(eq)
Ru(1)	1673(1)	1825(1)	3405(1)	12(1)
S(1)	1114(1)	2045(1)	1623(1)	17(1)
C(1)	-721(3)	1172(1)	4264(1)	18(1)
C(2)	817(3)	1502(1)	4988(1)	19(1)
C(3)	2750(3)	1179(1)	4904(1)	20(1)
C(4)	3166(3)	491(1)	4105(1)	19(1)
C(5)	1660(3)	161(1)	3401(1)	18(1)
C(6)	-300(2)	521(1)	3451(1)	16(1)
C(7)	-1895(3)	209(1)	2649(1)	21(1)
C(8)	-1459(3)	375(1)	1508(1)	22(1)
C(9)	-1189(3)	1450(1)	1198(1)	22(1)
C(10)	2796(3)	1286(2)	950(2)	25(1)
C(11)	550(3)	3296(1)	3481(1)	21(1)
C(12)	4421(2)	2624(1)	3182(1)	14(1)

Table 2.10. Bond lengths [Å] and angles [°] for $Ru(CH_3)_2(Ph(CH_3)_3SCH_3)$ (**2.4**).

Ru(1)-Cnt	1.712
Ru(1)-C(11)	2.1411(17)
Ru(1)-C(3)	2.2004(16)
Ru(1)-C(2)	2.2016(17)
Ru(1)-C(12)	2.2041(16)
Ru(1)-C(1)	2.2197(16)
Ru(1)-C(6)	2.2253(16)
Ru(1)-C(4)	2.2351(16)
Ru(1)-C(5)	2.2532(17)
Ru(1)-S(1)	2.3187(4)
S(1)-C(10)	1.807(2)
S(1)-C(9)	1.8197(18)
C(1)-C(6)	1.412(2)
C(1)-C(2)	1.428(2)
C(2)-C(3)	1.403(3)
C(3)-C(4)	1.431(2)
C(4)-C(5)	1.398(2)
C(5)-C(6)	1.432(2)
C(6)-C(7)	1.510(2)
C(7)-C(8)	1.534(2)
C(8)-C(9)	1.525(3)
Cnt-Ru(1)-S(1)	131.1
Cnt-Ru(1)-C(11)	128.4
Cnt-Ru(1)-C(12)	130.3
C(11)-Ru(1)-C(3)	115.44(7)
C(11)-Ru(1)-C(2)	91.35(7)
C(3)-Ru(1)-C(2)	37.18(7)
C(11)-Ru(1)-C(12)	81.97(7)
C(3)-Ru(1)-C(12)	94.10(6)
C(2)-Ru(1)-C(12)	120.02(6)
C(11)-Ru(1)-C(1)	93.96(7)
C(3)-Ru(1)-C(1)	67.60(6)
C(2)-Ru(1)-C(1)	37.69(6)
C(12)-Ru(1)-C(1)	157.54(6)

C(11)-Ru(1)-C(6)	121.17(7)
C(3)-Ru(1)-C(6)	80.13(6)
C(2)-Ru(1)-C(6)	67.54(6)
C(12)-Ru(1)-C(6)	156.47(6)
C(1)-Ru(1)-C(6)	37.05(6)
C(11)-Ru(1)-C(4)	152.81(7)
C(3)-Ru(1)-C(4)	37.63(6)
C(2)-Ru(1)-C(4)	66.97(6)
C(12)-Ru(1)-C(4)	94.54(6)
C(1)-Ru(1)-C(4)	79.00(6)
C(6)-Ru(1)-C(4)	66.98(6)
C(11)-Ru(1)-C(5)	158.42(7)
C(3)-Ru(1)-C(5)	66.75(6)
C(2)-Ru(1)-C(5)	78.59(6)
C(12)-Ru(1)-C(5)	119.60(6)
C(1)-Ru(1)-C(5)	66.42(6)
C(6)-Ru(1)-C(5)	37.29(6)
C(4)-Ru(1)-C(5)	36.30(6)
C(11)-Ru(1)-S(1)	83.70(5)
C(3)-Ru(1)-S(1)	160.36(5)
C(2)-Ru(1)-S(1)	154.79(5)
C(12)-Ru(1)-S(1)	83.86(4)
C(1)-Ru(1)-S(1)	117.80(5)
C(6)-Ru(1)-S(1)	93.96(4)
C(4)-Ru(1)-S(1)	122.91(5)
C(5)-Ru(1)-S(1)	97.26(4)
C(10)-S(1)-C(9)	99.81(9)
C(10)-S(1)-Ru(1)	109.44(7)
C(9)-S(1)-Ru(1)	108.76(6)
C(6)-C(1)-C(2)	120.05(16)
C(6)-C(1)-Ru(1)	71.69(9)
C(2)-C(1)-Ru(1)	70.47(9)
C(3)-C(2)-C(1)	120.53(16)
C(3)-C(2)-Ru(1)	71.36(10)
C(1)-C(2)-Ru(1)	71.84(9)
C(2)-C(3)-C(4)	119.49(16)

C(2)-C(3)-Ru(1)	71.45(10)
C(4)-C(3)-Ru(1)	72.50(9)
C(5)-C(4)-C(3)	120.03(16)
C(5)-C(4)-Ru(1)	72.55(10)
C(3)-C(4)-Ru(1)	69.87(9)
C(4)-C(5)-C(6)	120.85(16)
C(4)-C(5)-Ru(1)	71.15(10)
C(6)-C(5)-Ru(1)	70.30(9)
C(1)-C(6)-C(5)	118.94(15)
C(1)-C(6)-C(7)	120.49(15)
C(5)-C(6)-C(7)	120.58(15)
C(1)-C(6)-Ru(1)	71.26(9)
C(5)-C(6)-Ru(1)	72.41(9)
C(7)-C(6)-Ru(1)	127.93(11)
C(6)-C(7)-C(8)	115.79(14)
C(9)-C(8)-C(7)	115.19(15)
C(8)-C(9)-S(1)	117.48(13)

Table 2.11. Torsion angles [°] for $Ru(CH_3)_2(Ph(CH_3)_3SCH_3)$ (**2.4**).

C(11)-Ru(1)-S(1)-C(10)	152.40(9)
C(3)-Ru(1)-S(1)-C(10)	-15.14(16)
C(2)-Ru(1)-S(1)-C(10)	-127.90(13)
C(12)-Ru(1)-S(1)-C(10)	69.84(8)
C(1)-Ru(1)-S(1)-C(10)	-116.43(9)
C(6)-Ru(1)-S(1)-C(10)	-86.64(8)
C(4)-Ru(1)-S(1)-C(10)	-21.60(9)
C(5)-Ru(1)-S(1)-C(10)	-49.31(8)
C(11)-Ru(1)-S(1)-C(9)	-99.50(9)
C(3)-Ru(1)-S(1)-C(9)	92.96(16)
C(2)-Ru(1)-S(1)-C(9)	-19.80(13)
C(12)-Ru(1)-S(1)-C(9)	177.93(8)
C(1)-Ru(1)-S(1)-C(9)	-8.34(9)
C(6)-Ru(1)-S(1)-C(9)	21.46(8)
C(4)-Ru(1)-S(1)-C(9)	86.49(9)
C(5)-Ru(1)-S(1)-C(9)	58.79(8)
C(11)-Ru(1)-C(1)-C(6)	140.30(10)
C(3)-Ru(1)-C(1)-C(6)	-103.78(11)
C(2)-Ru(1)-C(1)-C(6)	-132.62(15)
C(12)-Ru(1)-C(1)-C(6)	-141.17(14)
C(4)-Ru(1)-C(1)-C(6)	-66.20(10)
C(5)-Ru(1)-C(1)-C(6)	-30.39(9)
S(1)-Ru(1)-C(1)-C(6)	55.34(10)
C(11)-Ru(1)-C(1)-C(2)	-87.08(11)
C(3)-Ru(1)-C(1)-C(2)	28.84(10)
C(12)-Ru(1)-C(1)-C(2)	-8.6(2)
C(6)-Ru(1)-C(1)-C(2)	132.62(15)
C(4)-Ru(1)-C(1)-C(2)	66.42(10)
C(5)-Ru(1)-C(1)-C(2)	102.22(11)
S(1)-Ru(1)-C(1)-C(2)	-172.04(8)
C(6)-C(1)-C(2)-C(3)	-0.5(2)
Ru(1)-C(1)-C(2)-C(3)	-54.28(14)
C(6)-C(1)-C(2)-Ru(1)	53.81(14)
C(11)-Ru(1)-C(2)-C(3)	-132.83(11)

C(12)-Ru(1)-C(2)-C(3)	-51.32(12)
C(1)-Ru(1)-C(2)-C(3)	132.44(15)
C(6)-Ru(1)-C(2)-C(3)	103.77(11)
C(4)-Ru(1)-C(2)-C(3)	30.27(10)
C(5)-Ru(1)-C(2)-C(3)	66.40(11)
S(1)-Ru(1)-C(2)-C(3)	149.15(10)
C(11)-Ru(1)-C(2)-C(1)	94.73(11)
C(3)-Ru(1)-C(2)-C(1)	-132.44(15)
C(12)-Ru(1)-C(2)-C(1)	176.24(9)
C(6)-Ru(1)-C(2)-C(1)	-28.67(10)
C(4)-Ru(1)-C(2)-C(1)	-102.17(11)
C(5)-Ru(1)-C(2)-C(1)	-66.03(10)
S(1)-Ru(1)-C(2)-C(1)	16.71(17)
C(1)-C(2)-C(3)-C(4)	-1.9(2)
Ru(1)-C(2)-C(3)-C(4)	-56.36(14)
C(1)-C(2)-C(3)-Ru(1)	54.50(14)
C(11)-Ru(1)-C(3)-C(2)	54.28(12)
C(12)-Ru(1)-C(3)-C(2)	137.34(10)
C(1)-Ru(1)-C(3)-C(2)	-29.21(10)
C(6)-Ru(1)-C(3)-C(2)	-65.66(10)
C(4)-Ru(1)-C(3)-C(2)	-130.55(15)
C(5)-Ru(1)-C(3)-C(2)	-102.13(11)
S(1)-Ru(1)-C(3)-C(2)	-139.46(13)
C(11)-Ru(1)-C(3)-C(4)	-175.17(10)
C(2)-Ru(1)-C(3)-C(4)	130.55(15)
C(12)-Ru(1)-C(3)-C(4)	-92.11(10)
C(1)-Ru(1)-C(3)-C(4)	101.34(11)
C(6)-Ru(1)-C(3)-C(4)	64.89(10)
C(5)-Ru(1)-C(3)-C(4)	28.42(10)
S(1)-Ru(1)-C(3)-C(4)	-8.9(2)
C(2)-C(3)-C(4)-C(5)	1.4(2)
Ru(1)-C(3)-C(4)-C(5)	-54.50(14)
C(2)-C(3)-C(4)-Ru(1)	55.85(14)
C(11)-Ru(1)-C(4)-C(5)	141.95(15)
C(3)-Ru(1)-C(4)-C(5)	132.37(15)
C(2)-Ru(1)-C(4)-C(5)	102.44(11)

C(12)-Ru(1)-C(4)-C(5)	-136.79(10)
C(1)-Ru(1)-C(4)-C(5)	64.93(10)
C(6)-Ru(1)-C(4)-C(5)	28.13(10)
S(1)-Ru(1)-C(4)-C(5)	-51.18(11)
C(11)-Ru(1)-C(4)-C(3)	9.6(2)
C(2)-Ru(1)-C(4)-C(3)	-29.93(10)
C(12)-Ru(1)-C(4)-C(3)	90.84(11)
C(1)-Ru(1)-C(4)-C(3)	-67.44(11)
C(6)-Ru(1)-C(4)-C(3)	-104.24(11)
C(5)-Ru(1)-C(4)-C(3)	-132.37(15)
S(1)-Ru(1)-C(4)-C(3)	176.45(8)
C(3)-C(4)-C(5)-C(6)	1.5(2)
Ru(1)-C(4)-C(5)-C(6)	-51.77(14)
C(3)-C(4)-C(5)-Ru(1)	53.25(14)
C(11)-Ru(1)-C(5)-C(4)	-130.04(18)
C(3)-Ru(1)-C(5)-C(4)	-29.40(10)
C(2)-Ru(1)-C(5)-C(4)	-66.47(11)
C(12)-Ru(1)-C(5)-C(4)	51.71(12)
C(1)-Ru(1)-C(5)-C(4)	-104.03(11)
C(6)-Ru(1)-C(5)-C(4)	-134.25(15)
S(1)-Ru(1)-C(5)-C(4)	138.75(9)
C(11)-Ru(1)-C(5)-C(6)	4.2(2)
C(3)-Ru(1)-C(5)-C(6)	104.85(11)
C(2)-Ru(1)-C(5)-C(6)	67.78(10)
C(12)-Ru(1)-C(5)-C(6)	-174.04(9)
C(1)-Ru(1)-C(5)-C(6)	30.21(9)
C(4)-Ru(1)-C(5)-C(6)	134.25(15)
S(1)-Ru(1)-C(5)-C(6)	-87.01(9)
C(2)-C(1)-C(6)-C(5)	3.2(2)
Ru(1)-C(1)-C(6)-C(5)	56.49(13)
C(2)-C(1)-C(6)-C(7)	-176.85(15)
Ru(1)-C(1)-C(6)-C(7)	-123.60(15)
C(2)-C(1)-C(6)-Ru(1)	-53.25(14)
C(4)-C(5)-C(6)-C(1)	-3.8(2)
Ru(1)-C(5)-C(6)-C(1)	-55.92(13)
C(4)-C(5)-C(6)-C(7)	176.32(15)

Ru(1)-C(5)-C(6)-C(7)	124.17(15)
C(4)-C(5)-C(6)-Ru(1)	52.15(14)
C(11)-Ru(1)-C(6)-C(1)	-48.14(12)
C(3)-Ru(1)-C(6)-C(1)	65.71(10)
C(2)-Ru(1)-C(6)-C(1)	29.14(10)
C(12)-Ru(1)-C(6)-C(1)	143.13(14)
C(4)-Ru(1)-C(6)-C(1)	102.62(11)
C(5)-Ru(1)-C(6)-C(1)	130.06(14)
S(1)-Ru(1)-C(6)-C(1)	-133.17(9)
C(11)-Ru(1)-C(6)-C(5)	-178.19(9)
C(3)-Ru(1)-C(6)-C(5)	-64.35(10)
C(2)-Ru(1)-C(6)-C(5)	-100.92(11)
C(12)-Ru(1)-C(6)-C(5)	13.07(19)
C(1)-Ru(1)-C(6)-C(5)	-130.06(14)
C(4)-Ru(1)-C(6)-C(5)	-27.43(9)
S(1)-Ru(1)-C(6)-C(5)	96.78(9)
C(11)-Ru(1)-C(6)-C(7)	66.37(17)
C(3)-Ru(1)-C(6)-C(7)	-179.79(16)
C(2)-Ru(1)-C(6)-C(7)	143.64(17)
C(12)-Ru(1)-C(6)-C(7)	-102.37(19)
C(1)-Ru(1)-C(6)-C(7)	114.51(19)
C(4)-Ru(1)-C(6)-C(7)	-142.87(17)
C(5)-Ru(1)-C(6)-C(7)	-115.44(19)
S(1)-Ru(1)-C(6)-C(7)	-18.66(15)
C(1)-C(6)-C(7)-C(8)	126.25(18)
C(5)-C(6)-C(7)-C(8)	-53.8(2)
Ru(1)-C(6)-C(7)-C(8)	37.1(2)
C(6)-C(7)-C(8)-C(9)	-63.2(2)
C(7)-C(8)-C(9)-S(1)	75.66(19)
C(10)-S(1)-C(9)-C(8)	62.43(16)
Ru(1)-S(1)-C(9)-C(8)	-52.12(15)

2.6 Experimental Section References

(1) Brookhart, M.; Grant, B.; Volpe, A. F. *Organometallics* **1992**, *11*, 3920-3922.
(2) Daugulis, O.; Brookhart, M.; White, P. S. *Organometallics* **2002**, *21*, 5935-5943.
(3) Shevchenko, N. E.; Nenajdenko, V. G.; Balenkova, E. S. *Synthesis* **2003**, *2003*, 1191-1200.
(4) Birch, A. J. *Journal of the Chemical Society (Resumed)* **1944**, *0*, 430-436.
(5) APEX2 Version 2010.9-0, Bruker AXS, Inc.; Madison, WI 2010.
(6) SAINT Version 7.68a, Bruker AXS, Inc.; Madison, WI 2009.
(7) G. M. Sheldrick, SADABS, Version 2008/1, Bruker AXS, Inc.; Madison, WI 2008.
(8) G. M. Sheldrick, SHELXTL, Version 2008/4, Bruker AXS, Inc.; Madison, WI 2008.
(9) International Tables for X-Ray Crystallography 1992, Vol. C., Dordrecht: Kluwer Academic Publishers.

Chapter 3

Heteroatom Effect on η⁶-Arene Tethered Ru(II) Complexes for Ethylene Polymerization Catalysis: Experimental and DFT Studies.

3.1 Introduction

Commercial olefin polymerization is mainly catalyzed by early transition metal (ETM) based catalysts due to their high activities and stereo- and regio-control of α-olefins polymerization and copolymerization.[1,2] In contrast, their oxophilicity hinders their capability of copolymerizing polar monomers with ethylene.[1-3] Late transition metals (LTM) based on Ni(II) and Pd(II) tolerate polar monomers but activities and molecular weights are low generally.[4-22] Middle-late periodic table transition metal catalysts of Fe and Co display high activity but do not incorporate polar monomers.[23,24] Group VIII metal "ruthenium" exhibits varied chemistry and tolerance to the presence of polar groups in other catalytic reactions.[25-28] Despite its importance, very little attention has been paid to ruthenium for olefin polymerization catalysis and only a handful of studies have been published.[29-33] For all these studies no active species were identified and nature of active catalytic species remained unclear.

We recently tested a η⁶-arene tethered Ru(II) complex (**3.1**) (Chart 3.1) for ethylene polymerization and found it to be active when activated with $AlMe_2Cl$. We also synthesized a dimethylated version (**3.1a**) (Chart 3.1) that was also found to be active for ethylene

polymerization when activated with HBArF ($[H(Et_2O)_2]^+[BAr'_4]^-$(where Ar'= 3,5-$(CF_3)_2C_6H_3$). Moreover, NMR and MS studies on **3.1a,** upon activation with HBArF in the presence of ethylene, demonstrated for the first time an ethylene coordination migratory insertion (Cossess-Arlman mechanism) for a ruthenium complex.[34] Recently, we also reported a bis((arenesulfonate)phosphine)Ru(IV)complex that was found to be the most active ruthenium complex to date.[35] After these satisfactory results, in this paper, we wish to explore the effect of different coordinating heteroatoms in the tethered arm of the η^6-arene tethered ruthenium(II) complexes.

For this purpose, we decided to study the effect of nitrogen and oxygen as coordinating heteroatoms and compare them with reported complex **3.1** that has a sulfur heteroatom. We synthesized complexes containing nitrogen (complex **3.2**, Chart 3.1) and oxygen (complex **3.3**[36], Chart 3.1) as pendant heteroatoms and tested them for ethylene polymerization.

Chart 3.1. η^6-arene tethered Ru(II) complexes for ethylene polymerization catalysis.

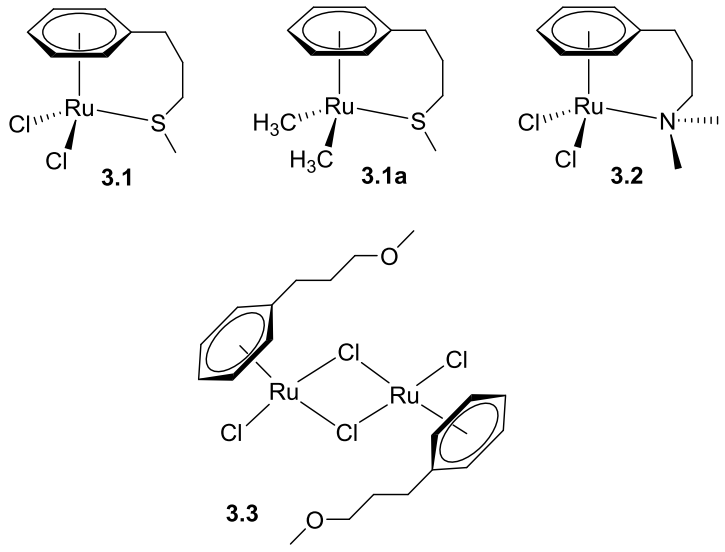

3.2 Synthesis, Characterization, and Polymerization Results

The synthesis of the complexes is depicted in Schemes 3.1 and 3.2 for amine complex **3.2** and ether complex **3.3,** respectively. Complex **3.2** starts with nucleophilic substitution followed by a Birch reduction.[37] Reduced ligand **3.2b** is treated with hydrochloric acid prior to complexation with $RuCl_3xH_2O$, as reported with a similar complex.[38] Complexation affords the dimeric species **3.2c** that upon treatment with an organic base yields to complex **3.2**. Complex **3.2** is air and moisture stable and decomposes slowly in chlorinated solvents. Single crystal X-ray diffraction of **3.2** reveals that the complex adopts a three legged piano stool conformation (Figure 3.1). One of the methyls attached to the nitrogen atoms is located *cis* to one of the chlorides while the other bisects the Cl-Ru-Cl angle. Table 3.1 compares selected bond distances and angles for complexes **3.1** and **3.2**. The ruthenium-nitrogen bond distance is shorter than for ruthenium-sulfur as expected due to atom size difference. The ruthenium-chloride bond distances are slightly larger for complex **3.2**. The average ruthenium-carbon (arene) bond distances are very similar. The Cl-Ru-Cl angle for complex **3.1** (86.879 °) is significantly smaller than for complex **3.2** (89.813 °). This is probably due to the sulfur's unpaired electron increasing repulsion with the vicinal chloride atom.

The ligand for complex **3.2** was synthesized in a similar fashion as depicted in Scheme 3.2, and the complexation was carried out as previously reported.[36]

Table 3.1. Complex **3.1** and **3.2** comparison of selected bonds (Å) and bond angles (°).

3.1[34]		**3.2**	
Ru(1)-S(1)	2.3670(4)	Ru(1)-N(1)	2.2387(13)
Ru(1)-Cl(1)	2.4032(4)	Ru(1)-Cl(1)	2.4195(4)
Ru(1)-Cl(2)	2.4228(4)	Ru(1)-Cl(2)	2.4369(4)
Ru(1)-C(arene)	2.1901	Ru(1)-C(arene)	2.1796
Cl(1)-Ru(1)-Cl(2)	86.879(13)	Cl(1)-Ru(1)-Cl(2)	89.813(13)

Scheme 3.1. Synthesis of η^6-$C_6H_5(CH_2)_3N(CH_3)_2RuCl_2$ (**3.2**).

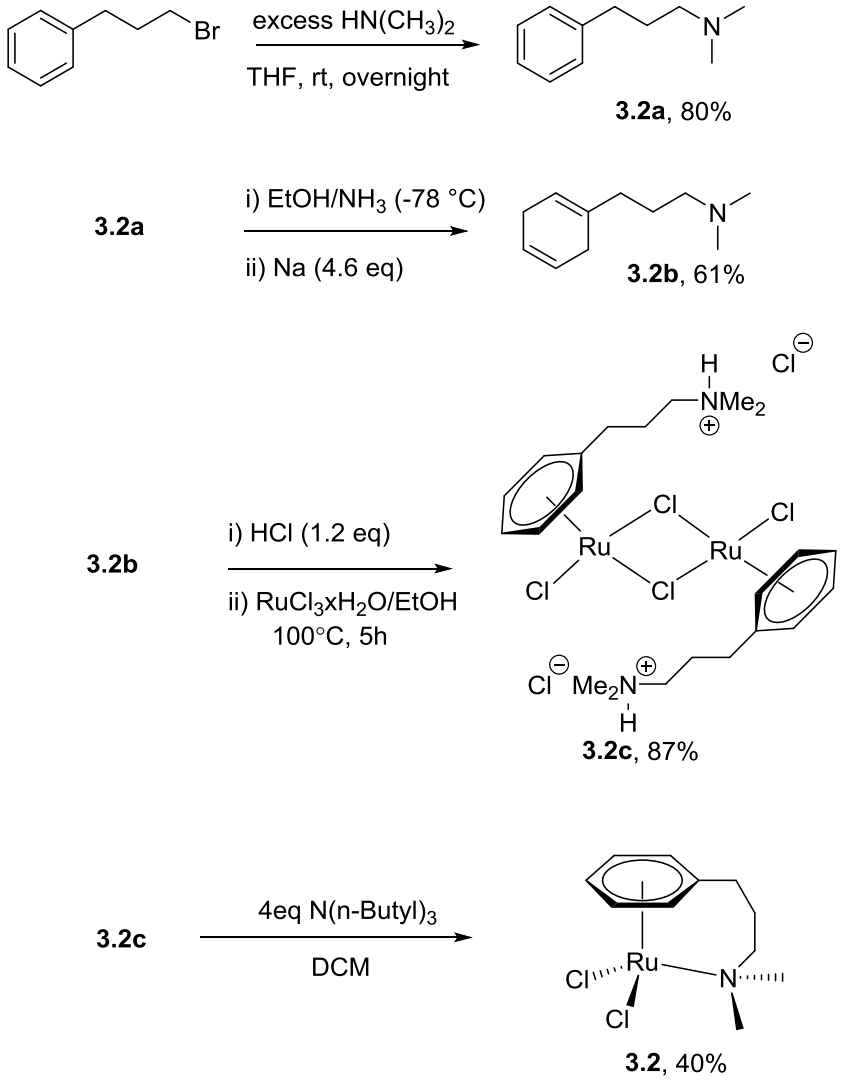

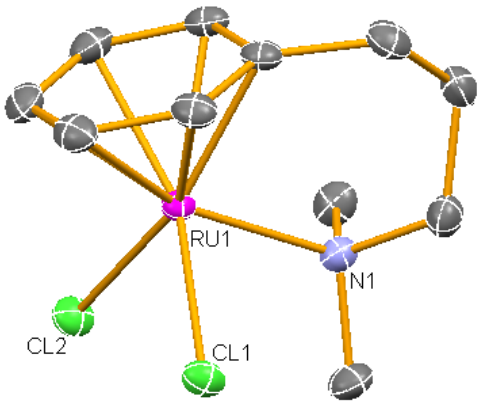

Figure 3.1. X-Ray crystal structure of **3.2**. ORTEP drawing, ellipsoids at 60% probability radius, hydrogens omitted for clarity.

Scheme 3.2. Synthesis of $[(\eta^6\text{-}C_6H_5(CH_2)_3OCH_3RuCl_2)]_2$ (**3.3**).

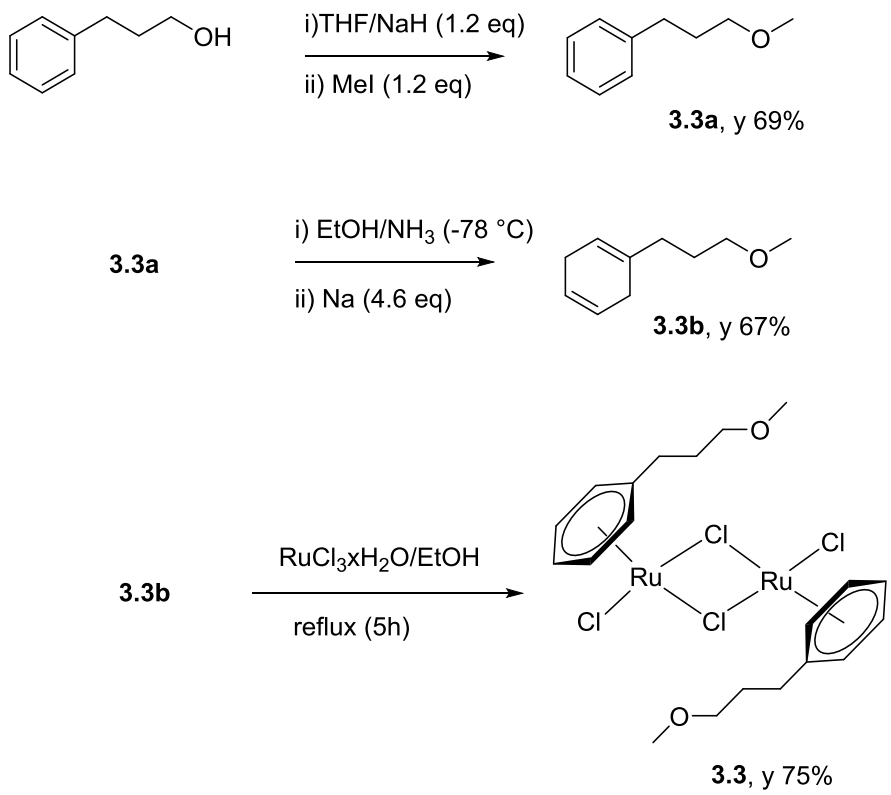

Polymerization studies were carried out with both complexes **3.2** and **3.3**. The data are compiled in Table 3.1, which also contains previous polymerization data on complexes **3.1** and **3.1a** (entries 14-17) for comparison purposes. Complex **3.3** was found to be inactive (entries 18-21) for olefin polymerization under the same conditions used for complexes **3.1** and **3.2**. Complex **3.2**, in contrast, was found to be active (entries 3-11) when activated with $AlMe_2Cl$ but not with MAO or $AlMe_3$ (entries 1 and 2). The same results were obtained for complex **3.1** which was only capable of making polyethylene when $AlMe_2Cl$ was used as a cocatalyst (entries 12 and 13). Like complex **3.1**, complex **3.2** is poorly soluble in DCM and insoluble in toluene or other non-polar solvents. For this reason, all polymerizations were run in DCM.

Polymerization with **3.2** at 25 °C (entries 3 and 4) yielded polyethylene in contrast to polymerizations with complex **3.1**, which did not afford any polyethylene at this temperature. This indicates that **3.2** is easier to activate with $AlMe_2Cl$ at lower temperatures than **3.1**. The polyethylene obtained shows a bimodal molecular weight distribution similar to that obtained with **3.1** suggesting the presence of two active species. One fraction exhibits a high molecular weight (175 kg·mol^{-1} for entry 3 and 189 kg·mol^{-1} for entry 4) while the other is of low molecular weight (<1000 g·mol^{-1}). In the case of **3.1**, the low molecular weight fraction was attributed to ruthenium(II) cationic species because polymerizations with complex **3.1a** only yielded a monomodal low molecular weight polymer (entries 16 and 17). High molecular weight polyethylene can only be attributed to Ru-aluminum species, as we proposed with **3.1** and also suggested for other metal complexes by others.[22,34,39-43] The narrow PDIs (1.52-1.89) for both fractions suggest that each of the active species act as a single site catalyst. Polymer melting temperatures (Tm)

for these two runs are ~127 °C, but the Tm are only relevant for the high molecular weight fraction, because the low molecular weight fraction is not expected to have a high Tm. The melting temperatures for the high molecular weights are low which indicates a moderate branching density. Branching is reported by NMR analysis, which cannot differentiate between the low and high molecular fractions. Therefore, the Tm found for these polymers is higher than expected from the branching calculated by NMR analysis.

Increasing the polymerization temperature to 50 °C resulted in a substantial increase in activity (more than double, entries 5 and 6). This higher activity can be attributed to the activation of more complexes and as a result, a higher number of active species. Also, higher temperatures might help to overcome the migratory insertion barrier, therefore increasing activity. The polymers obtained once again presented a bimodal distribution with PDIs that indicate a single site catalyst for both active species. In the case of the low molecular weight fraction for **3.2**, PDIs are slightly higher (1.45-1.60) than for those obtained by **3.1** (1.19-1.23, entries 16 and 17) at 50 °C. In contrast, the PDI of high molecular weight polymers produced by **3.1** (1.85-2.14, entries 5 and 6) are lower than for high molecular weight polyethylene produced by **3.2** (2.03-3.03, entries 14 and 15) under similar conditions. The high molecular weight fractions produced by complex **3.2** display lower molecular weights (125 $kg \cdot mol^{-1}$ and 137 $kg \cdot mol^{-1}$) than the high molecular weight fractions produced by complex **3.1** (198 $kg \cdot mol^{-1}$ and 262 $kg \cdot mol^{-1}$) at 50 °C. Branching of polymer produced by **3.1** is reduced, and its effect can be reflected by a slightly higher Tm of the high molecular weight polymer. To test complex **3.2** activities at higher temperatures, polymerization was carried out at 80 °C (entry 7), which resulted in a reduction of activity and indicates poor thermal stability of **3.2**. Complex **3.1** was also tested at this temperature

Table 3.2. Polymerization results with **3.2** and **3.3** compared with **3.1** and **3.1a**.

Entry	cat.	Cocat.	*t* (h)	*P*(psi)	*T* (°C)	yield (mg)	Mn[a] (kg·mol^{-1})	PDI[b] (Mw/Mn)	T_m[c] (°C)	Activ.[d] (10^3)	N_{br}[e]
1	**3.2**	MAO	4	600	50	0	-	-	-	-	-
2	**3.2**	$AlMe_3$	4	600	50	0	-	-	-	-	-
3	**3.2**	$AlMe_2Cl$	4	600	25	20	0.509, 119	1.52, 1.75	126.7	432	95
4	**3.2**	$AlMe_2Cl$	4	600	25	14	0.761, 161	1.77, 1.89	126.9	302	100
5	**3.2**	$AlMe_2Cl$	4	600	50	60	0.625, 137	1.60, 1.85	127.4	1295	83
6	**3.2**	$AlMe_2Cl$	4	600	50	50	0.600, 125	1.45, 2.14	126.3	1079	71
7	**3.2**	$AlMe_2Cl$	4	600	80	15	0.708, 161	1.81, 1.89	127.8	324	47
8	**3.2**	$AlMe_2Cl$	4	400	50	21	0.491, 140	1.43, 1.77	127.6	680	200
9	**3.2**	$AlMe_2Cl$	4	200	50	10	0.276, 55	1.91, 3.41	118.9	648	238
10	**3.2**	$AlMe_2Cl$	12	600	50	143	0.427, 120	1.38, 2.06	123.6	1065	91
11	**3.2**	$AlMe_2Cl$	24	600	50	344	0.435, 134	1.66, 2.05	123.4	1237	91
12	**3.1**	MAO	4	600	50	0	-	-	-	-	-
13	**3.1**	$AlMe_3$	4	600	50	0	-	-	-	-	-
14	**3.1**	$AlMe_2Cl$	4	400	50	15	0.638, 198	1.27, 2.03	129	809	18
15	**3.1**	$AlMe_2Cl$	12	800	50	93	0.848, 262	1.15, 3.03	131	836	8
16	**3.1a**	HBArF	12	400	50	28	0.610	1.19	61	55	36
17	**3.1a**	HBArF	12	800	50	55	0.657	1.23	75	54	27
18	**3.3**	MAO	4	600	50	-	-	-	-	-	-
19	**3.3**	$AlMe_3$	4	600	50	-	-	-	-	-	-
20	**3.3**	$AlMe_2Cl$	4	600	50	-	-	-	-	-	-
21	**3.3**	$AlMe_2Cl$	4	600	80	-	-	-	-	-	-

All polymerizations in 100 mL of DCM with 10 μmol [Ru], for complexes **3.1** and **3.1a** see Chapter 2. [a]Determined by high temperature GPC. [b]Polydispersity=Mw/Mn. [c]Melting transition temperature. [d]Activity=(molC_2H_4)/(mol[Ru]·h·bar) assuming all Ru is activated. [e]Branching=Me/1000C.

but was inactive. Once the temperature effect was established, we proceeded to study the effect of ethylene concentration.

Polymerization at 400 psi (entry 8) and 50 °C decreases the yield significantly indicating that the activity is dependent on ethylene concentration. Molecular weight for the low molecular weight fraction (491 $g \cdot mol^{-1}$) decreases slightly while the high molecular weight fraction does not vary dramatically (140 $kg \cdot mol^{-1}$). When ethylene pressure is reduced to 200 psi (entry 9), the activity is also low but comparable with polymerizations at 400 psi. In contrast, the molecular weight varies significantly. At 200 psi, the low molecular weight fraction is even lower (276 $g \cdot mol^{-1}$), and the high molecular weight fraction also decreases to obtain a moderate molecular weight polyethylene (55 $kg \cdot mol^{-1}$). Branching is greatly increased compared to 600 psi polymerizations, which indicates rapid β-hydrogen elimination due to a lower ethylene concentration. At 400 psi, the high molecular fraction has a Tm of 127.6 °C, almost identical to polymerizations at 600 psi, which indicates that the calculated branching corresponds mostly to the low molecular weight fraction. In contrast, polymerization at 200 psi gives a moderate molecular weight fraction with a Tm of 118.9 °C, which is consistent with a more branched polyethylene with a lower molecular weight.

Longer polymerization times were also tried at 50 °C for 12 and 24 hours (entries 10 and 11). Increasing the polymerization time does not have any significant effect on activity. Possible explanations are long induction times and decomposition of the active species. The activity is maintained because more catalyst is activated over time while the active species decomposes. Otherwise, we should see an increase in molecular weight as we increase the polymerization time. The bimodal distribution is persistent showing low and

high molecular weight polymer fractions. The melting temperature reveals that the high molecular weight fraction might be more branched than the previous polymerizations at 600 psi; this might indicate a higher chance *o*f *β*-hydrogen elimination and chain walking with longer polymerization times.

We can conclude from the polymerization experiments that complex **3.2** containing a nitrogen coordinating heteroatom is more active than the sulfur containing complex **3.2**. For both catalysts, the polymers obtained display a bimodal molecular weight distribution indicating the presence of two active species, one making the high molecular weight fraction and another the low molecular weight. For both fractions, narrow PDIs indicate that both of the two active species act as single site catalysts. For complex **3.2,** the high molecular fraction displays a slightly lower molecular weight than the high molecular fraction produced by complex **3.1**. Additionally, the PDIs for the low molecular weight fraction produced by complex **3.1a** are significantly narrower. From branching and Tm, we can infer that complex **3.2** produces a higher amount of the low molecular weight fraction.

3.3 Molecular Modeling of Chain Initiation and Chain Propagation. Determination of Migratory Insertion Barriers.

DFT Calculations. DFT calculations were carried out for the thiol (**3.2**) and amine (**3.1**) complexes. The thiol complex exists as two different isomers (see Chapter 2, *cis* (**2.5B**) and *trans* (**2.5A**)), and both complexes were modeled to see the effect of the methyl group on the thiol moiety during the ethylene migratory insertion.

a) Chain Initiation for Thiol Complex. As mentioned above, the thiol-Ru(II) complex exists as two isomers, *cis* and *trans*. For both isomers, the chain initiation energy profile was calculated and found to be almost identical, suggesting that the sterics of the methyl group on sulfur does not have any effect on the polymerization activity. Chart 3.2 depicts the optimized structures for all the minima and transition states calculated for the *cis* isomer (*trans* isomer optimized structures can be found in the appendix section). We only discuss the *cis* isomer, because any conclusion can also be applied to the *trans* isomer. The chain initiation energy profile in Figure 3.2 shows the energies for both isomers.

The demethylation of complex **3.1a** generates *α*-agostic complex **S1** (Chart 3.2 and Figure 3.2). Ethylene uptake happens in a barrierless manner to form ethylene π-complex **S2**. Ethylene uptake is exothermic by 16.6 kcal·mol^{-1} (Figure 3.2). We previously demonstrated the formation of **S2** by NMR.[34] Coordination of ethylene can occur in a perpendicular or planar fashion. For some late transition metals, perpendicular coordination is preferred and the rotation of ethylene has to happen to proceed with insertion.[44,45] In this case, ethylene prefers to coordinate in a planar fashion, and it is already in-plane with the Ru-Me bond, ready to proceed with migratory insertion. Carbon atoms in the ethylene monomer lose sp^2 character becoming more sp^3-like as reflected by a substantial elongation of the C=C to 1.412 Å (Chart 3.2, **S2**). This is due to strong back-bonding of the metal to ethylene, which is also suggested in the NMR experiments.[34] A perpendicular coordinated ethylene complex, **S2p**, was calculated to be 9.2 kcal·mol^{-1} less stable; this energy is also associated with the ethylene rotation barrier for complex **S2**. The ethylene-methyl distance in **S2** is 2.768 Å and forms an angle of 78.54 °. Ethylene migratory insertion (**S2 → S3γ**) through transition state $\mathbf{TS_{S2\text{-}S3\gamma}}$ was found to be 23.0 kcal·mol^{-1}. This

energy is the insertion barrier for chain initiation. This is in excellent agreement with the experimental 22.8 kcal·mol^{-1} calculated by variable temperature NMR experiments.[34] The ethylene-methyl distance is reduced to 2.028 Å at the transition state before relaxing to the kinetically favored migratory insertion product **S3γ**. The migratory insertion product is a *γ*-agostic complex that sits 21.7 kcal·mol^{-1} below the transition state and 1.3 kcal·mol^{-1} above the ethylene coordinated complex **S2**. This was found not to be the more stable product. Fast isomerization, **S3γ→ S4β**, to form a thermodynamic stable *β*-agostic complex **S4β** happens via transition state $\mathbf{TS_{S3\gamma\text{-}S4\beta}}$ with a 2.9 kcal·mol^{-1} isomerization barrier.

Chart 3.2. Optimized structures for thiol *cis* isomer chain initiation.

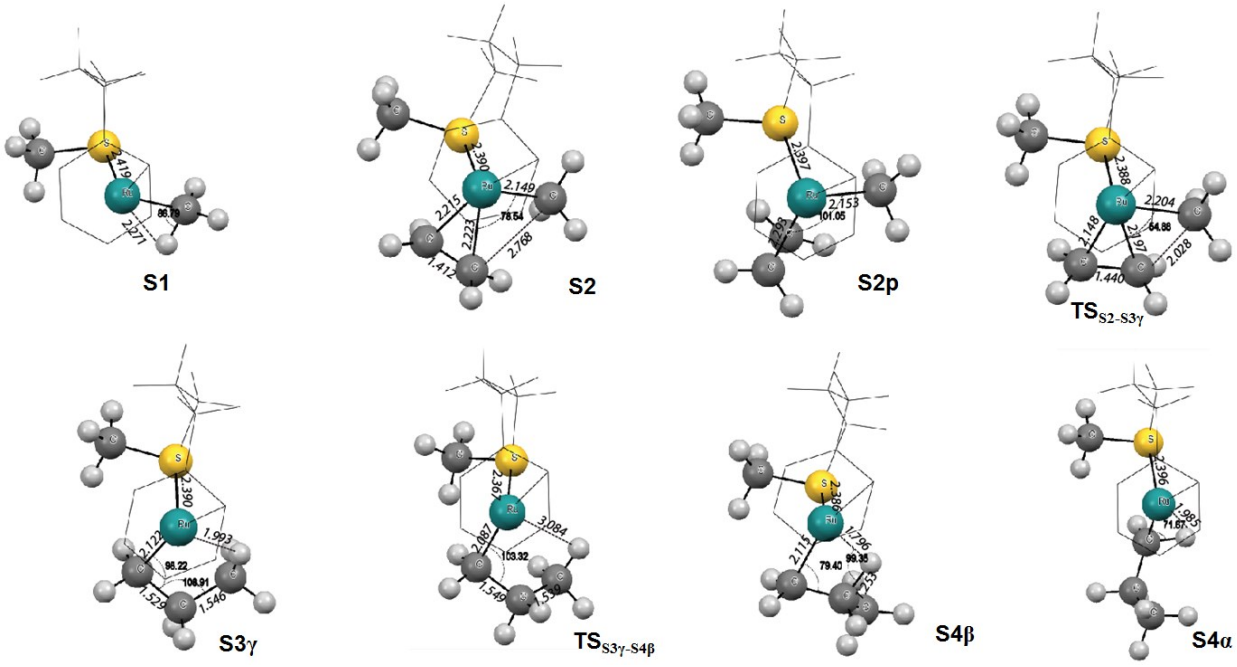

Ethylene coordination and migratory insertion to final product **S4β** is an exothermic process releasing 26.9 kcal·mol^{-1}. To complete the potential energy surface, we also

calculated the formation of an *α*-agostic complex **S4α** that was found to lay 8.9 kcal·mol^{-1} higher in energy than the more stable product **S4β**.

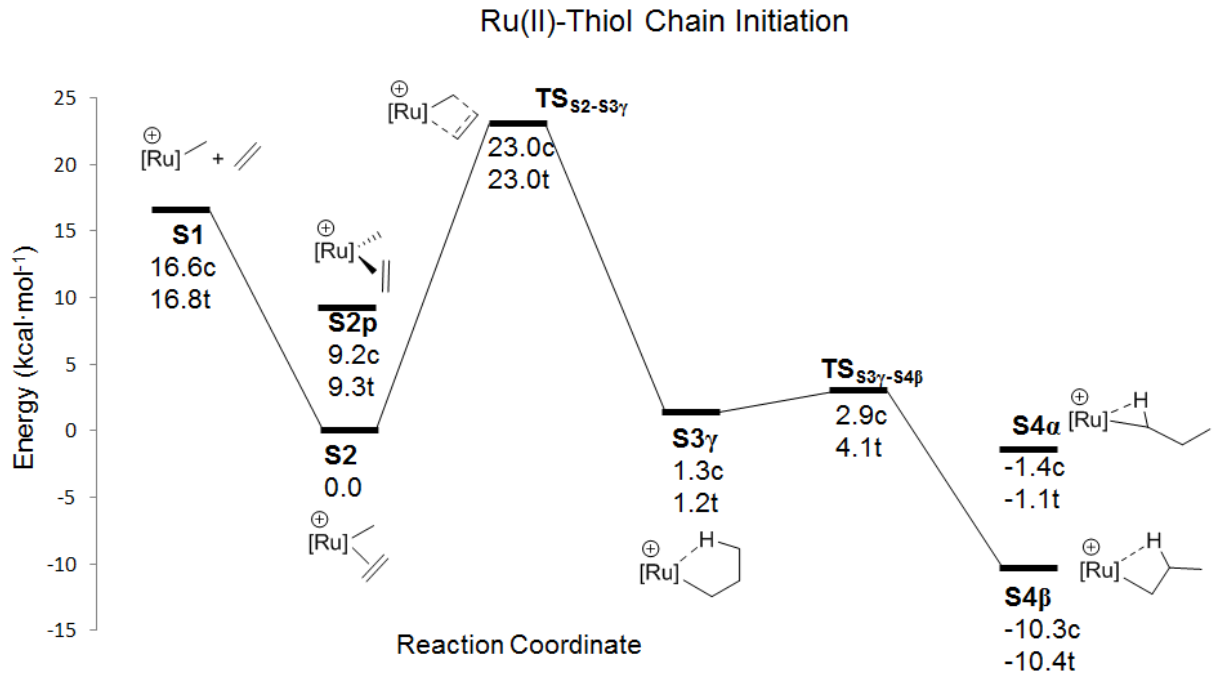

Figure 3.2. Thiol-Ru(II) relative energy profile of the proposed chain initiation for the active species. Annotations "c" and "t" indicate *cis* and *trans* isomers, respectively. Complex **S2** is made zero energy for comparison purposes.

b) Chain Propagation for Thiol Complex. For the chain propagation, the potential energy surface of the insertion product of only the *trans* isomer was used for DFT calculations. We can assume that identical energy profiles will be obtained as in the case of chain initiation. Chart 3.3 displays important bond distances angles for the optimized minima and transition states. Figure 3.3 depicts the potential energy surface for the chain propagation mechanism. Chain propagation starts from the *β*-agostic **S4β** complex and ethylene coordination. Ethylene binding is also favored, but the energy gained (5.3

kcal·mol^{-1}) is lower than for the chain initiation; this is due to opening of chelate **S4β**, which makes ethylene coordination more challenging. Complex **S5** is formed with ethylene bounded in-plane, as in the case of complex **S2** for chain initiation. Surprisingly, the ethylene-methyl distance is exactly the same for complexes **S2** and **S5**. The perpendicular coordinated complex was not calculated for chain propagation under the safe assumption that it will be higher in energy, as calculated for complex **S2**. After ethylene uptake, complex **S5** is formed and proceeds with ethylene insertion (**S5 → S6γ**) through transition state **$TS_{S5\text{-}S6\gamma}$**.

Chart 3.3. Optimized structures for thiol *trans* chain propagation.

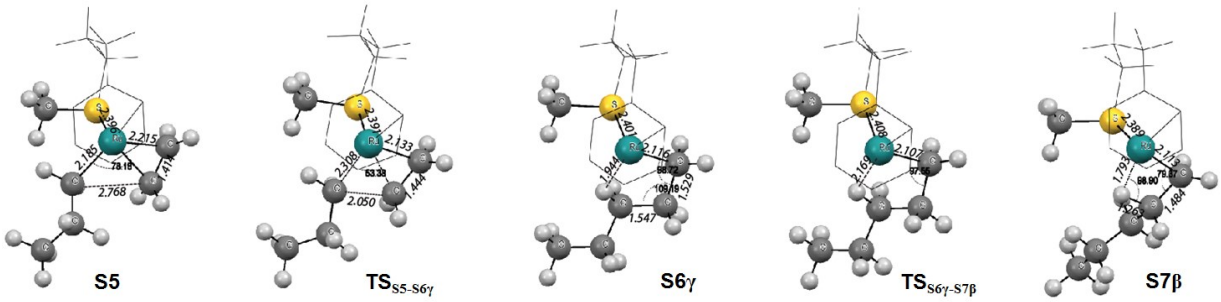

The migratory insertion barrier for chain propagation is 21.8 kcal·mol^{-1}, which is lower than chain initiation and also lower than the (>25 kcal·mol^{-1}) migratory insertion barrier calculated[46] for Nomura's[31,32] and Brookhart's[47] ruthenium complexes. This migratory insertion barrier for chain propagation seems to agree with the experimental results in which moderate activity was observed. This insertion barrier is higher than the ones calculated for ETM[44,48,49] and LTM[44] which explains lower activity. The difference in the migratory insertion barrier between chain initialization and propagation is only 1.2

kcal·mol^{-1}; such a small difference can be only attributed to the slightly more sterically hindered propyl moiety, because electron density in the metal should not change significantly by changing methyl to propyl. Steric effects have also been proposed by experiments and molecular modeling to decrease the migratory insertion barrier on LTM.[7,50] The ethylene-methyl distance of the migratory insertion transition state is 2.050 Å, which is slightly shorter than for the chain initiation transition state.

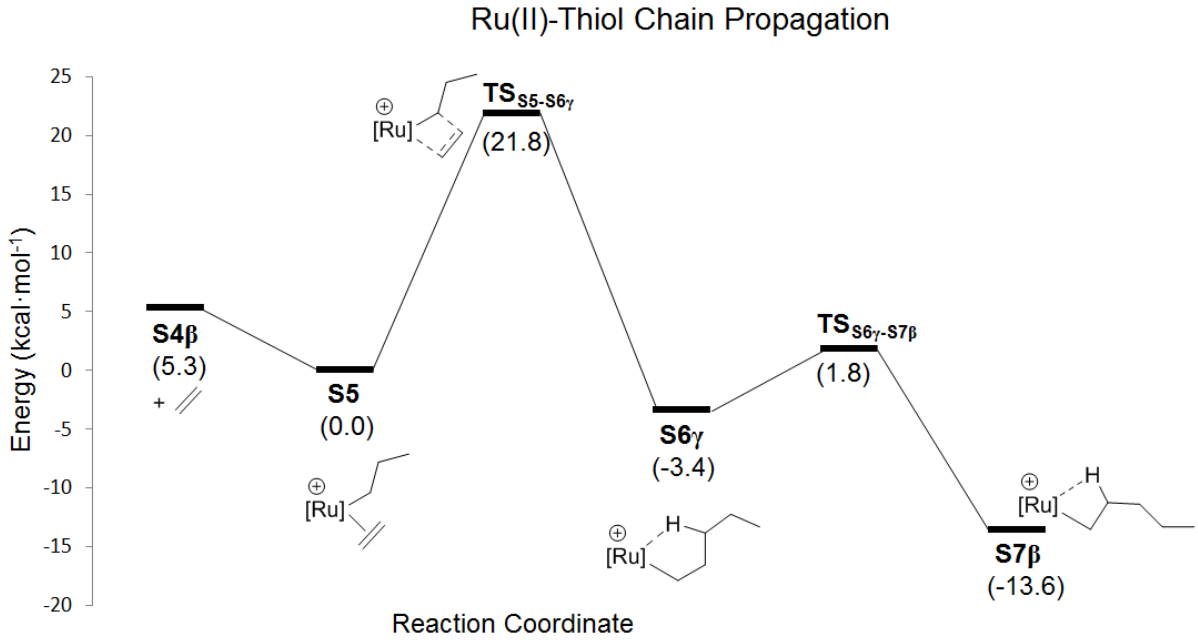

Figure 3.3. Thiol-Ru(II) relative energy profile of the proposed chain propagation for the active species. Complex **S5** is made zero energy for comparison purposes.

c) Chain Initiation for Amine Complex. To be able to compare results, DFT calculations with amine complex **3.2** were carried out using the same level of theory as for the thiol complex. Chart 3.4 and Figure 3.4 depict optimized structures for all the calculated structures and the energy profile for chain initiation, respectively. Methyl abstraction affords monocationic ruthenium complex **N1**. Ethylene coordination proceeds

exothermically by 5.3 kcal·mol^{-1} to form π-complex **N2**. Ethylene prefers to bind in-plane as complex **S2**. Perpendicular coordination of ethylene was also modeled (**N2p**), and it was found to be 7.4 kcal·mol^{-1} above the in-plane coordination complex **N2**. This energy is also the associated ethylene rotation barrier associated with complex **N2,** and it is slightly smaller than for complex **S2**. This difference is probably due to stronger π-back-bonding in **S2**. Migratory insertion (**N2→ N3γ**) proceeds through transition state $\mathbf{TS_{N2\text{-}N3\gamma}}$ with a migratory insertion barrier of 19.8 kcal·mol^{-1}. This insertion barrier for the chain initiation is lower compared to the thiol complex **S2** by 3.2 kcal·mol^{-1} for the *cis* and *trans* isomers.

Chart 3.4. Optimized structures for amine complex chain initiation.

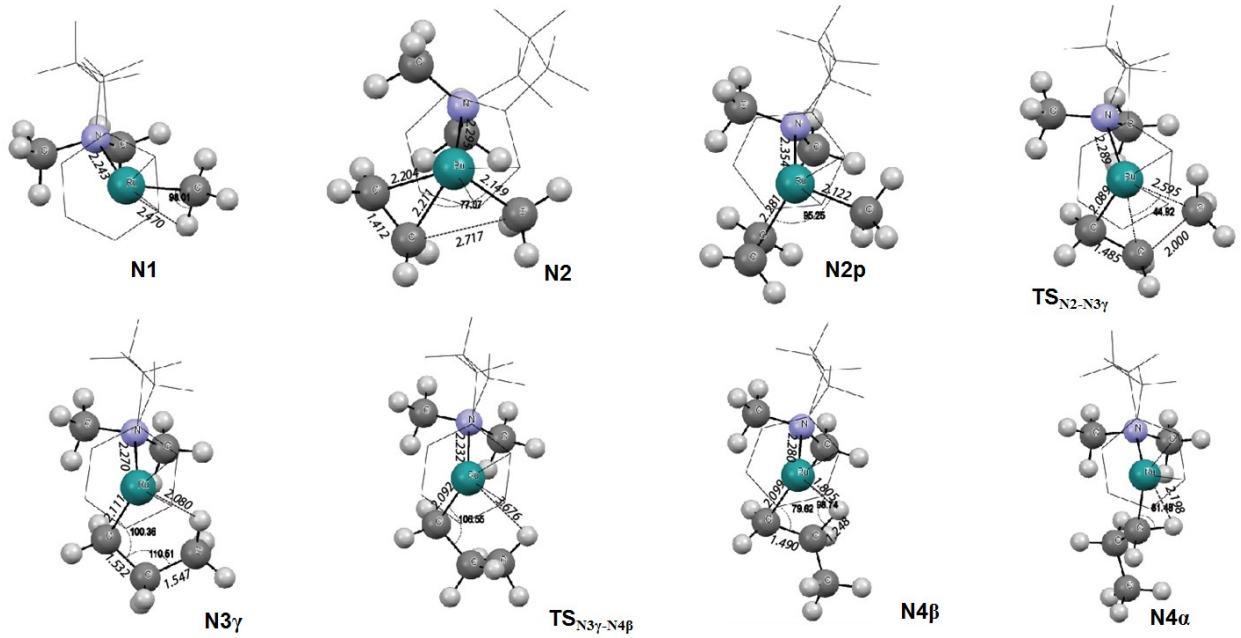

Transition state $\mathbf{TS_{N2\text{-}N3\gamma}}$ relaxes to *γ*-agostic chelate complex **N3γ** that through transition state $\mathbf{TS_{N3\gamma\text{-}N4\beta}}$ isomerizes easily to *β*-agostic complex **N4β,** which lies 13.3

kcal·mol^{-1} below ethylene coordinated complex **N2** and 33.1 kcal·mol^{-1} below transition state **$TS_{N2\text{-}N3\gamma}$**. The formation of an *α*-agostic complex **N4α** is predicted to be 10.5 kcal·mol^{-1} higher in energy than **N4β**. These results suggest that in amine complex **3.2,** chain initiation requires less energy than in thiol complex **3.1**. Chain propagation is the factor that is most likely to determine which complex is more active. Therefore, chain propagation was also modeled and compared with propagation of the thiol complex's active species.

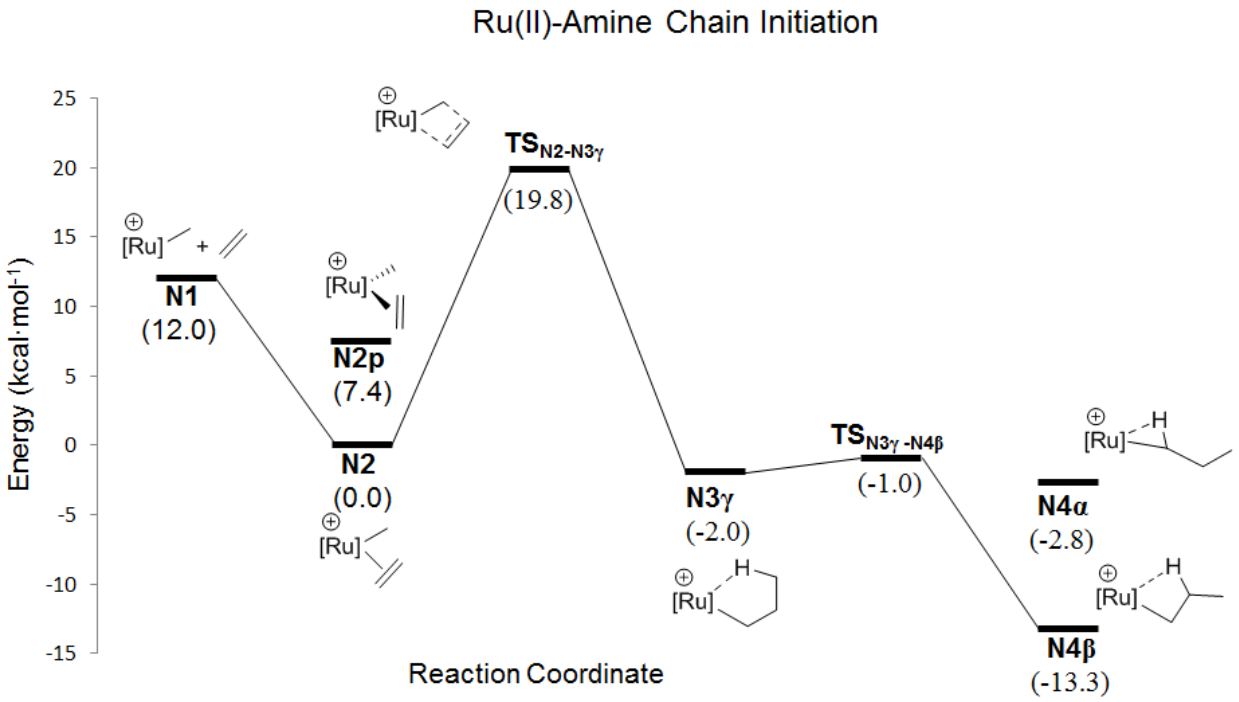

Figure 3.4. Amine-Ru(II) relative energy profile of the proposed chain initiation for active species.

d) Chain Propagation for Amine Complex. Chart 3.5 and Figure 3.5 depicts optimized structures calculated and the energy profile for chain propagation, respectively. Ethylene coordination **N4β→N5** is also exothermic but significantly less favored than for the thiol active species or chain initiation for this catalyst, and it is only 1.9 kcal·mol^{-1}. This low energy is partially due to opening of chelate. Additionally, ethylene uptake is dependent

on electron density at the metal center. Ruthenium-sulfur is a soft-soft interaction, which results in better orbital overlap and therefore, a more electron rich metal. This extra electron density on the metal enhances back-bonding to the coordinated ethylene resulting in better ethylene binding and in a higher insertion barrier. In the case of ruthenium-nitrogen, it is a soft-hard interaction. This is also reflected on the chain initiation mechanism in which ethylene uptake by the amine complex **N2** was exothermic by 12 kcal·mol^{-1}, that is 4.6-4.8 kcal·mol^{-1} less than ethylene uptake for the thiol complex **S2**.

The migratory insertion barrier **N5→N6γ** happens through transition state **TS$_{N5\text{-}N6\gamma}$** and has a total energy of 19.4 kcal·mol^{-1}, which is only 0.4 kcal·mol^{-1} lower than the migratory insertion barrier for the chain initiation mechanism. In the case of the amine complex, the insertion barrier is almost identical for chain initiation and chain propagation. Compared to the thiol complex, the amine complex insertion barrier is 2.4 kcal·mol^{-1} lower than the thiol complex, which explains the higher activities of the amine complex in ethylene polymerization.

Chart 3.5. Optimized structures for amine complex chain propagation.

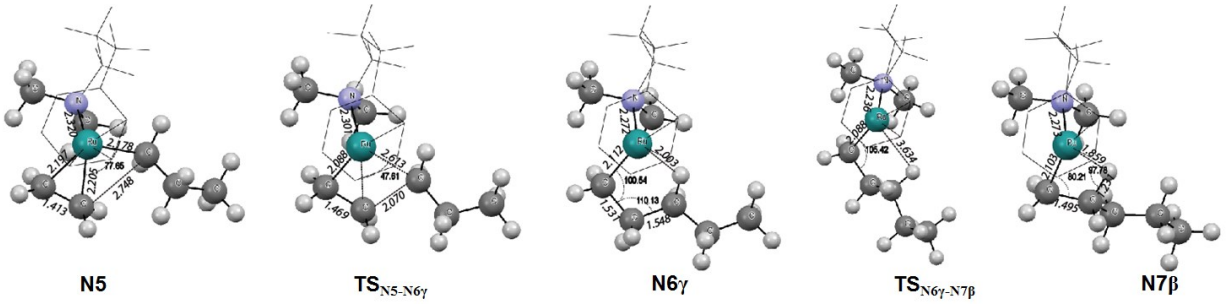

After migratory insertion, the expected kinetic *γ*-agostic complex **N6γ** is observed, which then isomerizes to the *β*-agostic complex **N7β** through the transition state **TSN$_{6\gamma\text{-}N7\beta}$** with an isomerization barrier of only 2.4 kcal·mol^{-1}. The *α*-agostic complex was not

calculated because it is expected to be higher in energy, as demonstrated for the chain initiation of the thiol and amine complexes.

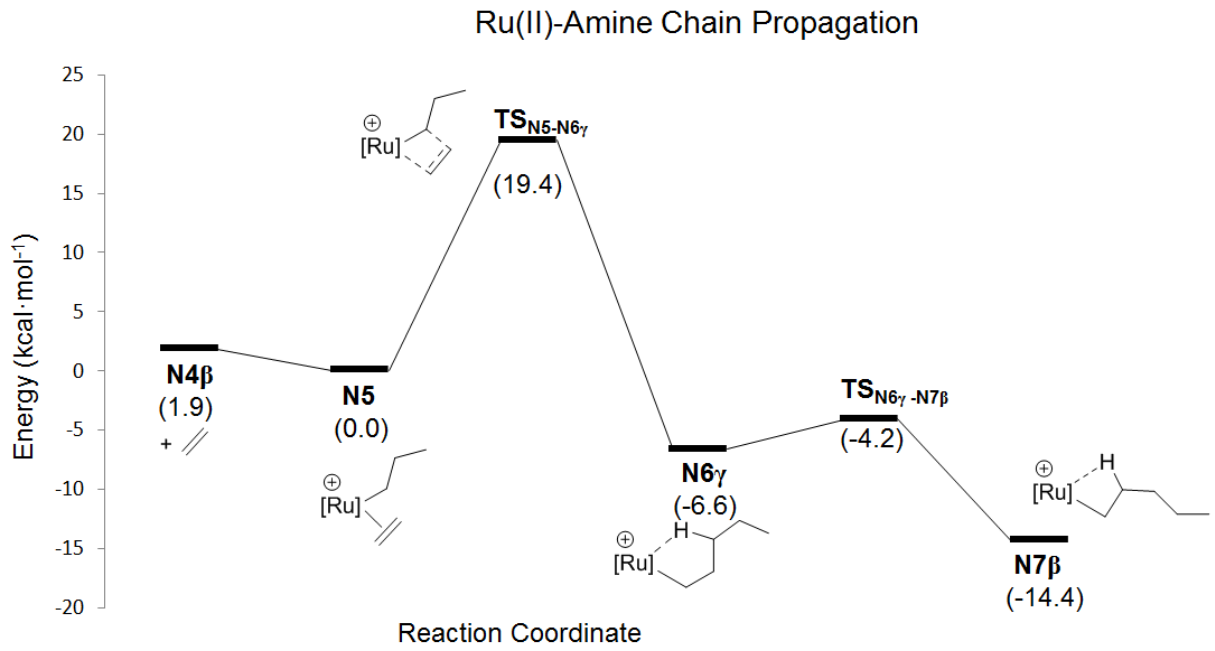

Figure 3.5. Amine-Ru(II) relative energy profile of the proposed chain propagation for active species.

Thus, the DFT calculations confirm the experimental results. The amine complex **3.2** is more active than the thiol complex **3.1** due to a lower migratory insertion barrier. The reason behind this lower insertion barrier has to be due to the nature of the heteroatom, sulfur or nitrogen, because the rest of the ligand framework is almost identical. Migratory insertion barrier difference of 2.4 kcal·mol^{-1} between amine and thiol complex should lead to larger difference in activity than the experimentally observed difference. DFT calculations results should be considered qualitatively in comparing activity difference since other factors such as counterion and solvent are not taking into account that might reduce the migratory insertion gap between the two catalysts.

3.4 Conclusions

In conclusion, we have studied the effect of the heteroatom on the polymerization activity of η^6-arene tethered ruthenium (II) complexes. Three complexes with oxygen, nitrogen, or sulfur on the tethered arm were compared for activity in ethylene polymerization. The oxygen tethered complex **3.3** was found to be inactive. The null activity of complex **3.3** can be justified by a lack of coordination of the oxygen atom; the active species generated cannot be stabilized and probably leads to decomposition. Previously synthesized complex **3.1**, containing thiol-ether in tethered arm, was active for ethylene polymerization with moderate activities. Complex **3.2**, with amine in the tethered arm, was synthesized and found to be 1.5-fold more active for ethylene polymerization than complex **3.1** (Table 1, entry 5 vs 15). Both complexes make polyethylene with a bimodal distribution, a high molecular weight fraction and a low molecular weight fraction, indicating the presence of two active species. The polydispersities of both fractions are generally narrow, indicating a single site catalyst. The molecular weights of the polymers produced with amine complex **3.2** are lower than those made using thiol-ether complex **3.1**. Computational modeling was used to compare the energy profiles of ethylene migratory insertion for complexes **3.1** and **3.2**. DFT calculations of the chain initiation and chain propagation mechanism demonstrate that amine complex **3.2** requires 3.2 and 2.4 kcal·mol^{-1} less than thiol-ether complex **3.1,** respectively. Although complex **3.2** has lower migratory insertion barriers, the calculated energies are still higher than those for ETM and LTM[44,48,49] but smaller than those calculated for other Ru(II) complexes.[46]

Molecular modeling has shown that metal electron density has a great effect on the insertion barrier for ETM catalysts.[48,49] Increasing electron donation to the metal center increases π back-bonding to ethylene, which results in higher insertion barriers.[49,51,52] The difference on activation barriers and polymerization activity are attributed to a heteroatom effect. Ruthenium-sulfur is a soft-soft interaction while ruthenium-nitrogen is a soft-hard interaction. The soft-soft ruthenium-sulfur interaction will favor better orbital overlap and electron donation from the sulfur to ruthenium, which is expected to be more favored than for ruthenium-nitrogen, a soft-hard interaction. A nitrogen atom is more electronegative than a sulfur atom, 3.04 and 2.58, respectively, using the Pauling scale. This difference in electronegativity suggests that nitrogen will donate less electron density to ruthenium, consequently reducing π back-bonding to ethylene and favoring migratory insertion into the Ru-alkyl bond. Additionally, the sulfur atom has an extra set of unpaired electrons that could also participate in electron donation to ruthenium. This effect is reflected by the inversion barrier of coordinated sulfides to transition metals[53-56], and we calculated it to be 14.4 ± 0.1 kcal·mol^{-1} for complex **3.1**.[34]

3.5 References

(1) *Transition Metal Polymerization Catalysts*; John Wiley & Sons, Inc.: New Yersey, 2009.
(2) *Organometallic Catalysts and Olefin Polymerization*; Springer: Berlin, 2009.
(3) *Topics in Organometallic Chemistry*; Springer: Berlin/Heidelberg, 2009; Vol. 29.
(4) Johnson, L. K.; Killian, C. M.; Brookhart, M. *J. Am. Chem. Soc.* **1995**, *117*, 6414-6415.
(5) Johnson, L. K.; Mecking, S.; Brookhart, M. *J. Am. Chem. Soc.* **1996**, *118*, 267-268.
(6) Svejda, S. A.; Johnson, L. K.; Brookhart, M. *J. Am. Chem. Soc.* **1999**, *121*, 10634-10635.
(7) Ittel, S. D.; Johnson, L. K.; Brookhart, M. *Chem. Rev.* **2000**, *100*, 1169-1203.
(8) Drent, E.; van Dijk, R.; van Ginkel, R.; van Oort, B.; Pugh, R. I. *Chem. Commun.* **2002**, 744-745.
(9) Boffa, L. S.; Novak, B. M. *Chem. Rev.* **2000**, *100*, 1479-1494.
(10) Nakamura, A.; Ito, S.; Nozaki, K. *Chem. Rev.* **2009**, *109*, 5215-5244.
(11) Carrow, B. P.; Nozaki, K. *J. Am. Chem. Soc.* **2012**, *134*, 8802-8805.
(12) Anselment, T. M. J.; Wichmann, C.; Anderson, C. E.; Herdtweck, E.; Rieger, B. *Organometallics* **2011**, *30*, 6602-6611.
(13) Rose, J. M.; Cherian, A. E.; Coates, G. W. *J. Am. Chem. Soc.* **2006**, *128*, 4186-4187.
(14) Berkefeld, A.; Mecking, S. *Angew. Chem. Int. Ed.* **2008**, *47*, 2538-2542.
(15) Berkefeld, A.; Drexler, M.; Möller, H. M.; Mecking, S. *J. Am. Chem. Soc.* **2009**, *131*, 12613-12622.
(16) Guironnet, D.; Caporaso, L.; Neuwald, B.; Göttker-Schnetmann, I.; Cavallo, L.; Mecking, S. *J. Am. Chem. Soc.* **2010**, *132*, 4418-4426.
(17) Kochi, T.; Noda, S.; Yoshimura, K.; Nozaki, K. *J. Am. Chem. Soc.* **2007**, *129*, 8948-8949.
(18) Wu, F.; Foley, S. R.; Burns, C. T.; Jordan, R. F. *J. Am. Chem. Soc.* **2005**, *127*, 1841-1853.
(19) Luo, S.; Vela, J.; Lief, G. R.; Jordan, R. F. *J. Am. Chem. Soc.* **2007**, *129*, 8946-8947.
(20) Weng, W.; Shen, Z.; Jordan, R. F. *J. Am. Chem. Soc.* **2007**, *129*, 15450-15451.
(21) Camacho, D. H.; Salo, E. V.; Ziller, J. W.; Guan, Z. *Angew. Chem. Int. Ed.* **2004**, *43*, 1821-1825.
(22) Leung, D. H.; Ziller, J. W.; Guan, Z. *J. Am. Chem. Soc.* **2008**, *130*, 7538-7539.
(23) Small, B. L.; Brookhart, M.; Bennett, A. M. A. *J. Am. Chem. Soc.* **1998**, *120*, 4049-4050.
(24) Britovsek, G. J. P.; Bruce, M.; Gibson, V. C.; Kimberley, B. S.; Maddox, P. J.; Mastroianni, S.; McTavish, S. J.; Redshaw, C.; Solan, G. A.; Strömberg, S.; White, A. J. P.; Williams, D. J. *J. Am. Chem. Soc.* **1999**, *121*, 8728-8740.
(25) Noyori, R.; Takaya, H. *Acc. Chem. Res.* **1990**, *23*, 345-350.
(26) Grubbs, R. H.; Miller, S. J.; Fu, G. C. *Acc. Chem. Res.* **1995**, *28*, 446-452.
(27) Trnka, T. M.; Grubbs, R. H. *Acc. Chem. Res.* **2001**, *34*, 18-29.
(28) Ueda, J.; Matsuyama, M.; Kamigaito, M.; Sawamoto, M. *Macromolecules* **1998**, *31*, 557-562.
(29) James, B. R.; Markham, L. D. *J. Catal.* **1972**, *27*, 442-451.
(30) Komiya, S.; Yamamoto, A.; Ikeda, S. *Bull. Chem. Soc. Jpn.* **1975**, *48*, 101-107.
(31) Nomura, K.; Warit, S.; Imanishi, Y. *Macromolecules* **1999**, *32*, 4732-4734.
(32) Nomura, K.; Sidokmai, W.; Imanishi, Y. *Bull. Chem. Soc. Jpn.* **2000**, *73*, 599-605.

(33) Piche, L.; Daigle, J.-C.; Claverie, J. P. *Chem. Commun.* **2011**, *47*, 7836-7838.
(34) Camacho-Fernandez, M. A.; Yen, M.; Ziller, J. W.; Guan, Z. *Chem. Sci.* **2013**, *4*, 2902-2906.
(35) Friedberger, T.; Ziller, J. W.; Guan, Z. *Organometallics* **2014**, *33*, 1913-1916.
(36) Čubrilo, J.; Hartenbach, I.; Schleid, T.; Winter, R. F. *Z. Anorg. Allg. Chem.* **2006**, *632*, 400-408.
(37) Birch, A. J. *Journal of the Chemical Society (Resumed)* **1944**, *0*, 430-436.
(38) Miyaki, Y.; Onishi, T.; Kurosawa, H. *Inorg. Chim. Acta* **2000**, *300-302*, 369-377.
(39) R. Kumar, K.; Sivaram, S. *Macromol. Chem. Phys.* **2000**, *201*, 1513-1520.
(40) Maldanis, R. J.; Wood, J. S.; Chandrasekaran, A.; Rausch, M. D.; Chien, J. C. W. *J. Organomet. Chem.* **2002**, *645*, 158-167.
(41) Fernando de Souza, R.; Simon, L. C.; Alves, M. d. C. M. *J. Catal.* **2003**, *214*, 165-168.
(42) de Souza, C. G.; de Souza, R. F.; Bernardo-Gusmão, K. *Applied Catalysis A: General* **2007**, *325*, 87-90.
(43) Evans, W. J.; Champagne, T. M.; Giarikos, D. G.; Ziller, J. W. *Organometallics* **2005**, *24*, 570-579.
(44) Deng, L.; Margl, P.; Ziegler, T. *J. Am. Chem. Soc.* **1997**, *119*, 1094-1100.
(45) Michalak, A.; Ziegler, T. *Organometallics* **2003**, *22*, 2660-2669.
(46) Heyndrickx, W.; Occhipinti, G.; Minenkov, Y.; Jensen, V. R. *J. Mol. Catal. A: Chem.* **2010**, *324*, 64-74.
(47) Dias, E. L.; Brookhart, M.; White, P. S. *Organometallics* **2000**, *19*, 4995-5004.
(48) Margl, P.; Deng, L.; Ziegler, T. *Organometallics* **1998**, *17*, 933-946.
(49) Margl, P.; Deng, L.; Ziegler, T. *J. Am. Chem. Soc.* **1998**, *120*, 5517-5525.
(50) Deng, L.; Woo, T. K.; Cavallo, L.; Margl, P. M.; Ziegler, T. *J. Am. Chem. Soc.* **1997**, *119*, 6177-6186.
(51) Jensen, V. R.; Thiel, W. *Organometallics* **2001**, *20*, 4852-4862.
(52) Schmid, R.; Ziegler, T. *Organometallics* **2000**, *19*, 2756-2765.
(53) Albéniz, A. C.; Espinet, P.; Lin, Y.-S. *Organometallics* **1996**, *15*, 5010-5017.
(54) Dupont, J.; Gruber, A. S.; Fonseca, G. S.; Monteiro, A. L.; Ebeling, G.; Burrow, R. A. *Organometallics* **2000**, *20*, 171-176.
(55) Canovese, L.; Lucchini, V.; Santo, C.; Visentin, F.; Zambon, A. *J. Organomet. Chem.* **2002**, *642*, 58-63.
(56) Shan, X.; Espenson, J. H. *Organometallics* **2003**, *22*, 1250-1254.
(57) Dolg, M.; Stoll, H.; Preuss, H. *Theoretica chimica acta* **1993**, *85*, 441-450.

3.6 Experimental Section

General. All organometallic manipulations were conducted under inert atmosphere by using standard Schlenk, vacuum, or glove box (N_2) techniques. All reagents were used as received from commercial suppliers unless otherwise noted. Anhydrous solvents were passed through a column of activated alumina (type A2, size 12x32, Purify) under argon pressure. Ethanol was degassed by passing a stream of N2 through the solvent. Deuterated solvents were purchased from Cambridge Isotope Laboratories and were placed over activated 4Å molecular sieves. Ultrahigh pure grade ethylene gas was purchased from Praxair and used without further purification. ^{1}H and ^{13}C-NMR spectra of organic compounds (ligands) were recorded at 500 MHz on a Bruker GN-500. Organometallic compounds ^{1}H NMR were recorded at 500 MHz on a Bruker GN-500 or Cryo-500, and ^{13}C-NMR on Cryo-500 spectrometer. All NMR chemical shifts are reported as δ in parts per million (ppm). ^{1}H and ^{13}C NMR spectra are relative to residual solvent. Molecular weights (Mn and Mw) and polydispersity indices (Mw/Mn) were determined by high-temperature gel permeation chromatography (GPC), using an Agilent PL-GPC 220 GPC equipped with a refractive index (dRI) detector and in-line viscometer. The column set consisted of two PLgel 5μm mixed-C 300x7.5 mm (and precolumn) and the samples were eluted at 150 °C with 1,2,4-trichlorobenzene containing 0.01 wt % di-tert-butyl-hydroxytoluene (BHT) at 1.0 mL/min rate. Universal calibration with polystyrene standards was used. Polymers solutions were placed in a heating plate at 150 °C prior to sample analysis and hot filtration was used before sampling. Branching was determined by ^{1}H-NMR and expressed as the number of Me's per 1000 carbons.[1] Electrospray Ionization Mass Spectrometric analyses

(ESI-MS) were obtained on a Waters Micromass LCT ESI-MS. Complexation of **3b** with $RuCl_3xH_2O$ to form **3** was done following published procedures.[2]

General procedure for ethylene polymerization. A 600 mL autoclave (Parr reactor) was heated under high vacuum to 120 °C for two hours then twice purged with ethylene and cooled to the desired polymerization temperature. A 100 mL Schlenk flask was kept in an oven overnight and introduced into the glove box. Dry DCM solvent (100 mL) was measured placed in a 100 mL round bottom flask. An aliquot of 10 mL of the solvent were used to dissolve the desired amount of complex **6** or **7** and introduced in a 12 mL syringe. Another 10 mL of DCM were loaded into a syringe for later rising of the flask. The left 80 ml solution (DCM) was loaded with the desired amount of alkyl aluminum cocatalyst. The cocatalyst solution was then transferred into the reactor through cannula under ethylene atmosphere. The reactor was then filled with ethylene at 200 psi for 10 minutes. Solution of complex was introduced through cannula under ethylene atmosphere and the flask was rinsed with the previously loaded 10 mL of solvent syringe. Parr reactor was closed and pressurized at the desired ethylene pressure. Polymerization was quenched with a methanol-acidic solution (100 mL). Polyethylene was filtrated and washed with MeOH and acetone, and finally dried under high vacuum overnight.

Computational details. DFT calculations were carried using TURBOMOLE version 6.5 program package.[3] Initial guess structures were obtained from available experimental crystal structures of by modification of them. Initial gas-phase optimizations were carried out using a double-zeta quality split-valence basis set with inclusion of polarization functions [def2-SV(P)][4] on all atoms and the inclusion of relativistic small-core pseudopotentials[557] for Ru. An open shell configuration (unrestricted wave function) was

used for all compounds. The non-hybrid GGA functional BP86[6,7] was used for all structures optimizations. Transition states search were performed initially manually and refinement of the transition state was done by scanning the potential energy surface along the corresponding coordinate. Full frequency calculations were carried out using the same level of theory to determine true minima in the potential energy surface. Also, full frequency calculations were used to determine true transition states by the finding of one negative frequency. TmoleX software was used to visualize negative frequencies and verify that correspond to the correct transition state. Energy single-point (SP) calculations were carried using the hybrid-GGA functional B3LYP[6,8] as implemented in Turbomole, together with triple-zeta quality basis sets (def2-TZVP)[9] for all atoms with an open shell configuration. Zero point energy (ZPE) corrections to the total energy were also applied by running a complete frequency calculation at the same level of theory.

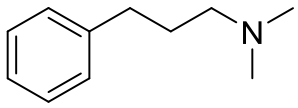

3.2a

Synthesis of N,N-dimethyl-3-phenylpropan-1-amine (3.2a). A 25 ml round bottom flask was charged with 1.0 g of 1-bromo-3-phenylpropane (5 mmol). A total volume of 3.75 mL (7.5 mmol) of dimethyl amine solution in THF (2.0 M) was added to the 25 mL flask dropwise under inert atmosphere. A white precipitate can be observed after 3 hours. Reaction was stopped after 5 hours. The product was washed with a $NaHCO_3$ solution and extracted with ether. Flash column chromatography, hexanes first and increasing gradually the amount of ethyl acetate (50%), afforded a yellowish oil that was further purified by high vacuum distillation (40-42 °C at 0.30 mm) to afford a colorless oil. Yield: 0.61 g, 80%. ^1H

NMR (500 MHz, $CDCl_3$): δ 7.27 (m, 2H, *aryl*), 7.18 (m, 3H, *aryl*), 2.67 (t, *J* = 7.5 Hz, 2H), 2.31 (t, *J* = 6.0 Hz, 2H), 2.25 (s, 6H), 1.82 (tt, *J* = 6.0, 7.5 Hz, 2H). ^{13}C NMR (500 MHz, $CDCl_3$): δ 142.3, 128.4, 125.8, 59.3, 45.6, 33.7, 29.6. ESI-MS (ESI+, CH_2Cl_2/MeOH) *m/z* calcd for $C_{11}H_{17}N$ $[M]^+$, 163.14; found $[M+H]^+$, 164.22.

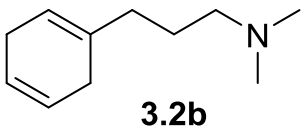

3.2b

Synthesis of 3-(cyclohexa-1,4-dienyl)-N,N-dimethylpropan-1-amine (3.2b). A two-neck 500 mL round bottom flask was flame dried before being cooled down in a dry ice/acetone bath (-78 °C) and was kept at this temperature the whole time. 60 mL of degassed ethanol was added, and 2.342 g (0.014 mol, 1 eq) of **2a** was added. Gaseous NH_3 (~240 mL) was liquefied into the flask with the help of dry ice/acetone mixture in a cold finger apparatus and stirred for 10 minutes. Metal sodium 1.5000 g (0.064 mol, 4.6 eq) was added portion wise. The solution was left to reach room temperature, and NH_3 was slowly evaporated. The flask was covered, and the solution was left stirring for 72 hours. A 500 mL saturated solution of ammonium chloride (NH_4Cl) was added to the reaction flask. The mixture was extracted with ether (3 x 500 mL), and the organic phase was dried over sodium sulfate. The evaporation of the ether *in vacuo*, afforded a colorless oil. ^1H NMR of the crude material showed no presence of starting material. Purification was carried out by high vacuum distillation (41 °C at 0.30-0.35 mm, b.p. ~ 220 °C) to afford a colorless oil. Yield: 1.45 g, 61%. ^1H NMR (500 MHz, $CDCl_3$): δ 5.70 (m, 2H), 5.43 (m, 1H), 2.67 (m, 2H), 2.60 (m, 1H), 2.24 (t, *J* = 7.5, 2H), 2.21 (s, 6H), 1.97 (t, *J* = 7.5, 2H), 1.59 (m, 2H). ^{13}C NMR

(500 MHz, $CDCl_3$): δ 134.9, 124.5, 118.5, 59.9, 45.8, 35.4, 29.2, 27.0, 25.8. ESI-MS (ESI+, CH_2Cl_2/MeOH) *m/z* calcd for $C_{11}H_{19}N$ $[M]^+$, 165.15; found $[M+H]^+$, 166.16.

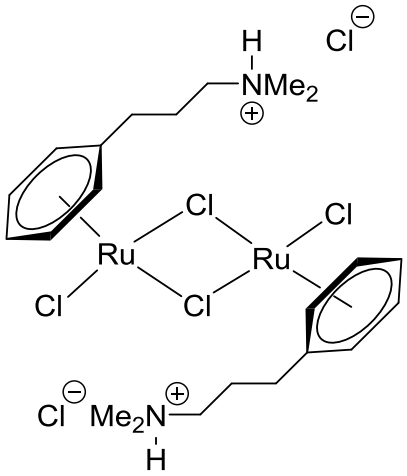

3.2c

Synthesis of [Ru(η^6- Ph$(CH_2)_3$NH$(CH_3)_2$Cl$_2$]$_2$Cl$_2$ (3.2c). Compound **2b** (1.0059 g, 0.0061 mol) was added to degassed ethanol (25 mL) in a 50 mL round bottom flask and stirred for 10 minutes. An excess of aqueous HCl was added. A total of 0.6430 g (0.0031 mol, 1 equiv) of $RuCl_3xH_2O$ was added to the solution. The mixture was heated under reflux for 5 hours. The solution was left to reach room temperature and dried *in vacuo* to obtain a light-brown solid. The solid was filtered, washed with ether and hexanes and dried overnight under house vacuum. Yield: 1.0030 g, 87%. ^{1}H NMR (500 MHz, d^6-DMSO): δ 9.86 (s, 1H) 6.02 (m, 2H), 5.82 (m, 3H), 3.13 (m, 2H), 2.76 (s, 6H), 2.53 (m, 2H), 2.00 (m, 2H). ^{13}C NMR (500 MHz, d^6-DMSO): δ 105.6, 88.4, 58.5, 83.7, 42.4, 29.1, 23.0. ESI-MS (ESI+, DMSO/MeOH) *m/z* calcd for $C_{22}H_{36}Cl_4N_2Ru_2$ $[M]^{2+}$,671.97; found $[M]^{2+}$/2, 335.99. $[M]^+$, 617.99.

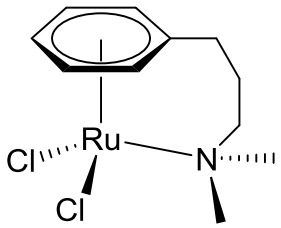

3.2

Synthesis of Ru(η^6- Ph$(CH_2)_3$N$(CH_3)_2Cl_2)_2$ (3.2). To a solution of **2c,** 0.4032 g (0.00054 mol, 1 eq) in DCM (40 ml), was added 0.4078 g (0.0022 mol, 4 equiv, 0.52 ml) of tri(n-butyl)amine and stirred for two hours. The solution turned dark. The solution was filtrated and dried *in vacuo*. A light brown solid is precipitated and washed with ether, ethyl acetate and ether again. Recrystallization by slow diffusion of dichloromethane/hexanes gave dark brown crystals suitable for x-ray analysis. Yield: 0.1454 g, 40%. The unreacted complex 2c can also be treated with more organic base to increase yield. We noticed that the use of strong bases, such as NaOH, yielded decomposed material, probably due to the acidity of the methyl-amine protons. ^{1}H NMR (500 MHz, d^6- $CDCl_3$): δ 5.77 (m, 1H,) 5.65 (m, 2H), 5.31 (m, 2H), 2.76 (m, 2H), 2.57 (s, 6H), 2.38 (m, 2H), 1.60 (m, 2H). ^{13}C NMR (500 MHz, $CDCl_3$): δ 91.7, 86.4, 83.7, 82.7, 63.8, 53.4, 29.7, 24.3. ESI-MS (ESI+, CH_2Cl_2) *m/z* calcd for $C_{11}H_{17}Cl_2NRu$ $[M]^+$, 335.24; found $[M\text{-}Cl]^+$, 299.95.

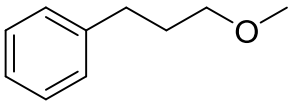

3.3a

Synthesis of 1-(3-methoxypropyl)benzene (3.3a). The compound 3-phenyl-1-propanol 10 g (0.073 mol) was added to 100 ml of THF. NaH 3.5250 g (0.088 mol) was added to the solution under an argon balloon atmosphere for five minutes. MeI 12.5040 g (0.088 mol) was added through a needle. The reaction was left stirring at room

temperature for 48 hours. Extraction by H_2O/Ether and organic phase evaporation *in vacuo* afforded a colorless oil. Further purification was carried out under high vacuum distillation Yield: 7.5525 g, 69%. ^{1}H NMR (500 MHz, d^6- $CDCl_3$): δ 7.20 (m, 2H,) 7.11 (m, 3H), 3.32 (t, *J* = 6.5, 2H), 3.26 (s, 3H), 2.62 (t, *J* = 7.5, 2H), 1.82 (tt, *J* = 6.5, 7.5, 2H).

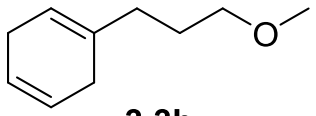

3.3b

Synthesis of (methoxypropyl)cyclohexa-1,4-diene (3.3b). Birch reduction was carried out the same way it was carried out for **2b**. Yield: 2.005 g, 67%. ^{1}H NMR (500 MHz, $CDCl_3$): δ 5.68 (m, 2H), 5.42 (m, 1H), 3.33 (m, 2H), 3.30 (s, 3H), 2.68 (m, 2H), 2.58 (m, 2H), 2.00 (m, 2H), 1.68 (m, 2H). ^{13}C NMR (500 MHz, $CDCl_3$): δ 134.4, 124.3, 118.5, 77.1, 58.5, 33.8, 28.9, 27.3, 26.8.

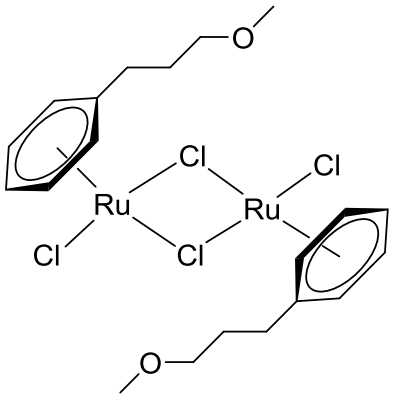

3.3

Synthesis of [Ru(η^6- $Ph(CH_2)_3O(CH_3)_2Cl_2$](3). Synthesized following published procedures.[36] ^{1}H NMR (500 MHz, d^6 $CDCl_3$): δ 5.65 (t, *J* = 5.5 Hz, 2H), 5.58 (t, *J* = 5.5 Hz, 1H), 5.40 (m, *J* = 7.5 Hz, 2H), 3.39 (t, *J* = 6.0 Hz, 2H), 3.29 (s, 3H), 2.64 (t, *J* = 7.5 Hz, 2H), 1.86 (tt, *J* = 6.0, 7.5 Hz, 2H). ^{13}C NMR (500 MHz, $CDCl_3$): δ 101.3, 84.2, 80.7, 80.0, 71.6, 58.8, 30.1, 29.6.

X-ray Data Collection, Structure Solution and Refinement for XX. A red crystal of approximate dimensions 0.13 x 0.34 x 0.39 mm was mounted on a glass fiber and transferred to a Bruker SMART APEX II diffractometer. The APEX2[10] program package was used to determine the unit-cell parameters and for data collection (10 sec/frame scan time for a sphere of diffraction data). The raw frame data was processed using SAINT[11] and SADABS[12] to yield the reflection data file. Subsequent calculations were carried out using the SHELXTL[13] program. The systematic absences were consistent with the hexagonal space groups R3 and $R\bar{3}$. The centrosymmetric space group $R\bar{3}$ was assigned and later determined to be correct.

The structure was solved by direct methods and refined on F^2 by full-matrix least-squares techniques. The analytical scattering factors[14] for neutral atoms were used throughout the analysis. Hydrogen atoms were located from a difference-Fourier amp and refined (x,y,z and U_{iso}) At convergence, wR2 = 0.0442 and Goof = 1.059 for 247 variables refined against 3612 data (0.74 Å), R1 = 0.0174 for those 3367 data with $I > 2.0\sigma(I)$.

Table 3.3. Crystal data and structure refinement for **3.2**.

Identification code	zg33 (Miguel Camacho)	
Empirical formula	C_{14} H_{21} Cl_2 N Ru	
Formula weight	375.29	
Temperature	88(2) K	
Wavelength	0.71073 Å	
Crystal system	Rhombohedral	
Space group	$R\bar{3}$	
Unit cell dimensions	a = 30.212(2) Å	α= 90°.
	b = 30.212(2) Å	β= 90°.
	c = 8.1946(6) Å	γ = 120°.
Volume	6477.7(8) $Å^3$	
Z	18	
Density (calculated)	1.732 Mg/m^3	
Absorption coefficient	1.442 mm^{-1}	
F(000)	3420	
Crystal color	red	
Crystal size	0.39 x 0.34 x 0.13 mm^3	
Theta range for data collection	2.34 to 28.84°	
Index ranges	$-40 \le h \le 40$, $-40 \le k \le 40$, $-11 \le l \le 11$	
Reflections collected	25987	
Independent reflections	3612 [R(int) = 0.0211]	
Completeness to theta = 25.50°	100.0 %	
Absorption correction	Numerical	
Max. and min. transmission	0.8381 and 0.6053	
Refinement method	Full-matrix least-squares on F^2	
Data / restraints / parameters	3612 / 0 / 247	
Goodness-of-fit on F^2	1.059	
Final R indices [I>2sigma(I) = 3367 data]	R1 = 0.0174, wR2 = 0.0434	
R indices (all data; 0.74Å)	R1 = 0.0193, wR2 = 0.0442	
Largest diff. peak and hole	1.138 and -0.383 $e.Å^{-3}$	

Table 3.4. Atomic coordinates (x 10^4) and equivalent isotropic displacement parameters ($Å^2$x 10^3) for **3.2** U(eq) is defined as one third of the trace of the orthogonalized U^{ij} tensor.

	x	y	z	U(eq)
Ru(1)	8279(1)	884(1)	4554(1)	15(1)
Cl(1)	8829(1)	1770(1)	3845(1)	20(1)
Cl(2)	8861(1)	1006(1)	6789(1)	18(1)
N(1)	8763(1)	705(1)	2916(1)	17(1)
C(1)	7655(1)	936(1)	3479(2)	20(1)
C(2)	7690(1)	1070(1)	5167(2)	21(1)
C(3)	7690(1)	736(1)	6357(2)	21(1)
C(4)	7644(1)	260(1)	5883(2)	20(1)
C(5)	7600(1)	125(1)	4227(2)	19(1)
C(6)	7612(1)	466(1)	2989(2)	19(1)
C(7)	7622(1)	345(1)	1214(2)	22(1)
C(8)	8045(1)	225(1)	788(2)	22(1)
C(9)	8585(1)	657(1)	1176(2)	21(1)
C(10)	9320(1)	1114(1)	2947(2)	20(1)
C(11)	9682(1)	974(1)	2084(2)	24(1)
C(12)	9624(1)	472(1)	2701(2)	25(1)
C(13)	9062(1)	56(1)	2636(2)	22(1)
C(14)	8729(1)	222(1)	3544(2)	17(1)

Table 3.5. Bond lengths [Å] and angles [°] for **3.2**.

Ru(1)-Cnt	1.656
Ru(1)-C(1)	2.1551(15)
Ru(1)-C(2)	2.1753(15)
Ru(1)-C(6)	2.1801(14)
Ru(1)-C(3)	2.1803(15)
Ru(1)-C(4)	2.1929(14)
Ru(1)-C(5)	2.1996(14)
Ru(1)-N(1)	2.2420(12)
Ru(1)-Cl(1)	2.4112(4)
Ru(1)-Cl(2)	2.4352(4)
N(1)-C(14)	1.5027(18)
N(1)-C(9)	1.5049(18)
N(1)-C(10)	1.5101(18)
C(1)-C(6)	1.417(2)
C(1)-C(2)	1.430(2)
C(2)-C(3)	1.404(2)
C(3)-C(4)	1.426(2)
C(4)-C(5)	1.404(2)
C(5)-C(6)	1.433(2)
C(6)-C(7)	1.504(2)
C(7)-C(8)	1.533(2)
C(8)-C(9)	1.528(2)
C(10)-C(11)	1.528(2)
C(11)-C(12)	1.522(2)
C(12)-C(13)	1.526(2)
C(13)-C(14)	1.524(2)
Cnt-Ru(1)-N(1)	129.2
Cnt-Ru(1)-Cl(1)	124.7
Cnt-Ru(1)-Cl(2)	125.8
C(1)-Ru(1)-C(2)	38.56(6)
C(1)-Ru(1)-C(6)	38.14(5)
C(2)-Ru(1)-C(6)	69.34(6)
C(1)-Ru(1)-C(3)	68.82(6)
C(2)-Ru(1)-C(3)	37.62(6)

C(6)-Ru(1)-C(3)	81.77(6)
C(1)-Ru(1)-C(4)	81.01(6)
C(2)-Ru(1)-C(4)	68.27(6)
C(6)-Ru(1)-C(4)	68.63(6)
C(3)-Ru(1)-C(4)	38.07(6)
C(1)-Ru(1)-C(5)	68.42(5)
C(2)-Ru(1)-C(5)	80.81(6)
C(6)-Ru(1)-C(5)	38.21(5)
C(3)-Ru(1)-C(5)	68.16(6)
C(4)-Ru(1)-C(5)	37.28(6)
C(1)-Ru(1)-N(1)	118.19(5)
C(2)-Ru(1)-N(1)	156.51(5)
C(6)-Ru(1)-N(1)	91.89(5)
C(3)-Ru(1)-N(1)	156.90(5)
C(4)-Ru(1)-N(1)	119.05(5)
C(5)-Ru(1)-N(1)	93.20(5)
C(1)-Ru(1)-Cl(1)	87.92(4)
C(2)-Ru(1)-Cl(1)	88.17(4)
C(6)-Ru(1)-Cl(1)	115.20(4)
C(3)-Ru(1)-Cl(1)	115.50(4)
C(4)-Ru(1)-Cl(1)	153.58(4)
C(5)-Ru(1)-Cl(1)	153.40(4)
N(1)-Ru(1)-Cl(1)	87.33(3)
C(1)-Ru(1)-Cl(2)	152.53(4)
C(2)-Ru(1)-Cl(2)	114.12(4)
C(6)-Ru(1)-Cl(2)	156.58(4)
C(3)-Ru(1)-Cl(2)	88.51(4)
C(4)-Ru(1)-Cl(2)	90.66(4)
C(5)-Ru(1)-Cl(2)	118.38(4)
N(1)-Ru(1)-Cl(2)	88.77(3)
Cl(1)-Ru(1)-Cl(2)	88.218(12)
C(14)-N(1)-C(9)	112.57(11)
C(14)-N(1)-C(10)	107.19(11)
C(9)-N(1)-C(10)	107.05(11)
C(14)-N(1)-Ru(1)	107.11(8)
C(9)-N(1)-Ru(1)	110.19(9)

C(10)-N(1)-Ru(1)	112.77(8)
C(6)-C(1)-C(2)	121.00(14)
C(6)-C(1)-Ru(1)	71.89(8)
C(2)-C(1)-Ru(1)	71.49(8)
C(3)-C(2)-C(1)	119.63(14)
C(3)-C(2)-Ru(1)	71.38(9)
C(1)-C(2)-Ru(1)	69.95(8)
C(2)-C(3)-C(4)	119.99(14)
C(2)-C(3)-Ru(1)	71.00(9)
C(4)-C(3)-Ru(1)	71.44(8)
C(5)-C(4)-C(3)	120.27(14)
C(5)-C(4)-Ru(1)	71.62(8)
C(3)-C(4)-Ru(1)	70.49(8)
C(4)-C(5)-C(6)	120.66(13)
C(4)-C(5)-Ru(1)	71.10(8)
C(6)-C(5)-Ru(1)	70.16(8)
C(1)-C(6)-C(5)	118.43(14)
C(1)-C(6)-C(7)	120.98(13)
C(5)-C(6)-C(7)	120.41(13)
C(1)-C(6)-Ru(1)	69.97(8)
C(5)-C(6)-Ru(1)	71.63(8)
C(7)-C(6)-Ru(1)	125.80(10)
C(6)-C(7)-C(8)	113.44(12)
C(9)-C(8)-C(7)	114.23(13)
N(1)-C(9)-C(8)	117.17(12)
N(1)-C(10)-C(11)	115.09(12)
C(12)-C(11)-C(10)	112.33(13)
C(11)-C(12)-C(13)	109.66(13)
C(14)-C(13)-C(12)	110.86(12)
N(1)-C(14)-C(13)	114.69(12)

Table 3.6. Anisotropic displacement parameters ($Å^2$x 10^3) for **3.2**. The anisotropic displacement factor exponent takes the form: $-2\pi^2[h^2 a^{*2} U^{11} + ... + 2 h k a^* b^* U^{12}]$

	U^{11}	U^{22}	U^{33}	U^{23}	U^{13}	U^{12}
Ru(1)	16(1)	12(1)	15(1)	-1(1)	-1(1)	6(1)
Cl(1)	23(1)	13(1)	22(1)	0(1)	-1(1)	7(1)
Cl(2)	19(1)	20(1)	15(1)	-1(1)	-1(1)	11(1)
N(1)	19(1)	16(1)	14(1)	0(1)	0(1)	8(1)
C(1)	18(1)	17(1)	26(1)	1(1)	-3(1)	9(1)
C(2)	17(1)	19(1)	30(1)	-3(1)	0(1)	10(1)
C(3)	18(1)	23(1)	21(1)	-3(1)	1(1)	9(1)
C(4)	16(1)	18(1)	22(1)	3(1)	2(1)	6(1)
C(5)	17(1)	14(1)	23(1)	-1(1)	-3(1)	6(1)
C(6)	16(1)	17(1)	22(1)	-1(1)	-5(1)	7(1)
C(7)	26(1)	18(1)	21(1)	-2(1)	-9(1)	11(1)
C(8)	29(1)	20(1)	18(1)	-3(1)	-6(1)	13(1)
C(9)	28(1)	22(1)	13(1)	0(1)	-1(1)	12(1)
C(10)	19(1)	17(1)	19(1)	-1(1)	2(1)	6(1)
C(11)	22(1)	25(1)	20(1)	-2(1)	5(1)	9(1)
C(12)	21(1)	27(1)	26(1)	-6(1)	2(1)	13(1)
C(13)	23(1)	22(1)	22(1)	-5(1)	-1(1)	13(1)
C(14)	19(1)	16(1)	17(1)	-1(1)	-1(1)	9(1)

Table 3.7. Hydrogen coordinates (x 10^4) and isotropic displacement parameters ($Å^2$x 10^3) for **3.2**.

	x	y	z	U(eq)
H(1A)	7708(7)	1173(7)	2690(20)	22(5)
H(2A)	7755(7)	1385(7)	5490(20)	22(5)
H(3A)	7752(7)	835(7)	7350(20)	19(4)
H(4A)	7661(7)	40(7)	6690(20)	21(4)
H(5A)	7596(7)	-163(7)	3940(20)	18(4)
H(7A)	7663(7)	630(7)	590(20)	25(5)
H(7B)	7287(8)	62(8)	920(20)	27(5)
H(8A)	7974(7)	-88(7)	1250(20)	23(5)
H(8B)	8041(7)	173(7)	-410(20)	24(5)
H(9A)	8607(6)	984(7)	920(20)	16(4)
H(9B)	8828(7)	618(7)	480(20)	25(5)
H(10A)	9411(6)	1179(7)	4100(20)	16(4)
H(10B)	9357(7)	1419(7)	2480(20)	22(4)
H(11A)	9618(8)	952(8)	900(20)	31(5)
H(11B)	10014(7)	1247(7)	2270(20)	25(5)
H(12A)	9749(7)	514(7)	3820(20)	28(5)
H(12B)	9816(8)	372(7)	2050(20)	28(5)
H(13A)	8946(7)	-40(7)	1540(20)	22(4)
H(13B)	9006(7)	-259(7)	3160(20)	21(4)
H(14A)	8380(7)	-51(6)	3500(20)	14(4)
H(14B)	8834(7)	292(7)	4660(20)	23(5)

Table 3.8. Torsion angles [°] for **3.2**.

C(1)-Ru(1)-N(1)-C(14)	-121.00(9)
C(2)-Ru(1)-N(1)-C(14)	-128.00(13)
C(6)-Ru(1)-N(1)-C(14)	-92.06(9)
C(3)-Ru(1)-N(1)-C(14)	-18.79(17)
C(4)-Ru(1)-N(1)-C(14)	-25.55(10)
C(5)-Ru(1)-N(1)-C(14)	-53.84(9)
Cl(1)-Ru(1)-N(1)-C(14)	152.79(8)
Cl(2)-Ru(1)-N(1)-C(14)	64.52(8)
C(1)-Ru(1)-N(1)-C(9)	1.76(11)
C(2)-Ru(1)-N(1)-C(9)	-5.24(18)
C(6)-Ru(1)-N(1)-C(9)	30.71(10)
C(3)-Ru(1)-N(1)-C(9)	103.98(15)
C(4)-Ru(1)-N(1)-C(9)	97.21(10)
C(5)-Ru(1)-N(1)-C(9)	68.93(9)
Cl(1)-Ru(1)-N(1)-C(9)	-84.44(9)
Cl(2)-Ru(1)-N(1)-C(9)	-172.71(9)
C(1)-Ru(1)-N(1)-C(10)	121.32(10)
C(2)-Ru(1)-N(1)-C(10)	114.32(14)
C(6)-Ru(1)-N(1)-C(10)	150.26(10)
C(3)-Ru(1)-N(1)-C(10)	-136.47(13)
C(4)-Ru(1)-N(1)-C(10)	-143.23(9)
C(5)-Ru(1)-N(1)-C(10)	-171.52(10)
Cl(1)-Ru(1)-N(1)-C(10)	35.11(9)
Cl(2)-Ru(1)-N(1)-C(10)	-53.16(9)
C(2)-Ru(1)-C(1)-C(6)	-132.93(13)
C(3)-Ru(1)-C(1)-C(6)	-104.17(10)
C(4)-Ru(1)-C(1)-C(6)	-66.68(9)
C(5)-Ru(1)-C(1)-C(6)	-30.18(9)
N(1)-Ru(1)-C(1)-C(6)	51.54(10)
Cl(1)-Ru(1)-C(1)-C(6)	137.40(8)
Cl(2)-Ru(1)-C(1)-C(6)	-140.49(8)
C(6)-Ru(1)-C(1)-C(2)	132.93(13)
C(3)-Ru(1)-C(1)-C(2)	28.76(9)
C(4)-Ru(1)-C(1)-C(2)	66.24(9)

C(5)-Ru(1)-C(1)-C(2)	102.75(10)
N(1)-Ru(1)-C(1)-C(2)	-175.53(8)
Cl(1)-Ru(1)-C(1)-C(2)	-89.68(8)
Cl(2)-Ru(1)-C(1)-C(2)	-7.57(14)
C(6)-C(1)-C(2)-C(3)	1.0(2)
Ru(1)-C(1)-C(2)-C(3)	-53.24(13)
C(6)-C(1)-C(2)-Ru(1)	54.29(13)
C(1)-Ru(1)-C(2)-C(3)	132.70(13)
C(6)-Ru(1)-C(2)-C(3)	103.80(10)
C(4)-Ru(1)-C(2)-C(3)	29.40(9)
C(5)-Ru(1)-C(2)-C(3)	65.96(9)
N(1)-Ru(1)-C(2)-C(3)	142.62(12)
Cl(1)-Ru(1)-C(2)-C(3)	-138.34(9)
Cl(2)-Ru(1)-C(2)-C(3)	-51.12(9)
C(6)-Ru(1)-C(2)-C(1)	-28.90(8)
C(3)-Ru(1)-C(2)-C(1)	-132.70(13)
C(4)-Ru(1)-C(2)-C(1)	-103.30(9)
C(5)-Ru(1)-C(2)-C(1)	-66.75(9)
N(1)-Ru(1)-C(2)-C(1)	9.92(17)
Cl(1)-Ru(1)-C(2)-C(1)	88.96(8)
Cl(2)-Ru(1)-C(2)-C(1)	176.18(7)
C(1)-C(2)-C(3)-C(4)	-1.5(2)
Ru(1)-C(2)-C(3)-C(4)	-54.03(12)
C(1)-C(2)-C(3)-Ru(1)	52.58(12)
C(1)-Ru(1)-C(3)-C(2)	-29.43(9)
C(6)-Ru(1)-C(3)-C(2)	-66.66(9)
C(4)-Ru(1)-C(3)-C(2)	-132.31(13)
C(5)-Ru(1)-C(3)-C(2)	-103.78(10)
N(1)-Ru(1)-C(3)-C(2)	-141.93(12)
Cl(1)-Ru(1)-C(3)-C(2)	47.40(10)
Cl(2)-Ru(1)-C(3)-C(2)	134.71(9)
C(1)-Ru(1)-C(3)-C(4)	102.89(10)
C(2)-Ru(1)-C(3)-C(4)	132.31(13)
C(6)-Ru(1)-C(3)-C(4)	65.66(9)
C(5)-Ru(1)-C(3)-C(4)	28.53(9)
N(1)-Ru(1)-C(3)-C(4)	-9.61(18)

Cl(1)-Ru(1)-C(3)-C(4)	179.71(7)
Cl(2)-Ru(1)-C(3)-C(4)	-92.97(8)
C(2)-C(3)-C(4)-C(5)	0.3(2)
Ru(1)-C(3)-C(4)-C(5)	-53.55(13)
C(2)-C(3)-C(4)-Ru(1)	53.82(12)
C(1)-Ru(1)-C(4)-C(5)	65.98(9)
C(2)-Ru(1)-C(4)-C(5)	103.87(10)
C(6)-Ru(1)-C(4)-C(5)	28.46(9)
C(3)-Ru(1)-C(4)-C(5)	132.94(13)
N(1)-Ru(1)-C(4)-C(5)	-51.36(10)
Cl(1)-Ru(1)-C(4)-C(5)	132.35(9)
Cl(2)-Ru(1)-C(4)-C(5)	-140.32(8)
C(1)-Ru(1)-C(4)-C(3)	-66.96(9)
C(2)-Ru(1)-C(4)-C(3)	-29.07(9)
C(6)-Ru(1)-C(4)-C(3)	-104.48(10)
C(5)-Ru(1)-C(4)-C(3)	-132.94(13)
N(1)-Ru(1)-C(4)-C(3)	175.70(8)
Cl(1)-Ru(1)-C(4)-C(3)	-0.59(15)
Cl(2)-Ru(1)-C(4)-C(3)	86.74(9)
C(3)-C(4)-C(5)-C(6)	1.3(2)
Ru(1)-C(4)-C(5)-C(6)	-51.68(12)
C(3)-C(4)-C(5)-Ru(1)	53.03(12)
C(1)-Ru(1)-C(5)-C(4)	-104.03(10)
C(2)-Ru(1)-C(5)-C(4)	-66.01(9)
C(6)-Ru(1)-C(5)-C(4)	-134.15(13)
C(3)-Ru(1)-C(5)-C(4)	-29.10(9)
N(1)-Ru(1)-C(5)-C(4)	136.85(9)
Cl(1)-Ru(1)-C(5)-C(4)	-132.73(9)
Cl(2)-Ru(1)-C(5)-C(4)	46.52(9)
C(1)-Ru(1)-C(5)-C(6)	30.13(9)
C(2)-Ru(1)-C(5)-C(6)	68.14(9)
C(3)-Ru(1)-C(5)-C(6)	105.05(10)
C(4)-Ru(1)-C(5)-C(6)	134.15(13)
N(1)-Ru(1)-C(5)-C(6)	-89.00(9)
Cl(1)-Ru(1)-C(5)-C(6)	1.42(15)
Cl(2)-Ru(1)-C(5)-C(6)	-179.32(7)

C(2)-C(1)-C(6)-C(5)	0.5(2)
Ru(1)-C(1)-C(6)-C(5)	54.64(12)
C(2)-C(1)-C(6)-C(7)	-174.58(14)
Ru(1)-C(1)-C(6)-C(7)	-120.48(13)
C(2)-C(1)-C(6)-Ru(1)	-54.10(13)
C(4)-C(5)-C(6)-C(1)	-1.7(2)
Ru(1)-C(5)-C(6)-C(1)	-53.84(12)
C(4)-C(5)-C(6)-C(7)	173.42(13)
Ru(1)-C(5)-C(6)-C(7)	121.31(13)
C(4)-C(5)-C(6)-Ru(1)	52.10(13)
C(2)-Ru(1)-C(6)-C(1)	29.20(9)
C(3)-Ru(1)-C(6)-C(1)	65.99(9)
C(4)-Ru(1)-C(6)-C(1)	103.10(10)
C(5)-Ru(1)-C(6)-C(1)	130.91(13)
N(1)-Ru(1)-C(6)-C(1)	-136.32(9)
Cl(1)-Ru(1)-C(6)-C(1)	-48.39(9)
Cl(2)-Ru(1)-C(6)-C(1)	132.40(10)
C(1)-Ru(1)-C(6)-C(5)	-130.91(13)
C(2)-Ru(1)-C(6)-C(5)	-101.71(10)
C(3)-Ru(1)-C(6)-C(5)	-64.92(9)
C(4)-Ru(1)-C(6)-C(5)	-27.81(9)
N(1)-Ru(1)-C(6)-C(5)	92.77(9)
Cl(1)-Ru(1)-C(6)-C(5)	-179.30(7)
Cl(2)-Ru(1)-C(6)-C(5)	1.49(16)
C(1)-Ru(1)-C(6)-C(7)	114.37(16)
C(2)-Ru(1)-C(6)-C(7)	143.57(14)
C(3)-Ru(1)-C(6)-C(7)	-179.64(13)
C(4)-Ru(1)-C(6)-C(7)	-142.53(14)
C(5)-Ru(1)-C(6)-C(7)	-114.72(16)
N(1)-Ru(1)-C(6)-C(7)	-21.95(12)
Cl(1)-Ru(1)-C(6)-C(7)	65.99(13)
Cl(2)-Ru(1)-C(6)-C(7)	-113.22(13)
C(1)-C(6)-C(7)-C(8)	122.88(15)
C(5)-C(6)-C(7)-C(8)	-52.15(19)
Ru(1)-C(6)-C(7)-C(8)	36.29(18)
C(6)-C(7)-C(8)-C(9)	-59.09(17)

C(14)-N(1)-C(9)-C(8)	56.03(17)
C(10)-N(1)-C(9)-C(8)	173.56(13)
Ru(1)-N(1)-C(9)-C(8)	-63.47(14)
C(7)-C(8)-C(9)-N(1)	81.12(17)
C(14)-N(1)-C(10)-C(11)	52.57(16)
C(9)-N(1)-C(10)-C(11)	-68.44(16)
Ru(1)-N(1)-C(10)-C(11)	170.21(10)
N(1)-C(10)-C(11)-C(12)	-53.66(18)
C(10)-C(11)-C(12)-C(13)	51.96(17)
C(12)-C(13)-C(14)-N(1)	58.36(17)

3.7 Experimental Section References

(1) Daugulis, O.; Brookhart, M.; White, P. S. *Organometallics* **2002**, *21*, 5935-5943.
(2) Čubrilo, J.; Hartenbach, I.; Schleid, T.; Winter, R. F. *Z. Anorg. Allg. Chem.* **2006**, *632*, 400-408.
(3) GmbH, T.; 6.5 ed. Karlsruhe 2013. http://www.turbomole.com
(4) Schäfer, A.; Horn, H.; Ahlrichs, R. *The Journal of Chemical Physics* **1992**, *97*, 2571-2577.
(5) Dolg, M.; Stoll, H.; Preuss, H. *Theoretica chimica acta* **1993**, *85*, 441-450.
(6) Becke, A. D. *Physical Review A* **1988**, *38*, 3098-3100.
(7) Perdew, J. P. *Physical Review B* **1986**, *33*, 8822-8824.
(8) Lee, C.; Yang, W.; Parr, R. G. *Physical Review B* **1988**, *37*, 785-789.
(9) Weigend, F.; Ahlrichs, R. *PCCP* **2005**, *7*, 3297-3305.
(10) APEX2 Version 2011.4-1, Bruker AXS, Inc.; Madison, WI 2011.
(11) SAINT Version 7.68a, Bruker AXS, Inc.; Madison, WI 2009.
(12) Sheldrick, G. M. SADABS, Version 2008/1, Bruker AXS, Inc.; Madison, WI 2008.
(13) Sheldrick, G. M. SHELXTL, Version 2013/1, Bruker AXS, Inc.; Madison, WI 2013.
(14) International Tables for X-Ray Crystallography 1992, Vol. C., Dordrecht: Kluwer Academic Publishers.

Chapter 4

Ethylene Polymerization with a Half-metallocene Dithiocarbamate Ruthenium (IV) Complex: An Experimental and Theoretical Study

4.1 Introduction

Polyolefins are the largest group of commodity plastics, and they continue to grow progressively.[1-3] Most polyolefins are obtained by catalytic polymerization of simple olefin monomers through the use of early transition metal (ETM) catalysts.[2,3] While ETM catalysts generally possess high activity for olefin polymerization, their oxophilicity hampers their ability to copolymerize ethylene with polar olefin monomers.[1-3] Copolymerization of ethylene with polar monomers will greatly improve properties such as dye retention, printability, and adhesion.[4-6] In contrast, late transition metal (LTM) catalysts based on Ni(II) and Pd(II) metals are more tolerant to polar groups and are active for ethylene polymerization, albeit with lower activities.[7-25] Although polar monomer incorporation is high in certain cases, polymerization activities and molecular weights are low which make these catalysts unfit for industrial scale production. Consequently, the search for a catalyst that incorporates polar monomers without sacrificing activity remains the greatest challenge in olefin polymerization catalysis.

Middle-late periodic table transition metal catalysts based on Fe and Co display high activity but do not incorporate polar monomers.[7,8] Ruthenium, which is in the same group as Fe and the same row (i.e., second) as Pd, displays varied chemistry and tolerance to the presence of polar groups in other catalytic reactions.[9-12] Despite its success in other areas of catalysis, there have been very few reports in the last four decades of the use of ruthenium for ethylene polymerization. Early studies performed in the 1970's showed that hydridoruthenium species (i.e., $HRuCl(PPh_3)_3$ or $(H)_2Ru(PPh_3)_4$) could polymerize ethylene.[13,14] However, it was not until three decades later that Nomura et al. reported a ruthenium-pybox complex **4.1** (Chart 4.1) that could polymerize ethylene when activated with MAO.[15,16] Notably, Brookhart et al. studied mechanistically a similar Ru-diiminopyridine (complex **4.2**) that was inactive for ethylene polymerization.[17] Complex **4.2** was not capable of polymerizing ethylene, even though it is in the activated form. The authors attributed the inactivity to the coordination geometry of the Ru complex, which is a distorted square pyramidal complex. This coordination results in non-degenerate coordination sites of olefin and alkyl groups relative to the tridentate ligand, resulting in energy barriers that are too high for migratory insertion. Moreover, high insertion barriers for Nomura and Brookhart's complexes have been corroborated by computational studies. These studies found that the calculated insertion barrier for migratory insertion was larger than 25 $kcal \cdot mol^{-1}$, which is too high for olefin insertion polymerization.[18] In addition, a Ru-di(phosphine-arenesulfonate) complex that unexpectedly made cross-linked polyethylene has been reported.[19] Remarkably, no active species were elucidated for any of the aforementioned examples.

In a recent paper, we showed that a η^6-arene-tethered Ru(II) (**4.3**) complex with equivalent coordination sites in *cis* geometry is capable of catalyzing ethylene polymerization in the absence of an aluminum cocatalyst.[20] Mass spectrometry (MS) and mechanistic studies by NMR spectroscopy also showed ruthenium complex-based ethylene polymerization via a Cossee-Arlman[21-23] coordination-insertion mechanism. The experimental insertion barrier for complex **4.3** has been calculated to be 22.8 kcal·mol^{-1} (see Chapter 3). This insertion barrier is lower than the insertion barrier calculated for Nomura's and Brookhart's complexes, but it is still significantly high compared with barriers associated with LTM catalysts.[24,25]

Chart 4.1. Reported ruthenium complexes and hafnium analog.

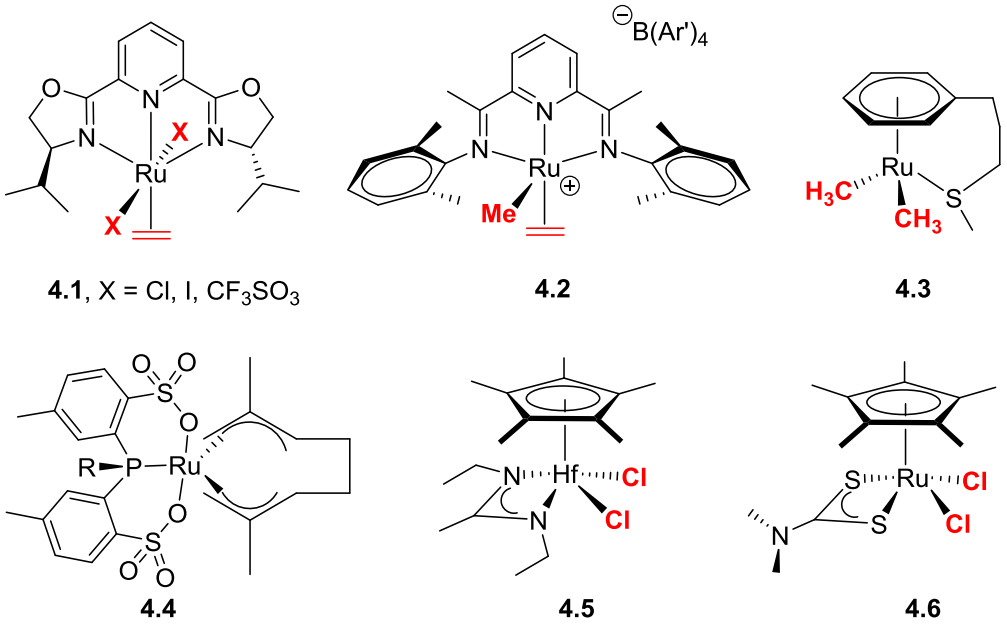

4.1, X = Cl, I, CF_3SO_3 **4.2** **4.3**

4.4 **4.5** **4.6**

We hypothesize that the electron rich nature of complex **4.3** is the reason for its high insertion barrier and ensuing lower activity. Molecular modeling has shown that metal

electron density has a great effect on the insertion barrier for ETM catalysts.[26,27] Increasing electron donation to the metal center increases π back-bonding to ethylene, which results in higher insertion barriers.[27-29] For these reasons, we envision that we can decrease the insertion barrier and increase the activity by reducing electron density in the ruthenium metal center. One approach to changing the electron density is to place electron-withdrawing groups on the ligand. A more drastic approach is to increase the metal oxidation state from Ru(II) to Ru(IV), which will lead to a more active complex. Indeed, this hypothesis has been tested by our group in a recent publication, where a bis(arenesulfonate)phosphine)Ru(IV) (complex **4.4**) displayed the highest activity to date of ethylene polymerization for a ruthenium complex.[30] We attribute this higher activity to the more electron-deficient nature of Ru(IV). These results inspired our group to search for new ruthenium (IV) complexes with a different ligand framework to study the effect on its activity and polymer properties.

To explore new complexes, we decided to look for existing ruthenium (IV) complexes that resemble some of the active ETM catalysts. One interesting ligand framework that works successfully for ETM is Sita's half-metallocene Hf(IV) complex **4.5**.[31-33] Hafnium complex **4.5** has been efficiently used for living coordinative chain-transfer polymerization of propene with $ZnEt_2$ as a chain transfer agent. Half-metallocene Ru(IV) complexes similar to Sita's have been synthesized by Goh.[34] Ru(IV) complex **4.6** is structurally very similar to Hf(IV) complex **4.5**: they differ only in the nature of the bidentate anionic ligand. Additionally, complex **4.6** has the chlorides in an equivalent *cis* geometry, which we proposed to be a necessary condition to obtain an active ruthenium

catalyst.[20] We decided to synthesize **4.6** following Goh's[34,35] procedure and attempt activation under ethylene pressure.

4.2 Synthesis, Characterization, and Polymerization Results.

Synthesis of complex dichloride complex **4.6** was carried out as depicted on Scheme 4.1. Tetramethylthiuram disulfide was added to a solution of $[Cp^*RuCl_2]_n$ in acetonitrile to obtain complex **4.6**.[34,35] Complex **4.6** was characterized by ^1H and ^{13}C-NMR before being tested for ethylene polymerization

Scheme 4.1. Synthesis of complex **4.6**.

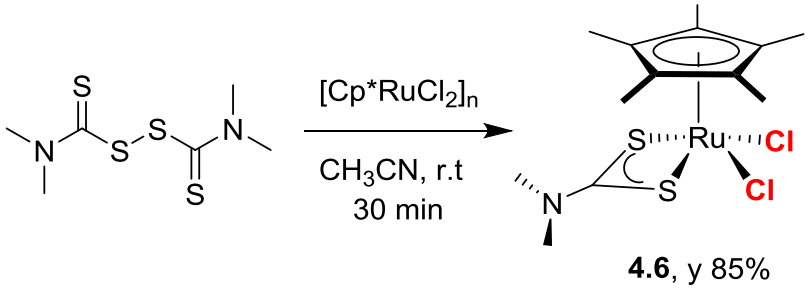

Polymerization results. Surprisingly, polymerization studies under ethylene pressure in toluene (500–600 psi, temperatures ranging from 50 to 80 °C, and polymerization times of 4 and 24 hours) with complex **4.6** did not yield any polymer using $AlMe_3$, $AlMe_2Cl$, $AlMe_3$-depleted MAO (dMAO), or MAO as cocatalysts. The polymerization solution color remained unchanged, which suggested that activation might not have occurred. Mass spectrometry analysis of the polymerization media before quenching

revealed that complex **4.6** was indeed still present in the polymerization solution. These results suggest that dichloride complex **4.6** is not effectively activated by aluminum activators.

Dimethylated complex **4.7** was synthesized by methylation with methyl lithium (Scheme 4.2) and characterized by ^{1}H, ^{13}C-NMR spectroscopies and single crystal X-ray crystallography (Figure 4.1). If a Cossee-Arlman mechanism is in place (see Chapter 1), complex **4.7** should be easier to activate than dichloride complex **4.6**.

Scheme 4.2. Synthesis of complex **4.7**.

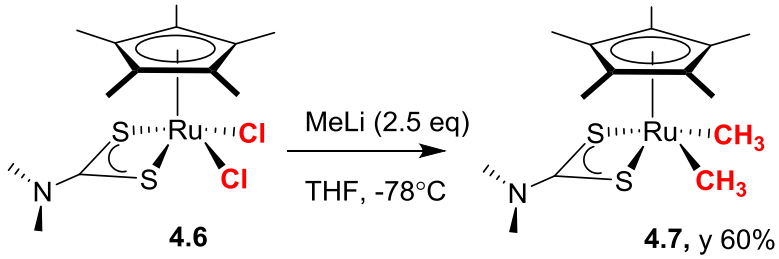

X-ray crystallography reveals that complex **4.7** adopts a four-legged piano stool (seven-coordinated) conformation. The dithiocarbamate ligand occupies two adjacent coordination sites, leaving the other two coordination sites for the methyl groups that are located *cis* to each other, as desired. The X-ray structure also reveals that nitrogen is in an almost perfect trigonal-planar geometry, which suggests that the unpaired electron on the nitrogen atom is participating in the donation to ruthenium by sharing its unpaired electrons to the dithiocarbamate carbon. Table 4.1 compares selected bond distances and bond angles of complexes **4.6** and **4.7**. The Ru-S bond distances are slightly larger for

complex **4.6**, which can be attributed to the chloride electron-withdrawing effect on ruthenium, which makes the Ru-S bond shorter. The sulfur-carbon and N-C(S_2) bond distances are very similar for both complexes. The Ru-Cl bond distance in complex **4.6** is larger than the Ru-CH_3 bond distance in complex **4.7** because of the larger size of chloride relative to carbon. The S-Ru-S bond angles are very similar for the two complexes. However, the S-C-S angle is two degrees larger for complex **4.7** because of steric repulsion between the two chlorides of complex **4.6**, which makes the Cl-Ru-Cl bond angle significantly larger than the C-Ru-C bond angle.

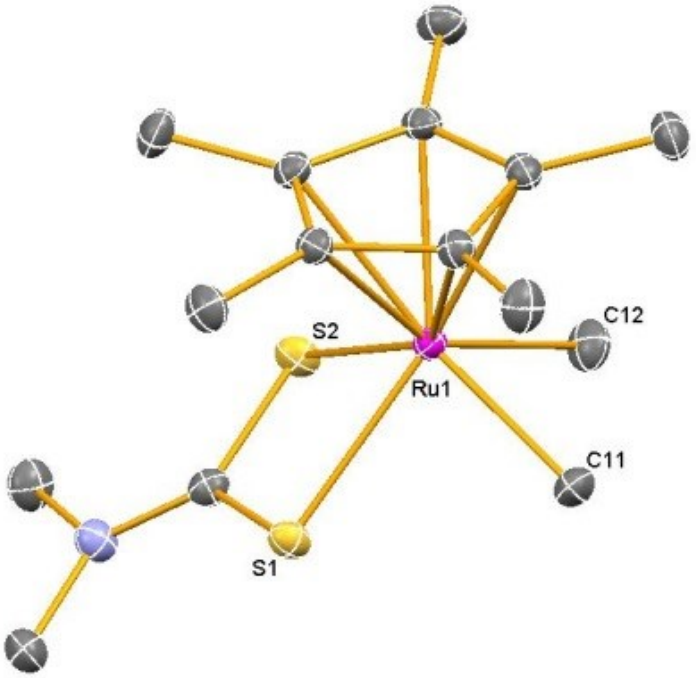

Figure 4.1. X-Ray crystal structure of complex **4.7**. ORTEP drawing with ellipsoids at 60% probability radius. The hydrogen atoms have been omitted for clarity.

The proposed X-ray structure is also retained in solution, as demonstrated by the ^{1}H and ^{13}C HMR data (Figure 4.2 a and b). The methyl groups attached to the nitrogen appear

as a singlet at 3.14 ppm in the ^{1}H-NMR spectrum and at 37.4 ppm in the ^{13}C-NMR spectrum (appendix section), suggesting retention of configuration or a very fast inversion of the $(CH_3)_2N$ moiety at room temperature. Low-temperature ^{1}H-NMR confirms that the $(CH_3)_2N$ protons are a sharp singlet, even at 220 K, suggesting that there is no rotation and that the nitrogen remains in a trigonal-planar geometry. Complex **4.7** is highly soluble both in non-polar solvents, such as pentane, and in polar solvents, such as dichloromethane. Our initial polymerization studies were performed with complex **4.7** activated with alkyl-aluminum cocatalysts.

Table 4.1. Comparison of selected bond distances (Å) and bond angles (°) for complexes **4.6** and **4.7**.

4.6[34]		**4.7**	
Ru(1)-S(1)	2.371(1)	Ru(1)-S(1)	2.3910(4)
Ru(2)-S(2)	2.3681(9)	Ru(2)-S(2)	2.3935(5)
S(1)-C(11)	1.713(5)	S(1)-C(13)	1.711(1)
S(2)-C(11)	1.724(5)	S(2)-C(13)	1.712(1)
N(1)-C(11)	1.304(6)	N(1)-C(13)	1.327(2)
Ru(1)-Cl(1)	2.406(1)	Ru(1)-C(11)	2.156(2)
Ru(1)-Cl(2)	2.406(1)	Ru(1)-C(12)	2.141(2)
S(1)-Ru(1)-S(2)	71.16(4)	S(1)-Ru(1)-S(2)	71.21(1)
S(1)-C(11)-S(2)	106.7(3)	S(1)-C(13)-S(2)	108.91(8)
Cl(1)-Ru(1)-Cl(2)	83.49(5)	C(11)-Ru(1)-C(12)	75.39(6)

When complex **4.7** was activated with $AlMe_2Cl$ or $AlMe_3$ in toluene at 50–80 °C (600 psi, 24 hours), trace amounts of polymer are formed. However, when MAO was used as the cocatalyst (Table 4.2, entry 1) with complex **4.7** in a toluene solution at 600 psi, 55 °C for 24 hours, more polymer is obtained (Table 4.2, entry 1). The polymer obtained has a molecular

weight of 89 kg·mol^{-1} and 2.5 polydispersity (PDI). Branching is very low, as reflected by the high melting transition temperature (Tm) of 134 °C. Although activity is low, this result is of great importance because complex **4.7** is active when activated MAO is used as the cocatalyst. Temperature has a great effect on polymer activity, and in the case of our previous Ru(IV) complex, high temperatures increased the activity.[30] Increasing the temperature to 70 °C resulted in a great enhancement in polymerization activity (entry 2). Additionally, longer polymerization times (entries 2–4) produced more polymer and tripled the activity of complex **4.7**. These results support our hypothesis that complex **4.7** would be easier to activate and imply that high temperatures and long polymerization times are required to activate complex **4.7**. In all cases, the obtained molecular weights are high (128–148 kg·mol^{-1}), with low branching, in general, which is reflected by high melting temperatures (>133 °C). Polydispersities are between 1.7 and 2.0, which indicates single site catalyst behavior. Additionally, high-temperature gel permeation chromatography (GPC) traces show evidence of monomodal distribution, indicating the presence of one active species. The cocatalyst MAO contains $AlMe_3$, which has been shown to have a negative effect on activity for our previous Ru(IV) complex **4.4**.[30] We decided to study activation with dMAO to determine whether the presence of $AlMe_3$ has any negative effect on polymerization activity.

Polyethylene was formed when complex **4.4** was activated with dMAO in toluene (in the presence of ethylene, 600 psi) for 4 hours at 70°C (entry 5). Additional polymerization for 12 and 24 hours at 70°C (entries 6 and 7) resulted in a substantial increase in activity, indicating time dependence, as in the case of MAO polymerization (vide supra). The molecular weights are also high (124–143 kg·mol^{-1}), and the monomodal PDIs (1.72–1.75)

are similar to the results obtained with MAO. There is a very slight increase in branching using dMAO. Compared to MAO, the activities are almost identical, indicating that the $AlMe_3$ contained in MAO does not impart a negative effect on polymerization activity. We do not know how much of the $AlMe_3$ in MAO was used, but it seems to be low based on the polymerization results. Therefore, we can conclude that the active species are identical whether complex **4.7** is activated with MAO or dMAO. In light of these results, we decided to further study the activity of complex **4.7** under different experimental conditions, such as temperature, pressure, and cocatalyst equivalents.

Polymerizations were performed at temperatures of 55–105 °C (entries 1–4, 8–13). The catalyst remains active in this temperature range, indicating thermal stability. However, a decrease in activity was observed as the temperature rose. For instance, the polymerization activity was almost eight-fold less at 105 °C relative to the polymerization activity at 70 °C, most likely due to thermal decomposition. The molecular weight of the polymer remains similar from 70 to 90 °C (>100 $kg{\cdot}mol^{-1}$). However, at higher temperatures, the molecular weights decrease slightly at 100 and 105 °C, falling below 100 $kg{\cdot}mol^{-1}$ (Table 4.2, entries 13 and 14), indicating a faster rate of decomposition of the active species at this temperatures. From these results, we can infer that complex **4.7** reaches its maximum activity at 70 °C. Additionally, branching appears to be little affected by high temperatures. Branching remains low at high temperatures, and polydispersities remain at approximately 2. GPC traces display monomodal profiles, suggesting single site catalyst at all temperatures. After studying the temperature effect, we decided to continue the study by varying the ethylene pressure.

All polymerizations up to this point were performed at 600 psi of ethylene; therefore, to examine the ethylene pressure effect on polymerization, we performed polymerizations at 200 and 400 psi at 70 °C (Table 4.2, entries 14–15). Lower ethylene pressures lead to less polyethylene, indicating a dependence on the concentration of the monomer. There is also an effect on molecular weight; polymerization at lower ethylene pressures generates polymers with lower molecular weights. Surprisingly, no effect on branching is observed under these conditions, indicating that insertion and coordination occur faster than *β*-hydrogen elimination at 70 °C, even at low ethylene pressures. At low ethylene pressures, an increase in polyethylene branching is expected because of *β*-hydride elimination and 2,1–reinsertion. Theoretical studies by Ziegler and others proposed that the vinyl chain end (formed after β-hydride elimination) must rotate before 2,1-reinsertion. The authors proposed that catalysts with a high degree of steric bulk hamper this rotation.[36,37] From single crystal X-ray crystallography, the C-Ru-C bite angle for complex **4.7** is only 75.36 degrees, which makes the active species significantly more sterically crowded than ETM (bite angle >97 degrees)[38] and LTM (bite angle >89 degrees) catalysts.[39,40] In the case of complex **4.7**, we can assume that rotation of the vinyl chain has a very high activation barrier after migratory insertion, even if there is *β*-hydrogen abstraction, which explains why polymers obtained with complex **4.7** have very low branching even at low ethylene pressure. Once again, GPC indicates monomodal distribution with PDI of approximately 2. Polymerizations at 1 atm did not yield any polyethylene; only high pressure results in polymer, highlighting the need for high ethylene concentrations to form polymers. After examining the polymerization time, temperature, and ethylene pressure, we decided to investigate the effect of cocatalyst equivalents.

All polymerizations up to this point were performed using 1000 equivalents of catalyst. To study the effect of the cocatalyst, polymerizations at 500 and 2000 equivalents of MAO (Table 4.2, entries 16–18) were performed. At 500 equivalents, there was a remarkable decrease in activity, meaning that a significant amount of cocatalyst is required to activate complex **4.7**. When 2000 equivalents of MAO were used, the activity increased, although only slightly relative to when 1000 equivalents were used. These results suggest a slow activation of complex **4.7** with MAO and that the increase in the number of equivalents from 1000 to 2000 equivalents does not yield a significant improvement in activity. Molecular weights increased significantly (>200 $kg \cdot mol^{-1}$), which was an unexpected result. Usually, molecular weights decrease with increasing MAO equivalents because of polymer chain transfer to MAO. In this case, we observed no chain transfer to MAO. The absence of change transfer also explains why complex **4.6** is not activated and complex **4.7** requires high temperatures and a large number of equivalents. If MAO were able to transmetalate with complex **4.6** or abstract a methyl group easily from complex **4.7**, we should expect to see a large degree of chain transfer. Higher molecular weight and activity can only be attributed to more catalyst activation and stabilization of the active species that remain active for longer periods of time. Next, we decided to examine catalyst **4.7** for α-olefin and polar monomer copolymerization with ethylene.

Copolymerizations with 1-hexene and methylacrylate were also tested. For 1-hexene (1.0 M), polyethylene was obtained (Table 4.2, entry 19) with lower activity. Analysis of the polymer obtained by ^{13}C-NMR spectroscopy indicated that 1-hexene was not incorporated into the polymer. Because of the lower activity and lower molecular weight obtained, it is clear that 1-hexene competes with ethylene. Unfortunately, copolymerization in the

presence of methylacryalte (0.1 M, Table 4.2, entry 20) afforded no polymer, which shows that the active catalyst generated from complex **4.7** activation is not tolerant toward polar groups.

NMR studies. Dimethyl complex **4.7** can also be activated by one equivalent of strong acid to obtain a monomethyl cationic active species. Activation with HBArF ([H($Et_2O)_2$]$^+$ [BAr'$_4$]$^-$ (where Ar'= 3,5-$(CF_3)_2C_6H_3$)) and the other demethylating reagents ($B(C_6F5)_3$, [Ph_3C][$B(C_6F_5)_4$], [$PhMe_2NH$][$B(C_6F_5)_4$]) under ethylene pressure (600 psi) was performed in toluene, but polymer was not obtained. We decided to examine the activation of complex **4.7** in the presence of ethylene by NMR (Scheme 4.3).

Scheme 4.3. Activation of complex **4.7** for NMR studies.

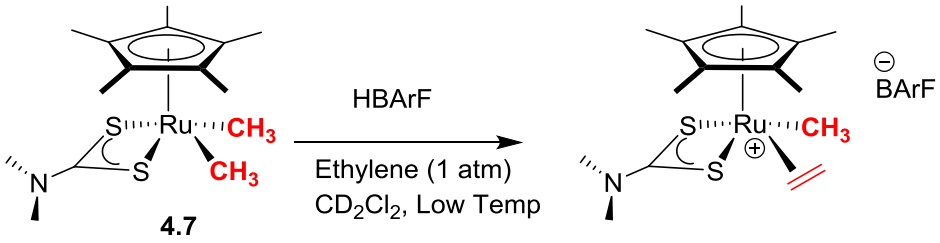

Figure 4.2 compares ^{1}H-NMR spectra at 298 K (top), 220 K (middle), and activation at 220 K (lower). There was a small shift in the peaks when the temperature was lowered to 220 K. When one equivalent of HBArF was added at low temperatures, mono-dimethylation was clearly observed, as the methylamine protons became non-equivalent (peaks *c* and *c'*). Additionally, the Ru-Me peak integrates for three protons (peak *a*), and observation of methane confirmed that one methyl group was protonated and that we obtained a mono-methylated cationic complex.

Table 4.2. Results of ethylene homopolymerization and copolymerization with **4.7** and **4.8**.

Entry	[Ru]	Cocat (1000 eq)	T (°C)	Yield (mg)	t (h)	P (psi)	Mn[a] (10^{-3})	PDI[b]	Tm[c] (°C)	Branch[d]	Activity[e] (10^3)
1	**4.7**	MAO	55	10	4	600	89	2.5	134.0	3	1.0
2	**4.7**	MAO	70	112	10	600	128	2.03	133.3	2	27.1
3	**4.7**	MAO	70	190	13	600	148	1.84	133.3	3	35.3
4	**4.7**	MAO	70	600	24	600	145	1.75	133.2	3	60.4
5	**4.7**	dMAO	70	35	4	600	124	1.75	133.4	3	21.2
6	**4.7**	dMAO	70	191	12	600	143	1.72	133.1	10	38.5
7	**4.7**	dMAO	70	614	24	600	126	1.78	133.5	6	61.8
8	**4.7**	MAO	80	194	12	600	113	1.84	132.6	<1	39.1
9	**4.7**	MAO	80	404	24	600	174	2.5	132.0	3	39.1
10	**4.7**	MAO	90	287	24	600	113	1.79	133.3	2	28.9
11	**4.7**	MAO	90	260	24	600	122	2.11	133.0	<1	26.2
12	**4.7**	MAO	100	112	24	600	92	2.04	133.1	7	11.3
13	**4.7**	MAO	105	79	24	600	89	2.18	133.0	5	8.0
14	**4.7**	MAO	70	76	24	200	90	1.90	133.8	2	23.0
15	**4.7**	MAO	70	260	24	400	100	1.79	133.9	1	39.3
16	**4.7**	MAO (500 eq)	70	174	24	600	121	1.81	133.5	<1	17.5
17	**4.7**	MAO (2000 eq)	70	707	24	600	270	1.69	134.0	7	71.2
18	**4.7**	MAO (2000 eq)	70	734	24	600	322	1.82	134.2	5	73.9
19	**4.7**[f]	dMAO	70	32	24	300	78	1.72	126	6	6.4
20	**4.7**[g]	dMAO	70	0	24	300	-	-	-	-	-
21	**4.8**	$Ni(COD)_2$ (2 eq)	70	0	24	600	-	-	-	-	-
22	**4.8**	$Ni(COD)_2$ (20 eq)	70	0	24	600	-	-	-	-	-
23	**4.8**	MAO (200 eq)	70	0	24	600	-	-	-	-	-
24	**4.8**	MAO (2000 eq)	70	0	24	600	-	-	-	-	-

All polymerizations were performed in 100 mL of toluene and 10 μmol of [Ru]. [a]Molecular weight in g·mol^{-1}. [b]Polydispersity Mw/Mn. [c]Melting transition temperature by differential scanning calorimetry (DSC). [d]Branching Me/1000C. [e]Activity as (grams of PE)/(mol of [Ru]·h·bar) and calculated assuming that all ruthenium is activated. [f] 1.0 M 1-hexene. [g] 0.1 M methylacrylate.

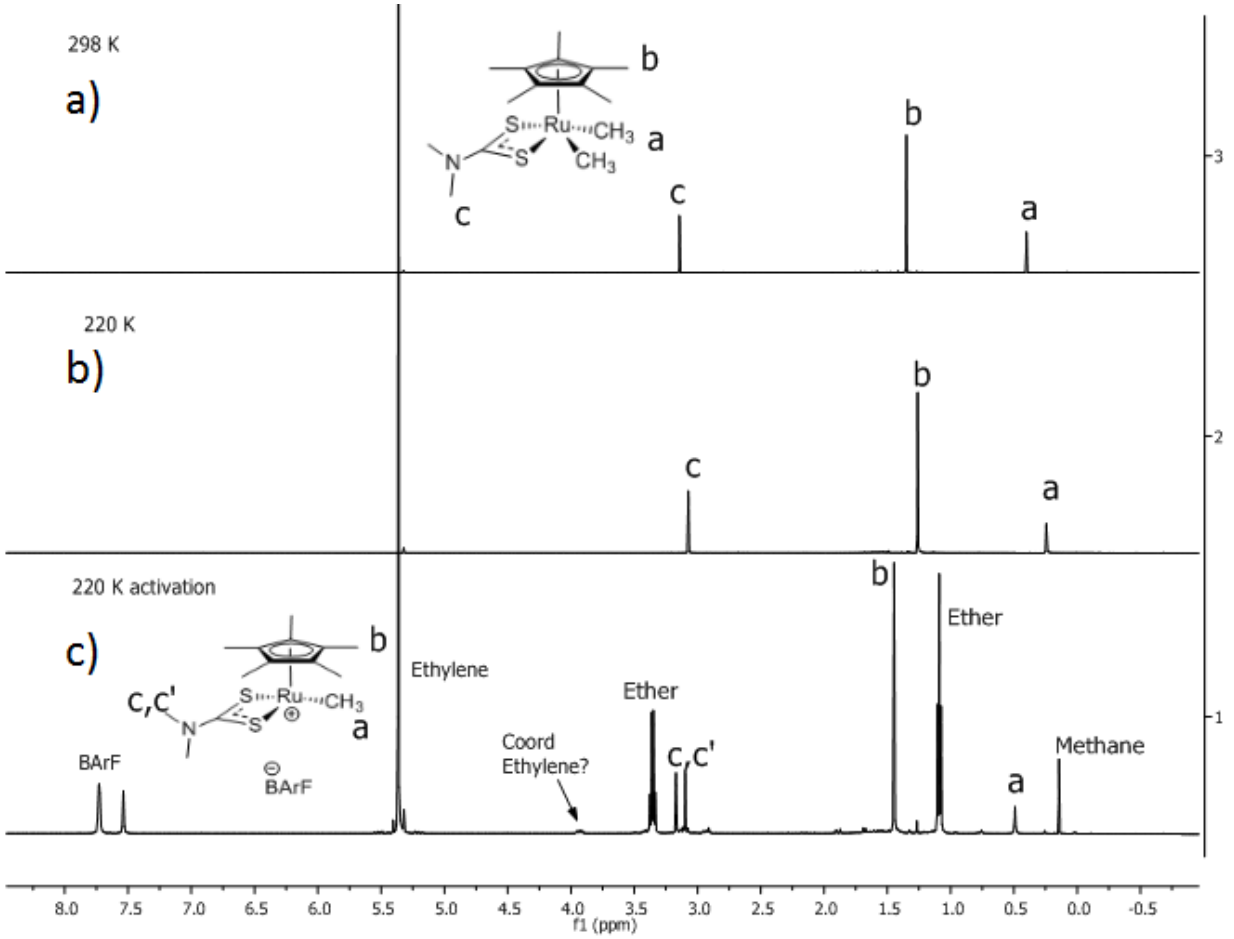

Figure 4.2. NMR activation studies of complex **7** in the presence of ethylene with HBArF at low temperature in CD_2Cl_2. a) Complex **7** at 298 K; b) Complex **7** at 220 K; c) Complex **7** activation with HBArF in the presence of ethylene (1 atm) at 220 K.

Ethylene coordination could not be determined at this temperature because of non-coordination at 1 atm or by slow rotation of ethylene, which made the proton signals too broad to be observed. Similar behavior was observed for complex **4.3** at low temperatures.[20] This problem can be solved by increasing the temperature in the NMR experiment, causing the proton signals of bound ethylene to coalesce and making them easier to identify. In this respect, new proton signals appeared immediately when the temperature was increased to 235 K (represented as *, Figure 4.3). Unfortunately, these

new signals did not appear to be due to ethylene but to the formation of a new complex. As the temperature is increased from 245 to 265 K, the new peaks in the NMR spectrum become predominant, and the signals due to the activated complex diminish. All new proton signals are singlets, and the integration agrees with the number of protons of complex **4.7**, but the structure cannot be assigned.

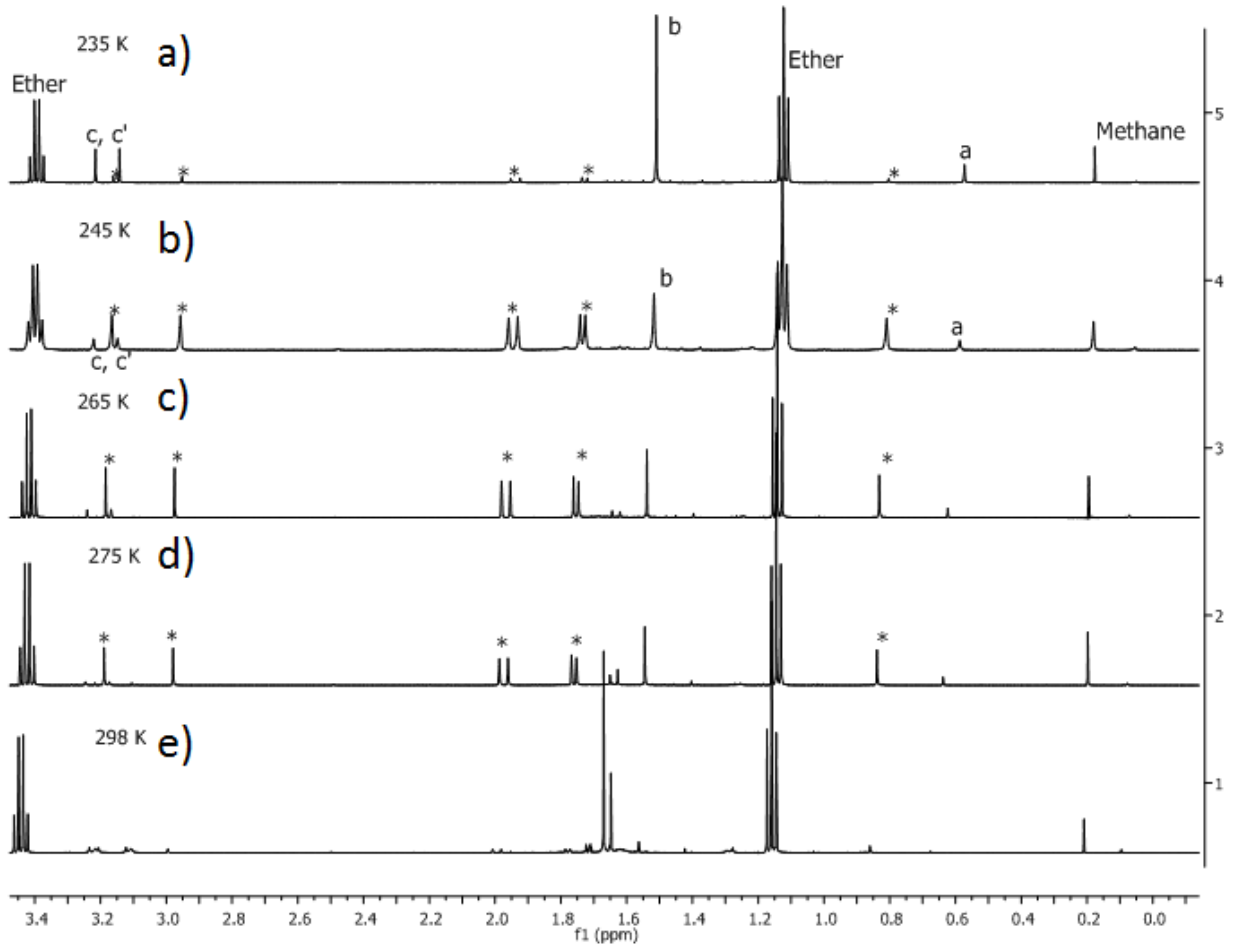

Figure 4.3. NMR activation studies of complex **4.7** in the presence of ethylene with HBArF at low temperature (* new peaks appearing when rising temperature). a) 235 K; b) 245 K; c) 265 K; d) 275 K; e) 298 K.

It is worth noting that the $(CH_3)_2N$ protons remain diastereotopic, but the pentamethylcyclopentadienyl (Cp*) singlet that integrates to fifteen protons is no longer present. Instead, five singlets that integrate to three protons each are present. These data suggest that the Cp* protons become diastereotopic, most likely because of slow rotation of Cp* in the newly formed complex. Increasing the NMR temperature (298 K, Figure 4.3) resulted in the appearance of two new proton signals, the disappearance of the original peaks and the disappearance of the peaks associated with the unknown species at lower temperatures. Mass spectrometry of the NMR solution indicated the presence of a ruthenium species with mass 356 $g \cdot mol^{-1}$, as in the case of the polymerization studies. Growing single crystals from the decomposition product was attempted, but no solid material was obtained.

The NMR studies indicate that complex **4.7** is activated to achieve a monocationic complex that decomposes at low temperatures. It appears that decomposition is faster than the ethylene coordination-insertion pathway. The presence of a counterion is known to have a great effect on active species and activity.[25]

Counterions can be classified into ions that coordinate and ions that do not coordinate, which has a great effect on catalysis.[41] When MAO is used as the cocatalyst, complex **4.7** is slowly activated, and MAO can coordinate to the active catalyst to stabilize it. MAO and other alkyl aluminum compounds have been found to coordinate and stabilize ETM and lanthanide catalysts.[42-48] Marks et al. observed, via ^{1}H-NMR spectroscopy, the activation of Cp_2ZrMe_2 with MAO to produce a Cp_2ZrMe^+ species stabilized by MAO.[42] Barron et al. were also able to study the activation of Cp_2ZrMe_2 with $(^tBuAlO)_6$, and they observed, via NMR spectroscopy, the formation of an active catalyst and coordination of

counter ion $^{-}(Me^{t}BuAlO)_6$.[44,49] They also found that the $Cp^*_2ZrMe_2$ complex is only activated by MAO or synthesized $(tBuAlO)_6$ clusters and not by trialkyl-aluminum ($Al^{t}Bu_3$). They also observed that the methyl groups in Cp_2ZrMe_2 bridge with aluminum in $Al^{t}Bu_3$, but methyl abstraction does not occur. Based on these results, we propose that similar active species are formed when complex **4.7** is activated by MAO, in which the active catalyst is stabilized by weak coordination with MAO clusters that can only be displaced under high ethylene pressure. This MAO stabilization cannot be provided by the $^{-}$BArF counterion or other non-coordinating counterions. We also attempted to study the activation of complex **4.7** with MAO by NMR spectroscopy, but we encountered severe solubility issues when complex **4.7** was activated. From these results we decided to synthesize a cationic monomethylated complex stabilized by a coordinating ligand that could be replaced by ethylene at high pressures.

Monomethylated cationic complex. Complex **4.8** was synthesized as depicted in Scheme 4.4. The structure features a triphenylphosphine coordinated to a cationic Ru(IV) complex, which precipitates as a dark solid in toluene. Other, weaker coordinating ligands were examined, such as acetonitrile, pyridine, lutidine, and dimethyl sulfoxide, but rapid decomposition was observed in all cases.

Scheme 4.4. Synthesis of complex **4.8**.

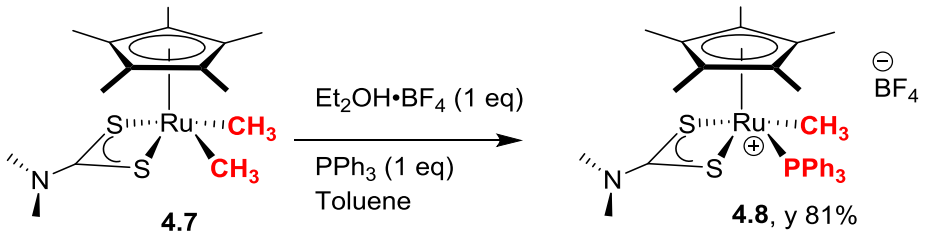

Complex **4.8** was characterized by ^{1}H, ^{13}C, ^{31}P, ^{19}F, and ^{11}B-NMR spectroscopy and single crystal x-ray crystallography (Figure 4.4). Complex **4.8** is monocationic with a distorted four-legged piano stool conformation. The piano stool is distorted by the large steric interactions of triphenylphosphine ligand that must coordinate out-of-plane to be accommodated. The nitrogen atom remains in trigonal planar geometry, as observed in complex **4.7**. The Ru-P bond in complex **4.8** is shorter that the Ru-S bond in complex **4.7**, which indicates very strong bonding of phosphorous to ruthenium. Additionally, the Ru(1)-S(2) bond distance is longer in complex **4.8** due to steric interactions of the vicinal triphenylphosphine ligand. The ruthenium methyl bond (Ru-CH_3) is also longer due to the proximity of triphenylphosphine. The remaining bonds and angles are very similar to the analogous metrics in complex **4.7** (Tables 4.1 and 4.3). Additionally, NMR spectroscopy confirms triphenylphosphine coordination to ruthenium by the diastereotopic $(CH_3)_2N$ proton signals and the Ru-CH_3 protons and carbon coupling with phosphine.

Ethylene polymerization was attempted with complex **4.8** under 600 psi of ethylene pressure at 70°C for 24 hours, but no polymer was obtained. Mass spectrometry of the polymerization media indicated that complex **4.8** remained intact, and ethylene was unable to displace triphenylphosphine. Polymerizations with **4.8** were attempted in the presence of phosphine scavengers (entries 21–24), such as $Ni(COD)_2$ and MAO, but no activation was achieved, even with 2000 equivalents of MAO. As before, mass spectrometry of the polymerization solution before quenching revealed that triphenylphosphine remains coordinated to ruthenium. This result suggests that complex **4.8** is highly stable and that triphenylphosphine binds with great strength to ruthenium, as it cannot be detached by $Ni(COD)_2$ or MAO.

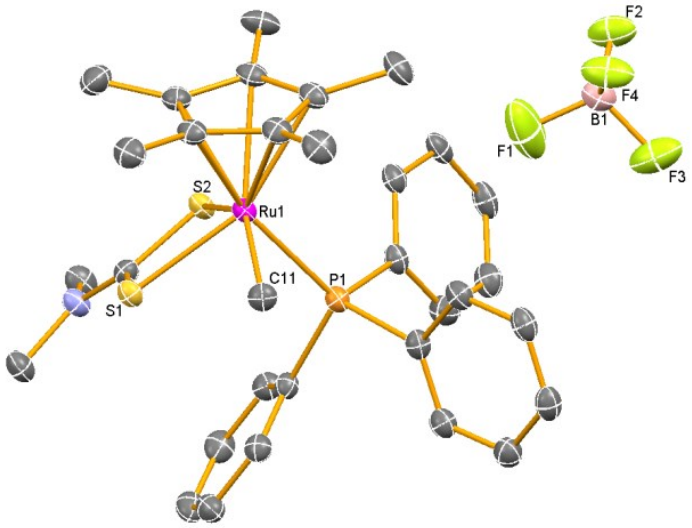

Figure 4.4. X-Ray crystal structure of complex **4.8**. ORTEP drawing with the ellipsoids at 60% probability radius. The hydrogen atoms have been omitted for clarity. Complex **4.8** crystallizes with one molecule of THF, which is omitted for clarity.

Table 4.3. Selected bond distances (Å) and bond angles (°) for complex **4.8**.

4.8			
Ru(1)-S(1)	2.3802(1)	Ru(1)-C(11)	2.1841(1)
Ru(2)-S(2)	2.4133(1)	Ru(1)-P(1)	2.3834(1)
S(1)-C(12)	1.7083(1)	S(1)-Ru(1)-S(2)	71.36(1)
S(2)-C(12)	1.7231(1)	S(1)-C(13)-S(2)	109.13(5)
N(1)-C(12)	1.3179(1)	C(11)-Ru(1)-P(1)	79.06(4)

Polymerization studies reveal one single active species when complex **4.7** is activated with MAO or dMAO in toluene at high ethylene pressures. We proposed an active species similar to the ones proposed for ETM under the same conditions.[44,49] Complex **4.7** is also significantly more active than our previous Ru(II) complex **4.3** and its dichloride analogs.[20] In the case of complex **4.3**, the migratory insertion barrier was calculated

experimentally to be 22.8 kcal·mol^{-1}, which is lower than the activation energy predicted for complexes **4.1** and **4.2**. NMR studies did not enable clear elucidation or calculation of the insertion barrier for the active species generated by the activation of complex **4.7**. To further investigate these energy barriers, we decided to use computational modeling, which has been used widely for determining insertion barriers for ethylene migratory insertion in many catalytic systems.[50]

4.3 Molecular Modeling of Chain Initiation and Chain Propagation. Determination of Migratory Insertion Barrier.

DFT studies. Density functional theory was used to calculate the insertion barrier for complex **4.7**. From NMR activation studies, it is reasonable to propose complex **4.9** (Figure 4.5) as the active catalyst. The counterion plays an important role in catalysis, perhaps by coordination with the active catalyst; however, we will not consider it in these DFT studies. Inclusion of the counterion, cages of MAO in this case, would be computationally too expensive[50] for our purposes.

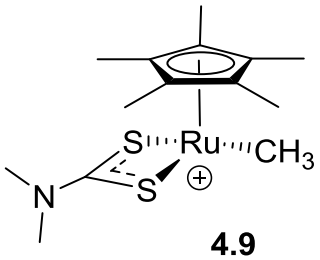

4.9

Figure 4.5. Proposed active species following MAO activation of complex **4.7**.

First, we calculated chain initiation or methyl insertion into the ethylene bond by migratory insertion. Figure 4.6 contains selected local minima structures and transition states with key bond distances and angles annotated. Figure 4.7 displays the energy profile for ethylene uptake to the migratory insertion step and the lowest energy structure following complete insertion. The optimized structure of complex **4.9** remains a four-legged piano stool conformation in which a vacant site is created upon activation. Structure **4.9** has a weak *α*-agostic interaction with the hydrogen atoms in the methyl moiety. Ethylene uptake by complex **4.9** into the vacant site is barrierless to form resting state complex **4.10**.

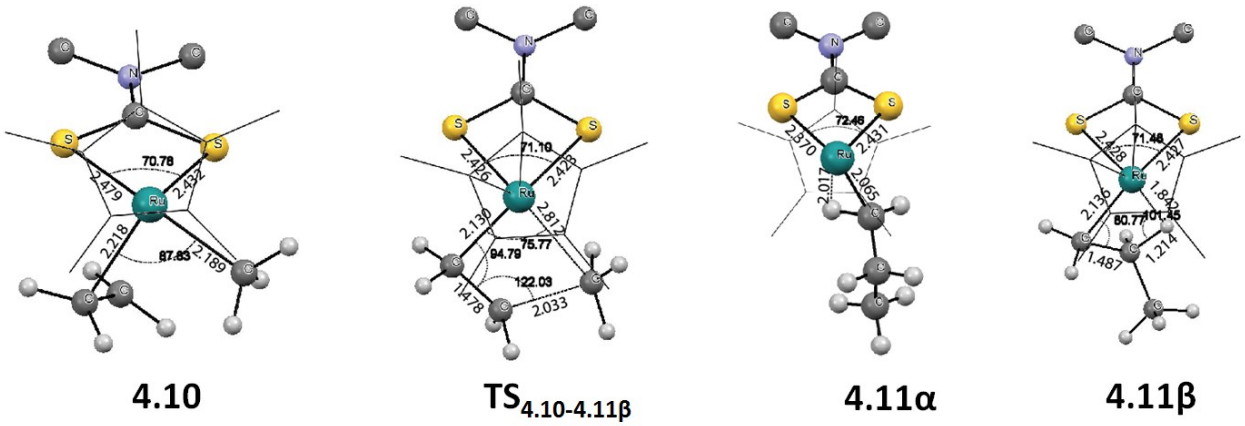

Figure 4.6. Relative energy profile of the proposed chain initiation for the active species. Bond distances are in Angstroms (Å), and bond angles are in degrees.

In the case of complex **4.10**, we found that a direct insertion pathway is favored. We monitored the ethylene–methyl bond distance and found that ethylene rotates as the distance between the ethylene and methyl carbon atoms decreases (see, e.g., the transition state complex **TS$_{4.10\text{-}4.11\beta}$**). Although there is steric crowding in the plane, ethylene can still

rotate to remain almost planar and proceed with the insertion reaction. The C=C-Ru-CH_3 dihedral angle was calculated to be 9.89 degrees. The migratory (**4.10 → 4.11β**) insertion barrier, through transition state **$TS_{4.10\text{-}4.11\beta}$**, is calculated to be 18.2 kcal·mol^{-1}, which is 4.6 kcal·mol^{-1} lower than the barrier determined experimentally for Ru(II) complexes (22.8 kcal·mol^{-1}).[20] Calculations on the Ru(II) complex reveal that the insertion barrier for chain initiation is 23.0 kcal·mol^{-1} using the same level of theory (see Chapter 3). Thus, the insertion barrier is overestimated by only 0.2 kcal·mol^{-1} for Ru(II). From these calculations, it is clear that our hypothesis that Ru(IV) will be more active than Ru(II) is supported not only by polymerization activity but also by molecular modeling calculations.

For LTM catalysts, the kinetic insertion product after migration is usually a η^2-γ-agostic complex in which the terminal methyl hydrogen atoms bind with the metal center before reaching the thermodynamic product. The γ-agostic chelate is easily opened by twisting the C_α-C_β bond and reorganizing to form a more stable β-agostic thermodynamic product.[36] In the case of the transition state complex **$TS_{4.10\text{-}4.11\beta}$**, rotation of the C_α-C_β bond occurs at the same time as migratory insertion and then relaxes directly to the β-agostic thermodynamic product **4.11β**. Once again, we attribute this outcome to the narrow bite angle that cannot accommodate a γ-agostic chelate because it is sterically more demanding than the β-agostic product.

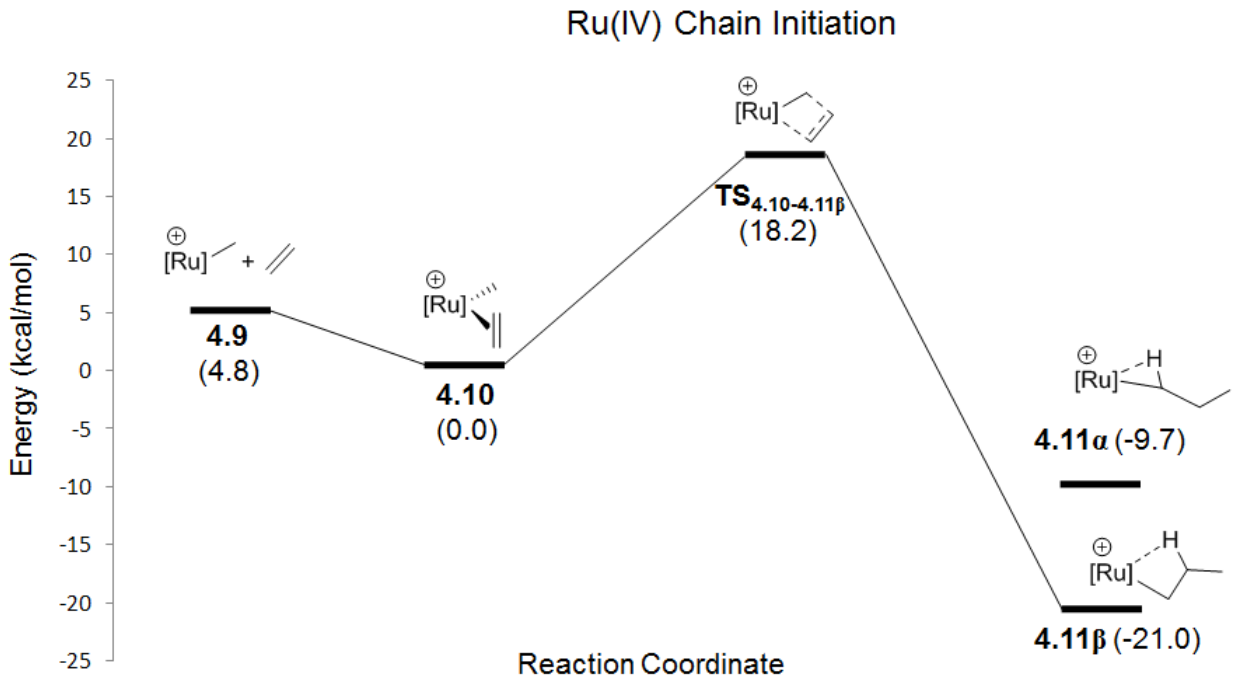

Figure 4.7. Relative energy profile of the proposed chain initiation for the active species. The active catalyst resting state complex **4.10** is assigned with zero energy for comparison purposes.

Complex **4.11β** forms a stable chelate 21.0 kcal·mol^{-1} lower in energy than complex **4.10**. The Ru-H bond is 1.842 Å, which is slightly longer than the analogous (calculated) bond in nickel *β*-agostic complexes.[36] Additionally, the C-H bond distance of the agostic hydrogen is slightly elongated. An *α*-agostic complex (**4.11α**) can also form, but it is thermodynamically less stable than complex **4.11β** by 11.3 kcal·mol^{-1}. Ethylene migratory insertion to a Ru-Me bond is just the chain initiation step. We also need to calculate the chain propagation migration barrier. Figure 4.8 contains selected local minima structures and transition states with key bond distances and angles annotated for the chain propagation. Figure 4.9 displays the energy profile for the chain propagation mechanism.

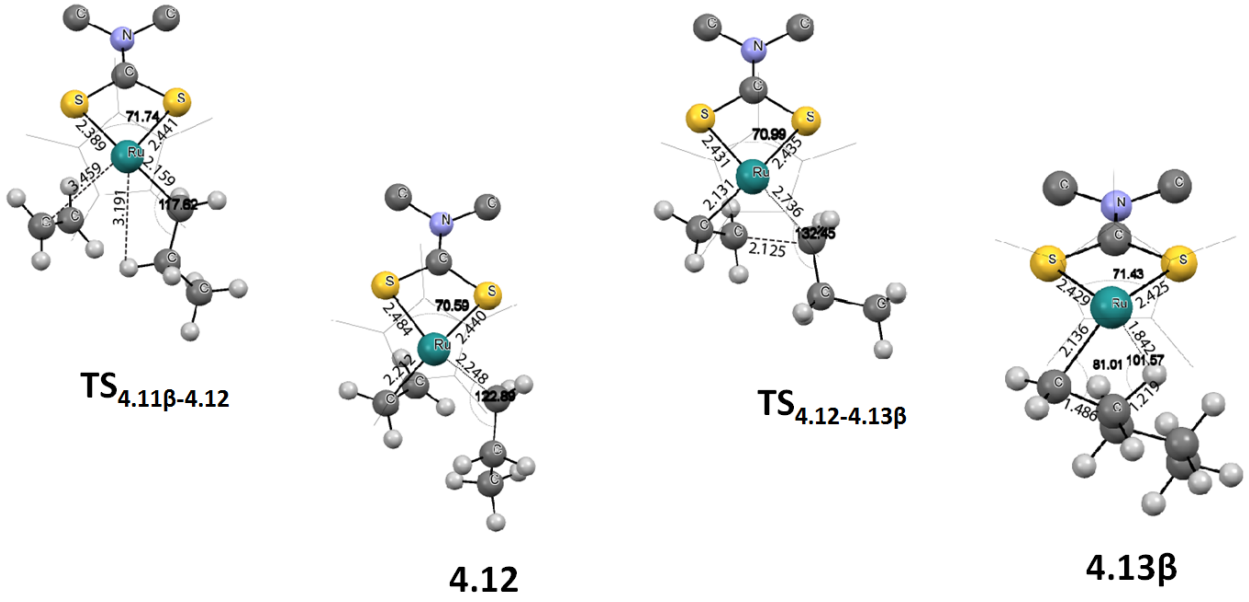

Figure 4.8. Relative energy profile of the proposed chain propagation for the active species. Bond distances are in Angstroms (Å), and bond angles are in degrees.

The formation of the highly stable complex **4.11β** implies that the chelate must be opened to accommodate the incoming ethylene monomer. In the case of ETM, LTM, and Ru(II) (see Chapter 3) complexes, this process is barrierless,[27,36] but in this case, we found that the opening of the chelate **4.11β** requires an activation barrier of 15.6 kcal·mol^{-1}, which is not energetically prohibitive but has a negative effect on the activity. The ethylene-bound complex **4.12** is formed after the chelate is opened, but it is only 3.4 kcal·mol^{-1} lower in energy than transition state **TS$_{4.11β-4.12}$** and 12.1 kcal·mol^{-1} higher in energy than complex **4.11β**. Steric interactions around the coordination plane are responsible for this activation barrier, in which ethylene must attack out of the plane to open the chelate. Once the chelate is opened, the formation of the ethylene bound complex **4.12** is less stable due to higher steric interactions involving the propyl moiety. In contrast, complex **4.10** possesses a methyl group and can easily accommodate the ethylene

monomer, being stabilized by 4.8 kcal·mol^{-1}. For complex **4.12**, the Ru-propyl bond is elongated compared to the Ru-Me bond in complex **4.10** (Figure 4.7). However, the sterically cumbersome complex **4.12** accelerates migratory insertion of ethylene into the Ru-propyl bond, and the calculated migratory insertion barrier is reduced greatly to 9.8 kcal·mol^{-1}. The migratory insertion (**4.12 → 4.13β**) transition state (**TS$_{4.12\text{-}4.13\beta}$**) occurs out of plane because steric interactions involving the propyl group do not allow the ethylene moiety to completely rotate. In this case, the C=C-Ru-propyl dihedral angle is 28.23 degrees. From the results of the migratory insertion barrier for chain propagation, one would expect a more active complex, but ethylene uptake is the rate-limiting step because of the steric interactions. This situation also explains why polymerizations at 1 atm do not yield polyethylene while high ethylene pressures are capable of producing polyethylene.

The total insertion barrier can be estimated to be 21.9 kcal·mol^{-1} for chain propagation if we consider ethylene uptake. We also expect complex **4.12** to be at low concentrations because of reversible coordination of ethylene. If the ethylene concentration is high enough, then more complex **4.12** is available to proceed with migratory insertion. The insertion barrier, 21.9 kcal·mol^{-1}, is in the same range for Ru(II) complexes (see Chapter 3), and we should expect similar activity. Instead, we observe that complex **4.7** is more active. We hypothesize that this discrepancy is due to the exclusion of the counterion effect in our calculations, as it certainly has a great effect on polymerization. Coordination of the MAO cluster (large excess MAO is present) might help to open or avoid the formation of β-agostic chelates, which might favor the coordination of ethylene. It is also worth mentioning that high ethylene pressures might kinetically favor chelate opening and

increase **4.12** concentration that requires only 9.8 kcal·mol^{-1} to proceed with insertion and form thermodynamically stable complex **4.13β**.

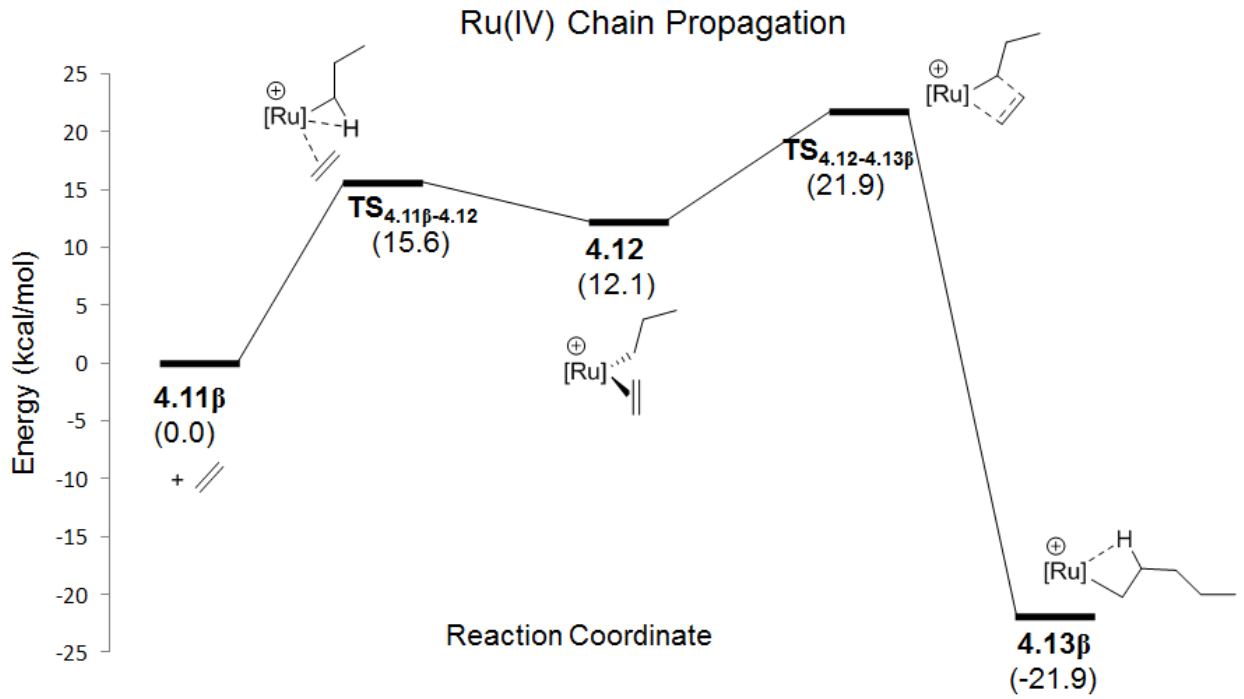

Figure 4.9. Relative energy profile of the proposed chain propagation for the active species. The active catalyst resting state complex **4.11β** is assigned with zero energy for comparison purposes.

In any case, for the proposed active species (**4.9**), the migratory insertion barrier is significantly lower, which we believe is why Ru(IV) complexes are more active than Ru(II) complexes. After migratory insertion, a very stable (**4.13β**) *β*–agostic complex is formed that will continue with change propagation in the same manner. The *α*-agostic complex following migratory insertion was not calculated for propagation because, as in the case of chain initiation, it is expected to be higher in energy.

4.4 Conclusions

In conclusion, half-metallocene dichloride complex **4.6** has been found to be inactive for ethylene polymerization. The inactivity of **4.6** is due to ineffective activation by alkyl-aluminum cocatalysts. The reason is the poor alkylating properties of alkyl-aluminum cocatalysts on complex **4.6**, as evidenced by MS experiments. We successfully synthesized dimethylated complex **4.7** and found it to be active for ethylene polymerization via activation by MAO or dMAO, as we proposed. This is the first report of a half-metallocene ruthenium (IV) complex capable of catalyzing ethylene polymerization. We also found complex **4.7** to be more active than Ru(II) complexes for ethylene polymerization, which we had hypothesized in terms of a more electron-deficient complex. Linear and high molecular weight polymers have been obtained. All polymers possessed monomodal distributions with narrow PDI, indicating that single site catalysts were formed. Complex **4.7** displays temperature, time, pressure, and catalyst equivalents dependence. Higher activities are found at 70 °C, 24 hours, 600 psi of ethylene, and 2000 equivalents of MAO. Low-temperature NMR studies of the activation of complex **4.7** with HBArF generated a monomethylated cationic species that decomposed at higher temperatures but indicated weak ethylene binding; this result was corroborated by DFT calculations, which explained the need for high ethylene pressures. Monomethylated cationic complex **4.8** stabilized with PPh_3 was also synthesized and used for polymerization. Complex **4.8** proved to be very stable, and PPh_3 could not be removed under harsh polymerization conditions. DFT calculations provide a qualitative understanding of active species and gives insights of migratory insertion barriers. Chain initialization was calculated to be 18.2 kcal·mol^{-1}, and

the chain propagation insertion barrier was calculated to be 21.9 kcal·mol^{-1}. Chain propagation was found to occur in two steps: ethylene uptake (15.6 kcal·mol^{-1}) and migratory insertion (9.8 kcal·mol^{-1}). Calculations indicate that the small bite angle controls polymerization activity in such Ru(IV) complexes in two different ways. The first is that steric interactions around the metal center decrease the migratory insertion barrier. Indeed, even smaller propagation migratory insertion barriers than observed for LTM of Ni and Pd catalysts were obtained.[25] The second effect is a higher ethylene uptake barrier, which is the reason for the lower activity displayed for complex **4.7**. Steric interactions involving the monomer are also responsible for the non-incorporation of 1-hexene. We hypothesized that fine-tuning the bite angle to favor ethylene uptake might increase the activity of this type complex. This tuning can be achieved by replacing the dithiocarbamate ligand with a less sterically demanding bidentate anionic ligand or a monodentate anionic ligand. This research opens a new research line to a class of tunable half-metallocene ruthenium (IV) complexes.

4.5 References

(1) *Topics in Organometallic Chemistry*; Springer: Berlin/Heidelberg, 2009; Vol. 29.
(2) *Transition Metal Polymerization Catalysts*; John Wiley & Sons, Inc.: New Yersey, 2009.
(3) *Organometallic Catalysts and Olefin Polymerization*; Springer: Berlin, 2009.
(4) Chung, T. C. *Functionalization of Polyolefins*; Academic Press: London, 2002.
(5) Dong, J.-Y.; Hu, Y. *Coord. Chem. Rev.* **2006**, *250*, 47-65.
(6) Yanjarappa, M. J.; Sivaram, S. *Prog. Polym. Sci.* **2002**, *27*, 1347-1398.
(7) Small, B. L.; Brookhart, M.; Bennett, A. M. A. *J. Am. Chem. Soc.* **1998**, *120*, 4049-4050.
(8) Britovsek, G. J. P.; Bruce, M.; Gibson, V. C.; Kimberley, B. S.; Maddox, P. J.; Mastroianni, S.; McTavish, S. J.; Redshaw, C.; Solan, G. A.; Strömberg, S.; White, A. J. P.; Williams, D. J. *J. Am. Chem. Soc.* **1999**, *121*, 8728-8740.
(9) Noyori, R.; Takaya, H. *Acc. Chem. Res.* **1990**, *23*, 345-350.
(10) Grubbs, R. H.; Miller, S. J.; Fu, G. C. *Acc. Chem. Res.* **1995**, *28*, 446-452.
(11) Trnka, T. M.; Grubbs, R. H. *Acc. Chem. Res.* **2001**, *34*, 18-29.
(12) Ueda, J.; Matsuyama, M.; Kamigaito, M.; Sawamoto, M. *Macromolecules* **1998**, *31*, 557-562.
(13) James, B. R.; Markham, L. D. *J. Catal.* **1972**, *27*, 442-451.
(14) Komiya, S.; Yamamoto, A.; Ikeda, S. *Bull. Chem. Soc. Jpn.* **1975**, *48*, 101-107.
(15) Nomura, K.; Warit, S.; Imanishi, Y. *Macromolecules* **1999**, *32*, 4732-4734.
(16) Nomura, K.; Sidokmai, W.; Imanishi, Y. *Bull. Chem. Soc. Jpn.* **2000**, *73*, 599-605.
(17) Dias, E. L.; Brookhart, M.; White, P. S. *Organometallics* **2000**, *19*, 4995-5004.
(18) Heyndrickx, W.; Occhipinti, G.; Minenkov, Y.; Jensen, V. R. *J. Mol. Catal. A: Chem.* **2010**, *324*, 64-74.
(19) Piche, L.; Daigle, J.-C.; Claverie, J. P. *Chem. Commun.* **2011**, *47*, 7836-7838.
(20) Camacho-Fernandez, M. A.; Yen, M.; Ziller, J. W.; Guan, Z. *Chem. Sci.* **2013**, *4*, 2902-2906.
(21) Cossee, P. *J. Catal.* **1964**, *3*, 80-88.
(22) Arlman, E. J. *J. Catal.* **1964**, *3*, 89-98.
(23) Arlman, E. J.; Cossee, P. *J. Catal.* **1964**, *3*, 99-104.
(24) Johnson, L. K.; Killian, C. M.; Brookhart, M. *J. Am. Chem. Soc.* **1995**, *117*, 6414-6415.
(25) Ittel, S. D.; Johnson, L. K.; Brookhart, M. *Chem. Rev.* **2000**, *100*, 1169-1203.
(26) Margl, P.; Deng, L.; Ziegler, T. *Organometallics* **1998**, *17*, 933-946.
(27) Margl, P.; Deng, L.; Ziegler, T. *J. Am. Chem. Soc.* **1998**, *120*, 5517-5525.
(28) Jensen, V. R.; Thiel, W. *Organometallics* **2001**, *20*, 4852-4862.
(29) Schmid, R.; Ziegler, T. *Organometallics* **2000**, *19*, 2756-2765.
(30) Friedberger, T.; Ziller, J. W.; Guan, Z. *Organometallics* **2014**, *33*, 1913-1916.
(31) Zhang, W.; Sita, L. R. *J. Am. Chem. Soc.* **2007**, *130*, 442-443.
(32) Zhang, W.; Wei, J.; Sita, L. R. *Macromolecules* **2008**, *41*, 7829-7833.
(33) Wei, J.; Zhang, W.; Wickham, R.; Sita, L. R. *Angew. Chem. Int. Ed.* **2010**, *49*, 9140-9144.
(34) Kuan, S. L.; Tay, E. P. L.; Leong, W. K.; Goh, L. Y.; Lin, C. Y.; Gill, P. M. W.; Webster, R. D. *Organometallics* **2006**, *25*, 6134-6141.
(35) Tay, E. P. L.; Kuan, S. L.; Leong, W. K.; Goh, L. Y. *Inorg. Chem.* **2007**, *46*, 1440-1450.

(36) Deng, L.; Margl, P.; Ziegler, T. *J. Am. Chem. Soc.* **1997**, *119*, 1094-1100.
(37) Deng, L.; Woo, T. K.; Cavallo, L.; Margl, P. M.; Ziegler, T. *J. Am. Chem. Soc.* **1997**, *119*, 6177-6186.
(38) Carpenetti, D. W.; Kloppenburg, L.; Kupec, J. T.; Petersen, J. L. *Organometallics* **1996**, *15*, 1572-1581.
(39) Tempel, D. J.; Johnson, L. K.; Huff, R. L.; White, P. S.; Brookhart, M. *J. Am. Chem. Soc.* **2000**, *122*, 6686-6700.
(40) Masuda, J. D.; Wei, P.; Stephan, D. W. *Dalton Transactions* **2003**, 3500-3505.
(41) Strauss, S. H. *Chem. Rev.* **1993**, *93*, 927-942.
(42) Sishta, C.; Hathorn, R. M.; Marks, T. J. *J. Am. Chem. Soc.* **1992**, *114*, 1112-1114.
(43) Gassman, P. G.; Callstrom, M. R. *J. Am. Chem. Soc.* **1987**, *109*, 7875-7876.
(44) Harlan, C. J.; Bott, S. G.; Barron, A. R. *J. Am. Chem. Soc.* **1995**, *117*, 6465-6474.
(45) Corker, J. M.; Evans, J. *J. Chem. Soc., Chem. Commun.* **1991**, 1104-1106.
(46) Fernando de Souza, R.; Simon, L. C.; Alves, M. d. C. M. *J. Catal.* **2003**, *214*, 165-168.
(47) Bryliakov, K. P.; Talsi, E. P.; Semikolenova, N. V.; Zakharov, V. A. *Organometallics* **2009**, *28*, 3225-3232.
(48) Evans, W. J.; Champagne, T. M.; Giarikos, D. G.; Ziller, J. W. *Organometallics* **2005**, *24*, 570-579.
(49) Mason, M. R.; Smith, J. M.; Bott, S. G.; Barron, A. R. *J. Am. Chem. Soc.* **1993**, *115*, 4971-4984.
(50) Rappé, A. K.; Skiff, W. M.; Casewit, C. J. *Chem. Rev.* **2000**, *100*, 1435-1456.

4.6 Experimental Section

General. All organometallic manipulations were conducted under inert atmosphere using standard Schlenk, vacuum, or glove box (N_2) techniques. All reagents were used as received from commercial suppliers unless otherwise noted. Anhydrous solvents were passed through a column of activated alumina (type A2, size 12x32, Purify) under argon pressure. Ethanol was degassed by passing a stream of N2 through the solvent. Deuterated solvents were purchased from Cambridge Isotope Laboratories and placed over activated 4Å molecular sieves. CD_2Cl_2 was dried over CaH_2 and distilled. Ultrahigh pure grade ethylene gas was purchased from Praxair and used without further purification. ^{1}H and ^{13}C-NMR spectra were recorded at 500 MHz on a Bruker GN-500 or Cryo-500 spectrometer. Low-temperature NMR spectra were recorded in the Bruker GN-500 spectrometer. ^{31}P and ^{19}F-NMR spectra were recorded using a DRX 400 MHz spectrometer. ^{11}B-NMR was recorded using a GN-500 spectrometer. All NMR chemical shifts are reported as δ in parts per million (ppm). ^{1}H and ^{13}C NMR spectra are relative to residual solvent. Molecular weights (Mn and Mw) and polydispersity indices (Mw/Mn) were determined by high-temperature gel permeation chromatography (GPC) using an Agilent PL-GPC 220 GPC equipped with a refractive index (dRI) detector and in-line viscometer. The column set consisted of two PLgel 5 μm mixed-C 300x7.5 mm (and pre-column), and the samples were eluted at 150 °C with 1,2,4-trichlorobenzene containing 0.01 wt % di-tert-butyl-hydroxytoluene (BHT) at a 1.0 mL/min rate. Universal calibration with polystyrene standards was used. Polymer solutions were placed on a heating plate at 150 °C prior to sample analysis, and hot filtration was used before sampling. Branching was determined by ^{1}H-NMR spectroscopy

and expressed as the number of Me's per 1000 carbons.[1] Electrospray Ionization Mass Spectrometric analyses (ESI-MS) were obtained on a Waters Micromass LCT ESI-MS. ESI-MS spectra analysis and isotope pattern simulations were performed using MassLynx Mass Spectrometry software to confirm the identity of the species. $[H(Et_2O)_2]^+$ $[BAr'_4]^-$ (where Ar'= 3,5-$(CF_3)_2C_6H_3$))[2] and **4.6**[3] were synthesized following published procedures.

General procedure for ethylene polymerization and copolymerization. A 600 mL autoclave (Parr reactor) was heated under high vacuum to 120 °C for two hours, then twice purged with ethylene and cooled to the desired polymerization temperature. A 100 mL Schlenk flask was kept in an oven overnight and introduced into the glove box. Dry toluene solvent (100 mL) was measured and placed in a 100 mL round bottom flask. An aliquot of 10 mL of the solvent was used to dissolve the desired amount of complex **4.6** or **4.7** and introduced in a 12 mL syringe. Another 10 mL of toluene was loaded into a syringe for later rinsing of the flask. Complex **4.8** was diluted in 2 mL of DCM and added to the 10 mL aliquot of toluene. The remaining 80 mL of solution (i.e., toluene) was loaded with the desired amount of alkyl aluminum cocatalyst. The cocatalyst solution was then transferred into the reactor through cannula under an ethylene atmosphere. The reactor was then filled with ethylene at 200 psi for 10 minutes. The solution of the complex was introduced through cannula under an ethylene atmosphere, and the flask was rinsed with the previously loaded 10 mL of solvent syringe. The Parr reactor was closed and pressurized with the desired ethylene pressure. Polymerization was quenched with a methanol-acidic solution (100 mL). Polyethylene was filtrated and washed with MeOH and acetone, then dried under high vacuum overnight.

Polymerizations with non-alkyl-aluminum cocatalysts: Complexes **4.6** and **4.7** were dissolved in 90 mL of toluene, whereas non-alkyl aluminum cocatalysts were dissolved in 10 mL of DCM and loaded in 12 mL syringes. Complex solutions were transferred through cannula under an ethylene atmosphere at room temperature, followed by the addition of cocatalyst and rinsing the flask with an extra 10 mL of toluene. Complex **4.8** was dissolved previously in 2 mL of DCM and added to 8 mL of toluene in a 12 mL syringe. $Ni(COD)_2$ was loaded as a suspension in 80 mL of toluene through cannula under an ethylene atmosphere, followed by the addition of the complex **4.8** solution and rinsed with 10 mL of toluene. The Parr reactor was pressurized at the desired pressure and heated to the target temperature.

Copolymerizations with 1-hexene (1.0 M) and methyl acrylate (0.1 M) were performed by addition of the co-monomer to the 80 mL toluene solution of MAO and transferred to the reactor via cannula, followed by addition of complex **4.7**, as described in the paragraph above, and pressurized to 300 psi of ethylene.

Computational details. DFT calculations were performed using the TURBOMOLE version 6.5 program package.[4] The initial guesses for the structures were obtained from available experimental crystal structures. Initial gas-phase optimizations were performed using a double-zeta quality split-valence basis set with inclusion of polarization functions [def2-SV(P)][5] on all atoms and the inclusion of relativistic small-core pseudopotentials[6] for Ru. An open-shell configuration (i.e., unrestricted wave function) was used for all compounds. The non-hybrid GGA functional BP86[7,8] was used for all structure optimizations. Initially, the search for transition states was performed manually. Once a reasonable guess was obtained, the structure was refined by scanning the potential energy surface along the corresponding coordinate. Full-frequency calculations were performed

using the same level of theory to determine the stable minima on the potential energy surface. Additionally, full frequency calculations were used to determine stable transition states by the presence of one negative frequency. TmoleX software was used to visualize negative frequencies and verify that the intended transition state was obtained. Single-point (SP) energy calculation was performed using the hybrid-GGA functional B3LYP[7,9] as implemented in Turbomole, together with triple-zeta quality basis sets (def2-TZVP)[10] for all atoms with an open-shell configuration. Zero point energy (ZPE) corrections to the total energy were also applied by running a complete frequency calculation at the same level of theory.

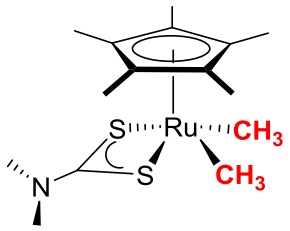

4.7

Synthesis of [Cp*RuMe$_2$(S$_2$CNMe$_2$)] (4.7). Complex **4.6** (0.1377 g, 0.322 mmol) was suspended in THF and cooled to -78 °C. A total of 0.5034 mL of a MeLi solution in hexanes (1.6 M) (0.805 mmol) was added dropwise. The solution was left to reach room temperature and stopped immediately. The reaction was dried under high vacuum and transferred to a glove box. The solid was washed with pentanes and the solution filtrated. Recrystallization was performed at -30 °C from a concentrated pentanes solution. Yield 0.0745 g, 60%, dark brown-red crystals. ^{1}H NMR (500 MHz, C_6D_6, 298 K): δ 2.47 (s, 6 H), 1.33 (s, 15 H), 1.17 (s, 6 H). ^{13}C NMR (500 MHz, C_6D_6, 298 K): δ 208.2, 128.4, 95.7, 36.2, 8.0, 5.8. MS(ESI) m/z calcd for $C_{15}H_{27}NS_2Ru$ M=387.06, found [M+H$^+$]=388.02, [M-Me$^+$]=372.01.

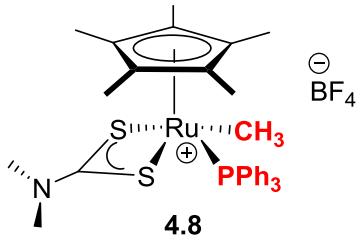

4.8

Synthesis of [Cp*(κ²-*S*₂CNMe₂)Ru(Me)PPh3][BF₄] (4.8). Complex **4.7** (0.1000 g, 0.259 mmol) and 0.0629 g of PPh_3(0.259 mmol) were weighed (in a glove box) and loaded in a 15 mL vial with 5 mL of toluene. The vial with attached septa was taken outside the glove box and cooled to -78 °C under a N2 atmosphere. A volume of 35.5 μL of $(Et_2O)H{\cdot}BF_4$ was added (0.0419 g, 0.259 mmol) to the toluene solution. The solution was left to reach room temperature, and after 30 minutes the reaction was stopped and the solvent evaporated under high vacuum. The crude material was introduced into a glove box, dissolved in THF and filtrated. Slow diffusion of diethylether into the THF solution afforded red crystals. Single crystal X-ray diffraction confirms crystallization with one THF molecule, which is confirmed by NMR spectroscopy of single crystals. Yield 0.1299 g, 81%. ^{1}H NMR (500 MHz, CD_2Cl_2, 298 K): δ 7.87–7.03 (br, 15H, PPh_3), 3.69 (m, 4H, THF), 3.02 (s, 3H), 2.91 (s, 3H), 1.82 (m, 4H, THF), 1.50 (s, 15H), 0.93–0.91 (d, J_{PH} 10 Hz, 3H). ^{13}C NMR (500 MHz, CD_2Cl_2, 298 K): δ 205.0, 133.6–128.0 (PPh_3), 103.4, 68.3 (THF), 38.1, 37.9, 26.1 (THF), 9.3–9.2 (d, J_{PC} 55 Hz), 8.9. ^{31}P {^{1}H}NMR (400 MHz, CD_2Cl_2, 298 K): δ 44.33. ^{19}F {^{1}H}NMR (400 MHz, CD_2Cl_2, 298 K): δ -153.50. ^{11}B NMR (500 MHz, CD_2Cl_2, 298 K): δ -1.15. MS(ESI) m/z calcd for $C_{31}H_{36}NPS_2Ru^+$ M=619.11, found [M^+]=619.19.

X-ray Data Collection, Structure Solution and Refinement for 4.7. A violet crystal of approximate dimensions 0.268 x 0.298 x 0.315 mm was mounted on a glass fiber and transferred to a Bruker SMART APEX II diffractometer. The APEX2[11] program package was used to determine the unit-cell parameters and for data collection (10 sec/frame scan time for a sphere of diffraction data). The raw frame data was processed using SAINT[12] and SADABS[13] to yield the reflection data file. Subsequent calculations were carried out using the SHELXTL[14] program. The diffraction symmetry was $2/m$ and the systematic absences were consistent with the monoclinic space group $P2_1/c$ that was later determined to be correct.

The structure was solved by direct methods and refined on F^2 by full-matrix least-squares techniques[15]. The analytical scattering factors[16] for neutral atoms were used throughout the analysis. Hydrogen atoms were located from a difference-Fourier map and refined (x,y,z and U_{iso}).

At convergence, wR2 = 0.0441 and Goof = 1.019 for 280 variables refined against 4000 data (0.74Å), R1 = 0.0169 for those 3742 data with $I > 2.0\sigma(I)$.

Table 4.4. Crystal data and structure refinement for **4.7**.

Identification code	zg67 (Miguel Camacho)	
Empirical formula	C15 H27 N Ru S2	
Formula weight	386.56	
Temperature	143(2) K	
Wavelength	0.71073 Å	
Crystal system	Monoclinic	
Space group	$P2_1/c$	
Unit cell dimensions	a = 8.2695(5) Å	α= 90°.
	b = 12.4074(7) Å	β= 95.9858(6)°.
	c = 16.5455(9) Å	γ = 90°.
Volume	1688.36(17) $Å^3$	
Z	4	
Density (calculated)	1.521 Mg/m^3	
Absorption coefficient	1.164 mm^{-1}	
F(000)	800	
Crystal color	violet	
Crystal size	0.315 x 0.298 x 0.268 mm^3	
Theta range for data collection	2.056 to 28.569°	
Index ranges	-10 ≤ h ≤ 11, -16 ≤ k ≤ 16, -21 ≤ l ≤ 21	
Reflections collected	19150	
Independent reflections	4000 [R(int) = 0.0176]	
Completeness to theta = 25.242°	100.0 %	
Absorption correction	Semi-empirical from equivalents	
Max. and min. transmission	0.7457 and 0.6708	
Refinement method	Full-matrix least-squares on F^2	
Data / restraints / parameters	4000 / 0 / 280	
Goodness-of-fit on F^2	1.019	
Final R indices [I>2sigma(I) = 3742 data]	R1 = 0.0169, wR2 = 0.0432	
R indices (all data, 0.74Å)	R1 = 0.0186, wR2 = 0.0441	
Largest diff. peak and hole	0.423 and -0.249 $e.Å^{-3}$	

Table 4.5. Atomic coordinates ($x10^4$) and equivalent isotropic displacement parameters ($Å^2x10^3$) for **4.7**. U(eq) is defined as one third of the trace of the orthogonalized U^{ij} tensor.

	X	y	z	U(eq)
Ru(1)	7451(1)	7027(1)	6286(1)	15(1)
S(1)	5469(1)	7316(1)	5148(1)	21(1)
S(2)	6233(1)	8759(1)	6420(1)	23(1)
N(1)	3533(2)	9027(1)	5361(1)	23(1)
C(1)	7550(2)	5278(1)	6663(1)	20(1)
C(2)	5929(2)	5614(1)	6745(1)	19(1)
C(3)	5995(2)	6483(1)	7302(1)	19(1)
C(4)	7676(2)	6684(1)	7584(1)	19(1)
C(5)	8638(2)	5927(1)	7193(1)	20(1)
C(6)	8013(2)	4304(1)	6204(1)	29(1)
C(7)	4406(2)	5129(1)	6331(1)	26(1)
C(8)	4546(2)	7009(1)	7603(1)	28(1)
C(9)	8270(2)	7442(1)	8256(1)	28(1)
C(10)	10430(2)	5763(1)	7369(1)	28(1)
C(11)	8798(2)	6444(1)	5327(1)	28(1)
C(12)	9578(2)	8021(1)	6354(1)	29(1)
C(13)	4858(2)	8463(1)	5604(1)	20(1)
C(14)	2416(2)	8685(1)	4669(1)	27(1)
C(15)	3059(2)	9965(1)	5812(1)	30(1)

Table 4.6. Bond lengths [Å] and angles [°] for **4.7**.

Ru(1)-Cnt	1.888
Ru(1)-C(12)	2.1410(15)
Ru(1)-C(11)	2.1555(15)
Ru(1)-C(4)	2.1796(13)
Ru(1)-C(5)	2.1849(13)
Ru(1)-C(1)	2.2577(14)
Ru(1)-C(3)	2.2715(13)
Ru(1)-C(2)	2.3311(13)
Ru(1)-S(1)	2.3909(4)
Ru(1)-S(2)	2.3935(4)
S(1)-C(13)	1.7111(14)
S(2)-C(13)	1.7123(14)
N(1)-C(13)	1.3271(18)
N(1)-C(14)	1.4577(19)
N(1)-C(15)	1.4581(19)
C(1)-C(2)	1.4236(19)
C(1)-C(5)	1.4370(19)
C(1)-C(6)	1.497(2)
C(2)-C(3)	1.4155(19)
C(2)-C(7)	1.4960(19)
C(3)-C(4)	1.4413(19)
C(3)-C(8)	1.495(2)
C(4)-C(5)	1.429(2)
C(4)-C(9)	1.499(2)
C(5)-C(10)	1.4937(19)
Cnt-Ru(1)-S(1)	122.2
Cnt-Ru(1)-S(2)	117.1
Cnt-Ru(1)-C(11)	114.3
Cnt-Ru(1)-C(12)	121.2
C(12)-Ru(1)-C(11)	75.39(7)
C(12)-Ru(1)-C(4)	94.35(6)
C(11)-Ru(1)-C(4)	131.48(6)
C(12)-Ru(1)-C(5)	90.92(6)
C(11)-Ru(1)-C(5)	93.80(6)
C(4)-Ru(1)-C(5)	38.22(5)
C(12)-Ru(1)-C(1)	122.25(6)
C(11)-Ru(1)-C(1)	82.77(6)

C(4)-Ru(1)-C(1)	62.78(5)
C(5)-Ru(1)-C(1)	37.70(5)
C(12)-Ru(1)-C(3)	128.93(6)
C(11)-Ru(1)-C(3)	143.07(6)
C(4)-Ru(1)-C(3)	37.71(5)
C(5)-Ru(1)-C(3)	62.63(5)
C(1)-Ru(1)-C(3)	61.04(5)
C(12)-Ru(1)-C(2)	152.18(6)
C(11)-Ru(1)-C(2)	108.98(6)
C(4)-Ru(1)-C(2)	61.64(5)
C(5)-Ru(1)-C(2)	61.67(5)
C(1)-Ru(1)-C(2)	36.10(5)
C(3)-Ru(1)-C(2)	35.79(5)
C(12)-Ru(1)-S(1)	116.57(5)
C(11)-Ru(1)-S(1)	80.53(4)
C(4)-Ru(1)-S(1)	141.85(4)
C(5)-Ru(1)-S(1)	148.94(4)
C(1)-Ru(1)-S(1)	111.32(4)
C(3)-Ru(1)-S(1)	104.74(4)
C(2)-Ru(1)-S(1)	91.14(3)
C(12)-Ru(1)-S(2)	80.18(5)
C(11)-Ru(1)-S(2)	128.65(5)
C(4)-Ru(1)-S(2)	94.43(4)
C(5)-Ru(1)-S(2)	131.32(4)
C(1)-Ru(1)-S(2)	147.22(4)
C(3)-Ru(1)-S(2)	86.40(4)
C(2)-Ru(1)-S(2)	113.44(3)
S(1)-Ru(1)-S(2)	71.212(12)
C(13)-S(1)-Ru(1)	89.27(5)
C(13)-S(2)-Ru(1)	89.15(5)
C(13)-N(1)-C(14)	121.32(12)
C(13)-N(1)-C(15)	121.56(13)
C(14)-N(1)-C(15)	116.94(13)
C(2)-C(1)-C(5)	108.27(12)
C(2)-C(1)-C(6)	125.31(13)
C(5)-C(1)-C(6)	125.78(13)
C(2)-C(1)-Ru(1)	74.76(8)
C(5)-C(1)-Ru(1)	68.40(7)

C(6)-C(1)-Ru(1)	129.71(10)
C(3)-C(2)-C(1)	108.23(12)
C(3)-C(2)-C(7)	125.30(13)
C(1)-C(2)-C(7)	126.46(13)
C(3)-C(2)-Ru(1)	69.81(7)
C(1)-C(2)-Ru(1)	69.14(7)
C(7)-C(2)-Ru(1)	127.64(10)
C(2)-C(3)-C(4)	108.24(12)
C(2)-C(3)-C(8)	124.89(13)
C(4)-C(3)-C(8)	126.58(13)
C(2)-C(3)-Ru(1)	74.40(7)
C(4)-C(3)-Ru(1)	67.68(7)
C(8)-C(3)-Ru(1)	128.46(10)
C(5)-C(4)-C(3)	107.68(12)
C(5)-C(4)-C(9)	126.38(13)
C(3)-C(4)-C(9)	125.39(13)
C(5)-C(4)-Ru(1)	71.09(8)
C(3)-C(4)-Ru(1)	74.60(7)
C(9)-C(4)-Ru(1)	126.53(10)
C(4)-C(5)-C(1)	107.56(12)
C(4)-C(5)-C(10)	126.11(13)
C(1)-C(5)-C(10)	126.03(13)
C(4)-C(5)-Ru(1)	70.69(8)
C(1)-C(5)-Ru(1)	73.90(8)
C(10)-C(5)-Ru(1)	125.77(10)
N(1)-C(13)-S(1)	125.28(11)
N(1)-C(13)-S(2)	125.81(11)
S(1)-C(13)-S(2)	108.91(8)

Table 4.7. Anisotropic displacement parameters ($Å^2$x 10^3) for **4.7**. The anisotropic displacement factor exponent takes the form: $-2\pi^2[h^2 a^{*2} U^{11} + ... + 2 h k a^* b^* U^{12}]$

	U^{11}	U^{22}	U^{33}	U^{23}	U^{13}	U^{12}
Ru(1)	15(1)	17(1)	15(1)	0(1)	2(1)	-1(1)
S(1)	24(1)	20(1)	18(1)	-3(1)	-1(1)	2(1)
S(2)	27(1)	18(1)	23(1)	-4(1)	-2(1)	0(1)
N(1)	24(1)	21(1)	24(1)	-1(1)	1(1)	3(1)
C(1)	19(1)	19(1)	21(1)	1(1)	2(1)	-1(1)
C(2)	18(1)	20(1)	19(1)	2(1)	2(1)	-3(1)
C(3)	19(1)	21(1)	18(1)	1(1)	4(1)	-3(1)
C(4)	20(1)	22(1)	15(1)	1(1)	2(1)	-4(1)
C(5)	18(1)	21(1)	20(1)	4(1)	1(1)	-1(1)
C(6)	29(1)	22(1)	38(1)	-6(1)	6(1)	3(1)
C(7)	21(1)	26(1)	31(1)	-2(1)	-1(1)	-6(1)
C(8)	22(1)	33(1)	30(1)	-4(1)	10(1)	-1(1)
C(9)	31(1)	32(1)	20(1)	-5(1)	1(1)	-8(1)
C(10)	18(1)	31(1)	34(1)	4(1)	-1(1)	1(1)
C(11)	26(1)	38(1)	20(1)	1(1)	7(1)	5(1)
C(12)	24(1)	27(1)	38(1)	3(1)	6(1)	-7(1)
C(13)	23(1)	17(1)	20(1)	0(1)	4(1)	-2(1)
C(14)	24(1)	31(1)	26(1)	1(1)	-2(1)	2(1)
C(15)	30(1)	23(1)	36(1)	-4(1)	4(1)	5(1)

Table 4.8. Hydrogen coordinates (x 10^4) and isotropic displacement parameters ($Å^2$x 10^3) for **4.7**.

	x	y	z	U(eq)
H(6A)	9070(30)	4372(16)	6058(12)	40(5)
H(6B)	7960(30)	3656(19)	6560(14)	53(6)
H(6C)	7290(30)	4184(17)	5746(13)	40(5)
H(7A)	3620(30)	5647(17)	6144(12)	40(5)
H(7B)	3900(20)	4706(17)	6717(12)	44(6)
H(7C)	4610(30)	4694(18)	5876(13)	46(6)
H(8A)	3750(20)	7212(15)	7175(12)	33(5)
H(8B)	4010(30)	6526(18)	7938(12)	42(5)
H(8C)	4810(30)	7590(20)	7920(13)	47(6)
H(9A)	7950(30)	8160(20)	8146(15)	60(7)
H(9B)	9320(30)	7480(20)	8333(15)	63(7)
H(9C)	7940(40)	7220(20)	8763(17)	82(9)
H(10A)	10940(20)	6394(17)	7544(11)	35(5)
H(10B)	10890(20)	5518(16)	6912(12)	39(5)
H(10C)	10670(30)	5250(18)	7787(13)	45(6)
H(11A)	9840(20)	6112(15)	5549(11)	34(5)
H(11B)	9030(20)	7041(15)	4993(13)	34(5)
H(11C)	8120(20)	5921(16)	5015(12)	36(5)
H(12A)	10570(30)	7605(18)	6324(12)	43(5)
H(12B)	9640(20)	8436(16)	6844(13)	36(5)
H(12C)	9480(30)	8557(18)	5922(13)	45(6)
H(14A)	2890(30)	8220(20)	4325(17)	68(8)
H(14B)	1540(30)	8310(20)	4838(16)	64(7)
H(14C)	2060(30)	9270(20)	4374(15)	66(7)
H(15A)	2120(30)	9840(20)	6089(15)	66(7)
H(15B)	3830(30)	10150(20)	6157(17)	76(9)
H(15C)	2830(30)	10540(20)	5462(15)	63(7)

Table 4.9. Torsion angles [°] for **4.7**.

C(5)-C(1)-C(2)-C(3)	1.51(15)
C(6)-C(1)-C(2)-C(3)	172.75(14)
Ru(1)-C(1)-C(2)-C(3)	-59.04(9)
C(5)-C(1)-C(2)-C(7)	-177.38(13)
C(6)-C(1)-C(2)-C(7)	-6.1(2)
Ru(1)-C(1)-C(2)-C(7)	122.08(14)
C(5)-C(1)-C(2)-Ru(1)	60.55(9)
C(6)-C(1)-C(2)-Ru(1)	-128.21(15)
C(1)-C(2)-C(3)-C(4)	-0.90(15)
C(7)-C(2)-C(3)-C(4)	178.00(13)
Ru(1)-C(2)-C(3)-C(4)	-59.53(9)
C(1)-C(2)-C(3)-C(8)	-175.03(13)
C(7)-C(2)-C(3)-C(8)	3.9(2)
Ru(1)-C(2)-C(3)-C(8)	126.34(14)
C(1)-C(2)-C(3)-Ru(1)	58.63(9)
C(7)-C(2)-C(3)-Ru(1)	-122.47(14)
C(2)-C(3)-C(4)-C(5)	-0.04(15)
C(8)-C(3)-C(4)-C(5)	173.96(14)
Ru(1)-C(3)-C(4)-C(5)	-63.86(9)
C(2)-C(3)-C(4)-C(9)	-172.02(13)
C(8)-C(3)-C(4)-C(9)	2.0(2)
Ru(1)-C(3)-C(4)-C(9)	124.17(14)
C(2)-C(3)-C(4)-Ru(1)	63.81(9)
C(8)-C(3)-C(4)-Ru(1)	-122.19(14)
C(3)-C(4)-C(5)-C(1)	0.96(15)
C(9)-C(4)-C(5)-C(1)	172.83(13)
Ru(1)-C(4)-C(5)-C(1)	-65.22(9)
C(3)-C(4)-C(5)-C(10)	-173.07(13)
C(9)-C(4)-C(5)-C(10)	-1.2(2)
Ru(1)-C(4)-C(5)-C(10)	120.74(14)
C(3)-C(4)-C(5)-Ru(1)	66.19(9)
C(9)-C(4)-C(5)-Ru(1)	-121.94(14)
C(2)-C(1)-C(5)-C(4)	-1.53(15)
C(6)-C(1)-C(5)-C(4)	-172.72(14)

Ru(1)-C(1)-C(5)-C(4)	63.11(9)
C(2)-C(1)-C(5)-C(10)	172.52(13)
C(6)-C(1)-C(5)-C(10)	1.3(2)
Ru(1)-C(1)-C(5)-C(10)	-122.85(14)
C(2)-C(1)-C(5)-Ru(1)	-64.63(10)
C(6)-C(1)-C(5)-Ru(1)	124.17(14)
C(14)-N(1)-C(13)-S(1)	1.8(2)
C(15)-N(1)-C(13)-S(1)	176.69(12)
C(14)-N(1)-C(13)-S(2)	-178.23(11)
C(15)-N(1)-C(13)-S(2)	-3.3(2)
Ru(1)-S(1)-C(13)-N(1)	-169.21(12)
Ru(1)-S(1)-C(13)-S(2)	10.81(6)
Ru(1)-S(2)-C(13)-N(1)	169.22(12)
Ru(1)-S(2)-C(13)-S(1)	-10.80(6)

X-ray Data Collection, Structure Solution and Refinement for zg80. An orange crystal of approximate dimensions 0.138 x 0.197 x 0.223 mm was mounted on a glass fiber and transferred to a Bruker SMART APEX II diffractometer. The APEX2[11] program package was used to determine the unit-cell parameters and for data collection (25 sec/frame scan time for a sphere of diffraction data). The raw frame data was processed using SAINT[12] and SADABS[13] to yield the reflection data file. Subsequent calculations were carried out using the SHELXTL[14] program. The diffraction symmetry was $2/m$ and the systematic absences were consistent with the monoclinic space group $P2_1/n$ that was later determined to be correct.

The structure was solved by direct methods and refined on F^2 by full-matrix least-squares techniques. The analytical scattering factors[15] for neutral atoms were used throughout the analysis. Hydrogen atoms were included using a riding model. There was one molecule of tetrahydrofuran solvent present.

At convergence, wR2 = 0.0725 and Goof = 1.060 for 432 variables refined against 7878 data (0.78Å), R1 = 0.0287 for those 6785 data with $I > 2.0\sigma(I)$.

Table 4.10. Crystal data and structure refinement for **4.8**.

Identification code	zg80 (Miguel Camacho)	
Empirical formula	C_{36} H_{47} B F_4 N O P Ru S_2	
Formula weight	792.71	
Temperature	88(2) K	
Wavelength	0.71073 Å	
Crystal system	Monoclinic	
Space group	$P2_1/n$	
Unit cell dimensions	a = 9.1914(6) Å	α= 90°.
	b = 18.9539(12) Å	β= 95.9872(8)°.
	c = 20.6718(13) Å	γ = 90°.
Volume	3581.6(4) $Å^3$	
Z	4	
Density (calculated)	1.470 Mg/m^3	
Absorption coefficient	0.650 mm^{-1}	
F(000)	1640	
Crystal color	orange	
Crystal size	0.223 x 0.197 x 0.138 mm^3	
Theta range for data collection	1.461 to 27.100°	
Index ranges	$-11 \le h \le 11$, $-24 \le k \le 24$, $-26 \le l \le 26$	
Reflections collected	39433	
Independent reflections	7878 [R(int) = 0.0322]	
Completeness to theta = 25.242°	100.0 %	
Absorption correction	Semi-empirical from equivalents	
Max. and min. transmission	0.8621 and 0.7566	
Refinement method	Full-matrix least-squares on F^2	
Data / restraints / parameters	7878 / 0 / 432	
Goodness-of-fit on F^2	1.060	
Final R indices [I>2sigma(I) = 6785 data]	R1 = 0.0287, wR2 = 0.0673	
R indices (all data, 0.78Å)	R1 = 0.0372, wR2 = 0.0725	
Largest diff. peak and hole	1.038 and -0.578 $e.Å^{-3}$	

Table 4.11. Atomic coordinates (x 10^4) and equivalent isotropic displacement parameters ($Å^2$x 10^3) for **4.8**. U(eq) is defined as one third of the trace of the orthogonalized U^{ij} tensor.

	x	y	z	U(eq)
Ru(1)	2626(1)	6740(1)	1657(1)	13(1)
S(1)	2005(1)	7905(1)	1956(1)	16(1)
S(2)	335(1)	6700(1)	2129(1)	15(1)
P(1)	3408(1)	6332(1)	2728(1)	14(1)
N(1)	-475(2)	7975(1)	2551(1)	18(1)
C(1)	3715(2)	6391(1)	767(1)	18(1)
C(2)	2754(2)	6980(1)	612(1)	18(1)
C(3)	1311(2)	6758(1)	697(1)	18(1)
C(4)	1379(2)	6026(1)	891(1)	19(1)
C(5)	2860(2)	5807(1)	943(1)	18(1)
C(6)	5283(2)	6349(1)	636(1)	24(1)
C(7)	3133(3)	7668(1)	316(1)	23(1)
C(8)	-54(3)	7175(1)	524(1)	25(1)
C(9)	75(3)	5558(1)	912(1)	25(1)
C(10)	3380(3)	5057(1)	1015(1)	25(1)
C(11)	4779(2)	7234(1)	1826(1)	18(1)
C(12)	457(2)	7598(1)	2252(1)	15(1)
C(13)	-201(3)	8720(1)	2711(1)	23(1)
C(14)	-1738(2)	7645(1)	2807(1)	22(1)
C(15)	2533(2)	5527(1)	2995(1)	16(1)
C(16)	1618(2)	5129(1)	2562(1)	18(1)
C(17)	952(2)	4516(1)	2768(1)	20(1)
C(18)	1189(2)	4315(1)	3416(1)	22(1)
C(19)	2114(3)	4702(1)	3849(1)	23(1)
C(20)	2800(3)	5303(1)	3640(1)	22(1)
C(21)	3023(2)	6985(1)	3344(1)	16(1)
C(22)	3891(2)	7589(1)	3452(1)	18(1)
C(23)	3493(3)	8131(1)	3851(1)	21(1)
C(24)	2211(3)	8075(1)	4149(1)	23(1)
C(25)	1351(2)	7478(1)	4058(1)	22(1)
C(26)	1747(2)	6935(1)	3658(1)	19(1)

C(27)	5338(2)	6099(1)	2956(1)	16(1)
C(28)	6073(2)	6254(1)	3565(1)	19(1)
C(29)	7505(2)	6024(1)	3723(1)	22(1)
C(30)	8214(2)	5638(1)	3279(1)	21(1)
C(31)	7479(2)	5474(1)	2673(1)	21(1)
C(32)	6057(2)	5703(1)	2513(1)	18(1)
B(1)	7615(3)	4115(1)	1002(1)	23(1)
F(1)	6986(2)	4760(1)	1089(1)	63(1)
F(2)	6539(2)	3605(1)	858(1)	36(1)
F(3)	8432(2)	3940(1)	1594(1)	43(1)
F(4)	8563(2)	4133(1)	531(1)	38(1)
O(1)	1377(2)	6420(1)	5691(1)	37(1)
C(33)	2479(3)	6420(2)	6236(1)	33(1)
C(34)	3738(3)	5945(1)	6062(1)	30(1)
C(35)	3342(3)	5805(2)	5339(1)	36(1)
C(36)	1687(3)	5850(2)	5272(1)	34(1)

Table 4.12. Bond lengths [Å] and angles [°] for **4.8**.

Ru(1)-Cnt	1.915
Ru(1)-C(11)	2.184(2)
Ru(1)-C(3)	2.212(2)
Ru(1)-C(2)	2.223(2)
Ru(1)-C(1)	2.282(2)
Ru(1)-C(4)	2.296(2)
Ru(1)-C(5)	2.327(2)
Ru(1)-S(1)	2.3801(5)
Ru(1)-P(1)	2.3834(6)
Ru(1)-S(2)	2.4133(5)
S(1)-C(12)	1.708(2)
S(2)-C(12)	1.723(2)
P(1)-C(15)	1.837(2)
P(1)-C(21)	1.837(2)
P(1)-C(27)	1.842(2)
N(1)-C(12)	1.318(3)
N(1)-C(13)	1.465(3)
N(1)-C(14)	1.467(3)
C(1)-C(5)	1.426(3)
C(1)-C(2)	1.440(3)
C(1)-C(6)	1.496(3)
C(2)-C(3)	1.420(3)
C(2)-C(7)	1.495(3)
C(3)-C(4)	1.444(3)
C(3)-C(8)	1.495(3)
C(4)-C(5)	1.416(3)
C(4)-C(9)	1.495(3)
C(5)-C(10)	1.502(3)
C(15)-C(16)	1.387(3)
C(15)-C(20)	1.397(3)
C(16)-C(17)	1.398(3)
C(17)-C(18)	1.388(3)
C(18)-C(19)	1.381(3)
C(19)-C(20)	1.391(3)

C(21)-C(22)	1.399(3)
C(21)-C(26)	1.401(3)
C(22)-C(23)	1.390(3)
C(23)-C(24)	1.390(3)
C(24)-C(25)	1.383(3)
C(25)-C(26)	1.392(3)
C(27)-C(28)	1.396(3)
C(27)-C(32)	1.403(3)
C(28)-C(29)	1.393(3)
C(29)-C(30)	1.389(3)
C(30)-C(31)	1.394(3)
C(31)-C(32)	1.384(3)
B(1)-F(1)	1.373(3)
B(1)-F(4)	1.373(3)
B(1)-F(2)	1.392(3)
B(1)-F(3)	1.407(3)
O(1)-C(36)	1.431(3)
O(1)-C(33)	1.434(3)
C(33)-C(34)	1.538(4)
C(34)-C(35)	1.524(4)
C(35)-C(36)	1.515(4)
Cnt-Ru(1)-S(1)	124.0
Cnt-Ru(1)-S(2)	111.1
Cnt-Ru(1)-P(1)	139.3
Cnt-Ru(1)-C(11)	107.7
C(11)-Ru(1)-C(3)	122.52(8)
C(11)-Ru(1)-C(2)	85.90(8)
C(3)-Ru(1)-C(2)	37.34(8)
C(11)-Ru(1)-C(1)	77.68(8)
C(3)-Ru(1)-C(1)	61.76(8)
C(2)-Ru(1)-C(1)	37.26(8)
C(11)-Ru(1)-C(4)	137.86(8)
C(3)-Ru(1)-C(4)	37.31(8)
C(2)-Ru(1)-C(4)	61.57(8)
C(1)-Ru(1)-C(4)	60.18(8)
C(11)-Ru(1)-C(5)	106.56(8)

C(3)-Ru(1)-C(5)	61.42(8)
C(2)-Ru(1)-C(5)	61.44(8)
C(1)-Ru(1)-C(5)	36.04(7)
C(4)-Ru(1)-C(5)	35.66(8)
C(11)-Ru(1)-S(1)	78.36(6)
C(3)-Ru(1)-S(1)	95.45(6)
C(2)-Ru(1)-S(1)	95.79(6)
C(1)-Ru(1)-S(1)	128.03(6)
C(4)-Ru(1)-S(1)	127.63(6)
C(5)-Ru(1)-S(1)	155.61(6)
C(11)-Ru(1)-P(1)	79.06(6)
C(3)-Ru(1)-P(1)	157.10(6)
C(2)-Ru(1)-P(1)	158.09(6)
C(1)-Ru(1)-P(1)	122.66(6)
C(4)-Ru(1)-P(1)	122.00(6)
C(5)-Ru(1)-P(1)	107.71(6)
S(1)-Ru(1)-P(1)	96.669(19)
C(11)-Ru(1)-S(2)	139.74(6)
C(3)-Ru(1)-S(2)	86.83(6)
C(2)-Ru(1)-S(2)	122.42(6)
C(1)-Ru(1)-S(2)	142.36(6)
C(4)-Ru(1)-S(2)	82.35(5)
C(5)-Ru(1)-S(2)	112.04(6)
S(1)-Ru(1)-S(2)	71.359(17)
P(1)-Ru(1)-S(2)	78.782(18)
C(12)-S(1)-Ru(1)	90.47(7)
C(12)-S(2)-Ru(1)	89.01(7)
C(15)-P(1)-C(21)	103.24(9)
C(15)-P(1)-C(27)	99.40(9)
C(21)-P(1)-C(27)	103.51(10)
C(15)-P(1)-Ru(1)	116.75(7)
C(21)-P(1)-Ru(1)	111.38(7)
C(27)-P(1)-Ru(1)	120.35(7)
C(12)-N(1)-C(13)	121.60(18)
C(12)-N(1)-C(14)	121.01(18)
C(13)-N(1)-C(14)	116.98(17)

C(5)-C(1)-C(2)	108.48(19)
C(5)-C(1)-C(6)	124.9(2)
C(2)-C(1)-C(6)	125.54(19)
C(5)-C(1)-Ru(1)	73.71(12)
C(2)-C(1)-Ru(1)	69.16(11)
C(6)-C(1)-Ru(1)	132.35(15)
C(3)-C(2)-C(1)	107.55(19)
C(3)-C(2)-C(7)	124.7(2)
C(1)-C(2)-C(7)	127.1(2)
C(3)-C(2)-Ru(1)	70.92(12)
C(1)-C(2)-Ru(1)	73.58(12)
C(7)-C(2)-Ru(1)	127.86(15)
C(2)-C(3)-C(4)	107.77(19)
C(2)-C(3)-C(8)	125.8(2)
C(4)-C(3)-C(8)	125.9(2)
C(2)-C(3)-Ru(1)	71.74(12)
C(4)-C(3)-Ru(1)	74.50(12)
C(8)-C(3)-Ru(1)	126.18(15)
C(5)-C(4)-C(3)	108.44(19)
C(5)-C(4)-C(9)	126.3(2)
C(3)-C(4)-C(9)	124.5(2)
C(5)-C(4)-Ru(1)	73.35(12)
C(3)-C(4)-Ru(1)	68.19(11)
C(9)-C(4)-Ru(1)	132.26(15)
C(4)-C(5)-C(1)	107.73(19)
C(4)-C(5)-C(10)	125.3(2)
C(1)-C(5)-C(10)	125.5(2)
C(4)-C(5)-Ru(1)	70.99(12)
C(1)-C(5)-Ru(1)	70.25(12)
C(10)-C(5)-Ru(1)	134.85(15)
N(1)-C(12)-S(1)	126.09(16)
N(1)-C(12)-S(2)	124.73(16)
S(1)-C(12)-S(2)	109.13(11)
C(16)-C(15)-C(20)	119.0(2)
C(16)-C(15)-P(1)	120.89(16)
C(20)-C(15)-P(1)	120.09(16)

C(15)-C(16)-C(17)	120.8(2)
C(18)-C(17)-C(16)	119.4(2)
C(19)-C(18)-C(17)	120.2(2)
C(18)-C(19)-C(20)	120.2(2)
C(19)-C(20)-C(15)	120.3(2)
C(22)-C(21)-C(26)	118.20(19)
C(22)-C(21)-P(1)	120.90(15)
C(26)-C(21)-P(1)	120.42(16)
C(23)-C(22)-C(21)	121.2(2)
C(22)-C(23)-C(24)	119.7(2)
C(25)-C(24)-C(23)	120.0(2)
C(24)-C(25)-C(26)	120.4(2)
C(25)-C(26)-C(21)	120.5(2)
C(28)-C(27)-C(32)	119.00(19)
C(28)-C(27)-P(1)	122.96(16)
C(32)-C(27)-P(1)	117.87(16)
C(29)-C(28)-C(27)	120.2(2)
C(30)-C(29)-C(28)	120.5(2)
C(29)-C(30)-C(31)	119.6(2)
C(32)-C(31)-C(30)	120.2(2)
C(31)-C(32)-C(27)	120.6(2)
F(1)-B(1)-F(4)	112.2(2)
F(1)-B(1)-F(2)	110.3(2)
F(4)-B(1)-F(2)	110.8(2)
F(1)-B(1)-F(3)	106.9(2)
F(4)-B(1)-F(3)	107.6(2)
F(2)-B(1)-F(3)	109.0(2)
C(36)-O(1)-C(33)	107.8(2)
O(1)-C(33)-C(34)	107.7(2)
C(35)-C(34)-C(33)	102.8(2)
C(36)-C(35)-C(34)	102.3(2)
O(1)-C(36)-C(35)	104.4(2)

Table 4.13. Anisotropic displacement parameters ($Å^2 x\ 10^3$) for **4.8**. The anisotropic displacement factor exponent takes the form: $-2\pi^2[h^2 a^{*2} U^{11} + ... + 2 h k a^* b^* U^{12}]$

	U^{11}	U^{22}	U^{33}	U^{23}	U^{13}	U^{12}
Ru(1)	12(1)	12(1)	14(1)	-1(1)	4(1)	-1(1)
S(1)	15(1)	13(1)	20(1)	0(1)	5(1)	-2(1)
S(2)	14(1)	13(1)	20(1)	-2(1)	6(1)	-2(1)
P(1)	13(1)	14(1)	16(1)	0(1)	5(1)	0(1)
N(1)	16(1)	16(1)	22(1)	-3(1)	6(1)	-1(1)
C(1)	22(1)	21(1)	13(1)	-2(1)	7(1)	-1(1)
C(2)	22(1)	19(1)	13(1)	-2(1)	4(1)	-1(1)
C(3)	20(1)	19(1)	14(1)	-3(1)	2(1)	-1(1)
C(4)	23(1)	19(1)	15(1)	-5(1)	5(1)	-3(1)
C(5)	23(1)	18(1)	15(1)	-3(1)	6(1)	-1(1)
C(6)	23(1)	28(1)	24(1)	-1(1)	12(1)	0(1)
C(7)	29(1)	22(1)	19(1)	3(1)	6(1)	-3(1)
C(8)	23(1)	30(1)	22(1)	-2(1)	-2(1)	3(1)
C(9)	26(1)	26(1)	24(1)	-9(1)	5(1)	-10(1)
C(10)	32(1)	17(1)	28(1)	-4(1)	10(1)	3(1)
C(11)	15(1)	20(1)	18(1)	1(1)	5(1)	-3(1)
C(12)	14(1)	16(1)	15(1)	1(1)	1(1)	0(1)
C(13)	23(1)	16(1)	29(1)	-3(1)	6(1)	2(1)
C(14)	17(1)	24(1)	29(1)	-3(1)	10(1)	-1(1)
C(15)	14(1)	14(1)	22(1)	1(1)	7(1)	1(1)
C(16)	18(1)	15(1)	21(1)	-1(1)	6(1)	3(1)
C(17)	17(1)	14(1)	32(1)	-5(1)	6(1)	1(1)
C(18)	20(1)	14(1)	33(1)	4(1)	12(1)	2(1)
C(19)	28(1)	21(1)	22(1)	6(1)	7(1)	1(1)
C(20)	25(1)	20(1)	23(1)	1(1)	4(1)	-3(1)
C(21)	16(1)	17(1)	15(1)	1(1)	3(1)	3(1)
C(22)	19(1)	19(1)	16(1)	2(1)	4(1)	1(1)
C(23)	26(1)	18(1)	19(1)	0(1)	2(1)	0(1)
C(24)	27(1)	25(1)	18(1)	-3(1)	6(1)	6(1)
C(25)	20(1)	30(1)	19(1)	1(1)	8(1)	5(1)
C(26)	17(1)	22(1)	18(1)	0(1)	4(1)	-1(1)
C(27)	13(1)	16(1)	21(1)	2(1)	6(1)	0(1)

C(28)	19(1)	17(1)	22(1)	0(1)	5(1)	0(1)
C(29)	21(1)	19(1)	25(1)	0(1)	1(1)	0(1)
C(30)	16(1)	19(1)	30(1)	3(1)	5(1)	1(1)
C(31)	19(1)	16(1)	28(1)	1(1)	10(1)	2(1)
C(32)	19(1)	16(1)	20(1)	0(1)	6(1)	-2(1)
B(1)	21(1)	24(1)	26(1)	-3(1)	7(1)	-4(1)
F(1)	36(1)	36(1)	119(2)	-6(1)	18(1)	8(1)
F(2)	36(1)	44(1)	27(1)	0(1)	3(1)	-23(1)
F(3)	37(1)	66(1)	26(1)	4(1)	-1(1)	-20(1)
F(4)	40(1)	48(1)	27(1)	-11(1)	15(1)	-20(1)
O(1)	36(1)	45(1)	30(1)	1(1)	1(1)	6(1)
C(33)	27(1)	43(2)	31(1)	-2(1)	4(1)	-4(1)
C(34)	30(1)	32(1)	29(1)	-1(1)	4(1)	-7(1)
C(35)	37(2)	42(2)	30(1)	-6(1)	6(1)	-3(1)
C(36)	37(2)	39(2)	27(1)	0(1)	2(1)	-5(1)

Table 4.14. Hydrogen coordinates (x 10^4) and isotropic displacement parameters ($Å^2$x 10^3) for **4.8**.

	x	y	z	U(eq)
H(6A)	5815	6034	954	36
H(6B)	5720	6820	671	36
H(6C)	5340	6164	196	36
H(7A)	2941	7638	-158	35
H(7B)	4170	7771	437	35
H(7C)	2535	8044	478	35
H(8A)	100	7663	672	38
H(8B)	-859	6967	735	38
H(8C)	-300	7169	51	38
H(9A)	-376	5472	469	38
H(9B)	-634	5788	1166	38
H(9C)	382	5109	1117	38
H(10A)	3189	4813	597	38
H(10B)	2857	4817	1341	38
H(10C)	4432	5051	1154	38
H(11A)	5539	6871	1825	26
H(11B)	4869	7475	2247	26
H(11C)	4895	7577	1480	26
H(13A)	37	8770	3182	34
H(13B)	-1078	8997	2571	34
H(13C)	620	8890	2487	34
H(14A)	-1921	7182	2603	34
H(14B)	-2602	7945	2711	34
H(14C)	-1536	7586	3279	34
H(16)	1441	5273	2121	22
H(17)	342	4241	2466	25
H(18)	713	3909	3562	26
H(19)	2283	4559	4290	28
H(20)	3453	5562	3938	27
H(22)	4768	7629	3248	21
H(23)	4095	8537	3919	25
H(24)	1926	8448	4416	28

H(25)	485	7438	4269	27
H(26)	1149	6527	3598	22
H(28)	5596	6518	3872	23
H(29)	8001	6133	4138	26
H(30)	9194	5485	3387	26
H(31)	7955	5205	2370	25
H(32)	5564	5591	2099	22
H(33A)	2070	6236	6627	40
H(33B)	2838	6905	6328	40
H(34A)	4691	6189	6142	36
H(34B)	3777	5500	6314	36
H(35A)	3769	6167	5069	43
H(35B)	3677	5333	5214	43
H(36A)	1299	5950	4816	41
H(36B)	1254	5404	5411	41

4.7 Experimental Section References

(1) Daugulis, O.; Brookhart, M.; White, P. S. *Organometallics* **2002**, *21*, 5935-5943.
(2) Brookhart, M.; Grant, B.; Volpe, A. F. *Organometallics* **1992**, *11*, 3920-3922.
(3) Kuan, S. L.; Tay, E. P. L.; Leong, W. K.; Goh, L. Y.; Lin, C. Y.; Gill, P. M. W.; Webster, R. D. *Organometallics* **2006**, *25*, 6134-6141.
(4) GmbH, T.; 6.5 ed. Karlsruhe 2013. http://www.turbomole.com
(5) Schäfer, A.; Horn, H.; Ahlrichs, R. *The Journal of Chemical Physics* **1992**, *97*, 2571-2577.
(6) Dolg, M.; Stoll, H.; Preuss, H. *Theoretica chimica acta* **1993**, *85*, 441-450.
(7) Becke, A. D. *Physical Review A* **1988**, *38*, 3098-3100.
(8) Perdew, J. P. *Physical Review B* **1986**, *33*, 8822-8824.
(9) Lee, C.; Yang, W.; Parr, R. G. *Physical Review B* **1988**, *37*, 785-789.
(10) Weigend, F.; Ahlrichs, R. *PCCP* **2005**, *7*, 3297-3305.
(11) APEX2 Version 2011.4-1, Bruker AXS, Inc.; Madison, WI 2011.
(12) SAINT Version 7.68a, Bruker AXS, Inc.; Madison, WI 2009.
(13) Sheldrick, G. M. SADABS, Version 2008/1, Bruker AXS, Inc.; Madison, WI 2008.
(14) Sheldrick, G. M. SHELXTL, Version 2013/1, Bruker AXS, Inc.; Madison, WI 2013.
(14) Sheldrick, G. M. SHELXL-2013/3
(15) International Tables for X-Ray Crystallography 1992, Vol. C., Dordrecht: Kluwer Academic Publishers.

APPENDIX

NMR Data and Coordinates for Optimized Structures

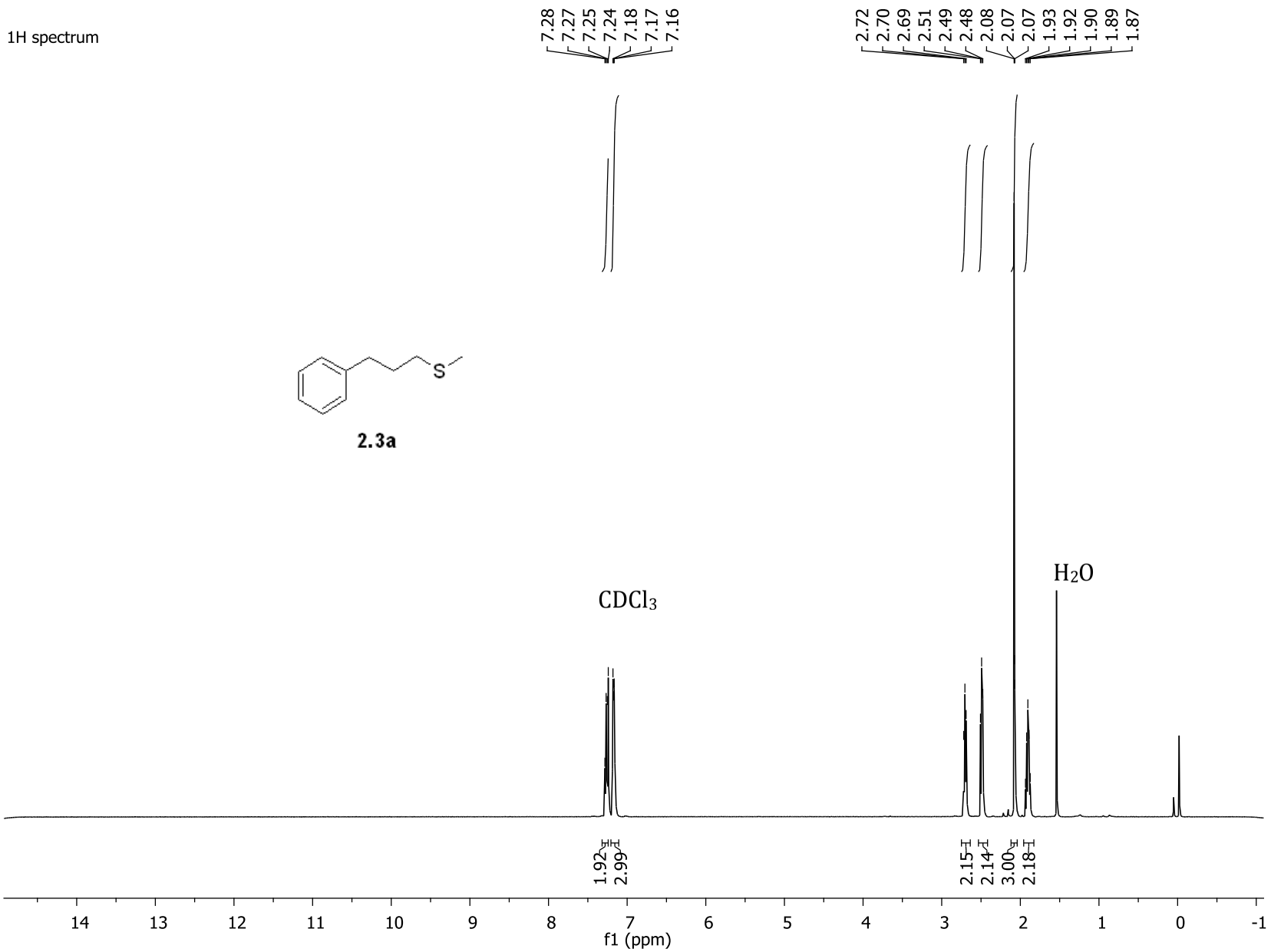
1H spectrum
7.28
7.27
7.25
7.24
7.18
7.17
7.16
2.72
2.70
2.69
2.51
2.49
2.48
2.08
2.07
2.07
1.93
1.92
1.90
1.89
1.87
S
2.3a
CDCl3
H2O
1.92
2.99
2.15
2.14
3.00
2.18
14
13
12
11
10
9
8
7
6
5
4
3
2
1
0
-1
f1 (ppm)

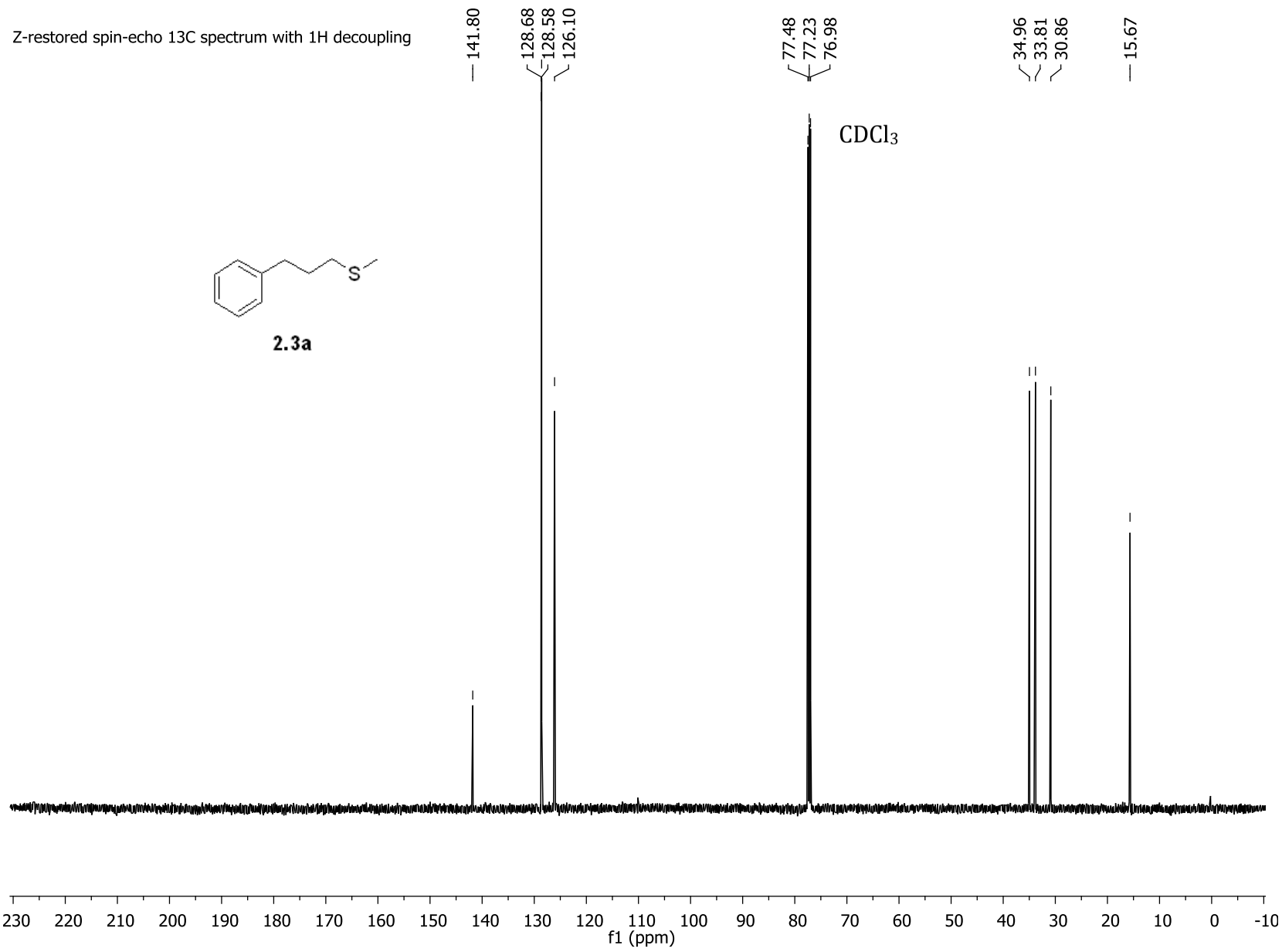
Z-restored spin-echo 13C spectrum with 1H decoupling
141.80
128.68
128.58
126.10
77.48
77.23
76.98
34.96
33.81
30.86
15.67
CDCl3
S
2.3a
230 220 210 200 190 180 170 160 150 140 130 120 110 100 90 80 70 60 50 40 30 20 10 0 -10
f1 (ppm)

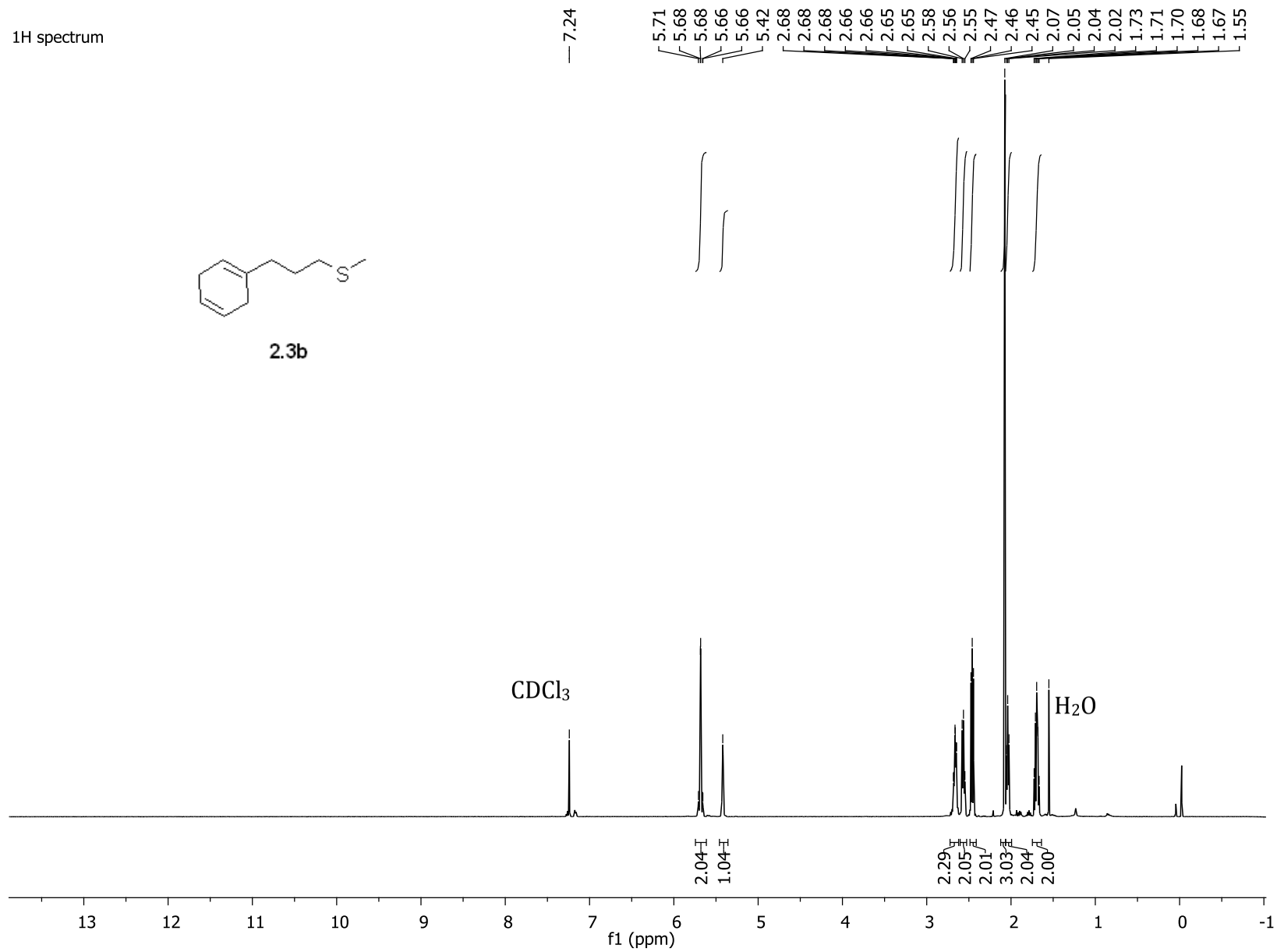
1H spectrum
7.24
5.71
5.68
5.68
5.66
5.66
5.42
2.68
2.68
2.68
2.66
2.66
2.65
2.65
2.58
2.56
2.55
2.47
2.46
2.45
2.07
2.05
2.04
2.02
1.73
1.71
1.70
1.68
1.67
1.55
S
2.3b
CDCl3
H2O
2.04
1.04
2.29
2.05
2.01
3.03
2.04
2.00
13
12
11
10
9
8
7
6
5
4
3
2
1
0
-1
f1 (ppm)

Z-restored spin-echo 13C spectrum with 1H decoupling

134.25
124.49
124.48
124.44
124.43
119.13
77.48
77.23
76.98
36.62
34.02
29.09
26.95
26.93
15.71

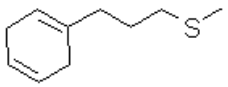

2.3b

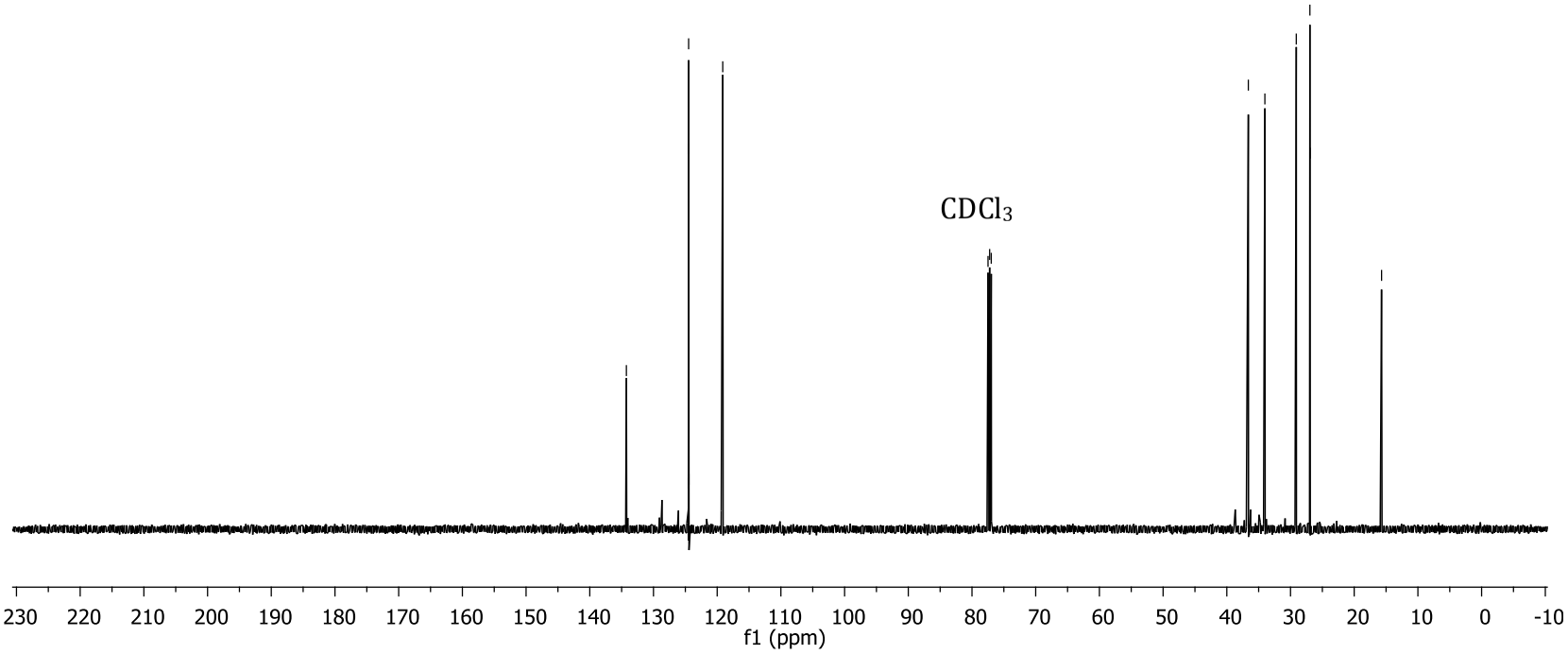

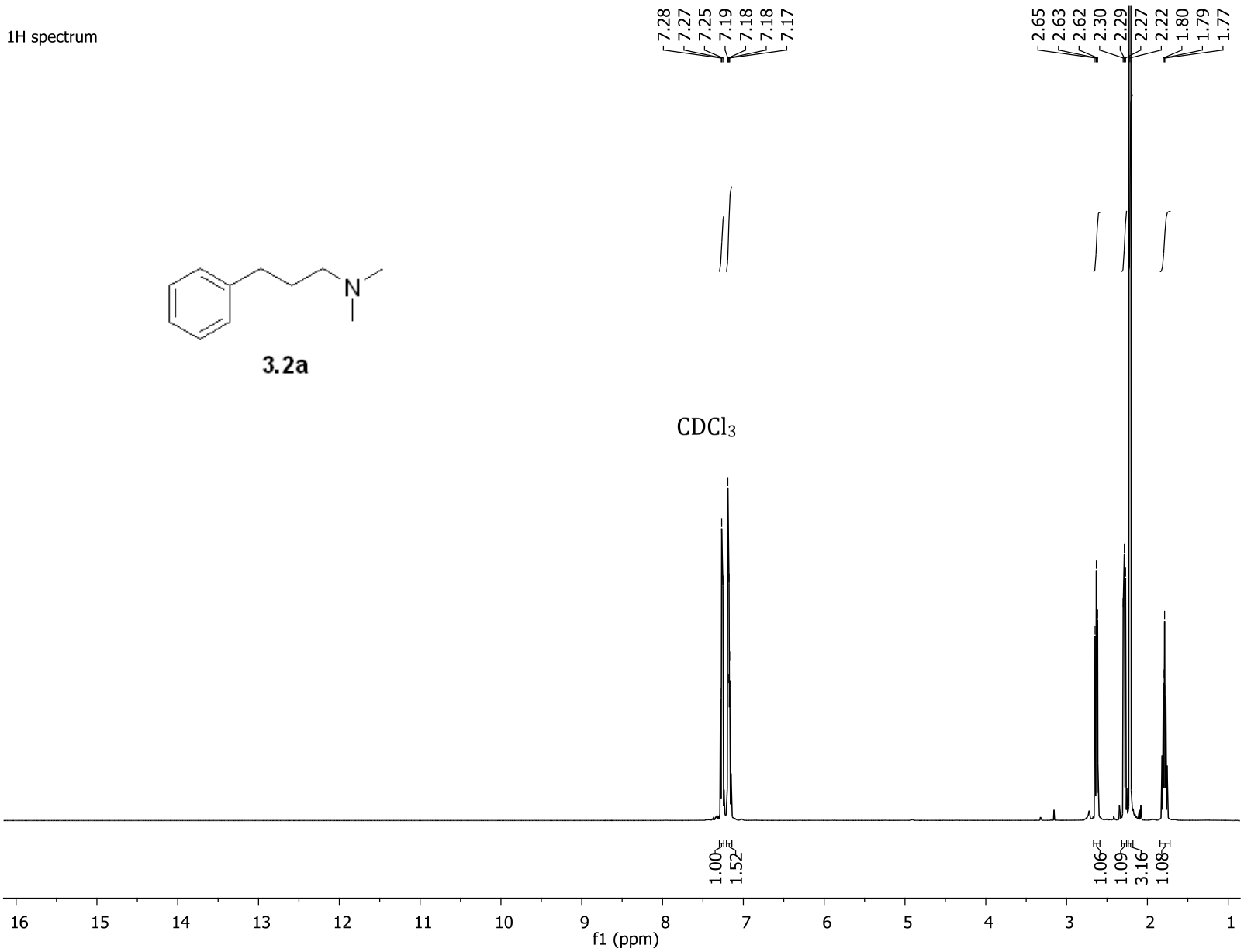
1H spectrum
7.28
7.27
7.25
7.19
7.18
7.18
7.17
2.65
2.63
2.62
2.30
2.29
2.27
2.22
1.80
1.79
1.77
N
3.2a
CDCl3
1.00
1.52
1.06
1.09
3.16
1.08
16
15
14
13
12
11
10
9
8
7
6
5
4
3
2
1
f1 (ppm)

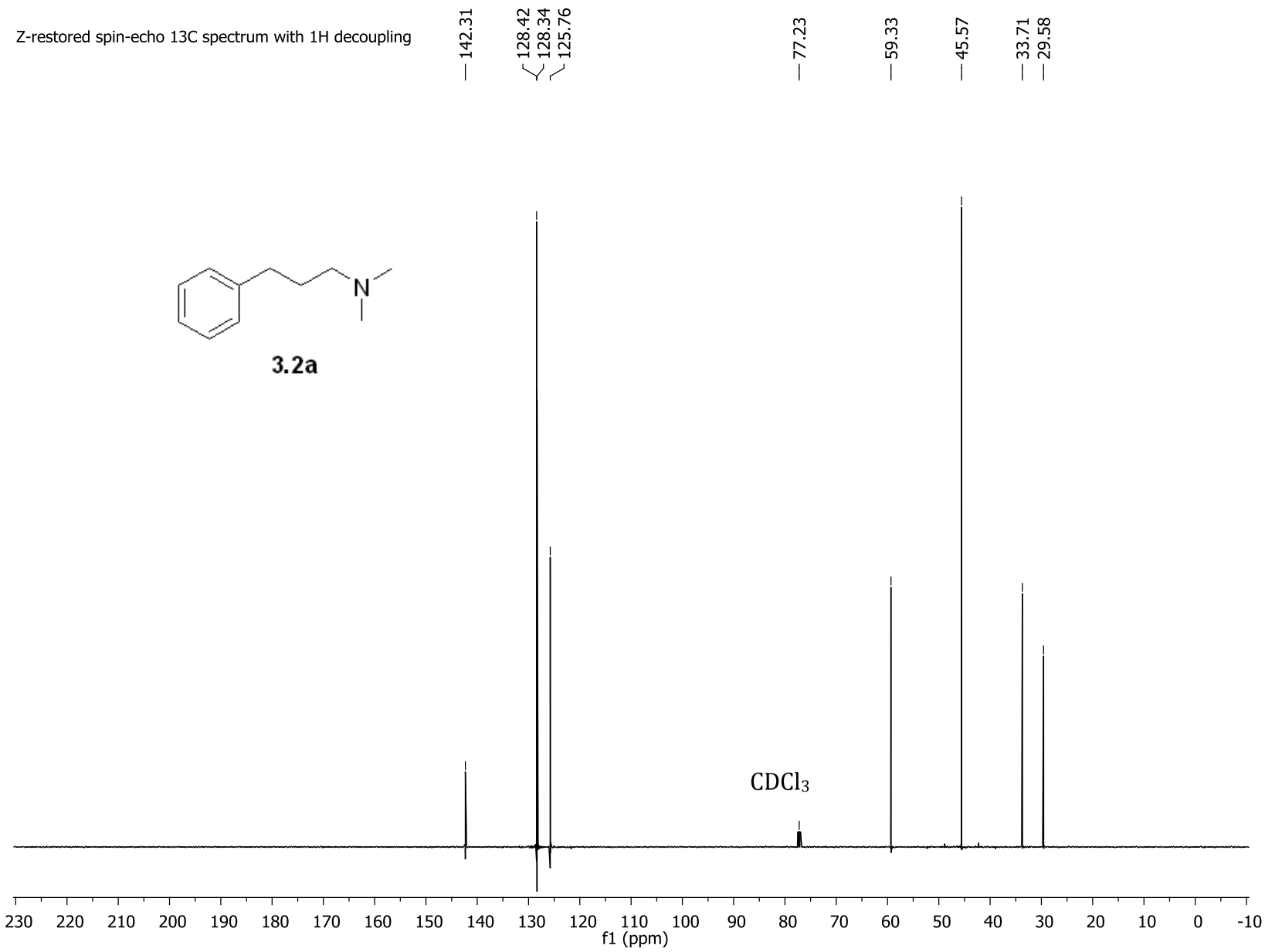
Z-restored spin-echo 13C spectrum with 1H decoupling
142.31
128.42
128.34
125.76
77.23
59.33
45.57
33.71
29.58
N
3.2a
CDCl3
230 220 210 200 190 180 170 160 150 140 130 120 110 100 90 80 70 60 50 40 30 20 10 0 -10
f1 (ppm)

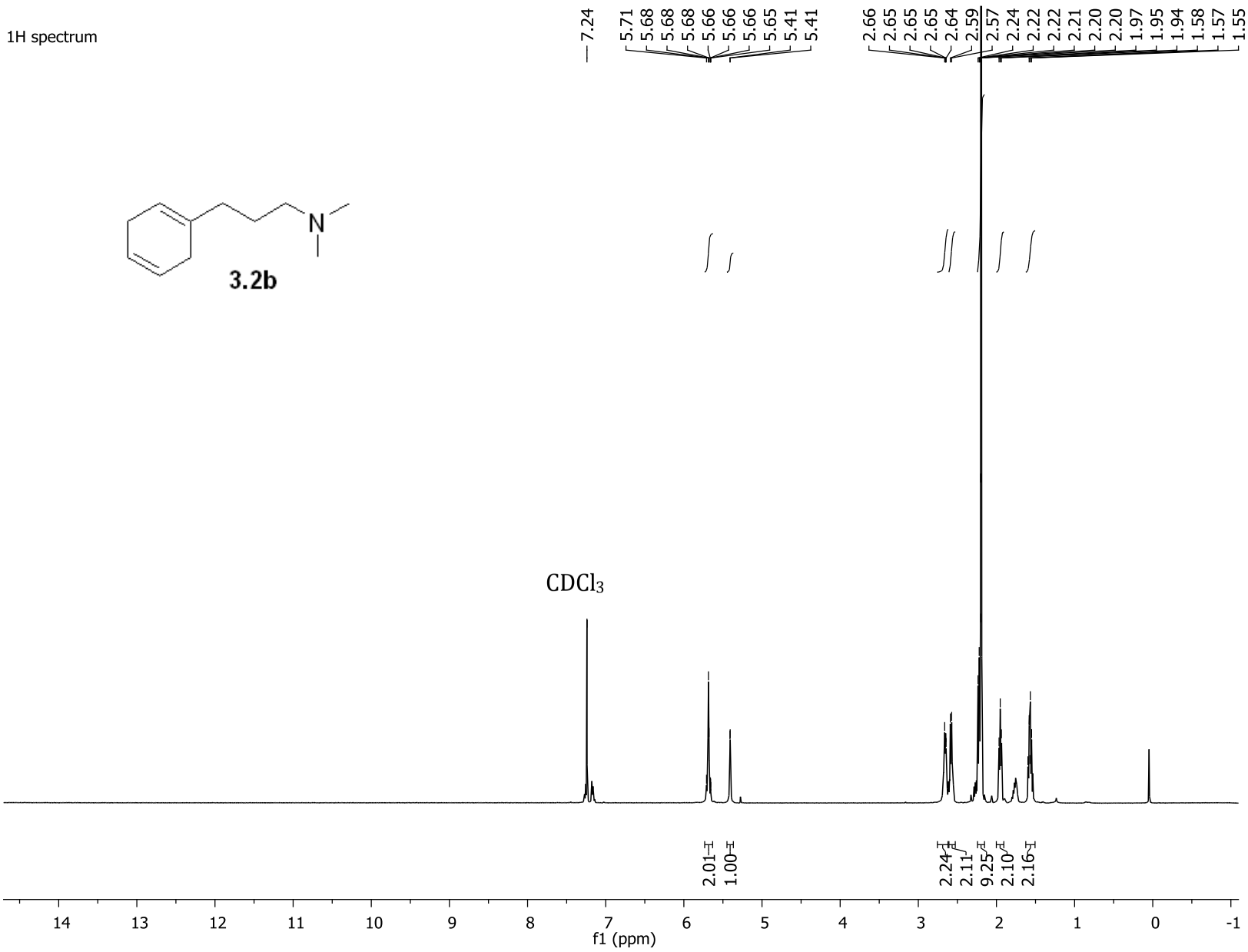
1H spectrum
7.24
5.71
5.68
5.68
5.68
5.66
5.66
5.66
5.65
5.41
5.41
2.66
2.65
2.65
2.65
2.64
2.59
2.57
2.24
2.22
2.22
2.21
2.20
2.20
1.97
1.95
1.94
1.58
1.57
1.55
N
3.2b
CDCl3
2.01
1.00
2.24
2.11
9.25
2.10
2.16
14
13
12
11
10
9
8
7
6
5
4
3
2
1
0
-1
f1 (ppm)

Z-restored spin-echo 13C spectrum with 1H decoupling

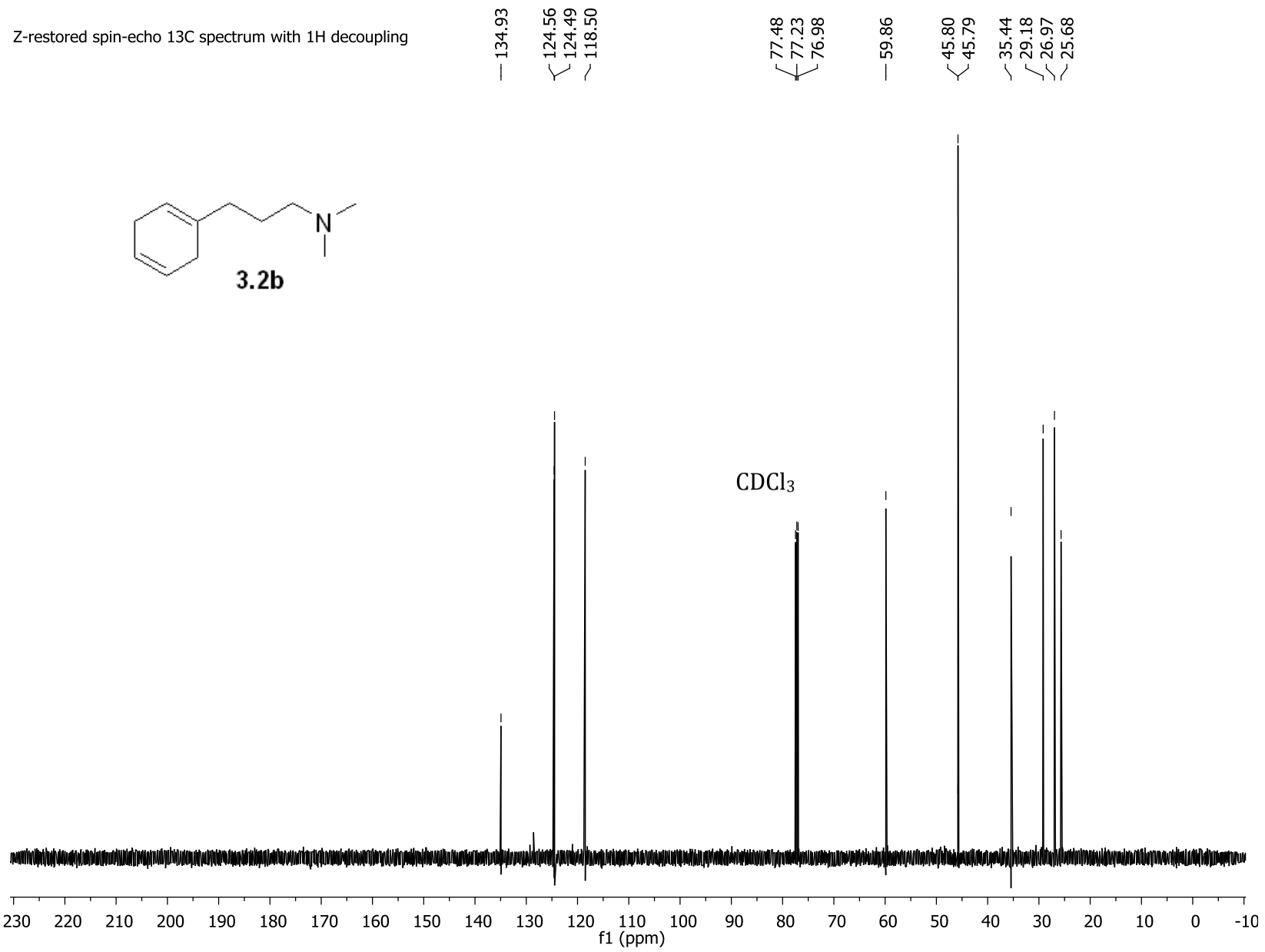

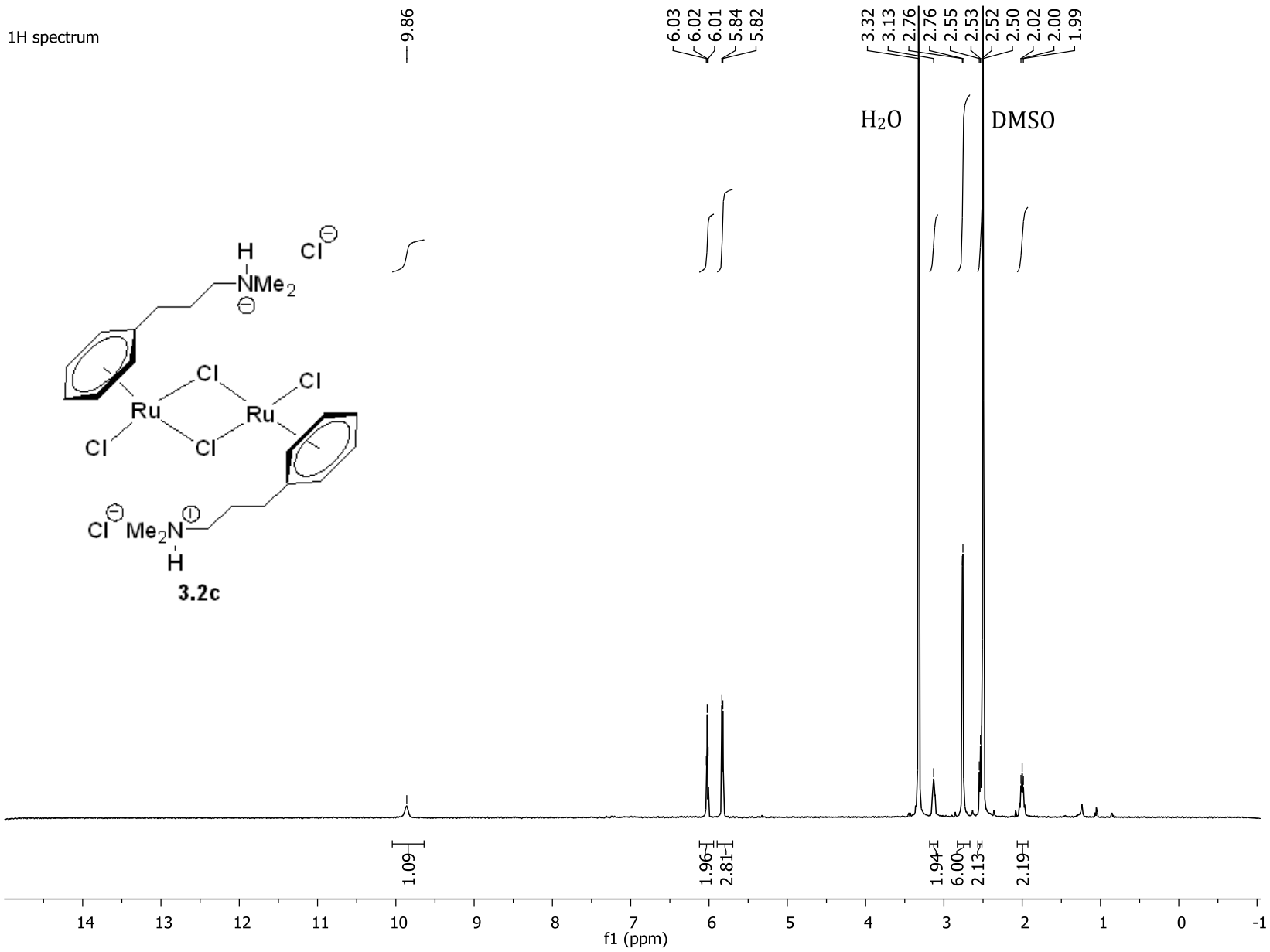
1H spectrum
9.86
6.03
6.02
6.01
5.84
5.82
3.32
3.13
2.76
2.76
2.55
2.53
2.52
2.50
2.02
2.00
1.99
H2O
DMSO
H
Cl
NMe2
Cl
Cl
Ru
Ru
Cl
Cl
Cl
Me2N
H
3.2c
1.09
1.96
2.81
1.94
6.00
2.13
2.19
14
13
12
11
10
9
8
7
6
5
4
3
2
1
0
-1
f1 (ppm)

Z-restored spin-echo 13C spectrum with 1H decoupling

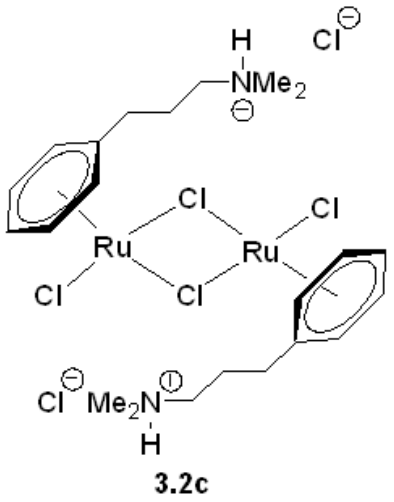

3.2c

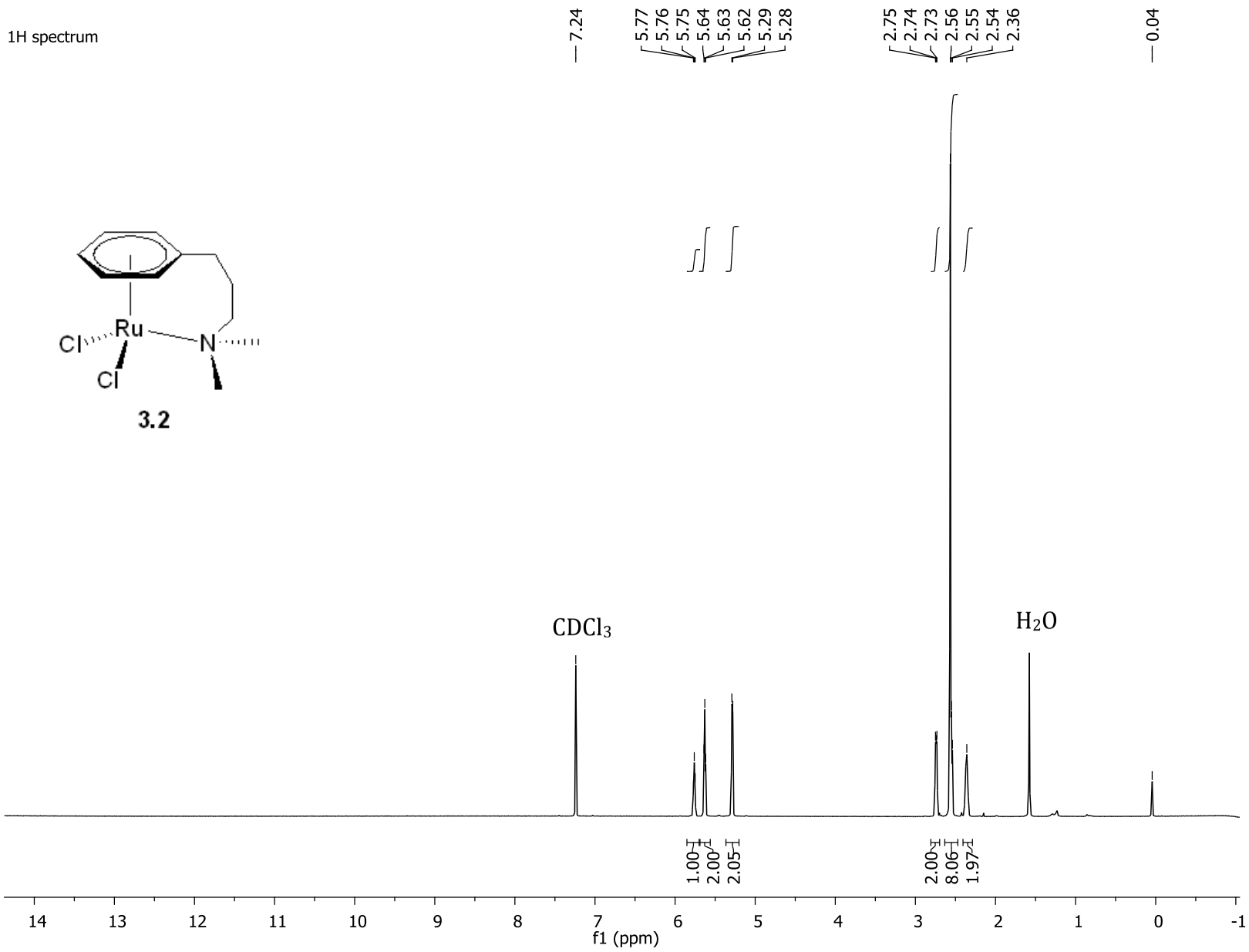
1H spectrum
7.24
5.77
5.76
5.75
5.64
5.63
5.62
5.29
5.28
2.75
2.74
2.73
2.56
2.55
2.54
2.36
0.04
Cl
Ru
N
Cl
3.2
CDCl3
H2O
1.00
2.00
2.05
2.00
8.06
1.97
14
13
12
11
10
9
8
7
6
5
4
3
2
1
0
-1
f1 (ppm)

Z-restored spin-echo 13C spectrum with 1H decoupling

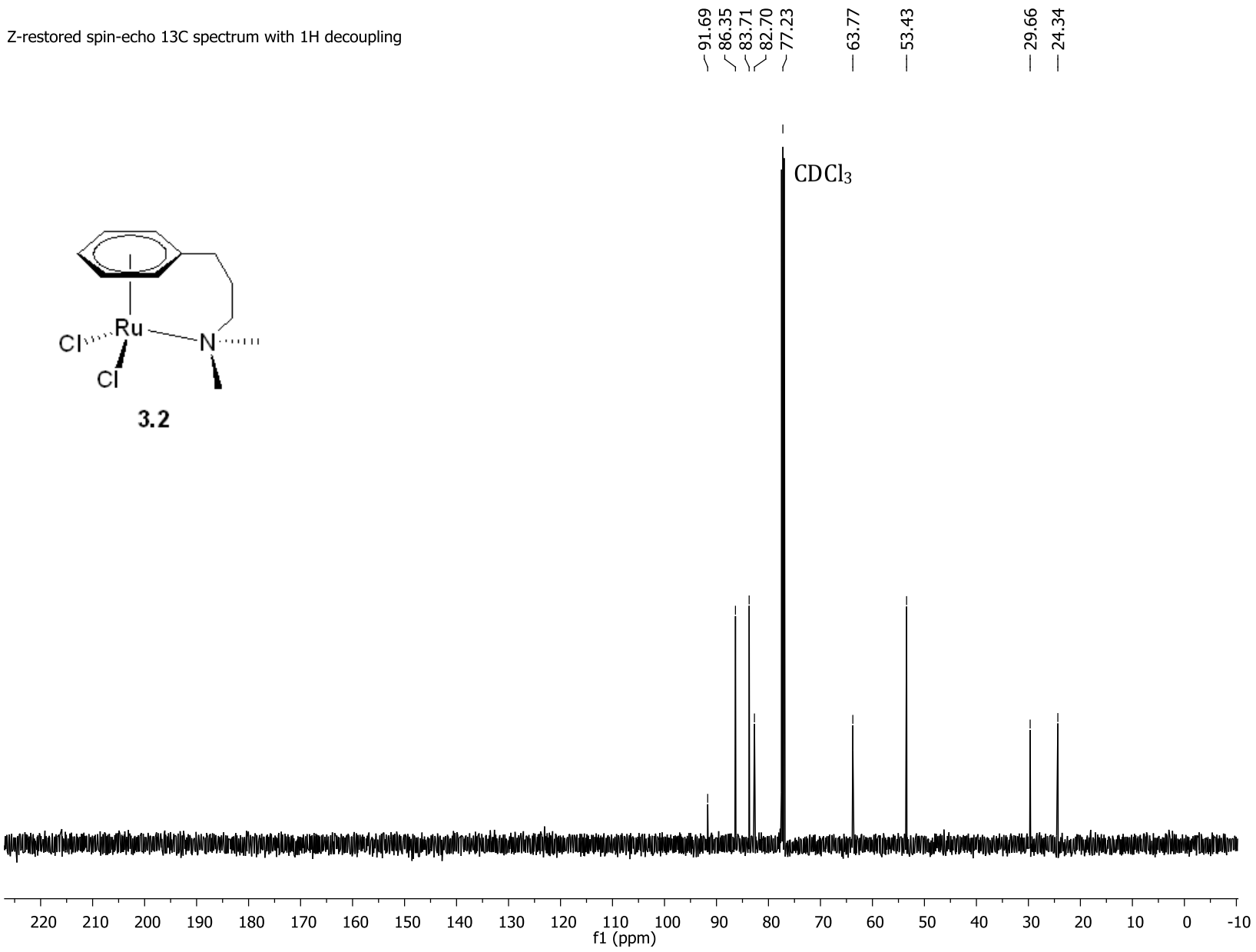

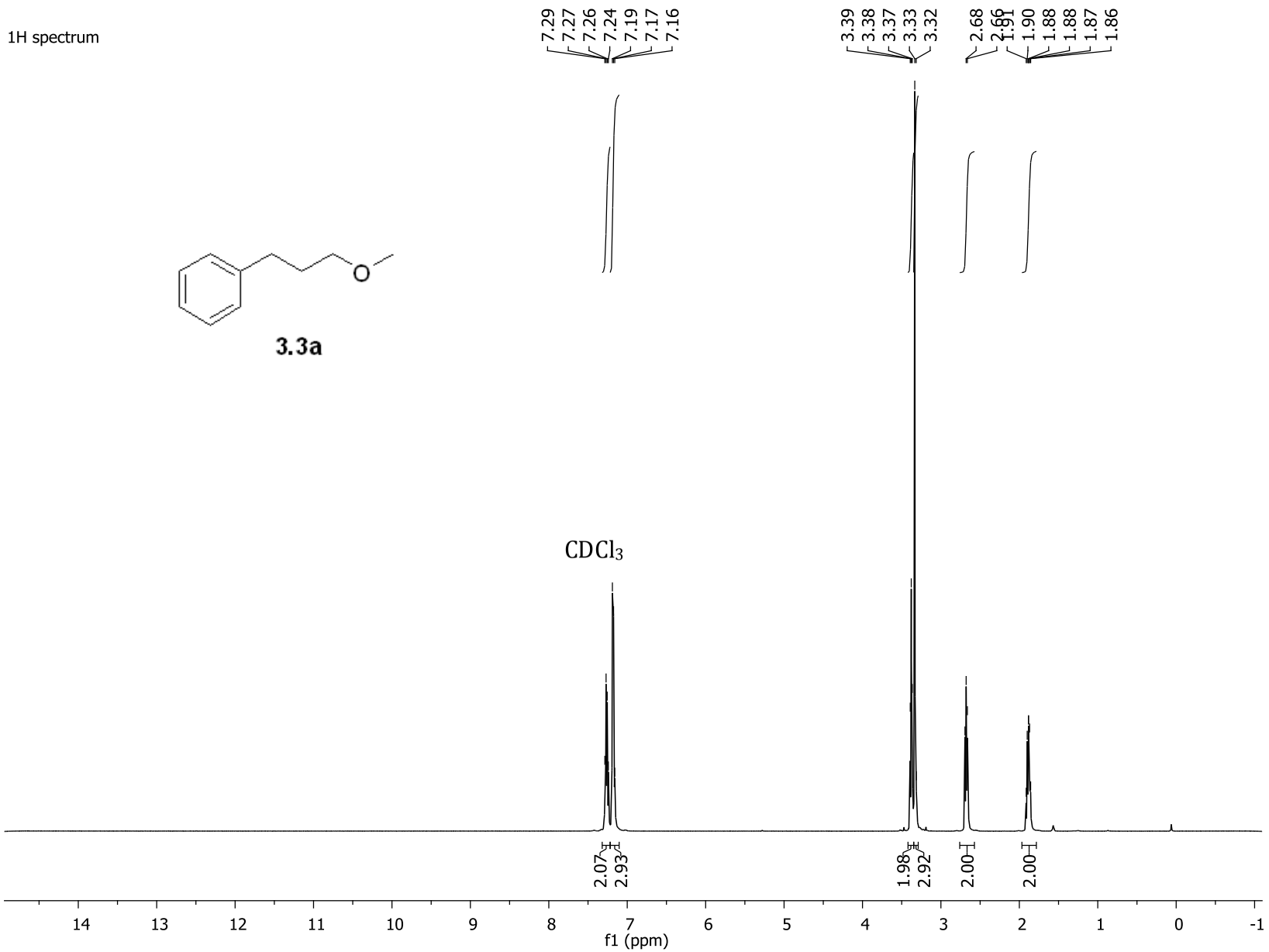
1H spectrum
7.29
7.27
7.26
7.24
7.19
7.17
7.16
3.39
3.38
3.37
3.33
3.32
2.68
2.66
1.91
1.90
1.88
1.88
1.87
1.86
O
3.3a
CDCl3
2.07
2.93
1.98
2.92
2.00
2.00
14
13
12
11
10
9
8
7
6
5
4
3
2
1
0
-1
f1 (ppm)

13C spectrum with 1H decoupling

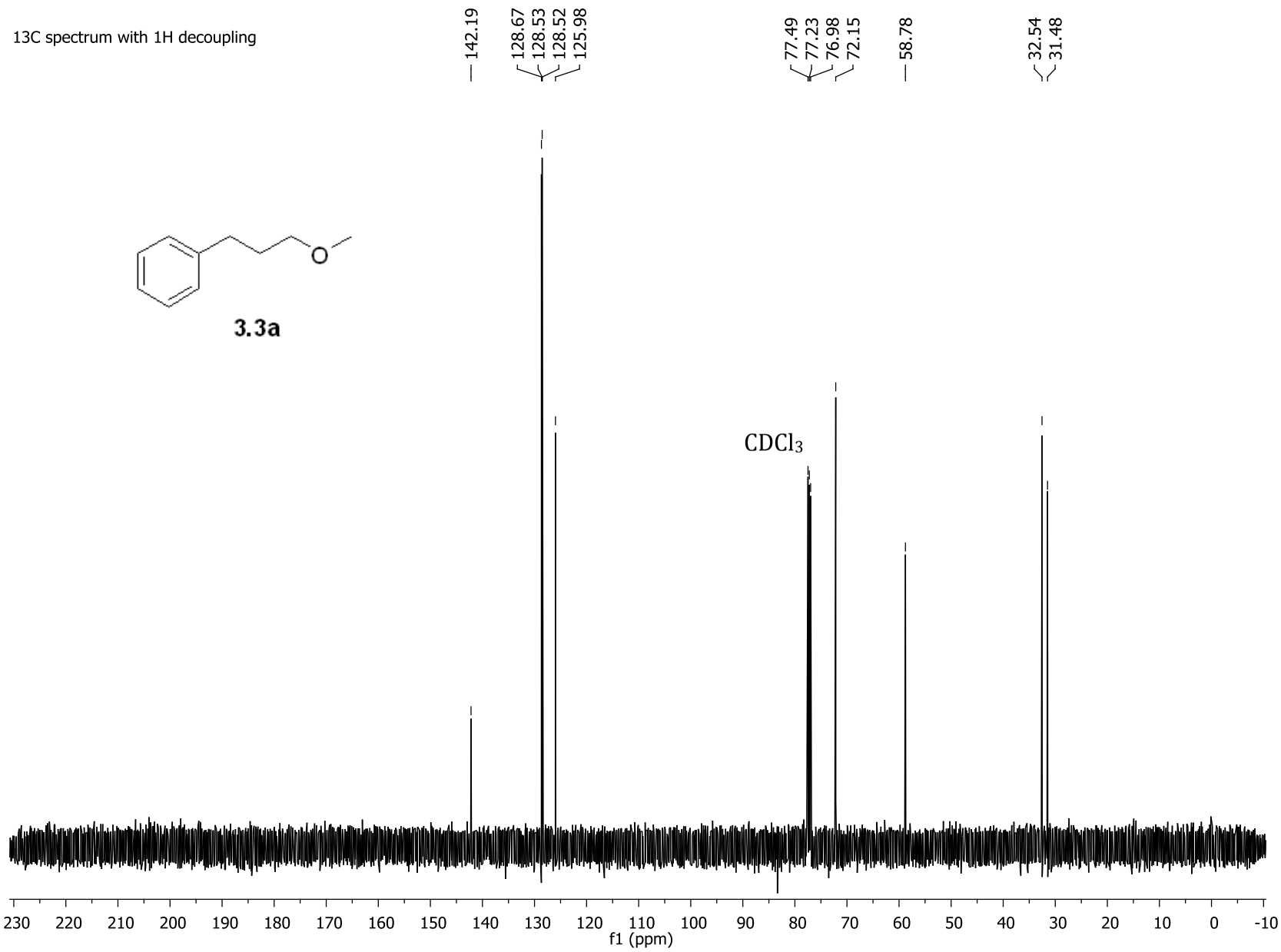

1H spectrum

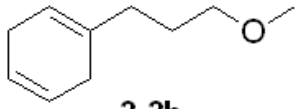

3.3b

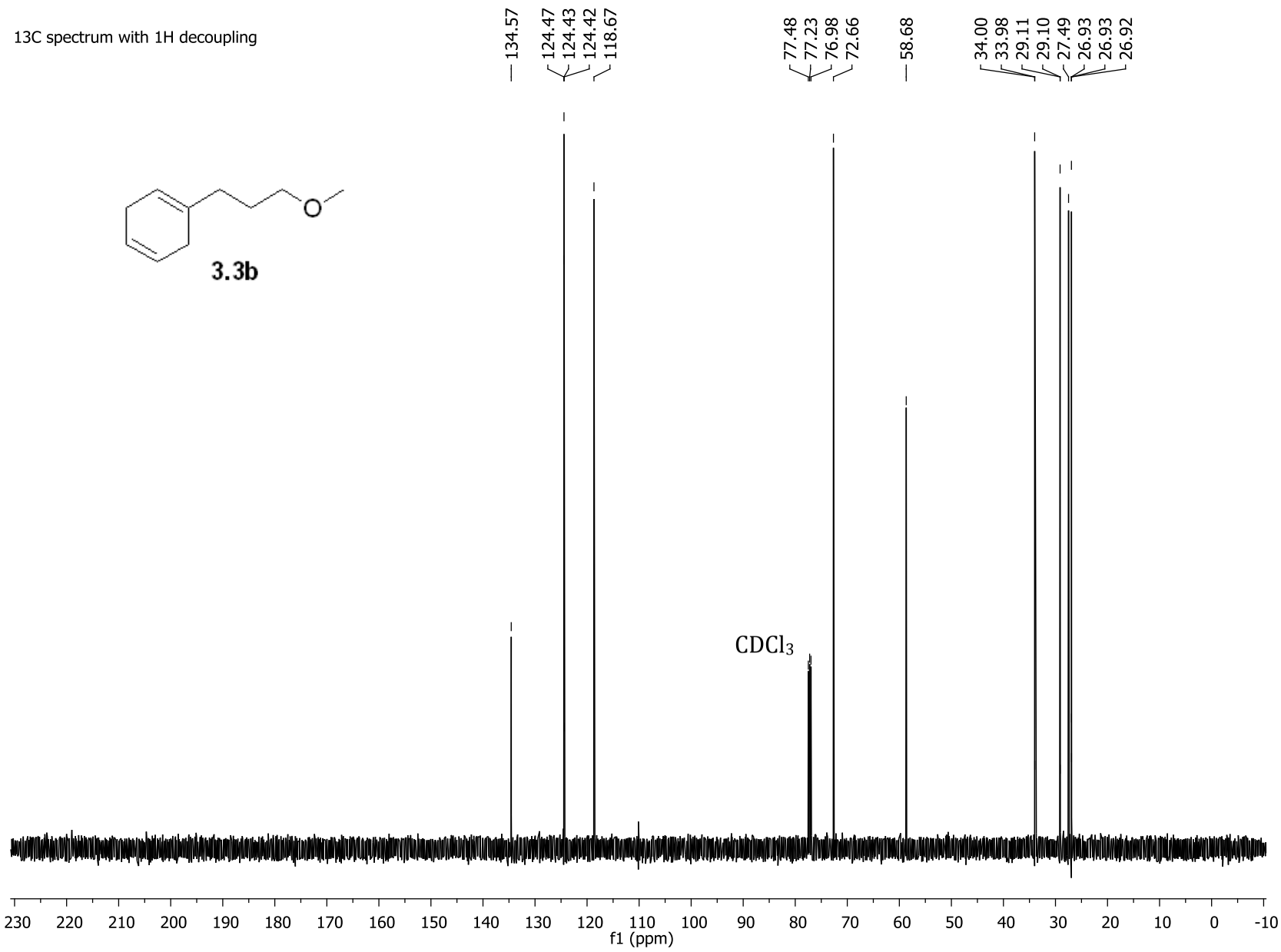
13C spectrum with 1H decoupling
134.57
124.47
124.43
124.42
118.67
77.48
77.23
76.98
72.66
58.68
34.00
33.98
29.11
29.10
27.49
26.93
26.92
3.3b
CDCl3
230 220 210 200 190 180 170 160 150 140 130 120 110 100 90 80 70 60 50 40 30 20 10 0 -10
f1 (ppm)

1H spectrum

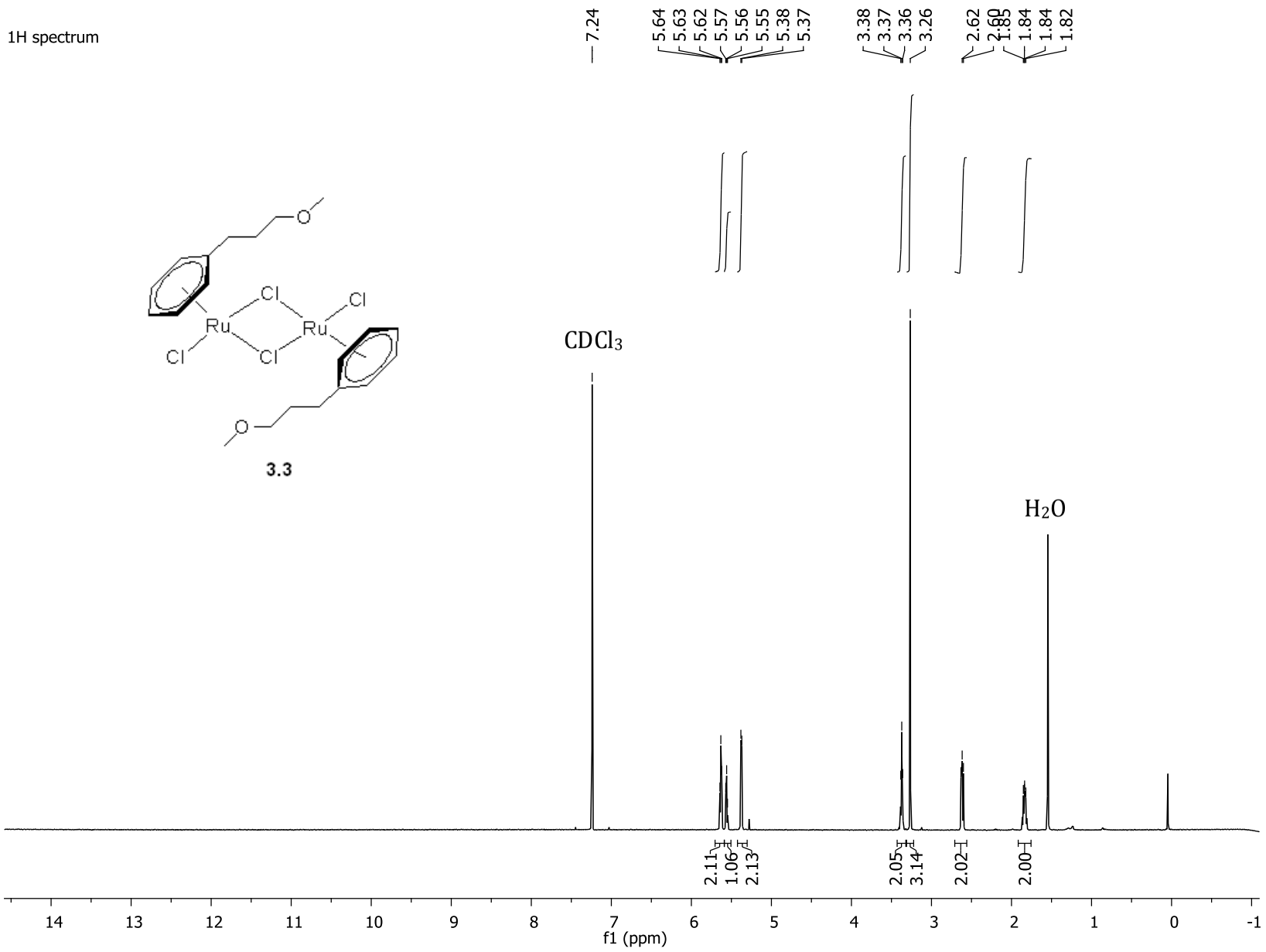

3.3

Z-restored spin-echo 13C spectrum with 1H decoupling

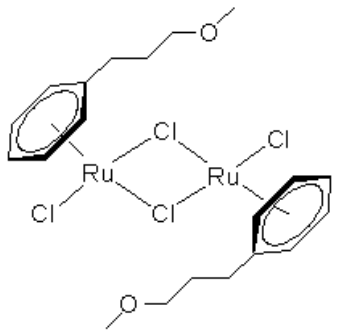

3.3

1H spectrum

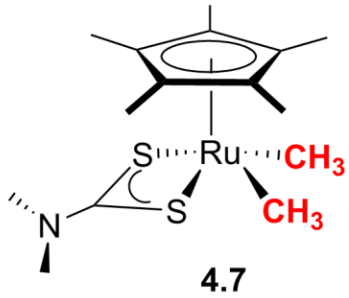

4.7

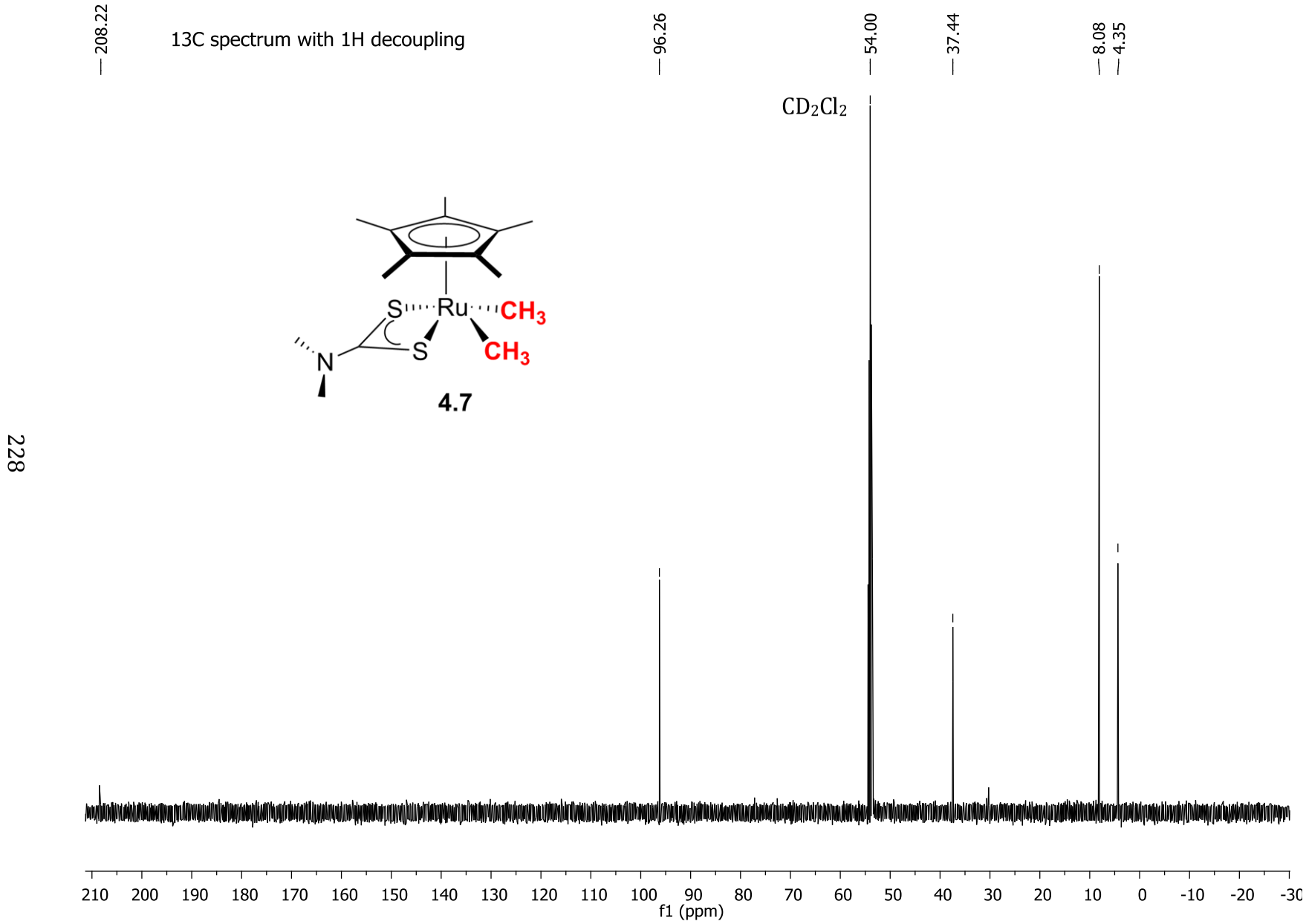
208.22
96.26
54.00
37.44
8.08
4.35
13C spectrum with 1H decoupling
CD2Cl2
S
Ru
CH3
CH3
S
N
4.7
210 200 190 180 170 160 150 140 130 120 110 100 90 80 70 60 50 40 30 20 10 0 -10 -20 -30
f1 (ppm)

1H spectrum

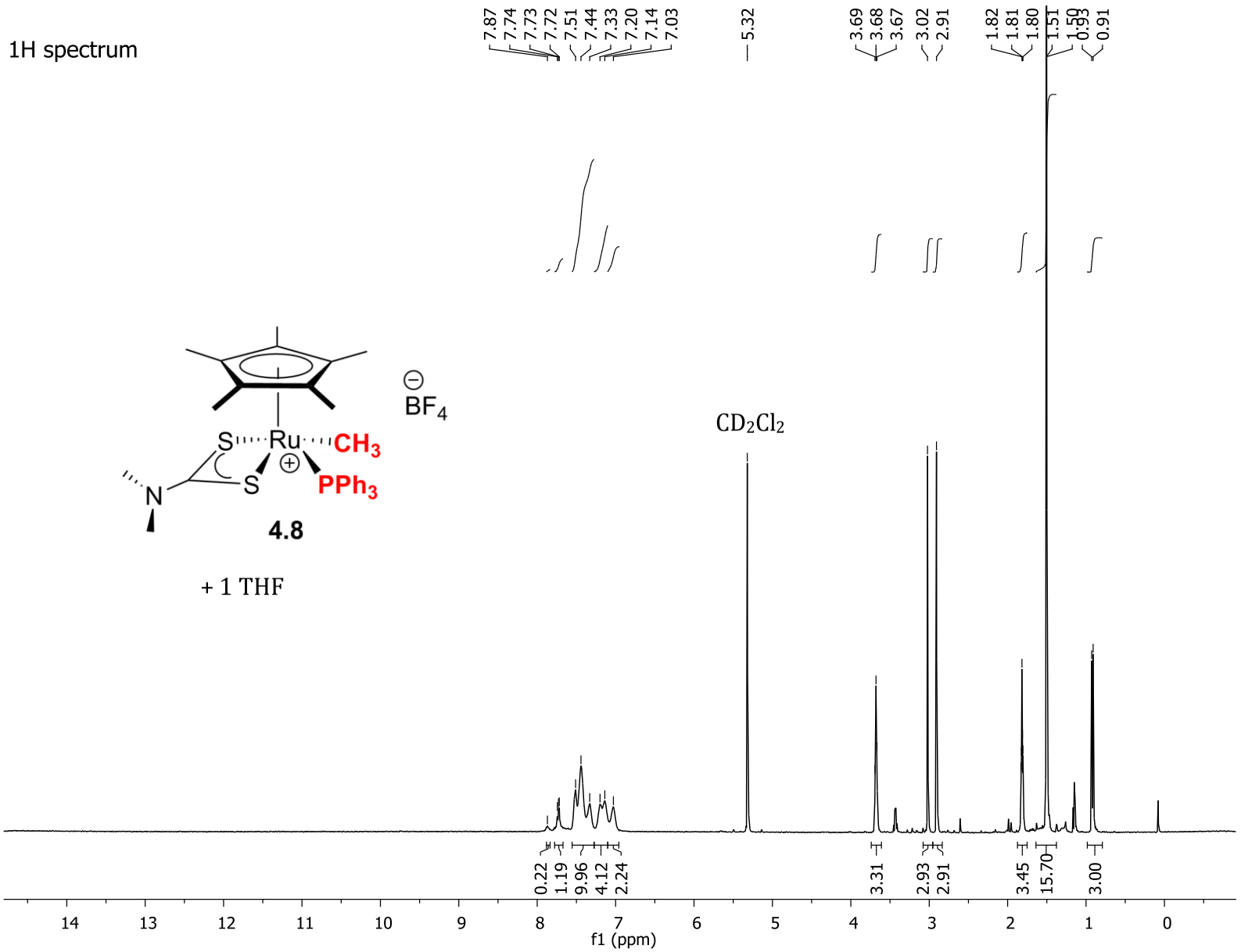
7.87
7.74
7.73
7.72
7.51
7.44
7.33
7.20
7.14
7.03
5.32
3.69
3.68
3.67
3.02
2.91
1.82
1.81
1.80
1.51
1.50
0.93
0.91
BF4
S
Ru
CH3
S
PPh3
N
4.8
+ 1 THF
CD2Cl2
0.22
1.19
9.96
4.12
2.24
3.31
2.93
2.91
3.45
15.70
3.00
14
13
12
11
10
9
8
7
6
5
4
3
2
1
0
f1 (ppm)

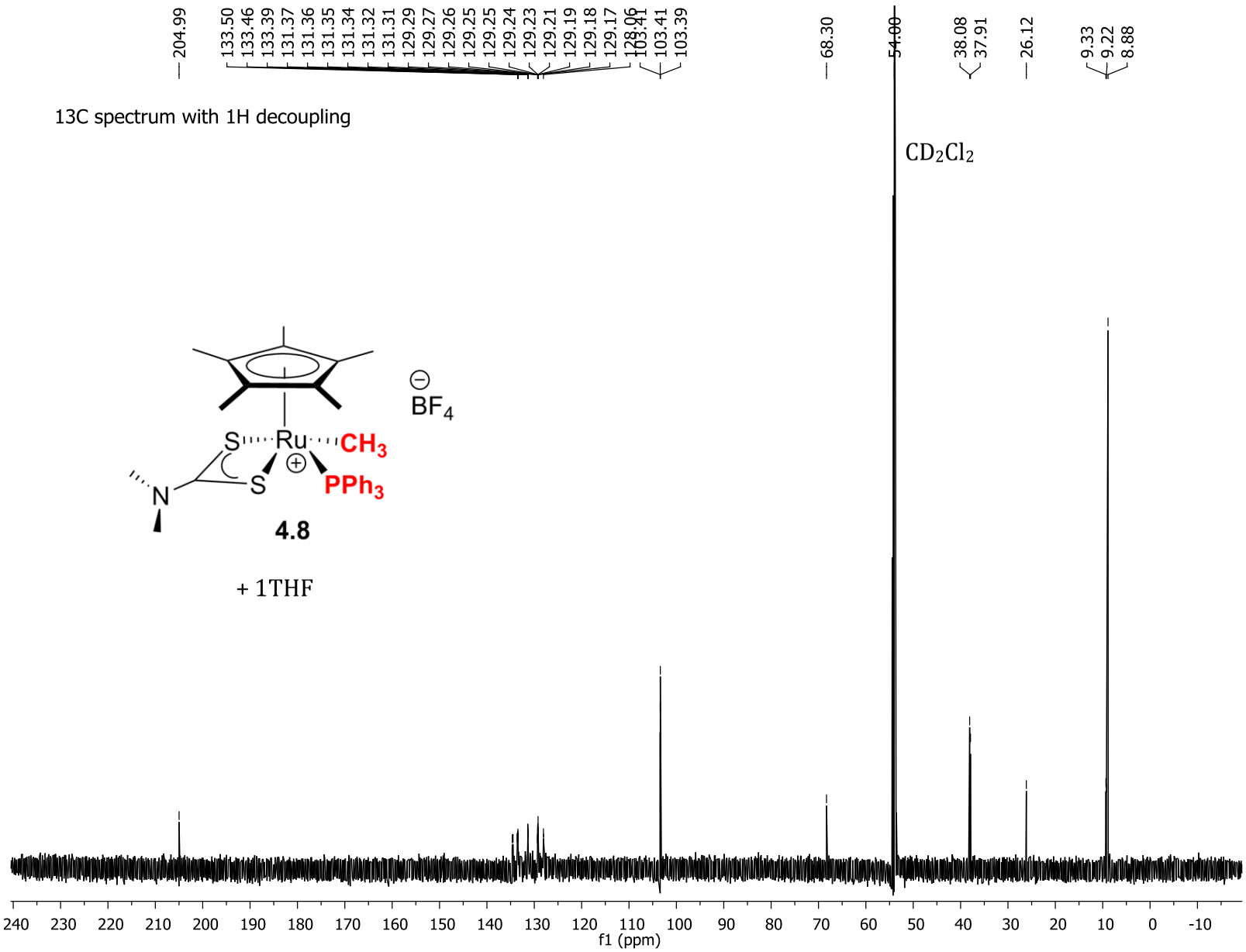
204.99
133.50
133.46
133.39
131.37
131.36
131.35
131.34
131.32
131.31
129.29
129.27
129.26
129.25
129.25
129.24
129.23
129.21
129.19
129.18
129.17
128.06
103.41
103.41
103.39
68.30
54.00
38.08
37.91
26.12
9.33
9.22
8.88
13C spectrum with 1H decoupling
CD2Cl2
BF4
S
Ru
CH3
PPh3
N
S
4.8
+ 1THF
240 230 220 210 200 190 180 170 160 150 140 130 120 110 100 90 80 70 60 50 40 30 20 10 0 -10
f1 (ppm)

31P spectrum with 1H decoupling

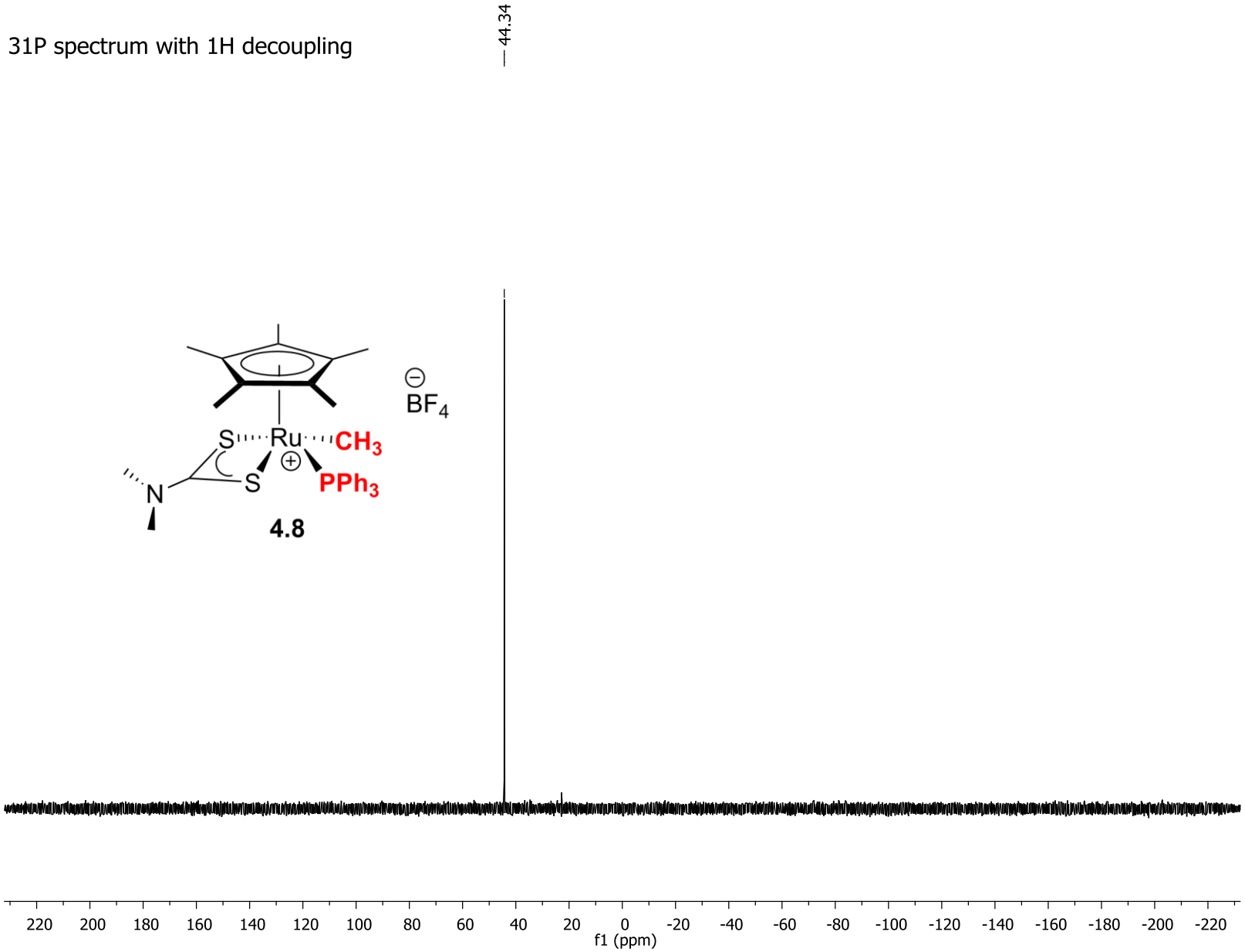

19F spectrum with 1H spectrum

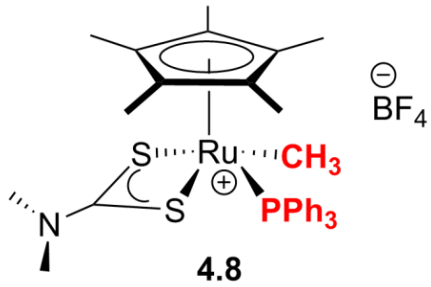

4.8

11B spectrum with 1H decoupling

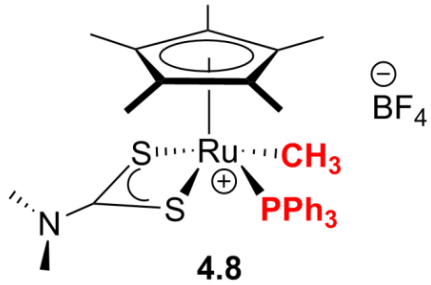

4.8

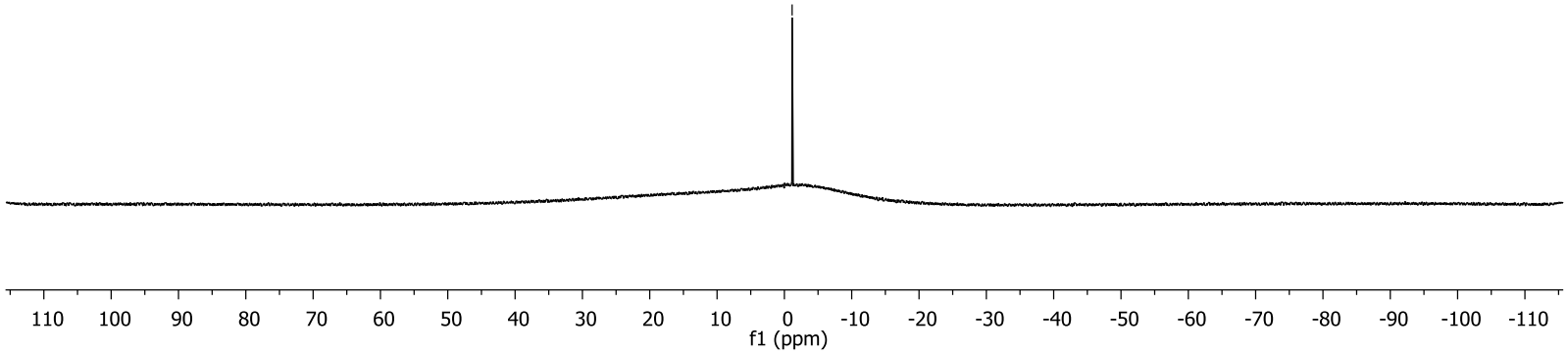

Optimized Structure Coordinates for **S1** *cis* isomer

Atom	X	Y	Z
Ru	0.044814	0.321906	0.369076
S	-0.227925	0.495693	-2.027825
C	-1.460234	-0.538706	1.604462
C	-0.461321	-0.032248	2.501367
C	0.892564	-0.414308	2.294023
C	1.241827	-1.439061	1.336399
C	0.244693	-2.011855	0.525511
C	-1.106792	-1.495663	0.570166
C	-2.166914	-1.989996	-0.392336
C	-1.825172	-1.923017	-1.894775
C	-1.707278	-0.51343	-2.484278
C	1.119355	-0.454017	-2.827662
H	-2.499954	-0.181042	1.676612
H	-0.720443	0.726459	3.25566
H	1.690777	0.0740962	0.876745
H	2.294432	-1.742948	1.221274
H	0.520194	-2.772187	-0.222228
H	-3.111703	-1.433615	-0.20713
H	-2.38111	-3.053239	-0.130792
H	-0.915913	-2.521403	-2.127808
H	-2.649841	-2.426618	-2.448373
H	-2.565403	0.128663	-2.187715
H	-1.689626	-0.546586	-3.595554
H	0.947437	-0.445755	-3.925325
H	1.182437	-1.493047	-2.446678
H	2.063513	-0.08448	2.605113
C	-0.517741	2.269496	0.355306
H	-0.939475	2.721895	-0.56818
H	0.597881	2.524632	0.37529
H	-1.008203	2.685172	1.260818

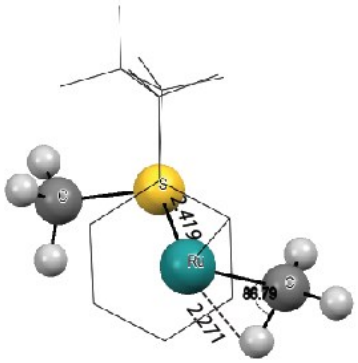

Optimized Structure Coordinates for **S2** *cis* isomer

Atom	X	Y	Z
Ru	0.347000	0.389000	0.410000
S	0.101000	0.495000	-1.965000
C	-1.343000	-0.488000	1.674000
C	-0.286000	-0.037000	2.521000
C	1.034000	-0.569000	2.344000
C	1.287000	-1.578000	1.367000
C	0.260000	-1.915000	0.458000
C	-1.084000	-1.374000	0.589000
C	-2.177000	-1.777000	-0.378000
C	-1.823000	-1.698000	-1.879000
C	-1.505000	-0.302000	-2.427000
C	1.280000	-0.643000	-2.782000
C	2.284000	1.322000	-0.122000
H	-2.355000	-0.071000	1.803000
H	-0.485000	0.703000	3.311000
H	1.852000	-0.223000	2.997000
H	2.289000	-2.025000	1.270000
H	0.473000	-2.643000	-0.341000
H	-3.081000	-1.160000	-0.180000
H	-2.468000	-2.829000	-0.149000
H	-1.008000	-2.411000	-2.136000
H	-2.708000	-2.066000	-2.446000
H	-2.272000	0.442000	-2.122000
H	-1.488000	-0.313000	-3.539000
H	1.095000	-0.601000	-3.876000
H	1.192000	-1.683000	-2.412000
H	2.298000	-0.259000	-2.569000
C	-0.968000	2.073000	0.175000
C	1.698000	2.079000	0.917000
H	-1.964000	1.722000	-0.174000
H	-0.576000	2.812000	-0.555000
H	-1.097000	2.575000	1.157000
H	2.055000	1.968000	1.956000
H	1.244000	3.058000	0.696000
H	3.109000	0.617000	0.088000
H	2.284000	1.744000	-1.144000

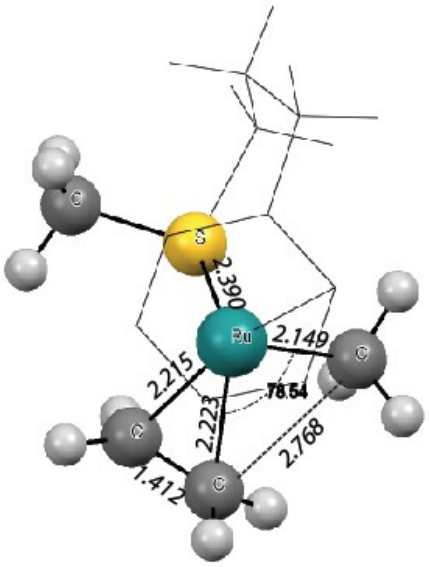

Optimized Structure Coordinates for **S2p** *cis* isomer

Atom	X	Y	Z
Ru	0.398129	0.243154	0.426771
S	0.117521	0.407666	-1.948476
C	-1.395541	-0.471118	1.537323
C	-0.414755	-0.102692	2.519479
C	0.856620	-0.719644	2.467148
C	1.138579	-1.768128	1.511545
C	0.172233	-2.120709	0.558628
C	-1.115170	-1.451520	0.537522
C	-2.183041	-1.851558	-0.457785
C	-1.803915	-1.768356	-1.949284
C	-1.485178	-0.359065	-2.452527
C	1.291209	-0.730636	-2.778294
C	2.067096	1.708396	-0.212830
H	-2.380426	0.020664	1.543605
H	-0.640397	0.661290	3.278206
H	1.633407	-0.424870	3.189013
H	2.122530	-2.262240	1.513488
H	0.392626	-2.911236	-0.176160
H	-3.091141	-1.235462	-0.279738
H	-2.474311	-2.903314	-0.229077
H	-0.974212	-2.469284	-2.194390
H	-2.674989	-2.135886	-2.537409
H	-2.250446	0.378181	-2.123266
H	-1.459363	-0.328561	-3.563850
H	1.106825	-0.686100	-3.873027
H	1.198181	-1.770515	-2.406600
H	2.313884	-0.356082	-2.569872
C	-0.588103	2.156972	0.402412
C	2.574316	0.873996	0.778581
H	-1.677757	2.017990	0.567093
H	-0.451288	2.700010	-0.557308
H	-0.180917	2.783039	1.225932
H	3.222094	0.017817	0.520876
H	2.656102	1.248985	1.812541
H	2.333983	1.541263	-1.271122
H	1.756011	2.736657	0.027107

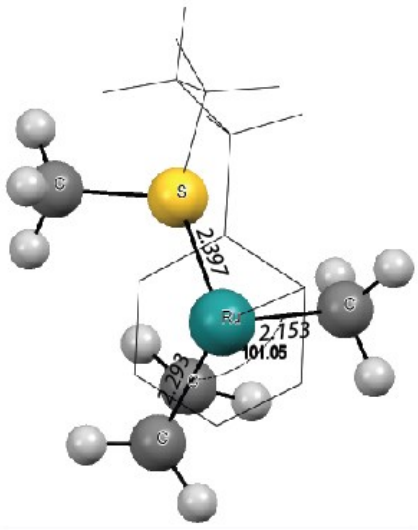

Optimized Structure Coordinates for **$TS_{S2\text{-}S3\gamma}$** *cis* isomer

Atom	X	Y	Z
Ru	0.30851	0.254723	0.539467
S	0.457678	0.419318	-1.838506
C	-1.629479	-0.728141	1.371915
C	-0.852305	-0.137841	2.421927
C	0.501869	-0.538319	2.629335
C	1.0883	-1.507151	1.750203
C	0.347419	-2.008976	0.650151
C	-1.035894	-1.620097	0.441633
C	-1.825833	-2.156261	-0.731386
C	-1.200638	-1.952687	-2.129412
C	-0.975717	-0.499163	-2.563256
C	1.84636	-0.581677	-2.488813
C	2.238325	1.197923	0.586518
H	-2.673168	-0.406607	1.223512
H	-1.309851	0.613623	3.084795
H	1.091227	-0.09915	3.449682
H	2.13608	-1.817598	1.889435
H	0.828502	-2.717964	-0.041289
H	-2.841402	-1.704197	-0.716952
H	-1.972377	-3.250772	-0.577566
H	-0.260423	-2.538289	-2.23541
H	-1.90138	-2.40214	-2.868747
H	-1.853717	0.14279	-2.331291
H	-0.808823	-0.440449	-3.661015
H	1.810159	-0.542791	-3.598197
H	1.811478	-1.630068	-2.131281
H	2.783193	-0.103698	-2.140673
C	-0.711913	2.193472	0.2984
C	1.250061	2.221946	0.810527
H	1.139155	2.576847	1.850518
H	1.2526	3.044882	0.079283
H	2.822525	0.797612	1.435386
H	2.799097	1.207928	-0.365992
H	-0.560652	2.701932	-0.674287
H	-1.73747	1.754041	0.243324
H	-0.784495	2.955999	1.097063

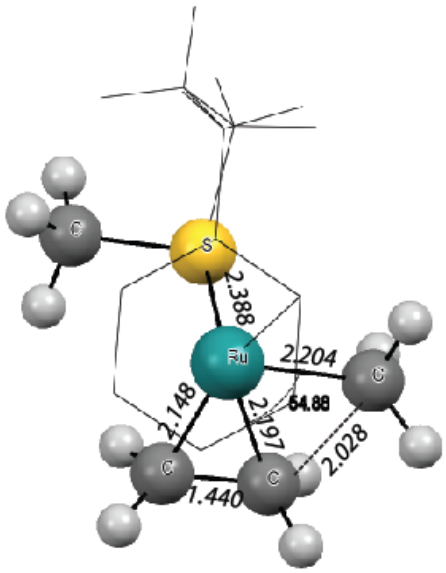

Optimized Structure Coordinates for **S3γ** *cis* isomer

Atom	X	Y	Z
Ru	0.112814	0.271231	0.462608
S	-0.194628	0.534528	-1.892239
C	-1.651195	-0.882858	1.498964
C	-0.800779	-0.218033	2.449126
C	0.604169	-0.466406	2.514206
C	1.18804	-1.302149	1.508294
C	0.360401	-1.877084	0.489528
C	-1.083489	-1.70424	0.492906
C	-1.938693	-2.337087	-0.580097
C	-1.527982	-2.04541	-2.041108
C	-1.566643	-0.570244	-2.456506
C	1.201835	-0.161492	-2.850667
C	1.870411	1.437209	0.224517
H	-2.734802	-0.686745	1.506214
H	-1.250529	0.497432	3.157441
H	1.227334	0.023086	3.277775
H	2.276563	-1.46789	1.480665
H	0.836597	-2.487032	-0.294357
H	-2.995352	-2.025305	-0.429161
H	-1.915844	-3.441939	-0.431726
H	-0.534832	-2.49076	-2.275708
H	-2.246047	-2.585302	-2.698527
H	-2.487877	-0.065543	-2.090899
H	-1.557015	-0.471505	-3.563997
H	0.982105	-0.024639	-3.930384
H	1.366756	-1.231898	-2.614561
H	2.105035	0.42176	-2.584355
C	-0.112718	2.934067	0.517442
C	1.372306	2.721292	0.88933
H	-0.798639	2.025788	0.710255
H	-0.252516	3.204666	-0.550117
H	-0.606466	3.702655	1.152628
H	1.46453	2.641073	1.995059
H	1.962235	3.620961	0.591482
H	2.750526	0.989077	0.731654
H	2.139515	1.611298	-0.839981

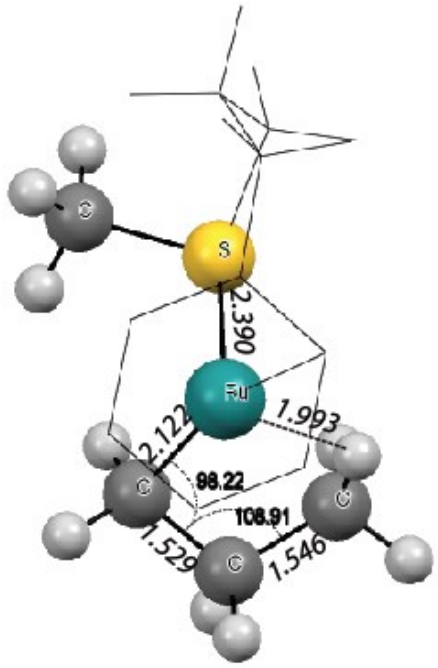

Optimized Structure Coordinates for $\mathbf{TS_{S3\gamma\text{-}S4\beta}}$ *cis* isomer

Atom	X	Y	Z
Ru	0.196765	0.181139	0.481159
S	-0.346623	0.580296	-1.788425
C	-1.678830	-0.899142	1.428402
C	-0.913898	-0.134967	2.373036
C	0.476705	-0.400361	2.616385
C	1.150238	-1.306697	1.748890
C	0.425595	-1.929525	0.671480
C	-1.017086	-1.787542	0.545770
C	-1.755005	-2.502983	-0.562505
C	-1.329569	-2.134924	-2.002815
C	-1.570380	-0.669219	-2.386483
C	1.013128	0.318170	-2.988216
C	1.954886	1.286480	0.275579
H	-2.758070	-0.709109	1.319225
H	-1.421190	0.647787	2.961241
H	1.025465	0.152766	3.393826
H	2.235187	-1.473268	1.843198
H	0.972004	-2.578591	-0.031860
H	-2.846132	-2.319238	-0.449470
H	-1.604795	-3.599069	-0.426075
H	-0.270229	-2.418686	-2.195280
H	-1.933840	-2.761277	-2.696837
H	-2.548081	-0.302811	-2.004110
H	-1.582134	-0.538685	-3.490045
H	0.624809	0.547707	-4.002113
H	1.399738	-0.719978	-2.934948
H	1.820176	1.033435	-2.736721
C	0.636990	3.540716	-0.070097
C	1.562122	2.684947	0.812708
H	-0.402100	3.144177	-0.129915
H	1.026166	3.616853	-1.110205
H	0.563433	4.574998	0.330478
H	1.141708	2.609145	1.844091
H	2.525605	3.236848	0.952075
H	2.764381	0.851481	0.900781
H	2.342159	1.364326	-0.763104

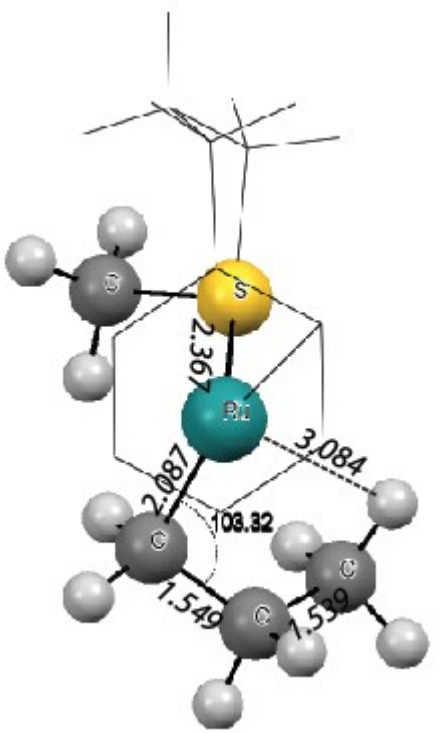

Optimized Structure Coordinates for **S4β** *cis* isomer

Atom	X	Y	Z
Ru	0.366364	0.257861	0.490076
S	0.070432	0.585981	-1.855101
C	-1.458281	-0.665169	1.549732
C	-0.510183	-0.156242	2.499223
C	0.852166	-0.586096	2.492327
C	1.292299	-1.498477	1.476771
C	0.365273	-1.959027	0.496749
C	-1.027048	-1.550983	0.522079
C	-1.993136	-2.036996	-0.535718
C	-1.581771	-1.797056	-2.004745
C	-1.432462	-0.329186	-2.418371
C	1.370056	-0.298896	-2.795320
C	2.108299	1.439959	0.290483
H	-2.505512	-0.327014	1.583996
H	-0.837643	0.588879	3.242515
H	1.562927	-0.186192	3.232434
H	2.344789	-1.818977	1.430540
H	0.720868	-2.632251	-0.298907
H	-2.986412	-1.570720	-0.355904
H	-2.134001	-3.133723	-0.392793
H	-0.662451	-2.369455	-2.263078
H	-2.380662	-2.232782	-2.646360
H	-2.279567	0.289708	-2.048561
H	-1.413092	-0.231453	-3.525865
H	1.175637	-0.160819	-3.880231
H	1.404981	-1.375939	-2.535165
H	2.336444	0.175285	-2.532958
C	0.926813	3.677698	-0.284554
C	1.112092	2.481317	0.657580
H	0.790282	3.351703	-1.337427
H	1.839466	4.311022	-0.235932
H	0.056424	4.304155	0.005742
H	-0.045186	1.999971	0.636372
H	1.175261	2.791451	1.721818
H	2.873340	1.188422	1.049085
H	2.553875	1.544813	-0.719148

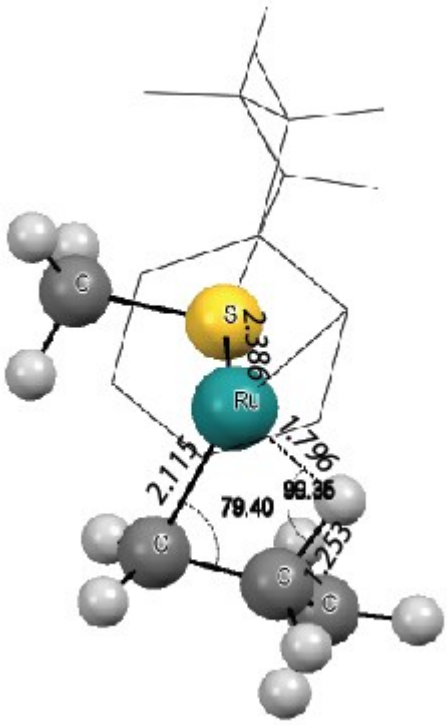

Optimized Structure Coordinates for **S4α** *cis* isomer

Atom	X	Y	Z
Ru	0.533973	0.005378	0.528688
S	0.199147	0.514980	-1.787962
C	-1.478734	-0.635897	1.510669
C	-0.501375	-0.224305	2.480980
C	0.778056	-0.857341	2.576322
C	1.143362	-1.804455	1.571626
C	0.199524	-2.141134	0.538509
C	-1.143353	-1.603706	0.529227
C	-2.115973	-1.979371	-0.566593
C	-1.641461	-1.723938	-2.014829
C	-1.373125	-0.257578	-2.375276
C	1.426326	-0.378351	-2.814265
C	2.194329	1.119935	0.353420
H	-2.464457	-0.145424	1.491865
H	-0.753911	0.590231	3.179668
H	1.492164	-0.557200	3.357492
H	2.147553	-2.256764	1.562784
H	0.508969	-2.844687	-0.250702
H	-3.073891	-1.440669	-0.398338
H	-2.346857	-3.065199	-0.466763
H	-0.758246	-2.354474	-2.264719
H	-2.449821	-2.079018	-2.693348
H	-2.168254	0.414212	-1.982993
H	-1.346486	-0.120247	-3.478317
H	1.233702	-0.136320	-3.880943
H	1.383001	-1.472868	-2.643035
H	2.425318	0.003688	-2.524782
H	1.311938	1.820165	0.735074
C	3.403041	1.166994	1.267487
H	2.449782	1.515859	-0.658741
H	4.135695	0.418515	0.880431
H	3.135433	0.839607	2.296165
C	4.083663	2.550271	1.320511
H	4.401958	2.886034	0.308735
H	4.988495	2.516889	1.965173
H	3.400267	3.323338	1.736616

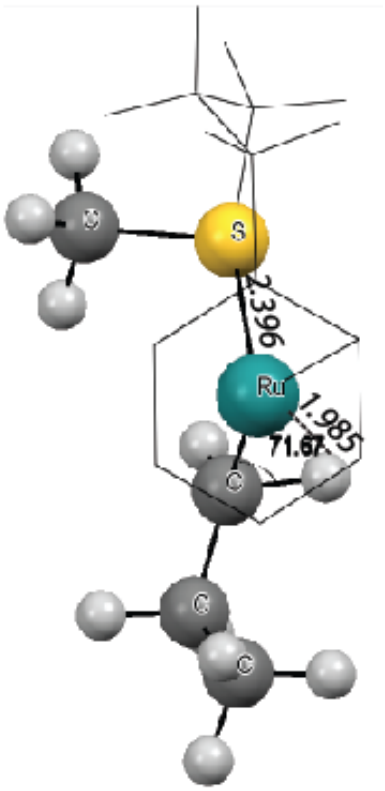

Optimized Structure Coordinates for **S1** *trans* isomer

Atom	X	Y	Z
Ru	0.536872	0.019007	0.518020
S	-0.165843	0.795004	-1.589119
C	-1.494032	-0.577893	1.534076
C	-0.550052	0.000064	2.443060
C	0.752266	-0.578101	2.653881
C	1.169885	-1.633862	1.800918
C	0.295781	-2.081025	0.744746
C	-1.070577	-1.595047	0.638223
C	-1.970687	-2.103703	-0.466991
C	-1.557924	-1.715267	-1.906704
C	-1.593395	-0.209234	-2.201320
C	1.026675	0.635174	-2.968594
C	2.486016	0.556984	0.088173
H	2.427154	1.678837	0.138082
H	2.854015	0.279964	-0.923215
H	3.217950	0.199158	0.842987
H	-2.500994	-0.140990	1.443054
H	-0.841953	0.889755	3.025850
H	1.439824	-0.145163	3.396827
H	2.190926	-2.040906	1.870095
H	0.658949	-2.840726	0.033282
H	-3.007330	-1.746988	-0.281026
H	-2.003069	-3.215230	-0.404048
H	-0.560976	-2.137041	-2.167146
H	-2.280850	-2.201728	-2.599928
H	-2.488958	0.273992	-1.753009
H	-1.627945	-0.011826	-3.293868
H	0.541828	1.021167	-3.889263
H	1.354188	-0.416501	-3.100069
H	1.894289	1.278161	-2.720945

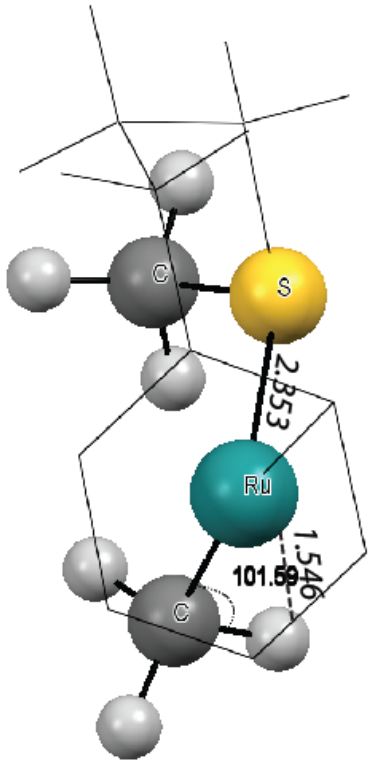

Optimized Structure Coordinates for **S2** *trans* isomer

Atom	X	Y	Z
Ru	0.329230	0.389223	0.468353
S	0.001570	0.661972	-1.882042
C	-1.481765	-0.585358	1.597091
C	-0.526195	-0.019514	2.500750
C	0.836315	-0.456929	2.500943
C	1.237985	-1.430395	1.538895
C	0.329473	-1.881476	0.545702
C	-1.061695	-1.462339	0.562470
C	-2.042342	-1.978472	-0.466057
C	-1.680130	-1.709549	-1.943764
C	-1.551791	-0.233820	-2.338898
C	1.211279	-0.285448	-2.877273
C	2.381916	0.758951	-0.075833
H	2.496393	1.554239	-0.842218
H	2.819638	-0.184078	-0.468698
H	2.944661	1.073712	0.827639
H	-2.533381	-0.259257	1.642538
H	-0.852229	0.736893	3.233052
H	1.554525	-0.054926	3.231722
H	2.286587	-1.767419	1.507769
H	0.677198	-2.596148	-0.216704
H	-3.045169	-1.548457	-0.252696
H	-2.142189	-3.080227	-0.330073
H	-0.766092	-2.271642	-2.240123
H	-2.496951	-2.142221	-2.564267
H	-2.364792	0.383354	-1.897009
H	-1.614377	-0.115832	-3.442788
H	0.871271	-0.256288	-3.933834
H	1.318328	-1.332120	-2.527969
H	2.182955	0.238405	-2.796219
C	-0.766184	2.322330	0.481394
C	0.564525	2.547906	0.899229
H	-1.591898	2.280701	1.214477
H	-1.075203	2.633876	-0.533408
H	0.801032	2.679461	1.970796
H	1.274502	3.034892	0.211056

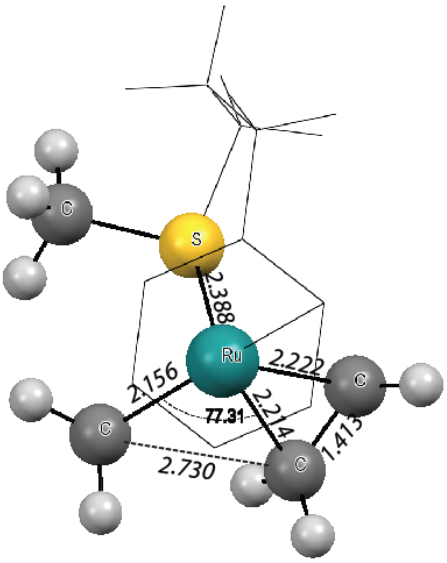

Optimized Structure Coordinates for **S2p** *trans* isomer

Atom	X	Y	Z
Ru	0.131671	0.321626	0.553888
S	-0.272628	0.604994	-1.816444
C	-1.595833	-0.926375	1.626279
C	-0.690434	-0.378421	2.588872
C	0.713014	-0.622045	2.533954
C	1.215533	-1.411299	1.450668
C	0.333190	-1.921131	0.458701
C	-1.091009	-1.665026	0.522625
C	-2.032744	-2.232406	-0.513719
C	-1.705341	-1.917440	-1.987470
C	-1.709161	-0.429832	-2.346634
C	1.059154	-0.178776	-2.800005
C	2.123766	0.976736	0.076127
H	2.168081	1.747293	-0.722418
H	2.734647	0.105728	-0.246183
H	2.576164	1.410839	0.993773
H	-2.676002	-0.733024	1.714677
H	-1.095716	0.235079	3.408494
H	1.388784	-0.215889	3.300973
H	2.295501	-1.609526	1.372191
H	0.747884	-2.513013	-0.371717
H	-3.064942	-1.886826	-0.287966
H	-2.041705	-3.340448	-0.388638
H	-0.747856	-2.392106	-2.298959
H	-2.485798	-2.407266	-2.612165
H	-2.594543	0.092740	-1.922325
H	-1.742569	-0.289820	-3.449294
H	0.766596	-0.126556	-3.869949
H	1.247182	-1.228117	-2.495391
H	1.974155	0.424522	-2.643834
C	-0.099684	2.622536	0.380227
C	-0.734806	2.215445	1.546262
H	-0.686571	2.834389	-0.529525
H	0.893421	3.096489	0.428216
H	-1.831089	2.090939	1.579756
H	-0.229648	2.349281	2.518373

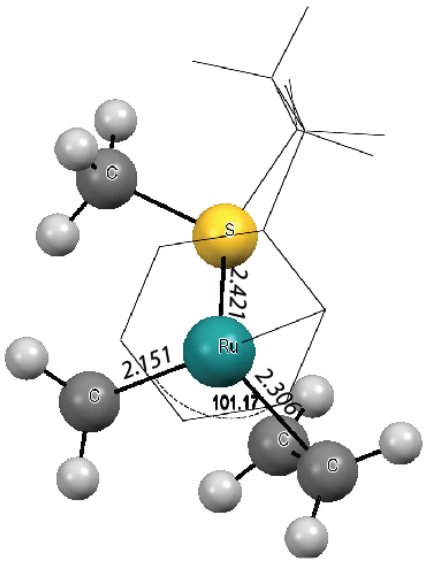

Optimized Structure Coordinates for **$TS_{S2\text{-}S3\gamma}$** *trans* isomer

Atom	X	Y	Z
Ru	0.239440	0.309043	0.484761
S	0.015511	0.610876	-1.880471
C	-1.445299	-0.583583	1.578362
C	-0.463573	-0.165995	2.539597
C	0.878331	-0.631483	2.422042
C	1.227973	-1.609060	1.426784
C	0.261677	-2.006989	0.480002
C	-1.087724	-1.474642	0.513666
C	-2.118123	-1.890511	-0.515379
C	-1.734308	-1.697323	-1.997268
C	-1.521559	-0.246190	-2.439898
C	1.284851	-0.366994	-2.767733
C	2.300251	1.439821	0.128133
H	2.430467	1.909451	-0.865332
H	2.619284	0.378901	0.068132
H	2.974147	1.920581	0.862501
H	-2.474139	-0.195006	1.638731
H	-0.731203	0.556687	3.326583
H	1.647928	-0.257827	3.117082
H	2.258028	-1.994817	1.364339
H	0.547266	-2.715095	-0.314843
H	-3.066866	-1.346744	-0.313025
H	-2.341855	-2.971046	-0.354047
H	-0.852651	-2.320780	-2.269096
H	-2.570386	-2.100232	-2.612681
H	-2.341967	0.414677	-2.082909
H	-1.495854	-0.169262	-3.548879
H	1.113828	-0.255319	-3.859642
H	1.267459	-1.436336	-2.476342
H	2.269542	0.071711	-2.509962
C	-0.566963	2.266660	0.546788
C	0.823317	2.583393	0.830869
H	-1.283499	2.341309	1.386641
H	-0.979497	2.660643	-0.402122
H	1.097431	2.677286	1.897170
H	1.278736	3.380196	0.216445

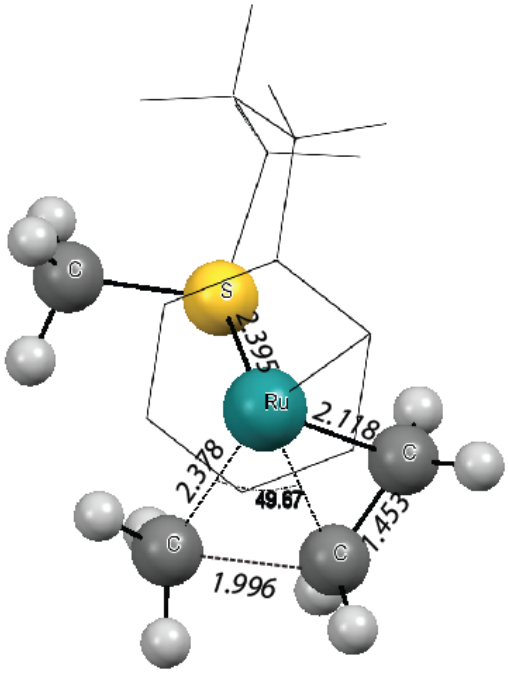

Optimized Structure Coordinates for **S3γ** *trans* isomer

Atom	X	Y	Z
Ru	0.265112	0.209844	0.471707
S	0.092149	0.549275	-1.902912
C	-1.477834	-0.455716	1.538107
C	-0.482287	-0.158768	2.530979
C	0.795408	-0.770151	2.416691
C	1.045041	-1.805138	1.437871
C	0.049045	-2.139024	0.505555
C	-1.204117	-1.405142	0.486374
C	-2.265285	-1.704493	-0.552512
C	-1.838524	-1.603444	-2.030157
C	-1.486451	-0.191180	-2.507921
C	1.320811	-0.536038	-2.722317
C	2.208190	2.007093	0.262986
H	2.246470	2.212887	-0.827692
H	2.143089	0.860845	0.396711
H	3.216555	2.198874	0.692905
H	-2.449177	0.063297	1.557340
H	-0.675691	0.592286	3.312055
H	1.604279	-0.466651	3.101278
H	2.028828	-2.299859	1.401701
H	0.247790	-2.911565	-0.254244
H	-3.138940	-1.038490	-0.380563
H	-2.627814	-2.742357	-0.363838
H	-1.011086	-2.311903	-2.260648
H	-2.695405	-1.947759	-2.652855
H	-2.260837	0.547881	-2.205867
H	-1.407529	-0.151436	-3.616316
H	1.204166	-0.431746	-3.822368
H	1.213926	-1.595023	-2.412805
H	2.322663	-0.163332	-2.426607
C	-0.266685	2.254015	0.571894
C	1.097870	2.812266	0.979153
H	-1.063706	2.444948	1.320868
H	-0.604374	2.652661	-0.409712
H	1.237427	2.722390	2.079420
H	1.213923	3.895652	0.736738

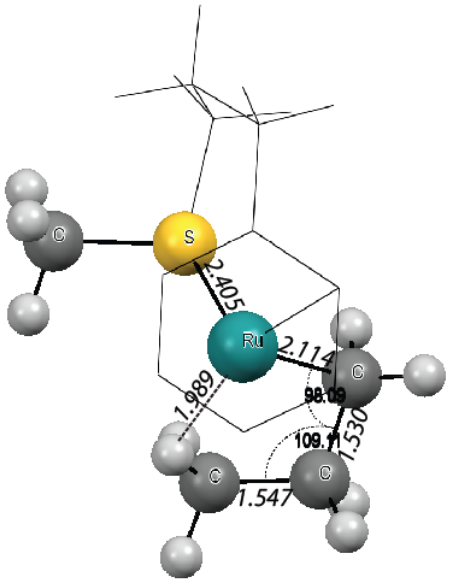

Optimized Structure Coordinates for **$TS_{S3\gamma\text{-}S4\beta}$** *trans* isomer

Atom	X	Y	Z
Ru	0.220035	0.189251	0.514201
S	0.096652	0.537856	-1.875742
C	-1.472452	-0.526020	1.589121
C	-0.478541	-0.231074	2.580306
C	0.817884	-0.797856	2.428171
C	1.086802	-1.811798	1.433936
C	0.086449	-2.163891	0.513823
C	-1.178196	-1.451064	0.509699
C	-2.235593	-1.747336	-0.533735
C	-1.801516	-1.648283	-2.008971
C	-1.463287	-0.234465	-2.492812
C	1.357192	-0.529671	-2.668745
C	2.206813	2.736357	-0.248725
H	1.783073	3.241285	-1.143964
H	2.538547	1.717845	-0.558510
H	3.126798	3.286420	0.045930
H	-2.458841	-0.036567	1.627864
H	-0.679116	0.502110	3.376715
H	1.631741	-0.473920	3.098131
H	2.086136	-2.271596	1.375997
H	0.299193	-2.913462	-0.264736
H	-3.108440	-1.079092	-0.365414
H	-2.602116	-2.784290	-0.345126
H	-0.965441	-2.348723	-2.232173
H	-2.650450	-2.004247	-2.636123
H	-2.251698	0.495210	-2.204653
H	-1.372580	-0.201082	-3.600607
H	1.250371	-0.437796	-3.770916
H	1.269557	-1.587772	-2.350828
H	2.347319	-0.131128	-2.367390
C	-0.233217	2.205874	0.605225
C	1.195447	2.716790	0.915146
H	-0.934785	2.441802	1.433741
H	-0.621423	2.661120	-0.332061
H	1.635709	2.183614	1.794646
H	1.065974	3.762598	1.291578

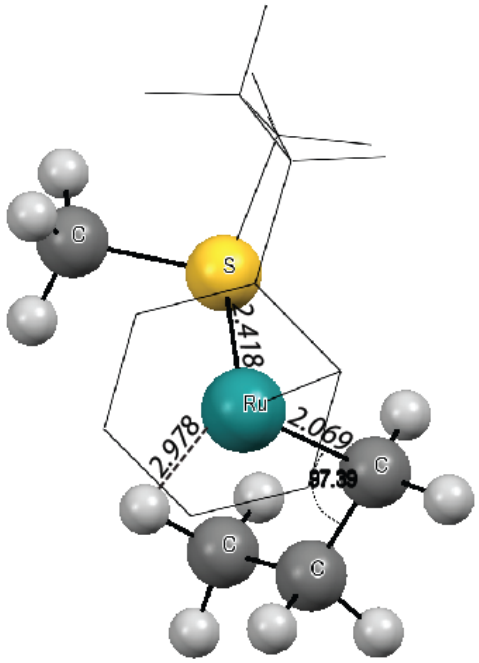

Optimized Structure Coordinates for **S4β** *trans* isomer

Atom	X	Y	Z
Ru	0.013858	0.407033	0.709252
S	-0.120894	0.935846	-1.617950
C	-1.670258	-0.709404	1.603609
C	-0.781925	-0.312761	2.659557
C	0.598791	-0.654448	2.588722
C	1.099808	-1.461440	1.506507
C	0.217199	-1.869186	0.480092
C	-1.174613	-1.462957	0.488955
C	-2.101208	-1.853205	-0.643112
C	-1.635513	-1.497609	-2.070636
C	-1.523091	-0.000130	-2.372524
C	1.304631	0.191619	-2.495167
C	1.500681	3.573289	0.132711
H	1.218310	4.603543	0.441889
H	1.157962	3.431605	-0.914292
H	2.608886	3.497956	0.163203
H	-2.729786	-0.410980	1.632899
H	-1.155071	0.300272	3.495176
H	1.291237	-0.289192	3.364512
H	2.164468	-1.739201	1.466803
H	0.607259	-2.461477	-0.362497
H	-3.100991	-1.401190	-0.462451
H	-2.247998	-2.957415	-0.592427
H	-0.685480	-2.018740	-2.326280
H	-2.389385	-1.910237	-2.778803
H	-2.425952	0.553825	-2.033212
H	-1.418221	0.177340	-3.465225
H	1.194039	0.389133	-3.582932
H	1.392186	-0.895814	-2.298955
H	2.210935	0.707947	-2.118422
C	-0.643921	2.395760	0.990427
C	0.826689	2.577864	1.085877
H	-1.226730	2.514357	1.922703
H	-1.131933	2.884022	0.123869
H	1.422113	1.511540	0.760877
H	1.190919	2.685436	2.129243

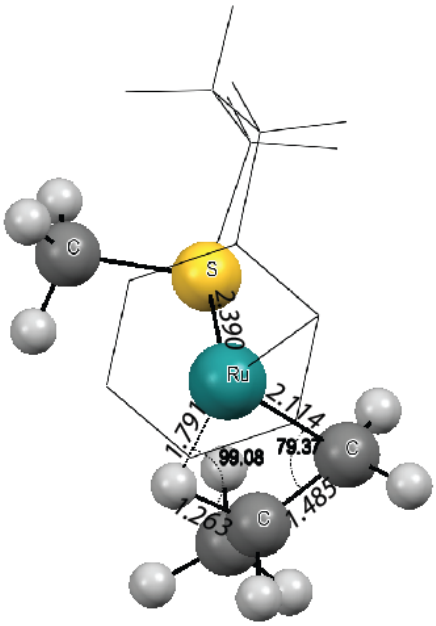

Optimized Structure Coordinates for **S4α** *trans* isomer

Atom	X	Y	Z
Ru	-0.287369	0.306384	0.777515
S	-0.435881	0.966326	-1.540719
C	-1.766328	-1.059284	1.561411
C	-0.970235	-0.637825	2.677989
C	0.443903	-0.756639	2.595783
C	1.064928	-1.432744	1.479948
C	0.268526	-1.949249	0.437011
C	-1.150432	-1.690728	0.415742
C	-2.003248	-2.118164	-0.761116
C	-1.543975	-1.645316	-2.155786
C	-1.640911	-0.136840	-2.403155
C	1.131614	0.498081	-2.366226
H	-2.855421	-0.894305	1.567414
H	-1.442342	-0.148742	3.543344
H	1.076643	-0.328620	3.390160
H	2.160993	-1.535106	1.443801
H	0.749702	-2.453624	-0.415347
H	-3.050415	-1.785790	-0.589457
H	-2.031876	-3.232973	-0.763670
H	-0.520106	-2.014450	-2.389736
H	-2.204527	-2.132381	-2.908547
H	-2.631863	0.263819	-2.095949
H	-1.510146	0.098816	-3.481908
H	1.047140	0.745320	-3.446116
H	1.373242	-0.574612	-2.224873
H	1.927370	1.122151	-1.910369
C	-0.802501	2.205331	1.135410
C	-1.349332	2.822115	2.405305
H	-1.022213	2.841378	0.247026
H	0.393567	2.097139	1.162199
H	-1.043589	2.235636	3.299213
H	-2.462421	2.751546	2.345177
C	-0.953973	4.302177	2.589916
H	-1.289268	4.922540	1.729599
H	0.148233	4.419434	2.686963
H	-1.419973	4.718316	3.509092

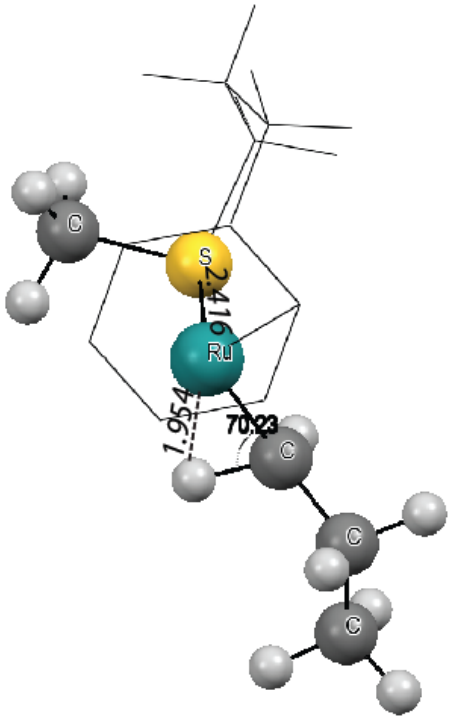

Optimized Structure Coordinates for **S5**

Atom	X	Y	Z
Ru	0.172016	0.459758	0.557292
S	-0.15241	0.788038	-1.79403
C	-1.53558	-0.7722	1.598425
C	-0.66814	-0.13874	2.546238
C	0.73373	-0.42096	2.562508
C	1.262145	-1.29934	1.569789
C	0.430725	-1.80293	0.536867
C	-1.00007	-1.54992	0.540094
C	-1.897	-2.13341	-0.52818
C	-1.55346	-1.75281	-1.98569
C	-1.59272	-0.25423	-2.30827
C	1.159856	0.02716	-2.81884
C	2.201216	1.091663	0.048935
H	2.131564	1.896846	-0.71692
H	2.63793	0.196191	-0.44908
C	3.13057	1.555004	1.174355
H	-2.61858	-0.57125	1.632946
H	-1.09287	0.540157	3.303549
H	1.383139	0.021912	3.331905
H	2.341537	-1.51873	1.550414
H	0.872283	-2.43848	-0.2469
H	-2.94747	-1.8391	-0.31373
H	-1.86323	-3.24435	-0.44416
H	-0.57752	-2.19065	-2.29356
H	-2.30784	-2.2463	-2.63896
H	-2.4723	0.243994	-1.84495
H	-1.66337	-0.09056	-3.40565
H	0.824214	0.070626	-3.87637
H	1.379117	-1.01762	-2.51966
H	2.067838	0.649464	-2.70361
C	-1.17881	2.214445	0.604609
C	0.107962	2.612439	1.034586
H	-1.99225	2.048773	1.333522
H	-1.52753	2.505288	-0.4037
H	0.311286	2.761329	2.11034
H	0.742459	3.210867	0.359546
H	3.272135	0.745517	1.926988
H	2.683624	2.411457	1.726367
C	4.513912	1.973208	0.638427
H	4.432272	2.822867	-0.07577
H	5.019653	1.134147	0.109833
H	5.179343	2.296376	1.469029

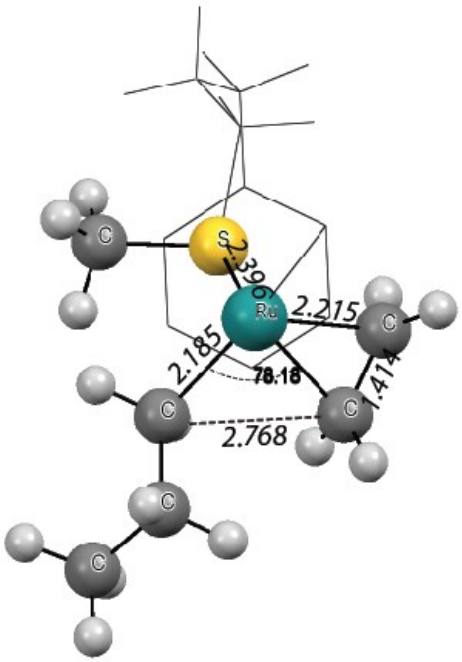

Optimized Structure Coordinates for **$TS_{S5\text{-}S6\gamma}$**

Atom	X	Y	Z
Ru	-0.04309	0.376524	0.589267
S	-0.27701	0.760007	-1.75866
C	-1.59209	-0.87668	1.591576
C	-0.71993	-0.33221	2.592533
C	0.684839	-0.5593	2.509523
C	1.217752	-1.40467	1.479213
C	0.360906	-1.89595	0.471481
C	-1.06537	-1.62511	0.494732
C	-1.98115	-2.15931	-0.58571
C	-1.61406	-1.80046	-2.04172
C	-1.64826	-0.30782	-2.38635
C	1.139913	0.053578	-2.67903
C	1.820259	1.712597	0.317813
H	1.814273	2.293785	-0.62724
H	2.306089	0.743602	0.061779
C	2.737423	2.373773	1.35836
H	-2.67432	-0.67669	1.642297
H	-1.13079	0.290056	3.40365
H	1.355978	-0.11269	3.260052
H	2.299951	-1.60467	1.430139
H	0.786277	-2.49465	-0.35022
H	-3.01818	-1.81615	-0.37787
H	-2.00151	-3.27078	-0.4999
H	-0.63423	-2.24422	-2.32945
H	-2.35838	-2.29889	-2.70306
H	-2.56839	0.180783	-1.99728
H	-1.63479	-0.15586	-3.48769
H	0.957135	0.198017	-3.76496
H	1.295745	-1.01899	-2.44726
H	2.037844	0.632364	-2.38373
C	-1.24862	2.131026	0.723488
C	0.094088	2.589712	0.991238
H	-1.95682	2.018794	1.564744
H	-1.72869	2.469221	-0.21462
H	0.361886	2.737879	2.051701
H	0.454636	3.408009	0.346049
H	2.633904	1.851708	2.337871
H	2.441789	3.43151	1.53795
C	4.210965	2.339068	0.917816
H	4.357864	2.86409	-0.05247
H	4.586741	1.297671	0.801158
H	4.854855	2.845091	1.67002

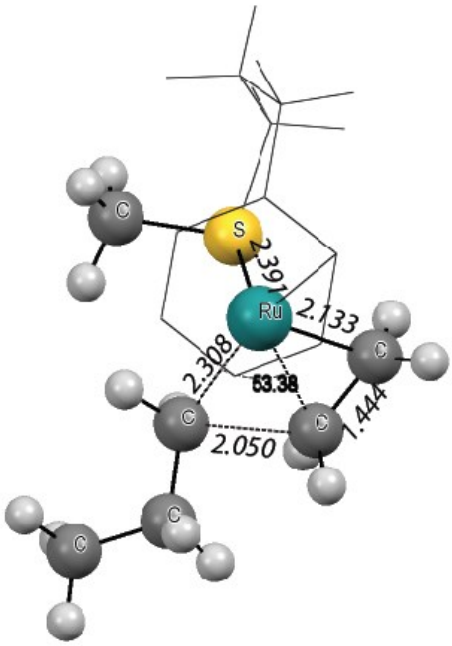

Optimized Structure Coordinates for **S6γ**

Atom	X	Y	Z
Ru	0.010373	0.161117	0.588315
S	-0.11182	0.617551	-1.7658
C	-1.6176	-0.9003	1.516292
C	-0.74207	-0.48146	2.575981
C	0.634116	-0.82673	2.499301
C	1.123258	-1.72471	1.477165
C	0.252031	-2.18009	0.472961
C	-1.11952	-1.70524	0.428425
C	-2.05412	-2.12908	-0.68535
C	-1.58579	-1.84933	-2.12745
C	-1.48846	-0.36756	-2.50266
C	1.338509	-0.15973	-2.57208
C	1.561644	2.353226	0.61323
H	1.545885	2.629148	-0.46547
H	1.660118	1.188797	0.623366
C	2.86927	2.826317	1.265016
H	-2.67179	-0.58016	1.513535
H	-1.11229	0.164899	3.386537
H	1.337158	-0.42128	3.245077
H	2.185186	-2.0166	1.465327
H	0.631359	-2.84482	-0.31952
H	-3.04601	-1.65228	-0.52615
H	-2.21989	-3.22695	-0.57963
H	-0.62817	-2.3722	-2.34913
H	-2.33115	-2.3058	-2.81753
H	-2.40357	0.189931	-2.2044
H	-1.36815	-0.23966	-3.60059
H	1.252953	-0.01163	-3.66988
H	1.425472	-1.23664	-2.32451
H	2.234453	0.378041	-2.20046
C	-0.92208	2.052127	0.773766
C	0.270913	2.846726	1.307268
H	-1.78284	2.026579	1.474876
H	-1.27918	2.444822	-0.20348
H	0.373845	2.696269	2.40596
H	0.166742	3.948225	1.150904
H	2.888331	2.500019	2.330074
H	2.823043	3.941234	1.290836
C	4.142078	2.370191	0.54504
H	4.165703	2.726954	-0.50897
H	4.230308	1.259414	0.532099
H	5.04953	2.766332	1.049389

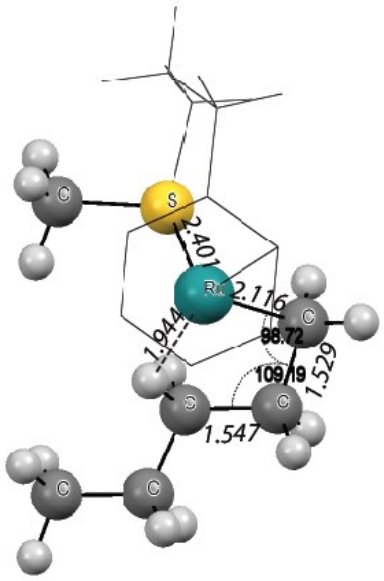

Optimized Structure Coordinates for **$TS_{S6\gamma\text{-}S7\beta}$**

Atom	X	Y	Z
Ru	-0.02097	0.292469	0.44556
S	-0.34752	0.670512	-1.90912
C	-1.49475	-0.84554	1.501192
C	-0.59888	-0.33605	2.501248
C	0.792937	-0.57076	2.348158
C	1.294426	-1.45409	1.318636
C	0.407586	-2.02596	0.391049
C	-0.99412	-1.65327	0.410232
C	-1.9561	-2.18972	-0.62885
C	-1.59658	-1.93456	-2.10574
C	-1.65845	-0.46699	-2.53751
C	1.12593	0.012681	-2.77872
C	1.355253	2.847603	0.305833
H	1.066813	3.281694	-0.67976
H	1.559427	1.730544	0.077844
C	2.676424	3.44777	0.795952
H	-2.56966	-0.60822	1.549458
H	-0.97354	0.307321	3.312509
H	1.505516	-0.08582	3.035205
H	2.376086	-1.64987	1.246019
H	0.793659	-2.68566	-0.40203
H	-2.97184	-1.78507	-0.42626
H	-2.02755	-3.29162	-0.47128
H	-0.60829	-2.37797	-2.36375
H	-2.33365	-2.48466	-2.73344
H	-2.60647	0.014085	-2.21071
H	-1.60442	-0.37058	-3.64399
H	0.961775	0.113961	-3.87291
H	1.335304	-1.04105	-2.50651
H	1.982073	0.651021	-2.47919
C	-0.98861	2.152127	0.652454
C	0.169288	2.909799	1.309852
H	-1.88857	2.080853	1.301724
H	-1.28542	2.618271	-0.31232
H	0.589268	2.339194	2.169057
H	-0.07346	3.954044	1.617538
H	2.958364	2.984341	1.770019
H	2.478971	4.52348	1.02065
C	3.835207	3.328818	-0.20048
H	3.59401	3.823094	-1.16831
H	4.083087	2.263436	-0.41367
H	4.755948	3.80738	0.19687

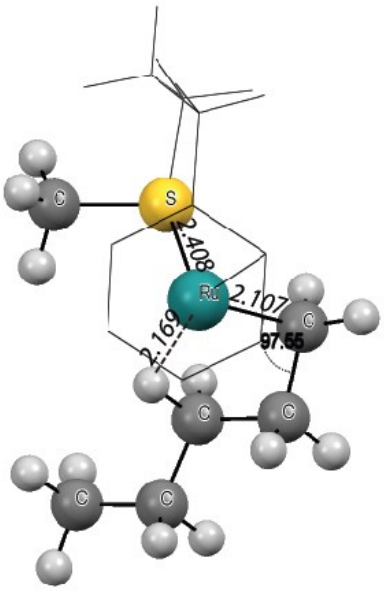

Optimized Structure Coordinates for **S7β**

Atom	X	Y	Z
Ru	0.010373	0.161117	0.588315
S	-0.11182	0.617551	-1.7658
C	-1.6176	-0.9003	1.516292
C	-0.74207	-0.48146	2.575981
C	0.634116	-0.82673	2.499301
C	1.123258	-1.72471	1.477165
C	0.252031	-2.18009	0.472961
C	-1.11952	-1.70524	0.428425
C	-2.05412	-2.12908	-0.68535
C	-1.58579	-1.84933	-2.12745
C	-1.48846	-0.36756	-2.50266
C	1.338509	-0.15973	-2.57208
C	1.561644	2.353226	0.61323
H	1.545885	2.629148	-0.46547
H	1.660118	1.188797	0.623366
C	2.86927	2.826317	1.265016
H	-2.67179	-0.58016	1.513535
H	-1.11229	0.164899	3.386537
H	1.337158	-0.42128	3.245077
H	2.185186	-2.0166	1.465327
H	0.631359	-2.84482	-0.31952
H	-3.04601	-1.65228	-0.52615
H	-2.21989	-3.22695	-0.57963
H	-0.62817	-2.3722	-2.34913
H	-2.33115	-2.3058	-2.81753
H	-2.40357	0.189931	-2.2044
H	-1.36815	-0.23966	-3.60059
H	1.252953	-0.01163	-3.66988
H	1.425472	-1.23664	-2.32451
H	2.234453	0.378041	-2.20046
C	-0.92208	2.052127	0.773766
C	0.270913	2.846726	1.307268
H	-1.78284	2.026579	1.474876
H	-1.27918	2.444822	-0.20348
H	0.373845	2.696269	2.40596
H	0.166742	3.948225	1.150904
H	2.888331	2.500019	2.330074
H	2.823043	3.941234	1.290836
C	4.142078	2.370191	0.54504
H	4.165703	2.726954	-0.50897
H	4.230308	1.259414	0.532099
H	5.04953	2.766332	1.049389

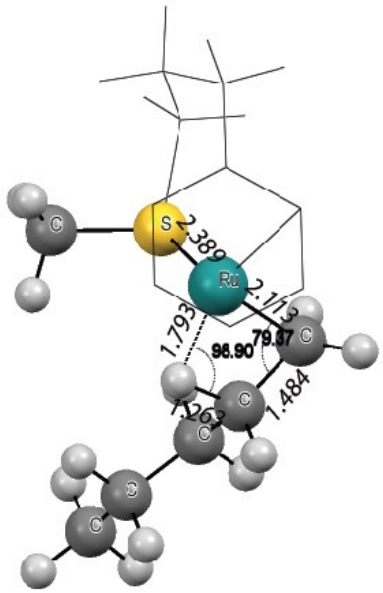

Optimized Structure Coordinates for **N1**

Atom	X	Y	Z
Ru	0.000129	0.320088	0.298959
C	-1.42312	-0.55302	1.596467
C	-0.36718	-0.06682	2.434855
C	0.970668	-0.44492	2.12363
C	1.244736	-1.51395	1.186472
C	0.200235	-2.06018	0.430926
C	-1.12553	-1.47355	0.51082
C	-2.19246	-1.84794	-0.49302
C	-1.77664	-1.6546	-1.96767
C	-1.4575	-0.21754	-2.40566
C	1.008496	-0.36529	-2.46479
H	-2.45137	-0.17773	1.72583
H	-0.56915	0.691779	3.206368
H	1.808332	0.040415	2.650676
H	2.282146	-1.85267	1.032114
H	0.412294	-2.84454	-0.31308
H	-3.11102	-1.2564	-0.28616
H	-2.46902	-2.91742	-0.33809
H	-0.94723	-2.34403	-2.24111
H	-2.63149	-1.98061	-2.60075
H	-2.26876	0.46488	-2.07123
H	-1.44392	-0.18707	-3.52169
H	0.982388	-0.38725	-3.58041
H	1.010224	-1.40173	-2.08337
H	1.948473	0.131102	-2.14551
C	-0.73569	2.222511	0.453548
H	-1.41427	2.572392	-0.35252
H	0.239868	2.778187	0.348295
H	-1.18639	2.474058	1.437224
N	-0.16264	0.397051	-1.93666
C	-0.07887	1.766309	-2.52576
H	0.833052	2.281291	-2.1614
H	-0.03132	1.698401	-3.63706
H	-0.96731	2.363863	-2.25086

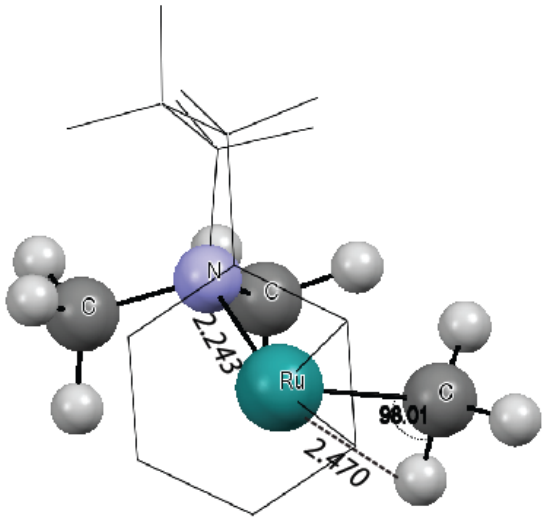

Optimized Structure Coordinates for **N2**

Atom	X	Y	Z
Ru	0.284791	0.405527	0.351259
C	-1.35751	-0.52087	1.639805
C	-0.28057	-0.04014	2.448472
C	1.044078	-0.53065	2.209562
C	1.264037	-1.58265	1.257469
C	0.216537	-1.95447	0.39884
C	-1.11592	-1.3886	0.539782
C	-2.1951	-1.73219	-0.45831
C	-1.78426	-1.49244	-1.92801
C	-1.36748	-0.06332	-2.30783
C	1.035025	-0.46334	-2.56463
C	2.315809	1.197287	0.02648
H	-2.36991	-0.11373	1.794153
H	-0.46495	0.695765	3.246044
H	1.880954	-0.15505	2.820406
H	2.266694	-2.02273	1.133368
H	0.40185	-2.71257	-0.3788
H	-3.10774	-1.14137	-0.22517
H	-2.48159	-2.80321	-0.34168
H	-1.01353	-2.22689	-2.24984
H	-2.6707	-1.7261	-2.55846
H	-2.09261	0.665846	-1.89068
H	-1.43088	0.021933	-3.41871
H	0.839022	-0.54359	-3.66011
H	1.017546	-1.47347	-2.12049
H	2.046327	-0.03935	-2.42114
C	-1.12989	2.024433	0.338331
C	1.55787	2.179138	0.700978
H	-2.12054	1.637577	0.014404
H	-0.83469	2.852283	-0.334
H	-1.23005	2.446381	1.36019
H	1.678566	2.334363	1.788375
H	1.20588	3.070663	0.156922
H	3.057876	0.58304	0.567927
H	2.549386	1.332607	-1.04292
N	0.014517	0.422499	-1.92823
C	0.170429	1.769447	-2.5523
H	1.132123	2.227201	-2.24849
H	0.158486	1.676816	-3.66296
H	-0.6596	2.433396	-2.24912

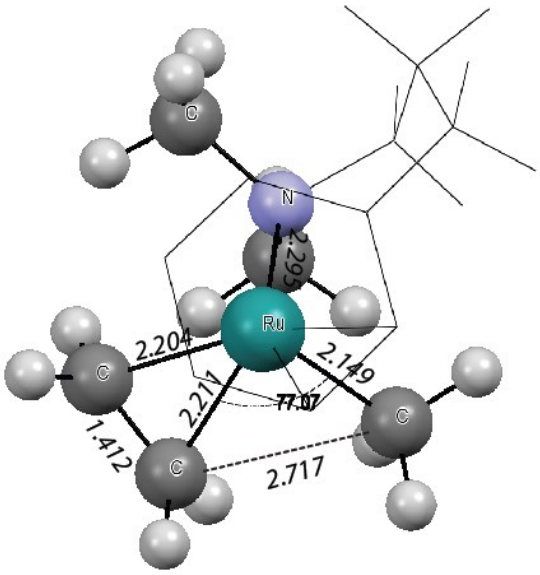

Optimized Structure Coordinates for **N2p**

Atom	X	Y	Z
Ru	0.35524	0.279322	0.424432
C	-1.41653	-0.52354	1.536083
C	-0.38554	-0.17208	2.466626
C	0.886164	-0.80213	2.349776
C	1.133358	-1.84541	1.384797
C	0.132578	-2.14035	0.455025
C	-1.15232	-1.46384	0.502274
C	-2.21286	-1.7949	-0.51767
C	-1.78719	-1.54624	-1.97446
C	-1.36698	-0.10871	-2.29143
C	1.034938	-0.5309	-2.54294
C	2.092299	1.621994	-0.13021
H	-2.40459	-0.04241	1.599245
H	-0.5685	0.569922	3.258077
H	1.676255	-0.53247	3.066278
H	2.104059	-2.36434	1.356807
H	0.309588	-2.91263	-0.31125
H	-3.1298	-1.20656	-0.29678
H	-2.49334	-2.8674	-0.39979
H	-1.00845	-2.27126	-2.2978
H	-2.66389	-1.76497	-2.62313
H	-2.08438	0.607022	-1.83495
H	-1.43962	0.028588	-3.39604
H	0.850068	-0.60028	-3.64179
H	1.007947	-1.54489	-2.1058
H	2.0478	-0.11363	-2.3865
C	-0.70208	2.118102	0.46402
C	2.328266	1.156087	1.161387
H	-1.64238	1.997798	-0.11958
H	-0.13977	2.982834	0.054511
H	-0.98278	2.374432	1.508711
H	3.049827	0.339039	1.328541
H	2.117235	1.800295	2.033547
H	2.658954	1.169493	-0.96213
H	1.73532	2.650709	-0.29167
N	0.019185	0.353889	-1.90456
C	0.157264	1.704828	-2.52716
H	1.170459	2.111115	-2.36202
H	-0.01135	1.626989	-3.62627
H	-0.59053	2.400613	-2.10407

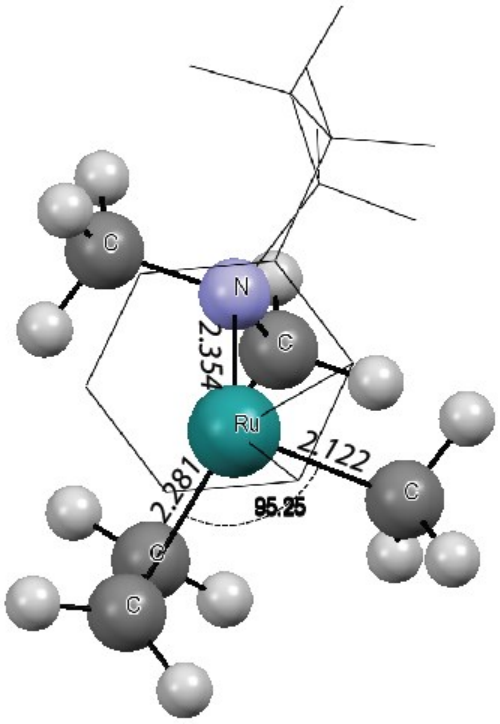

Optimized Structure Coordinates for $\mathbf{TS_{N2\text{-}N3\gamma}}$

Atom	X	Y	Z
Ru	0.153863	-0.21524	0.305362
C	-1.63898	-1.26781	1.40101
C	-0.69157	-0.65999	2.30127
C	0.693817	-1.00098	2.285129
C	1.170393	-1.88838	1.260255
C	0.243646	-2.39938	0.301192
C	-1.17987	-2.11435	0.36798
C	-2.0991	-2.59016	-0.72777
C	-1.61425	-2.23146	-2.15119
C	-1.34885	-0.74544	-2.43238
C	1.103092	-0.83628	-2.62357
C	1.864571	0.994552	0.193879
H	-2.7025	-0.98447	1.454789
H	-1.04781	0.085655	3.031207
H	1.388227	-0.54441	3.007528
H	2.237886	-2.14754	1.186603
H	0.62622	-3.04487	-0.50471
H	-3.11092	-2.15912	-0.56249
H	-2.21614	-3.69665	-0.6637
H	-0.7369	-2.84973	-2.44184
H	-2.41731	-2.53766	-2.85735
H	-2.16326	-0.12876	-1.99097
H	-1.39893	-0.59506	-3.53741
H	0.984025	-0.83739	-3.73334
H	1.172763	-1.87986	-2.26911
H	2.047664	-0.31915	-2.36639
C	-0.8241	2.0566	0.4881
C	1.1547	2.1702	0.7554
H	-1.41261	1.188099	0.095617
H	-0.94163	2.885383	-0.23302
H	-1.20652	2.330459	1.48761
H	1.201289	2.279844	1.85397
H	1.283822	3.141659	0.239428
H	2.668382	0.5998	0.849505
H	2.261857	1.145411	-0.83041
N	-0.04159	-0.12971	-1.98311
C	-0.04366	1.263363	-2.51443
H	0.856258	1.809133	-2.17225
H	-0.04311	1.247449	-3.62952
H	-0.95049	1.800331	-2.17842

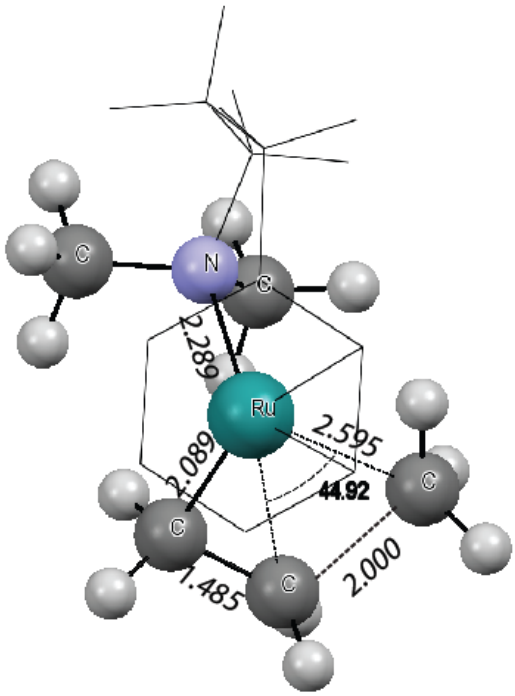

Optimized Structure Coordinates for **N3γ**

Atom	X	Y	Z
Ru	0.087456	0.169858	0.38122
C	-1.70338	-1.04599	1.345607
C	-0.93959	-0.26762	2.288056
C	0.466384	-0.45471	2.472774
C	1.154976	-1.30204	1.5499
C	0.419856	-1.9505	0.501943
C	-1.03224	-1.88048	0.428028
C	-1.75829	-2.55697	-0.70375
C	-1.26389	-2.11297	-2.09908
C	-1.27691	-0.59973	-2.35593
C	1.143104	-0.246	-2.55057
C	1.795137	1.40505	0.270377
H	-2.7945	-0.91103	1.280596
H	-1.46447	0.471329	2.916049
H	1.012312	0.101909	3.249105
H	2.249878	-1.41349	1.599582
H	0.972116	-2.56433	-0.22751
H	-2.84691	-2.3501	-0.61368
H	-1.6368	-3.66127	-0.6153
H	-0.26414	-2.54446	-2.32439
H	-1.94272	-2.5693	-2.85222
H	-2.18989	-0.14728	-1.91101
H	-1.33961	-0.43722	-3.45823
H	1.002169	-0.25505	-3.65729
H	1.409569	-1.26387	-2.2109
H	1.982149	0.431021	-2.30361
C	-0.15937	2.935355	0.761648
C	1.317645	2.608677	1.08786
H	-0.8333	2.012909	0.670939
H	-0.27483	3.486743	-0.19403
H	-0.65336	3.525422	1.564322
H	1.408887	2.385668	2.173585
H	1.944704	3.515599	0.911759
H	2.70828	0.938358	0.698188
H	2.025774	1.693059	-0.77886
N	-0.10224	0.227686	-1.87969
C	-0.36605	1.618422	-2.34668
H	0.467751	2.283883	-2.05323
H	-0.45886	1.640526	-3.45827
H	-1.31238	1.992054	-1.90682

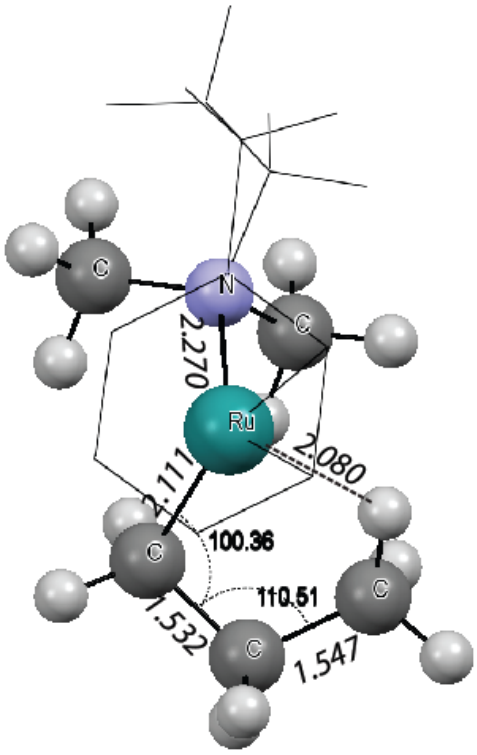

Optimized Structure Coordinates for $\mathbf{TS_{N3\gamma\text{-}N4\beta}}$

Atom	X	Y	Z
Ru	0.171364	0.123533	0.419031
C	-1.69936	-1.00981	1.32513
C	-0.98977	-0.1691	2.258855
C	0.393216	-0.37372	2.571067
C	1.132883	-1.27386	1.749351
C	0.462946	-1.96705	0.677903
C	-0.98225	-1.91253	0.514838
C	-1.63037	-2.6389	-0.63417
C	-1.09667	-2.18477	-2.0135
C	-1.18822	-0.67555	-2.2843
C	1.183132	-0.13077	-2.55557
C	1.842556	1.380729	0.370395
H	-2.78071	-0.86319	1.173073
H	-1.54593	0.62215	2.789323
H	0.893106	0.228	3.345106
H	2.220938	-1.38986	1.879857
H	1.059826	-2.61106	0.011292
H	-2.73015	-2.48142	-0.59366
H	-1.46138	-3.7349	-0.52707
H	-0.06059	-2.55394	-2.179
H	-1.70661	-2.69343	-2.79147
H	-2.12436	-0.26908	-1.84346
H	-1.25448	-0.51398	-3.38653
H	0.998761	-0.04026	-3.65215
H	1.508652	-1.1635	-2.32681
H	1.996868	0.561739	-2.27075
C	1.006349	3.887227	0.303222
C	1.446997	2.677356	1.140518
H	0.008995	3.749423	-0.16868
H	1.741498	4.115043	-0.50051
H	0.930956	4.792842	0.94411
H	0.66731	2.47153	1.915343
H	2.34002	2.972437	1.742273
H	2.696324	0.884883	0.880373
H	2.187407	1.632984	-0.65737
N	-0.05691	0.202757	-1.79982
C	-0.44106	1.609413	-2.10427
H	0.399984	2.289539	-1.87301
H	-0.70259	1.721751	-3.18385
H	-1.3286	1.897944	-1.50022

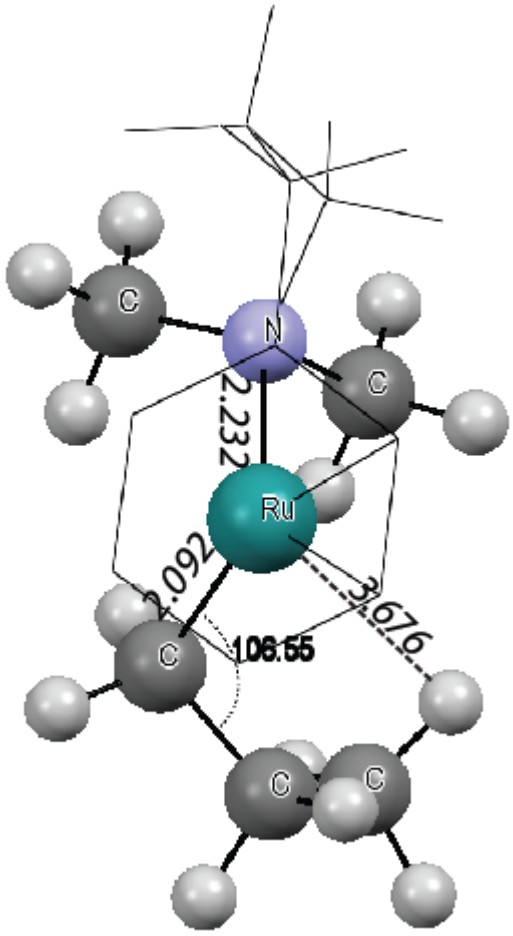

Optimized Structure Coordinates for **N4β**

Atom	X	Y	Z
Ru	0.383375	0.149193	0.501905
C	-1.43276	-0.88925	1.512173
C	-0.52026	-0.30511	2.456182
C	0.861979	-0.67494	2.4891
C	1.369655	-1.56838	1.490312
C	0.48659	-2.06723	0.491359
C	-0.92982	-1.74623	0.50205
C	-1.81748	-2.24076	-0.61079
C	-1.34632	-1.81021	-2.01578
C	-1.16795	-0.30106	-2.22115
C	1.272813	-0.25417	-2.47188
C	2.06804	1.396534	0.403141
H	-2.49897	-0.61563	1.529575
H	-0.89575	0.433736	3.182681
H	1.536139	-0.23937	3.24257
H	2.437984	-1.8346	1.466291
H	0.8885	-2.71894	-0.30026
H	-2.85279	-1.87387	-0.44043
H	-1.86574	-3.35337	-0.57418
H	-0.42903	-2.36213	-2.31711
H	-2.12232	-2.1367	-2.74238
H	-2.00228	0.248948	-1.73337
H	-1.23717	-0.09395	-3.31568
H	1.120662	-0.18774	-3.57566
H	1.400173	-1.31426	-2.18668
H	2.200361	0.287458	-2.20624
C	1.023566	2.385574	0.794342
H	2.834601	1.173229	1.171091
H	2.528525	1.536419	-0.59452
N	0.114176	0.350581	-1.75341
C	0.018677	1.775106	-2.18088
H	0.956722	2.31111	-1.94187
H	-0.13793	1.836649	-3.28354
H	-0.83555	2.267075	-1.67446
C	1.080101	3.010463	2.18984
H	1.885549	3.777258	2.207863
H	0.128123	3.516053	2.459585
H	1.314006	2.260128	2.973226
H	0.847846	3.16165	0.018248
H	-0.11034	1.875116	0.692244

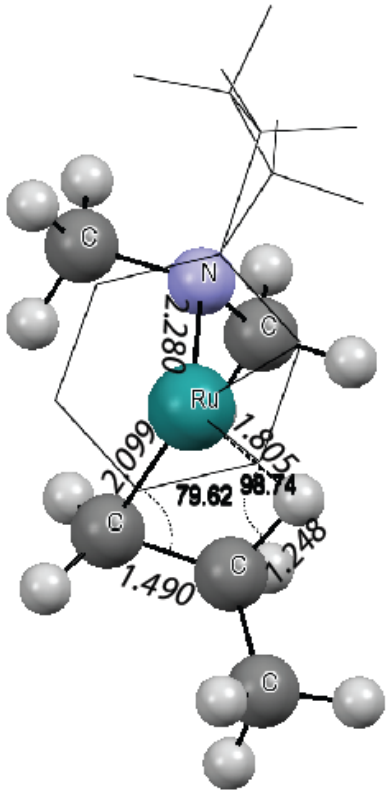

Optimized Structure Coordinates for **N4α**

Atom	X	Y	Z
Ru	0.35808	0.042052	0.163014
C	-1.58654	-0.72771	1.26039
C	-0.63694	-0.04148	2.102116
C	0.704578	-0.51664	2.274434
C	1.174485	-1.53158	1.391304
C	0.270689	-2.08597	0.412404
C	-1.14349	-1.75941	0.408315
C	-2.04274	-2.34431	-0.64925
C	-1.6338	-1.92771	-2.0823
C	-1.52136	-0.41312	-2.31276
C	0.83684	-0.24686	-2.93031
C	2.048932	1.197019	0.093623
H	-2.63099	-0.38041	1.219066
H	-0.9713	0.837732	2.678242
H	1.388666	-0.01484	2.976095
H	2.22906	-1.84947	1.406906
H	0.657599	-2.82601	-0.30693
H	-3.08964	-2.02433	-0.45667
H	-2.03065	-3.45552	-0.57975
H	-0.69957	-2.44527	-2.39116
H	-2.41426	-2.30796	-2.77706
H	-2.30675	0.117019	-1.7312
H	-1.72056	-0.20029	-3.38988
H	0.516409	-0.08265	-3.98706
H	1.00421	-1.32868	-2.7685
H	1.790464	0.280878	-2.75544
H	2.633393	1.048108	1.029655
N	-0.20538	0.259659	-1.9928
C	-0.41174	1.719242	-2.22885
H	0.542126	2.264012	-2.09899
H	-0.78295	1.899493	-3.26598
H	-1.16261	2.114077	-1.51241
H	1.281327	2.031337	0.311688
C	3.019671	1.628016	-1.00409
H	3.630201	0.740567	-1.29609
H	2.496985	1.965262	-1.92601
C	3.969825	2.75206	-0.54299
H	4.563908	2.440857	0.344735
H	4.684779	3.018962	-1.3513
H	3.40814	3.672976	-0.26911

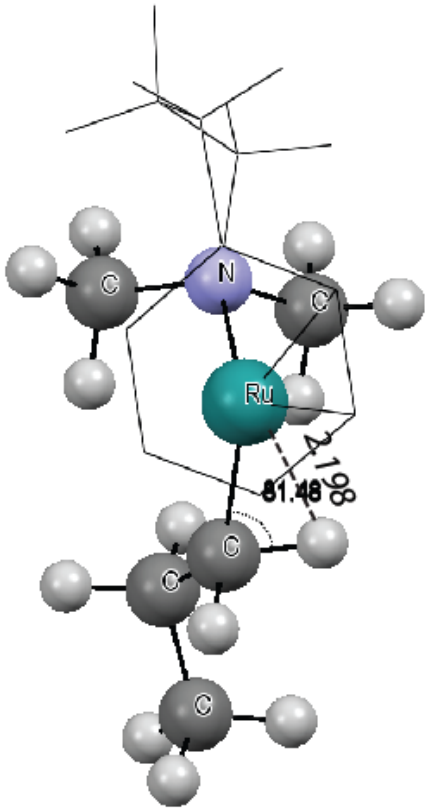

Optimized Structure Coordinates for **N5**

Atom	X	Y	Z
Ru	0.342503	0.372017	0.395796
C	-1.29656	-0.57574	1.677696
C	-0.19152	-0.15479	2.481308
C	1.117325	-0.65928	2.187051
C	1.289863	-1.68298	1.194557
C	0.214922	-2.0004	0.350926
C	-1.09676	-1.40099	0.538201
C	-2.2032	-1.6805	-0.45009
C	-1.80937	-1.42121	-1.92087
C	-1.35804	0.002677	-2.27886
C	1.030446	-0.4531	-2.56277
C	2.378614	1.115939	0.039806
H	-2.2976	-0.15784	1.871813
H	-0.33859	0.542193	3.319192
H	1.975616	-0.32814	2.793955
H	2.277951	-2.14364	1.033469
H	0.361993	-2.7378	-0.45436
H	-3.09044	-1.0639	-0.18712
H	-2.52568	-2.74338	-0.35411
H	-1.06541	-2.17031	-2.2709
H	-2.71214	-1.61591	-2.54124
H	-2.06178	0.742366	-1.84332
H	-1.42988	0.109202	-3.38753
H	0.823771	-0.51047	-3.65786
H	0.99185	-1.46962	-2.13531
H	2.053313	-0.05732	-2.421
C	-1.0521	2.043797	0.426279
C	1.672387	2.088282	0.782589
H	-1.99823	1.619262	0.018477
H	-0.67597	2.781274	-0.31001
C	-1.34995	2.777563	1.73598
H	1.846317	2.191851	1.868865
H	1.332825	3.01465	0.28981
H	3.123206	0.462198	0.52939
H	2.581027	1.29148	-1.03007
N	0.038036	0.447164	-1.90325
C	0.223017	1.797321	-2.51045
H	1.196966	2.228429	-2.20642
H	0.201955	1.720913	-3.62237
H	-0.58904	2.478121	-2.19475
C	-2.26285	3.999248	1.512551
H	-0.4054	3.117168	2.217212
H	-1.84492	2.100918	2.469214
H	-3.23589	3.705336	1.058739
H	-2.48266	4.510833	2.475372
H	-1.78674	4.744735	0.837116

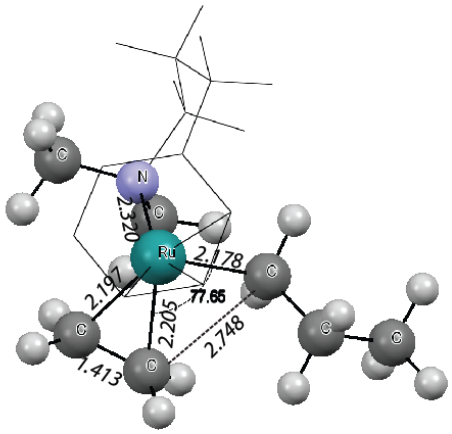

Optimized Structure Coordinates for **$TS_{N5\text{-}N6\gamma}$**

Atom	X	Y	Z
Ru	0.37976	0.122638	0.317294
C	-1.50597	-0.70515	1.47236
C	-0.46817	-0.22647	2.341982
C	0.865517	-0.73905	2.282452
C	1.196617	-1.67405	1.245825
C	0.193423	-2.06853	0.311554
C	-1.17188	-1.58842	0.416811
C	-2.18335	-1.96715	-0.63469
C	-1.74044	-1.63619	-2.07577
C	-1.34778	-0.17586	-2.33457
C	1.052465	-0.53567	-2.68641
C	2.277441	0.950491	0.038217
H	-2.53128	-0.31405	1.565319
H	-0.70854	0.543459	3.092588
H	1.633349	-0.38096	2.986068
H	2.22285	-2.06259	1.14619
H	0.465822	-2.76216	-0.4993
H	-3.14418	-1.45194	-0.4167
H	-2.38989	-3.06046	-0.56725
H	-0.93864	-2.32671	-2.41637
H	-2.60131	-1.85299	-2.74574
H	-2.06187	0.504044	-1.82016
H	-1.44914	0.01677	-3.42946
H	0.834475	-0.52505	-3.78113
H	1.053638	-1.5801	-2.32715
H	2.062561	-0.11465	-2.52431
C	-0.22716	2.642586	0.647516
C	1.786355	2.165421	0.702174
H	-1.06	1.91387	0.528552
H	-0.18432	3.277085	-0.25533
C	-0.36724	3.450751	1.929829
H	1.945407	2.217521	1.794388
H	2.003002	3.132987	0.20846
H	3.044623	0.388167	0.608435
H	2.598741	1.086296	-1.01288
N	0.042284	0.280978	-1.95368
C	0.162749	1.677983	-2.45545
H	1.133347	2.116037	-2.15243
H	0.101308	1.693659	-3.56937
H	-0.66237	2.296549	-2.05437
C	-1.70627	4.208905	1.988997
H	0.47207	4.179735	2.005384
H	-0.27757	2.787135	2.819614
H	-2.57591	3.51405	1.972559
H	-1.77371	4.809275	2.922323
H	-1.81609	4.910039	1.132092

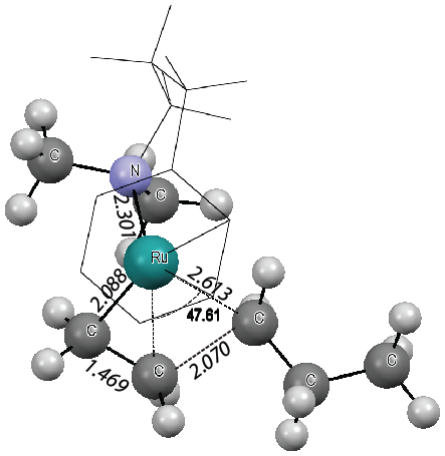

Optimized Structure Coordinates for **N6γ**

Atom	X	Y	Z
Ru	0.295143	0.052222	0.296347
C	-1.59401	-0.859	1.393792
C	-0.60741	-0.29474	2.279535
C	0.746763	-0.7547	2.306829
C	1.165429	-1.66551	1.287014
C	0.221951	-2.10729	0.302289
C	-1.18719	-1.7521	0.38036
C	-2.13692	-2.21373	-0.69248
C	-1.70498	-1.79124	-2.11476
C	-1.44572	-0.29149	-2.31151
C	0.967237	-0.40294	-2.74005
C	2.197473	0.936787	0.052903
H	-2.63972	-0.51797	1.449113
H	-0.91591	0.491971	2.987609
H	1.463068	-0.35709	3.041329
H	2.217407	-1.98518	1.218368
H	0.570031	-2.77649	-0.50078
H	-3.1506	-1.81092	-0.47896
H	-2.22302	-3.3242	-0.65986
H	-0.83608	-2.39147	-2.46229
H	-2.53075	-2.06429	-2.80772
H	-2.20468	0.301203	-1.75529
H	-1.58188	-0.05782	-3.39415
H	0.726062	-0.32723	-3.82706
H	1.057404	-1.46909	-2.46208
H	1.943047	0.085265	-2.55757
C	0.639007	2.774867	0.805021
C	2.052838	2.162862	0.958036
H	-0.17897	1.960251	0.67798
H	0.568243	3.349298	-0.14435
C	0.177323	3.644759	1.979779
H	2.202273	1.868045	2.021198
H	2.820967	2.946722	0.748431
H	3.033997	0.274875	0.363986
H	2.377943	1.23153	-1.00375
N	-0.09201	0.267299	-1.93155
C	-0.11849	1.704118	-2.32578
H	0.853099	2.180882	-2.09416
H	-0.30471	1.800501	-3.42167
H	-0.92845	2.230175	-1.78219
C	-1.20208	4.285532	1.792395
H	0.950882	4.437644	2.116682
H	0.201075	3.042425	2.917765
H	-1.99993	3.515562	1.679402
H	-1.47238	4.916897	2.665834
H	-1.23046	4.936112	0.889947

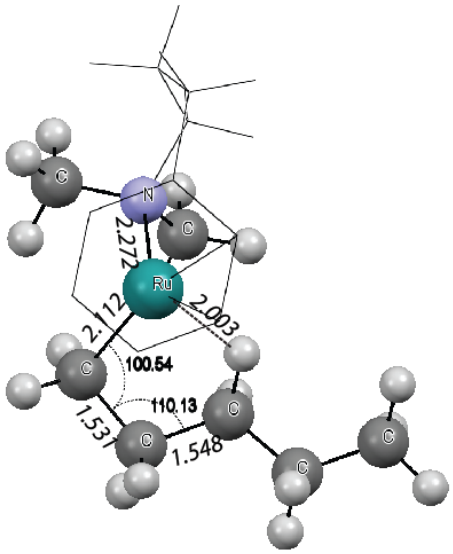

Optimized Structure Coordinates for **$TS_{N6\gamma\text{-}N7\beta}$**

Atom	X	Y	Z
Ru	0.178885	-0.07614	0.210684
C	-1.71936	-1.06105	1.227035
C	-0.8491	-0.35149	2.132413
C	0.526252	-0.71069	2.309014
C	1.095898	-1.63402	1.383411
C	0.26775	-2.19785	0.347549
C	-1.17175	-1.986	0.316163
C	-1.98784	-2.58202	-0.8003
C	-1.51972	-2.12438	-2.20196
C	-1.46103	-0.60351	-2.40615
C	0.932581	-0.31523	-2.83758
C	1.956909	1.010349	0.073498
H	-2.78767	-0.79724	1.178235
H	-1.27202	0.460824	2.74745
H	1.149571	-0.20444	3.061697
H	2.172563	-1.86669	1.410756
H	0.733651	-2.8637	-0.39736
H	-3.05603	-2.30774	-0.66023
H	-1.93516	-3.69353	-0.74939
H	-0.54968	-2.59678	-2.47061
H	-2.24559	-2.52419	-2.94319
H	-2.3097	-0.11814	-1.87662
H	-1.59225	-0.38532	-3.49258
H	0.68274	-0.16489	-3.91471
H	1.156472	-1.38483	-2.66326
H	1.83642	0.273907	-2.59466
C	1.35492	3.593644	0.160836
C	1.72001	2.301854	0.9143
H	0.325631	3.524447	-0.26194
H	2.043747	3.720619	-0.70836
C	1.43061	4.846913	1.051166
H	0.967424	2.135688	1.726961
H	2.665817	2.485501	1.481028
H	2.796702	0.424027	0.50481
H	2.248057	1.272394	-0.96788
N	-0.20563	0.124962	-1.98235
C	-0.45032	1.574824	-2.22337
H	0.474003	2.15135	-2.03347
H	-0.76758	1.749787	-3.27934
H	-1.25795	1.938583	-1.55201
C	1.049663	6.139567	0.318678
H	2.464009	4.939039	1.460325
H	0.765179	4.708208	1.936131
H	0.004218	6.10006	-0.06304
H	1.125295	7.020349	0.992392
H	1.71895	6.326806	-0.55106

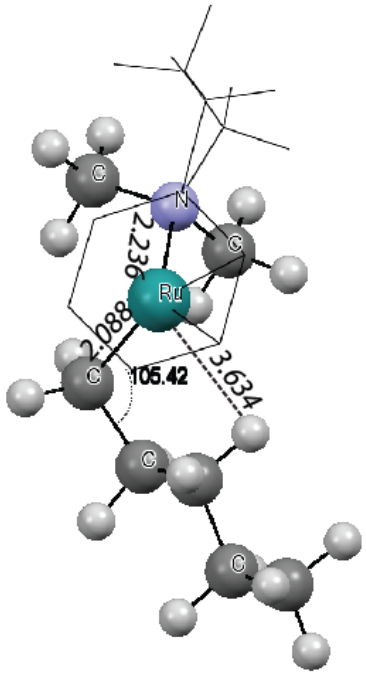

Optimized Structure Coordinates for **N7β**

Atom	X	Y	Z
Ru	0.526672	0.069132	0.230946
C	-1.38025	-0.4921	1.447484
C	-0.28588	-0.05083	2.268623
C	0.98755	-0.70539	2.239221
C	1.212473	-1.74375	1.278119
C	0.162674	-2.10587	0.384467
C	-1.15385	-1.49978	0.477961
C	-2.21828	-1.87335	-0.52088
C	-1.79767	-1.63311	-1.98528
C	-1.34381	-0.20544	-2.31168
C	1.025084	-0.65651	-2.76798
C	2.442629	0.882003	-0.06666
H	-2.36235	-0.0003	1.521014
H	-0.4358	0.800749	2.952933
H	1.800502	-0.36994	2.90268
H	2.197729	-2.23031	1.1985
H	0.352579	-2.87626	-0.37922
H	-3.1421	-1.29488	-0.30304
H	-2.47966	-2.949	-0.39222
H	-1.03607	-2.37494	-2.31006
H	-2.68338	-1.83776	-2.62608
H	-2.00467	0.528487	-1.80106
H	-1.46968	-0.04712	-3.40917
H	0.782971	-0.61326	-3.85692
H	0.9735	-1.70655	-2.42623
H	2.06002	-0.29592	-2.61662
C	1.953093	3.474386	-0.11291
C	1.74742	2.074504	0.505782
H	1.922587	3.428646	-1.22307
H	2.999142	3.760864	0.14578
C	0.977435	4.544211	0.400072
H	0.53256	1.921705	0.373611
H	1.870349	2.144981	1.607438
H	3.222956	0.419856	0.568319
H	2.795091	0.994739	-1.1121
N	0.078602	0.197496	-1.99384
C	0.219929	1.591987	-2.49505
H	1.264922	1.930827	-2.37379
H	-0.03763	1.643838	-3.57962
H	-0.45776	2.267301	-1.93519
C	1.274665	5.945779	-0.14792
H	1.008601	4.564458	1.514933
H	-0.06619	4.2512	0.1297
H	1.218865	5.970361	-1.25949
H	0.547595	6.690767	0.241065
H	2.292384	6.287029	0.144763

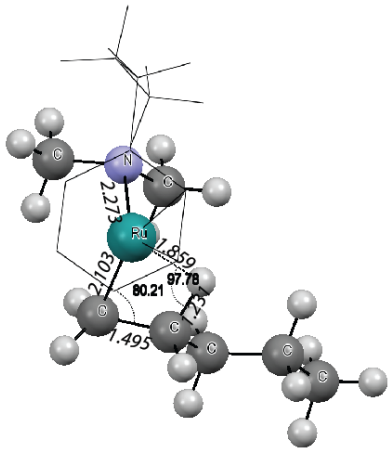

Optimized Structure Coordinates for **4.9**

Atom	X	Y	Z
Ru	0.371274	-0.12462	0.210268
S	-1.36105	0.173141	-1.34118
S	-0.23591	2.22694	0.270046
N	-2.17619	2.790793	-1.57423
C	0.862014	-2.33212	0.829269
C	-0.54934	-2.05385	0.911761
C	-0.74022	-0.94313	1.848527
C	0.583716	-0.55907	2.352884
C	1.552146	-1.43419	1.735435
C	1.504827	-3.41734	0.02036
C	-1.6402	-2.85128	0.258211
C	-2.04971	-0.43806	2.37875
C	0.848442	0.436015	3.443709
C	3.005289	-1.51612	2.088473
C	2.278809	0.652181	-0.10439
C	-1.38498	1.897897	-0.97071
C	-3.15409	2.409468	-2.59621
C	-2.1083	4.215183	-1.23577
H	2.509088	-3.12104	-0.34828
H	1.640952	-4.3337	0.642026
H	0.886252	-3.7029	-0.85523
H	-2.5589	-2.24988	0.100828
H	-1.91378	-3.71505	0.907982
H	-1.327	-3.26208	-0.72416
H	-2.87396	-0.57791	1.650138
H	-2.32003	-0.995	3.307022
H	-2.00003	0.63905	2.638955
H	0.116848	1.270296	3.425902
H	1.86577	0.872943	3.370059
H	0.765004	-0.05825	4.44014
H	3.41609	-0.54378	2.429057
H	3.629906	-1.88897	1.250081
H	3.128841	-2.239	2.929006
H	3.1172	-0.05718	0.031051
H	2.523024	1.644961	0.326139
H	2.048084	0.760789	-1.20074
H	-3.25905	1.306555	-2.63106
H	-4.13911	2.861948	-2.34979
H	-2.82879	2.776047	-3.59526
H	-2.95681	4.498072	-0.57316
H	-1.15204	4.434098	-0.71804
H	-2.16299	4.813104	-2.16994

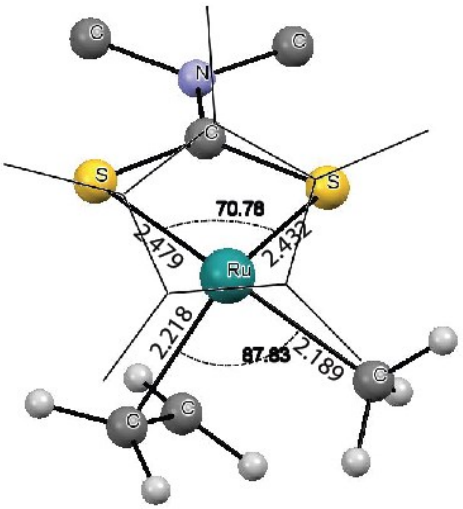

Optimized Structure Coordinates for **4.10**

Atom	X	Y	Z
Ru	0.435176	-0.31724	-0.14751
S	-1.42688	0.339269	-1.55833
S	-0.04123	2.030268	0.221923
N	-2.16484	2.95634	-1.24541
C	0.87939	-2.38314	0.781782
C	-0.53504	-2.08632	0.691424
C	-0.78828	-0.90804	1.526033
C	0.487708	-0.51765	2.134442
C	1.503488	-1.41135	1.657558
C	1.5701	-3.60143	0.244357
C	-1.58364	-2.93342	0.032244
C	-2.14065	-0.38631	1.914677
C	0.669	0.544338	3.178346
C	2.944715	-1.42511	2.073414
C	1.05191	-1.27692	-1.94727
C	2.800004	1.022471	-0.86954
C	-1.35306	1.939218	-0.9186
C	-3.22514	2.796899	-2.24115
C	-2.04347	4.276985	-0.62859
H	2.569699	-3.37477	-0.18468
H	1.73501	-4.32433	1.077
H	0.969021	-4.1276	-0.52464
H	-2.4592	-2.32822	-0.2811
H	-1.94962	-3.71262	0.740821
H	-1.19456	-3.45477	-0.86685
H	-2.87478	-0.49734	1.090577
H	-2.52833	-0.95611	2.7912
H	-2.1029	0.685543	2.198263
H	-0.05162	1.378878	3.053411
H	1.693381	0.972142	3.17084
H	0.501707	0.105538	4.189831
H	3.295146	-0.42831	2.412598
H	3.612776	-1.76848	1.255831
H	3.086839	-2.12815	2.927676
H	0.378306	-0.99919	-2.77996
H	1.103046	-2.37487	-1.84245
H	3.864404	1.01423	-1.17382
H	2.713264	0.92201	0.227323
H	2.244566	1.880449	-1.28351
H	-3.05598	1.872412	-2.82997
H	-4.22194	2.738938	-1.748
H	-3.21593	3.669078	-2.9301
H	-3.0341	4.599352	-0.23913
H	-1.32084	4.239801	0.211571
H	-1.69259	5.023003	-1.37673
C	2.375249	-0.6203	-1.99006
H	2.600787	-0.0915	-2.93677
H	3.221934	-1.24566	-1.64996

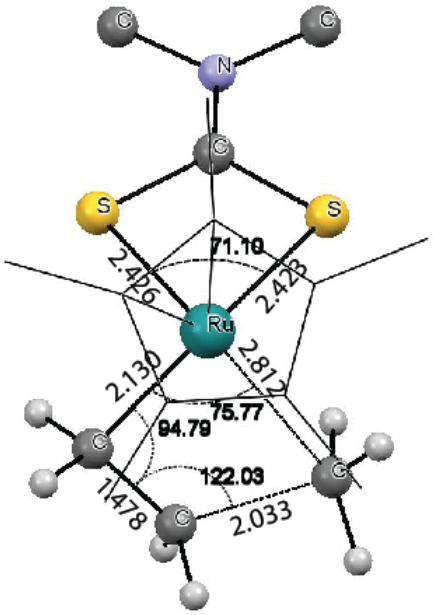

Optimized Structure Coordinates for **$TS_{4.10\text{-}4.11\beta}$**

Atom	X	Y	Z
Ru	0.435176	-0.31724	-0.14751
S	-1.42688	0.339269	-1.55833
S	-0.04123	2.030268	0.221923
N	-2.16484	2.95634	-1.24541
C	0.87939	-2.38314	0.781782
C	-0.53504	-2.08632	0.691424
C	-0.78828	-0.90804	1.526033
C	0.487708	-0.51765	2.134442
C	1.503488	-1.41135	1.657558
C	1.5701	-3.60143	0.244357
C	-1.58364	-2.93342	0.032244
C	-2.14065	-0.38631	1.914677
C	0.669	0.544338	3.178346
C	2.944715	-1.42511	2.073414
C	1.05191	-1.27692	-1.94727
C	2.800004	1.022471	-0.86954
C	-1.35306	1.939218	-0.9186
C	-3.22514	2.796899	-2.24115
C	-2.04347	4.276985	-0.62859
H	2.569699	-3.37477	-0.18468
H	1.73501	-4.32433	1.077
H	0.969021	-4.1276	-0.52464
H	-2.4592	-2.32822	-0.2811
H	-1.94962	-3.71262	0.740821
H	-1.19456	-3.45477	-0.86685
H	-2.87478	-0.49734	1.090577
H	-2.52833	-0.95611	2.7912
H	-2.1029	0.685543	2.198263
H	-0.05162	1.378878	3.053411
H	1.693381	0.972142	3.17084
H	0.501707	0.105538	4.189831
H	3.295146	-0.42831	2.412598
H	3.612776	-1.76848	1.255831
H	3.086839	-2.12815	2.927676
H	0.378306	-0.99919	-2.77996
H	1.103046	-2.37487	-1.84245
H	3.864404	1.01423	-1.17382
H	2.713264	0.92201	0.227323
H	2.244566	1.880449	-1.28351
H	-3.05598	1.872412	-2.82997
H	-4.22194	2.738938	-1.748
H	-3.21593	3.669078	-2.9301
H	-3.0341	4.599352	-0.23913
H	-1.32084	4.239801	0.211571
H	-1.69259	5.023003	-1.37673
C	2.375249	-0.6203	-1.99006
H	2.600787	-0.0915	-2.93677
H	3.221934	-1.24566	-1.64996

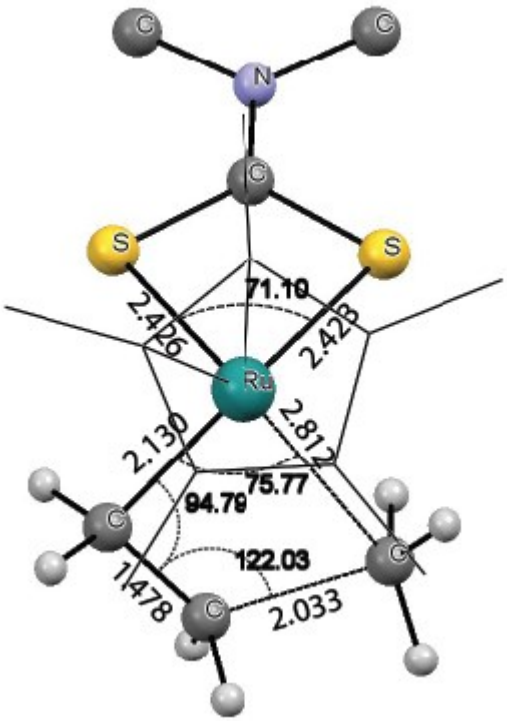

Optimized Structure Coordinates for **4.11α**

Atom	X	Y	Z
Ru	0.484735	-0.23256	0.148943
S	-1.33323	0.13931	-1.32486
S	-0.05564	2.135428	0.236086
N	-2.12	2.768299	-1.44543
C	0.818811	-2.42744	0.919503
C	-0.58081	-2.07674	0.916439
C	-0.76315	-0.91477	1.784433
C	0.551407	-0.56254	2.323544
C	1.509707	-1.51288	1.806931
C	1.423346	-3.61577	0.232294
C	-1.67626	-2.86197	0.256034
C	-2.07088	-0.32435	2.225641
C	0.812321	0.477004	3.372945
C	2.915552	-1.66395	2.30494
C	2.33281	0.420897	-0.50124
C	-1.3009	1.846788	-0.92306
C	-3.17908	2.423894	-2.39577
C	-2.00667	4.181298	-1.07714
H	2.496883	-3.46363	-0.0032
H	1.35563	-4.51455	0.889786
H	0.895693	-3.86142	-0.71287
H	-2.54668	-2.22457	-0.00342
H	-2.03875	-3.6568	0.948899
H	-1.33013	-3.36427	-0.67134
H	-2.86538	-0.46669	1.464693
H	-2.41221	-0.81432	3.167344
H	-1.98229	0.763041	2.428488
H	0.135296	1.349636	3.265147
H	1.857255	0.848316	3.340278
H	0.639046	0.044042	4.386243
H	3.38468	-0.69118	2.556027
H	3.57314	-2.19791	1.591517
H	2.892788	-2.26724	3.242869
H	2.455093	1.525164	-0.51365
H	1.702358	0.099975	-1.42392
H	-3.28714	1.322758	-2.46399
H	-4.14168	2.86187	-2.0524
H	-2.93854	2.828321	-3.4044
H	-2.79487	4.458746	-0.34136
H	-1.00888	4.376212	-0.6332
H	-2.1268	4.805479	-1.98789
C	3.674009	-0.27595	-0.51831
H	3.553281	-1.38032	-0.52778
H	4.231999	-0.00696	0.407456
C	4.524414	0.15236	-1.73749
H	5.517735	-0.34547	-1.70687
H	4.032628	-0.12807	-2.69518
H	4.693922	1.251439	-1.74859

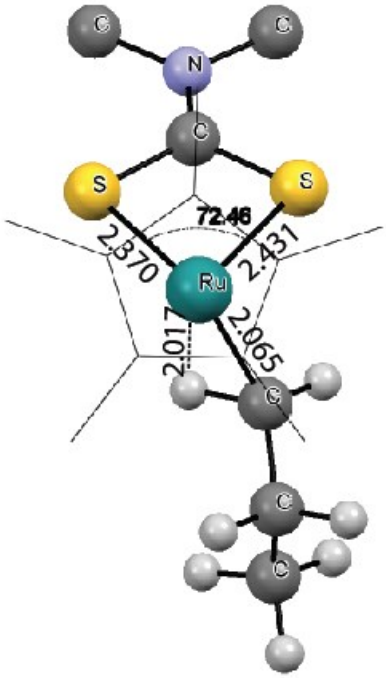

Optimized Structure Coordinates for **4.11β**

Atom	X	Y	Z
Ru	0.304855	-0.4094	-0.33532
S	-1.63689	0.247586	-1.63586
S	-0.06643	1.968973	-0.01942
N	-2.27072	2.89417	-1.35565
C	0.737529	-2.48622	0.57442
C	-0.66288	-2.12832	0.655525
C	-0.76369	-0.92768	1.482343
C	0.592433	-0.57022	1.90544
C	1.509714	-1.51485	1.324331
C	1.284548	-3.74811	-0.02229
C	-1.81529	-2.93475	0.132518
C	-2.03571	-0.32314	2.001796
C	0.948795	0.508267	2.885768
C	2.989901	-1.5713	1.566229
C	0.884218	-1.31949	-2.17919
C	-1.46229	1.866462	-1.05596
C	-3.41085	2.735186	-2.25913
C	-2.06615	4.231114	-0.79832
H	2.31265	-3.62365	-0.42242
H	1.341711	-4.52939	0.77184
H	0.639698	-4.15116	-0.82999
H	-2.69089	-2.29417	-0.09898
H	-2.13709	-3.6828	0.894094
H	-1.54819	-3.49069	-0.79016
H	-2.87197	-0.4503	1.284414
H	-2.33151	-0.8178	2.956039
H	-1.92131	0.761463	2.206078
H	0.250261	1.36879	2.832195
H	1.978993	0.891476	2.730371
H	0.898583	0.100557	3.92249
H	3.423403	-0.5637	1.733908
H	3.533713	-2.04429	0.722607
H	3.205278	-2.17925	2.476056
H	-3.33178	1.772861	-2.80441
H	-4.3673	2.755132	-1.68913
H	-3.41533	3.567387	-2.99636
H	-3.01688	4.598151	-0.35308
H	-1.28759	4.200475	-0.00948
H	-1.74706	4.938902	-1.59609
H	1.405286	-2.2884	-2.07098
H	0.065746	-1.36151	-2.92116
C	1.765889	-0.12282	-2.21617
H	1.3713	0.677994	-2.87759
H	1.749077	0.414602	-1.12819
C	3.274643	-0.35231	-2.40305
H	3.463059	-0.71919	-3.43557
H	3.853824	0.584822	-2.26124
H	3.661675	-1.11447	-1.69328

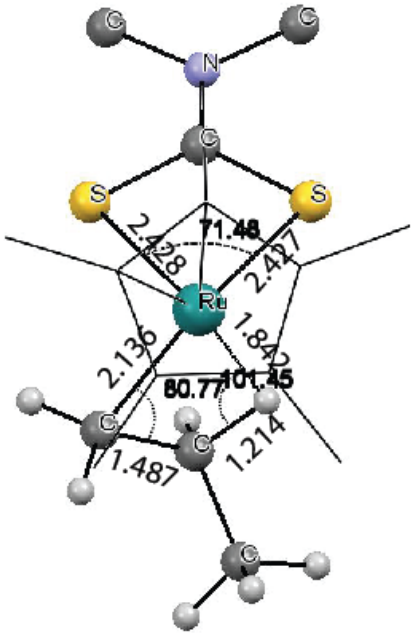

Optimized Structure Coordinates for **$TS_{4.11\beta\text{-}4.12}$**

Atom	X	Y	Z
Ru	0.466707	-0.30911	-0.03088
S	-1.51209	0.056321	-1.31835
S	0.007785	2.08763	-0.06465
N	-2.24697	2.695465	-1.48994
C	0.872836	-2.43636	0.910063
C	-0.5327	-2.10216	0.878505
C	-0.72395	-0.88118	1.664268
C	0.591079	-0.46428	2.151996
C	1.552872	-1.45289	1.723875
C	1.497653	-3.66986	0.32919
C	-1.62528	-2.95771	0.305049
C	-2.02952	-0.28676	2.10337
C	0.852222	0.648351	3.12272
C	2.947764	-1.55279	2.264066
C	1.111008	-0.70754	-3.53958
C	2.481451	0.408832	-0.33331
C	-1.38838	1.775274	-1.02638
C	-3.43342	2.334974	-2.26648
C	-2.04758	4.1219	-1.22737
H	2.541605	-3.49208	-0.00091
H	1.52465	-4.48153	1.094505
H	0.923544	-4.05717	-0.53714
H	-2.49733	-2.35363	-0.02275
H	-1.98866	-3.67759	1.075019
H	-1.27563	-3.55321	-0.56385
H	-2.85929	-0.55448	1.419145
H	-2.28736	-0.66468	3.120591
H	-1.9762	0.820301	2.16444
H	0.150313	1.495338	2.978278
H	1.886336	1.041553	3.035929
H	0.722538	0.278055	4.167011
H	3.502562	-0.59276	2.212641
H	3.548042	-2.3368	1.762048
H	2.884199	-1.82749	3.343265
H	2.157777	-0.42455	-3.75305
H	0.336524	0.048453	-3.7578
H	2.846437	0.98681	0.544109
H	2.229788	1.144796	-1.13116
H	-3.58046	1.236357	-2.24904
H	-4.32867	2.826833	-1.82671
H	-3.32246	2.670211	-3.32214

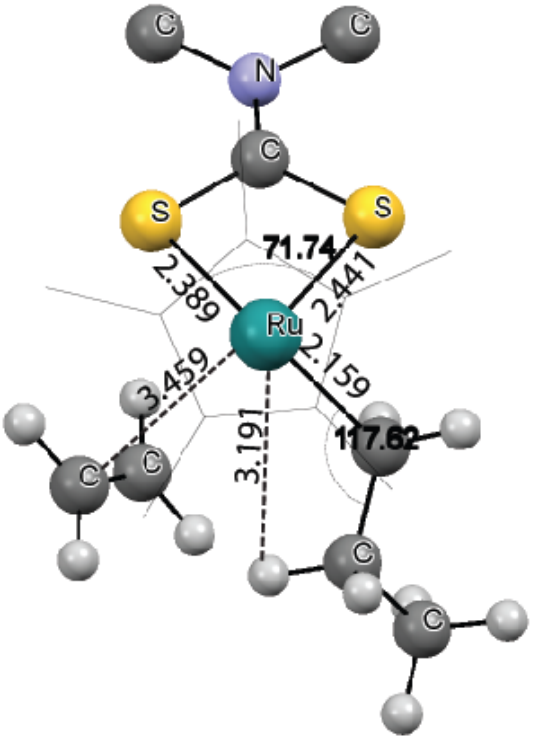

H	-2.73504	4.473441	-0.42477
H	-0.99929	4.305458	-0.91464
H	-2.25405	4.6968	-2.15545
C	0.78929	-1.93041	-3.07045
H	1.557938	-2.70272	-2.8876
H	-0.26255	-2.22674	-2.90799
C	3.516317	-0.5849	-0.84976
H	3.068343	-1.24174	-1.62595
H	3.877232	-1.25386	-0.04279
C	4.732171	0.150394	-1.4586
H	5.487198	-0.57963	-1.82533

Optimized Structure Coordinates for **4.12**

Atom	X	Y	Z
Ru	0.50965	-0.34211	-0.21286
S	-1.69445	0.095689	-1.27066
S	0.065686	2.057102	-0.19801
N	-2.31534	2.755715	-1.33804
C	0.803702	-2.4092	0.840497
C	-0.59625	-2.0545	0.771436
C	-0.79221	-0.83888	1.562172
C	0.494292	-0.4431	2.082332
C	1.466846	-1.43376	1.674169
C	1.412346	-3.68778	0.345151
C	-1.68206	-2.9101	0.188563
C	-2.10097	-0.23026	1.968984
C	0.740601	0.67929	3.045674
C	2.834883	-1.5777	2.262821
C	1.055506	-0.13093	-2.39921
C	2.607947	0.462841	-0.15197
C	-1.45469	1.788969	-0.97786
C	-3.59359	2.457103	-1.98235
C	-2.03186	4.168545	-1.08372
H	2.486012	-3.57389	0.090192
H	1.344527	-4.46522	1.142228
H	0.88739	-4.08698	-0.54615
H	-2.55186	-2.31021	-0.15244
H	-2.05284	-3.62255	0.962195
H	-1.32318	-3.51613	-0.66906
H	-2.93788	-0.56735	1.326838
H	-2.33319	-0.52371	3.019038
H	-2.06563	0.879724	1.936491
H	0.011873	1.504543	2.910283
H	1.760434	1.106394	2.940555
H	0.647172	0.309951	4.093511
H	3.335318	-0.60338	2.435345
H	3.503435	-2.217	1.654757
H	2.728703	-2.06588	3.260866
H	2.003909	0.402883	-2.54215
H	0.194742	0.298579	-2.93622
H	2.684181	0.802165	0.900179
H	2.552317	1.382422	-0.7681
H	-3.75717	1.361211	-2.01587
H	-4.42253	2.92876	-1.40941

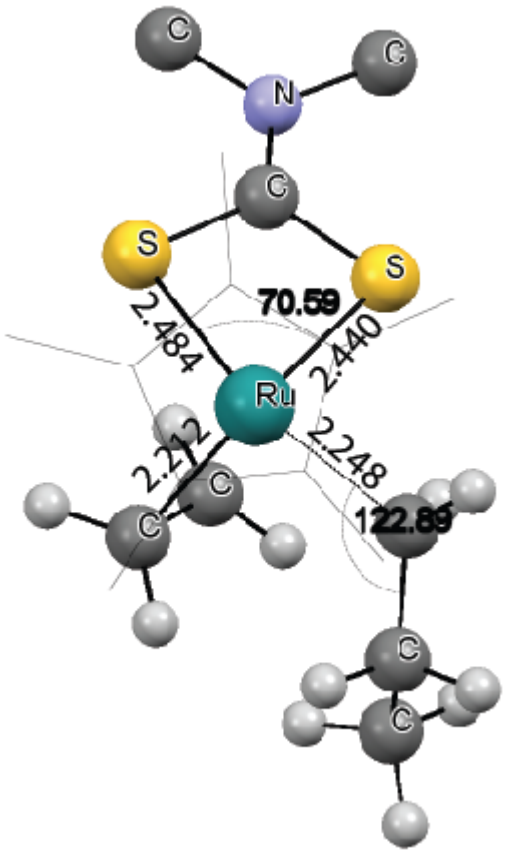

H	-3.60378	2.856717	-3.02121
H	-2.63348	4.543194	-0.22437
H	-0.95424	4.305389	-0.86042
H	-2.28932	4.762097	-1.98738
C	1.042253	-1.48872	-2.02796
H	1.993284	-2.0263	-1.8731
H	0.181575	-2.12474	-2.30443
C	3.841038	-0.37859	-0.54622
H	3.644832	-1.46988	-0.44607
H	4.629191	-0.16774	0.214133
C	4.462889	-0.11068	-1.92858
H	5.46108	-0.59589	-2.00046
H	3.85504	-0.5079	-2.76935
H	4.613876	0.978764	-2.09979

Optimized Structure Coordinates for **$TS_{4.12\text{-}4.13\beta}$**

Atom	X	Y	Z
Ru	0.269435	-0.44169	-0.15944
S	-1.68577	0.171093	-1.46728
S	-0.04871	1.970421	-0.02762
N	-2.26879	2.842403	-1.37496
C	0.572669	-2.47144	0.904406
C	-0.80257	-2.02062	0.926867
C	-0.84014	-0.76324	1.672462
C	0.526669	-0.4673	2.106145
C	1.386378	-1.51578	1.62792
C	1.050253	-3.80408	0.410088
C	-1.99505	-2.79358	0.445569
C	-2.08188	-0.056	2.132203
C	0.929911	0.654857	3.017783
C	2.84212	-1.68175	1.945459
C	0.694047	-1.58503	-1.90643
C	2.664923	0.605195	-0.9646
C	-1.46881	1.825073	-1.0177
C	-3.42466	2.6376	-2.24851
C	-2.03534	4.210852	-0.91468
H	2.090094	-3.76938	0.022747
H	1.044628	-4.52986	1.257191
H	0.396185	-4.22274	-0.38192
H	-2.82859	-2.1214	0.155587
H	-2.36887	-3.46447	1.253927
H	-1.75115	-3.431	-0.42958
H	-2.90419	-0.14975	1.393218
H	-2.43836	-0.49998	3.090594
H	-1.9004	1.024311	2.307387
H	0.297045	1.554963	2.873088
H	1.989547	0.953818	2.874242
H	0.819417	0.335932	4.080607
H	3.349476	-0.71092	2.123551
H	3.389022	-2.21789	1.14248
H	2.95893	-2.28473	2.876423
H	-0.2407	-1.81398	-2.45524
H	1.305619	-2.48821	-1.73153
H	2.416821	0.689055	0.109206
H	2.504139	1.581131	-1.46031
H	-3.35239	1.64991	-2.74778
H	-4.37191	2.683284	-1.66455

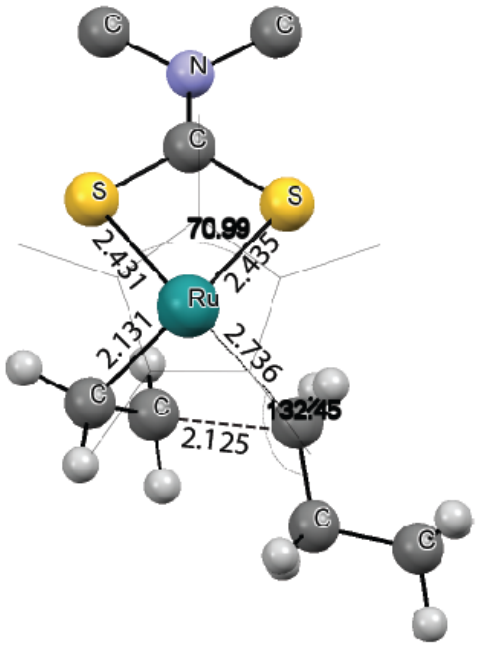

H	-3.44405	3.43242	-3.02559
H	-2.98026	4.631711	-0.50645
H	-1.26459	4.217529	-0.1175
H	-1.69154	4.852316	-1.75747
C	1.435456	-0.41519	-2.36562
H	0.853164	0.38313	-2.8598
H	2.395026	-0.62263	-2.87606
C	4.030269	-0.01612	-1.18815
H	4.272373	-0.03067	-2.27526
H	4.034092	-1.07821	-0.853
C	5.131328	0.761306	-0.4401
H	6.128661	0.31294	-0.6425
H	5.168554	1.824614	-0.76432
H	4.973772	0.748989	0.661452

Optimized Structure Coordinates for **4.13β**

Atom	X	Y	Z
Ru	0.362596	-0.8521	-0.03681
S	-1.35627	0.052021	-1.49501
S	0.532516	1.567219	-0.02408
N	-1.41172	2.788338	-1.5184
C	0.271531	-2.8452	1.122198
C	-1.00968	-2.17548	1.087141
C	-0.85445	-0.88896	1.764255
C	0.534393	-0.797	2.2215
C	1.225726	-1.9857	1.796927
C	0.537418	-4.25955	0.702525
C	-2.30252	-2.76142	0.600502
C	-1.96806	0.043234	2.14369
C	1.099203	0.284398	3.094608
C	2.651607	-2.34096	2.102313
C	0.794113	-2.07697	-1.73268
C	2.220342	-0.27199	-2.93799
C	-0.84486	1.65113	-1.08579
C	-2.55121	2.775987	-2.4358
C	-0.9291	4.104082	-1.09998
H	1.570427	-4.40724	0.322493
H	0.423157	-4.92818	1.587842
H	-0.17552	-4.6155	-0.06887
H	-2.99929	-1.97629	0.241742
H	-2.81085	-3.30782	1.428825
H	-2.14526	-3.48078	-0.22951
H	-2.79596	0.014534	1.405922
H	-2.38849	-0.24719	3.13451
H	-1.6155	1.092325	2.220709
H	0.615751	1.265287	2.907385
H	2.193282	0.407818	2.953973
H	0.927994	0.026362	4.166015
H	3.28428	-1.44018	2.241666
H	3.107513	-2.96165	1.302488
H	2.705732	-2.93333	3.045224
H	0.087253	-1.93402	-2.57142
H	0.948886	-3.14269	-1.49185
H	1.281643	0.298532	-3.12031
H	2.377811	-0.90929	-3.83915
H	-2.67714	1.763844	-2.8708
H	-3.486	3.062857	-1.90289

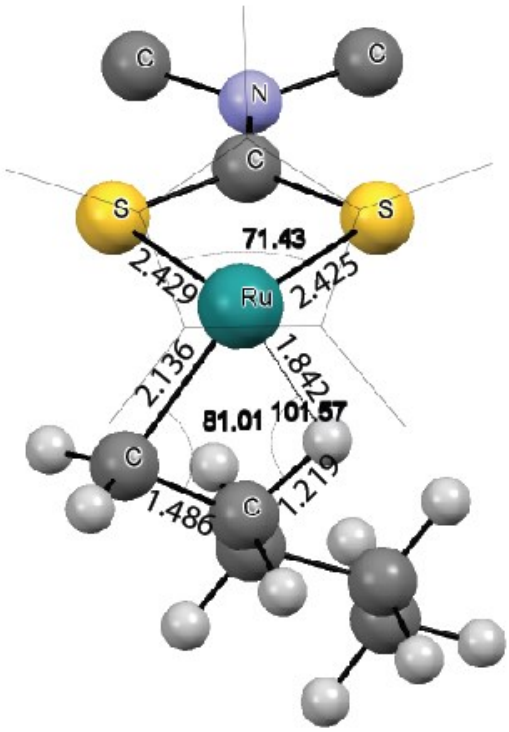

H	-2.37024	3.502083	-3.25793
H	-1.78325	4.714348	-0.73263
H	-0.18724	3.995623	-0.28336
H	-0.45241	4.63312	-1.95581
C	2.00911	-1.22126	-1.74978
H	2.931505	-1.79618	-1.50359
H	2.024388	-0.51272	-0.75841
C	3.407252	0.689286	-2.77103
H	4.329402	0.099807	-2.55428
H	3.231446	1.332627	-1.87684
C	3.643444	1.573208	-4.00248
H	4.505347	2.257245	-3.84648
H	3.860452	0.961518	-4.90666
H	2.752563	2.201395	-4.22903